Structural effects of oxidation of carbon/carbon composites

Crocker, P.

Award date:
1991

Awarding institution:
University of Bath

STRUCTURAL EFFECTS OF OXIDATION OF CARBON/CARBON COMPOSITES

submitted by P. CROCKER

for the degree of PhD
of the University of Bath

1991

ProQuest LLC
789 East Eisenhower Parkway
P.O. Box 1346
Ann Arbor, MI 48106-1346

ACKNOWLEDGEMENTS

The author would like to thank the following people who have helped in this research programme.

Prof. Brian McEnaney for all his help throughout the research.

Prof. Bryan Harris for helpful discussions and editing.

Dr. Graeme Proud of British Petroleum Plc for useful discussions.

Mark Deven and Ian Trussler of university of Bath for their technical assistance.

Mike Hallgarth for letting me use his computer.

The Science and Engineering Research Council, the University of Bath and British Petroleum Plc for financial support.

ABSTRACT

The aim of this work was to identify microstructural features which control the strength and other mechanical properties of carbon/carbon composites and to observe how these features and properties are affected by oxidation in air. Three commercially-manufactured, 2D woven composites, (KKarb, Sigri and FMI) having a range of fibre types, matrix types and weave patterns, were fractured in flexural, impact and tensile modes in the as-received condition and after oxidation between 500-700^{o}C in air.

In the unoxidised state, the KKarb material failed in flexure by delamination between plies, whereas flexural failure of the Sigri composite was dominated by large pores which blunted cracks; for the FMI material flexural failure was dominated by microcracks at cross-over points between fibre bundles. In tension the Sigri material failed with long fibre pull-out, whereas the tensile failure in the KKarb material was more brittle, implying a stronger degree of fibre/matrix adhesion. In Impact testing the KKarb material failed by cross-specimen cracking with some delamination; the Sigri material failed either by delamination or by cross-bundle cracking or by a mixture of the two; and the FMI material failed by cross-bundle cracking with some small amounts of fibre pullout.

After air oxidation for all three composites there was preferential attack of the matrix at the fibre/matrix interface. In the case of the KKarb material there was a change in flexural failure mode after oxidation from ply delamination to cross-bundle cracking; there was no change in failure mode for the other two composites after oxidation. There were substantial reductions in the mechanical properties for small amounts of oxidation with the KKarb material showing the greatest reduction.

The diverse nature of these composites leads to a large scatter of experimental results, this and the reduction in strength observed on oxidation mean that careful consideration must be given to the properties of these materials when designing components

CONTENTS

CHAPTER 1. INTRODUCTION

Carbon/carbon composites are used in aerospace applications, such as rocket nozzles and space shuttle wing leading edges, as well as other high temperature areas, e.g. aircraft brakes. The material is suited to these, and other, applications because of its high specific strength which is uniquely maintained to temperatures of up to 2000^{o}C, and its useful thermal characteristics, i.e. near zero coefficient of thermal expansion, good thermal shock resistance and good thermal conductivity. A range of composite properties can be achieved, where necessary for different applications, by using a variety of fibre and matrix precursors, fibre layups and temperatures and pressures during manufacture. These different processing conditions lead to various carbon forms ranging from graphite to non-graphitic which have varying strengths and interface characteristics. The interfaces, especially fibre/matrix interfaces, play an important role in the mechanical properties.

However the strength of carbon/carbon composites is severely reduced by oxidation at temperatures above about 450^{o}C and this is a major limitation since in most high temperature applications the composites are in contact with air. Although there has been much work published on the development of coatings to inhibit oxidation of commercial carbon/carbon composites, there

have been few studies of the effects of oxidation on the microstructure and strength of the uncoated composites. Such studies may lead to a better understanding of structure - property relationships for carbon/carbon composites undergoing oxidation, which in turn may lead to improvements in the oxidation resistance of commercial materials.

This thesis reports work performed on the effects of air oxidation on the strength, microstructure and fracture of carbon/carbon composites. Attempts are made to identify those microstructural features that are important for mechanical properties and fracture mechanisms when the material is subjected to oxidation in air.

The structure of the thesis is as follows: Chapter 2 reviews carbon/carbon composites, including manufacture, mechanical properties, oxidation and carbon fibres. Chapter 3 describes the experimental methods, Chapter 4 details the results which are discussed in Chapter 5. In Chapter 6 the conclusions are listed.

CHAPTER 2 LITERATURE SURVEY

This literature survey is intended to cover all aspects of carbon/carbon composites. The review concerns background information including the structure and properties of carbon fibres and graphite. The main part of the survey follows, and reviews carbon/carbon composites, with the major areas of manufacture, mechanical properties and oxidation being covered.

2.1 CARBON

Carbon has two main allotropes, namely diamond and graphite, although there is evidence for other types of solid carbon, Kroto (1990), Kasatochkin (1973). However, forms of carbon based on graphite are the most important for engineering purposes. Graphites consists of carbon atoms arranged in layers of regular hexagons. The layers are stacked parallel to one another in an ABAB stacking sequence, fig. 2.1, sometimes ABCABC stacking occurs where the C layer bears the same relationship to the B layer as B does to A. The carbon atoms within the layer planes are bonded together by strong covalent bonds, whereas the bonding between the layers are weak Van der Waals forces. The interlayer spacing of 3.35Å is a measure of the graphitic nature of a carbon as defects in the structure will increase this spacing.

The properties of graphite are highly anisotropic because of the strong bonds within the carbon layer planes and the weak bonds between the layer planes. The elastic modulus of a perfect single crystal of graphite parallel to the layer planes is 1021GPa however perpendicular to the layer planes is 37GPa; the shear modulus is 4GPa, Bacon(1973). Much graphite material is polycrystalline and contains stacking faults, dislocations, impurities and voids. These defects destroy the regularity of the layer planes, reducing the area of continuous hexagonal carbon layers. The strength is reduced by these defects giving typical values of 20MPa for tensile strength and 10GPa for elastic modulus, Brocklehurst (1972). Heat treatment can improve the structural integrity of graphite materials.

2.2 CARBON FIBRES

2.2.1 INTRODUCTION

Carbon fibres are one of many fibrës used as reinforcement in composite materials. The carbon layer planes are highly oriented with the fibres leading to strengths of 2-3 GPa, however structural defects occur and can limit the strength. Carbon fibres have diameters of between 5-10μm and they are manufactured from one of three precursors, either pitch,

polyacrylonitrile (PAN) or rayon. Rayon carbon fibres were the first to be used, but with advances in manufacturing techniques, pitch, and especially PAN, have become the more common fibres, Fitzer (1989a). Much experimental work is being carried out on vapour grown carbon fibres (VGCF), Tibbetts (1989), though they are not a feasible option for reinforcing materials at the moment.

2.2.2 MANUFACTURE

PAN

Carbon fibres made from PAN are manufactured by oxidising and stretching PAN fibres at temperatures of about 250^{o}C in air, fig 2.2. The nitrile groups react to form a hexagonal structure and the oxygen helps to cross link this structure, Dresselhaus et.al. (1988). Stretching is needed to align the structure and to stop shrinkage. The fibres are then carbonised by heating in an inert atmosphere at about 1000^{o}C. This expels the hydrogen and oxygen and most of the nitrogen leaving a hexagonal carbon structure. Fitzer(1989a) suggests 7% nitrogen remains until heat treatment at higher temperatures is applied. The carbon yield is about 50%.

PITCH

The pitch raw material used for carbon fibre production is normally mesophase pitch; although carbon fibres can be made from isotropic pitch, these will not be

reviewed here. The treatment of pitch to form suitable precursors is discussed by Edie (1989). Mesophase pitch is heated to 400°C, fig 2.3, where a liquid crystal spherical mesophase forms. As further heat is applied the mesophase spheres grow and coalesce to form a mesophase rich fluid from which mesophase fibres are extruded. The carbonisation temperature is above the melting point of the mesophase, therefore the mesophase fibres are heated in air to stabilise them, at temperatures of around 300°C. Carbonisation is then performed at about 800°C in an inert atmosphere, this produces a carbon fibre with about 70-80 % carbon yield.

RAYON

Carbon fibres are produced from rayon fibres by first heating them at 300°C-400°C, usually in an inert atmosphere, Bacon (1973). This expels water molecules, fig. 2.4. The fibres are carbonised by heating at about 1200°C in an inert atmosphere, leaving a porous carbon structure. The carbon yield is low at about 20%-30%. Hot stretching at high temperatures is required to produce carbon fibres with acceptable mechanical properties.

VAPOUR GROWN CARBON FIBRES

Vapour grown carbon fibres are formed by the pyrolytic deposition of carbon on a fine catalyst e.g. Fe, Ni, Cu. A hydrocarbon gas is passed over the catalyst and

at suitable temperatures of around 1000°C, Tibbetts (1989) it decomposes depositing carbon. Two stages of growth have been identified, a lengthening and a thickening stage, depending on the gas composition. The filaments have a shell/core structure, with a more graphitic and dense core, and can be graphitised at temperatures of 2300°C or more. Compared to PAN, pitch and rayon derived carbon fibres, vapour grown carbon fibres are easy to manufacture, but they can only be grown to lengths of about 10mm, with a large scatter of sizes being produced. Some very thin fibres are produced, which are potentially carcinogenic. These fibres will not be discussed further as they are not currently commercially used in carbon/carbon composites.

2.2.3 HEAT TREATMENT

After carbonisation all carbon fibres can be subjected to further heat treatment, this improves alignment of basal planes with the fibre axis and helps remove impurities. The rayon carbon fibres are often stretched when heat treated and the pitch carbon fibres graphitise when exposed to high temperatures. The temperature used for this heat treatment can determine the properties of the resultant fibres. Carbon fibres are classified into three types, Type I or high modulus, HM, type II or high strength, HS and type III or intermediate modulus, IM. HM fibres are formed by

heat treating at temperatures above 2500°C, fig 2.5, from PAN or pitch carbon fibres. HS fibres are formed by heat treatment between 1500°C and 2500°C from PAN or rayon carbon fibres. IM fibres are formed at lower heat treatment temperatures and are only used for lower specification composites. Heat treatments are all carried out in inert atmospheres because carbon fibres, like all carbon materials, oxidise easily when exposed to air at temperatures above 450°C.

2.2.4 MICROSTRUCTURE

Rayon carbon fibres have only partial alignment of the carbon layer planes along the fibre axis although this can be improved by stretching during heat treatment, Fitzer (1989a). Rayon carbon fibres will not graphitise when heated, however, Mochida et.al. (1985) suggest that catalysts, such as chromium, at temperatures above 1500°C can be used to graphitise these fibres.

Pitch derived carbon fibres have carbon layer planes that are well oriented along the fibre axis and this alignment is improved with graphitisation. The extrusion conditions, e.g. nozzle shape, stirring etc., influence the microstructure of pitch carbon fibres according to Dressellhaus et.al. (1988), producing either radial, random or circumferential orientation of the layer planes across the fibre diameter. White et. al. (1985) suggest that pitch fibres either have a

random core with radial crystallite orientation on the rim or are radially oriented across the whole cross section. Some fibres having both orientations causing local misorientations at regions where the cross section is changing from all radial to partially radial alignment.

Carbon fibres derived from PAN do not graphitise, but have good layer plane orientation with the fibre. For high modulus fibres the mean value of the angle of orientation of the layer planes with respect to the fibre axis is 10^{o} with a larger variation for lower modulus fibres, Smith (1970). PAN carbon fibres have a sheath/core structure which Watt and Johnson (1971) suggest is caused by more oxygen entering the outer part of the fibre than the centre, when the fibre is oxidised during manufacture. Much work has been done on the microstructure of PAN carbon fibres. The Johnson and Tyson (1969) model suggests that PAN carbon fibres are composed of structural units, called crystallites or fibrils, which are elongated or needle like, fig 2.6. They may be bonded together by a secondary carbon phase and are composed of graphite plates. The fibril blocks are stacked together at random angles, but not more than 10^{o} from the fibre axis. The more commonly used model is of PAN carbon fibre consisting of a ribbon like set of curved planes, which are cross linked enclosing many voids, fig 2.7.

2.2.5 MECHANICAL PROPERTIES

Carbon fibres have very anisotropic properties with strength of 3.5 GPa, according to Bennett and Johnson (1979), along fibre axis as covalently bonded carbon layer planes are roughly aligned with the fibre axis. Flaws within the fibres such as impurities and defects in the structure can reduce strength. Stretching during manufacture improves alignment and improves strength. Reynolds and Sharp (1974) proposed a mechanism for crack propagation, depicted by Johnson (1987), fig 2.8, suggesting that misoriented crystallites are locations of high shear stresses parallel to layer planes when fibres are loaded in tension. These stresses cause cracking across basal planes in the misoriented regions which can propagate along the basal planes and by stress transfer propagate across other layer planes. If Lc or La, i.e. the crystallite dimensions, are greater than a critical tensile crack size, the crack can propagate to failure. The fibre diameters also influence strength, smaller diameter lead to greater strength, fig 2.9.

2.3 CARBON/CARBON COMPOSITES

2.3.1 INTRODUCTION

Composite materials consist of one material reinforced with one or more other materials, or possibly the same material, in a different form, e.g. a bulk material can be reinforced with fibres or discrete particles. Fibre reinforcement produces a composite with high fracture toughness that the individual materials could not achieve. Carbon/carbon composites, CCC, consist of carbon fibres in a carbon or possibly graphitised carbon matrix; this matrix is derived from one or more of three precursors, i.e. pitch, resin or gaseous hydrocarbon.

The matrix type along with weave pattern and processing conditions can influence the mechanical properties as well as determine the fibre/matrix bonding and the porosity. Carbon/carbon composites have high strength and low density and, unlike carbon fibre reinforced plastics, they maintain their properties at elevated temperatures, fig 2.10, in inert atmospheres. The principal uses of carbon/carbon composites are for aircraft brakes, rocket nozzles and in the glass industry.

However carbon/carbon composites readily oxidise in air at temperatures above 450^{o}C, hence their use is limited

and coatings are needed for most high temperature applications. The manufacture, mechanical properties and oxidation of carbon/carbon composites are reviewed in sections 2.3.2, 2.3.3 and 2.3.4 respectively.

2.3.2 MANUFACTURE

a) PROCESS

The manufacture of carbon/carbon composites is a multi-stage process the general sequence of which is shown in fig 2.11. The carbon fibres are layered, woven or spun into the desired form, with a binder to form a prepreg. These prepregs are layered or joined to form the desired shape, then cured at 250^{o}C leaving a highly porous product.

To improve the density the matrix is impregnated with either liquid or vapour. The liquid impregnation uses either, pitch or resin, which is carbonised at about 1000^{o}C, Thomas and walker (1986), and in the case of pitch at pressures of around 100MPa, White and Sheaffer (1989). The vapour impregnation process is called Carbon Vapour Deposition, CVD, and involves passing a hydrocarbon gas over the prepreg and at suitable temperatures and pressures, e.g. 1100^{o}C and 50MPa which cause the hydrocarbon to degrade and deposits carbon, Savage (1988).

The process of impregnation/carbonisation is repeated several times until the required density is obtained. The whole component can then be heat treated to in excess of 2000^{o}C, to improve the structural integrity; heat treatment graphitises the CVD and pitch matrices and removes some impurities.

Chang and Okura (1986) have suggested a cheap, quick process for making a carbon/carbon composite, this uses fine pulverised coke in a binder laminated between layers of carbon fibres. The material is then hot pressed at about 49MPa and 600^{o}C. This leads to a carbon/carbon composite with different properties from those produced by the general method, but might have potential use in research and development applications. The resulting composite contains many pores and cracks.

b) PREPREGS AND FIBRE LAYUP

Carbon fibres are rather fragile to handle, therefore coated fibres are layed up; the coating is normally a resin formed by immersion of the fibres in a bath of resin prior to laying up. The resin on the layed up fibres is cured at about 200^{o}C and possibly under pressure. The result is a solid prepreg, which is easy to handle and assures the shape and alignment of the fibres are maintained.

Gill (1972) describes the manufacture of 1D prepregs in detail. Fibre bundles are immersed in a resin and lined up parallel and evenly spaced between two sheets of plastic. A roller rolls over the fibres at temperatures of about 150^{o}C to partially cure the resin, fig 2.12, forming a prepreg with uniform fibre distribution. These 1D prepregs can be layered, to produce thick flat samples, or can be moulded to a desired shape with a vacuum applied to remove solvents and excess air. An autoclave at 150^{o}C and 2.76MPa is then used to fully cure the resin and produce a final prepreg. A similar process is used for random chopped mats or woven mats, and 3D to 7D designs are cured in the same manner.

Carbon Fibres can be layed up in various ways, to reinforce the composite, i.e. 1D up to 7D or random chopped fibres, fig 2.13. 1D layup consists of fibres in the same direction, this leads to a composite with a low porosity and highly anisotropic properties

2D layup can be either layered or woven, fig 2.13. In the layered form plates of 1D prepregs are arranged at a variety of angles to each other usually 0^{o}±90^{o} or 0^{o}±45^{o} this leads to more isotropic properties in the plane of the fibres. Alternatively these fibres can be woven together. Bundles or tows of fibres are woven and these can contain a few hundred or, more commonly, a few thousand fibres. Various weave patterns can be used and these will affect the properties. The more tightly

woven the bundles, the more stress there will be in the weaves which may cause cracks and reduce the fibres reinforcing capabilities. Donnet and Bansal (1984) suggest that tightly woven plain weaves can only be used for flat samples, whereas 8 harness satin weaves, i.e. over one fibre bundle and under seven bundles, can be moulded into complex shapes. Weaving fibres is a delicate process as the fibres are very brittle. Gill (1972) suggests it is possible to weave oxidised PAN fibres rather than carbon fibres, as they are easier to handle and then carbonise after weaving.

The 3D layup leads to a higher porosity material with more isotropic properties and improved interlaminar shear strength compared with 1D and 2D layups. Further reinforcement along the diagonals is possible to give 4,5,6 or 7D composites. 3D composites can be manufactured with fibres in orthogonal directions; the simplest form is a layered 2D structure with fibres in the third direction, fig 2.13. Olry et. al. (1990) suggest a simple method for fabricating 3D composites, by using occasional weaves in the third direction to pin the 2D plies together. Oxidised PAN fibres were used.

3D materials can be made by filament winding to form cylindrical or spherical shapes. The filament winding technique requires a lathe to wind fibres onto a mandrel of the desired shape, e.g. a cone., the winding

arm of the lathe can be adjusted, along with the speed etc., to give helical, circumferential or cylindrical winding. Albugues and Grenie (1985) suggest a 3D helical form can be made by helically winding round metal rods, then the rods can be retracted and replaced with fibres. Radial 3D layups have to compensate for the space around the fibre tows increasing as the radius increases, this can be achieved by increasing the fibre size with distance or putting in extra fibres, fig 2.14.

Another arrangement of the carbon fibres is short random chopped fibres in which fibres of 10mm length or longer are randomly placed in a binder. This layup is easier to fabricate and leads to an isotropic composite, however the reinforcing capabilities are not as great as for the more normal 1-7D layup. On the other hand these layups are very flexible and can be moulded to complex shape prepregs.

c) IMPREGNATION AND CARBONISATION

The matrix material of the carbon/carbon composite is formed by impregnating the prepreg, with either pitch or resin, followed by carbonisation or by impregnation by carbon vapour deposition, CVD. The impregnation/carbonisation process is repeated many times, until the required density is achieved. Fig 2.15 shows how the density changes with impregnation and

carbonisation for a resin matrix precursor, Thomas and Walker (1986). Different precursors can be used on each impregnation/carbonisation step to give a composite with the desired properties.

RESIN

Thermo-setting resins, commonly phenolics and polyfurfuryl alcohol, are used as matrix precursors for carbon/carbon composites. They have a low viscosity and a good wetting, behaviour towards carbon which are desirable for infiltration. The impregnated composite is slowly heated in air to 200-250^{o}C, to polymerise the resin and produce a non melting, highly cross-linked and porous solid; the slow heating rate allows volatiles to escape. Carbonisation is achieved by heating in an inert atmosphere to 650-1000^{o}C.

The resultant carbon matrix is a hard, glassy carbon which is isotropic and non graphitising and contains many defects. The matrix is thought to consist of cross linked ribbons stacked in layers, called microfibrils, which are twisted and intertwined, fig. 2.16, Jenkins and Kawamura (1976), with only small regions of parallel graphitic ABAB stacking. The material is porous with low density.

The carbonisation process leads to high shrinkage due to weight loss when the polymer converts to carbon. Ward (1986) reports that phenolic resin has a linear

shrinkage of 20% on carbonisation. The carbon yield from most resins used as carbon/carbon composite matrix precursors is about 60%, with large amounts of volatiles given off, however increased pressure has no influence on carbon yield, according to Savage (1988).

There have been many reports of stress graphitisation of the resin carbon matrix in the region of the fibres. McAlister et.al. (1971) suggests that shrinkage stresses close to the fibres can cause glassy carbons to graphitise at temperatures above 2500^{o}C. Hishiyama et.al. (1974) found that for PAN carbon fibres in furfuryl alcohol carbon matrix stress graphitisation occurred at the fibre/matrix interface and expanded into the matrix. They suggest that induced graphitisation stresses are formed on carbonisation, not on curing, because of high volume shrinkage.

It has been suggested, Savage (1988), that resin matrices lead to weak fibre/matrix bonding of a mechanical keying type, however, carbon fibre surface treatment improves fibre/matrix adhesion because of chemical linkages.

PITCH

Mesophase pitch, which can be produced from, coal tar pitch or petroleum pitch can be used for the matrix of carbon/carbon composites. Pitch has good flow characteristics i.e. high wetting, low viscosity,

though not as good as for resins. White and Sheaffer (1989) found that wetting was independent of most factors i.e. fibre type, weave, pressure.

In a similar manner to pitch carbon fibres, the pitch is heated to 400^{o}C where mesophase spheres form then grow and coalesce. The composite is then heated in an inert atmosphere to 700-1000^{o}C under pressure, typically 100MPa. A slow heating rate is applied to allow low molecular weight substances to escape. The resultant matrix material has a coalesced mesophase microstructure and on graphitisation gives a highly oriented carbon.

At atmospheric pressure the carbon yield from pitch is only about 50%, though this increases as pressure increases. Hence a pressure of about 100MPa is often used to give a carbon yield between 80-90%. Higher pressure leads to a more coarse and isotropic microstructure, according to Savage (1988), possibly as volatiles are retained and the ability of the mesophase to coalesce is reduced, Forrest and Marsh (1982). It has been suggested Savage (1988) also that increased pressure reduces the temperature at which the mesophase forms.

Oxidation of the pitch can be used to prevent bloating, which can occur with high pressure carbonisation of pitch, White and Sheaffer (1989) used oxidation at

222^{o}C for 50-100 hrs before carbonisation to stabilise pitch and reduce bloating.

Pitch shrinks less than resin on carbonisation, therefore fewer impregnation/ carbonisation cycles are needed to give composite of required density. High densities can be achieved, with pitch derived matrix. Lewis and Bacon (1989) suggests low pressure pyrolysis of mesophase pitch leads to a matrix microstructure where carbon layer planes are oriented parallel to the fibre axis for several micrometers; high pressure pyrolysis leads to a microstructure where planes are oriented perpendicular to fibre axis for 0.5-1μm.

Additives can be used to hydrogenate and crosslink the pitch before decomposition. Ward (1986) suggests that Al_3Cl_5 can be added to promote carbon yield and small quantities of sulphur can give better translation of fibre strength without influencing the microstructure. Bashir (1988) states that sulphur is used as a cross linking agent for low weight molecular species, however too large a quantity of sulphur leads to excessive cross linking producing an isotropic carbon.

HOT ISOSTATIC PRESSURE IMPREGNATION and CARBONISATION

A method for impregnation and carbonisation sometimes used for large objects or woven, multi-dimensional, complex shapes is the hot isostatic impregnation carbonisation, HIPIC, process, Savage (1988). A prepreg

is infiltrated with molten pitch under vacuum, to fill the pores, and is placed in a thin walled stainless steel can which is then sealed. The temperature is increased gradually to 650-1000^{o}C and the pressure is increased to about 100MPa to carbonise the pitch. A constant pressure is applied around the specimen and stops any pitch escaping from the pores. After carbonisation the can is unsealed and the specimen is machined to remove excess products. The process can be repeated 4 or 5 times to achieve the required density. The final composite can be further heat treated.

CARBON VAPOUR DEPOSITION

The carbon vapour deposition, CVD, method is used to deposit the matrix carbon on the preform, using the isothermal, temperature gradient or pressure gradient methods, fig 2.17. A hydrocarbon gas usually methane or propane is passed with an inert gas carrier to help deposition, such as H_2 or He as they have good thermal conductivity, into a gas tight furnace under various pressure and temperature conditions. The vapour dehydrogenates and carbon is deposited on the substrate surfaces.

The isothermal method involves the substrate being heated by radiation so that the gas and substrate are at the same temperature around 1050-1100^{o}C and at reduced pressure e.g. 6KPa, which helps deposition to occur in the interior. In the thermal gradient method

the substrate is supported by an inductively heated mandril at about 1100^{o}C at atmospheric pressure and the hydrocarbon vapour is passed over at high gas flow rate. Carbon is deposited more readily on the interior of the substrate as it is the hottest part. In the pressure gradient method the gas is passed over the substrate at a higher pressure than the rest of the container forcing the gas to penetrate all of the interior of the sample. Because of the difficulty in processing, the gradient methods are used for one sample at a time, whereas the isothermal method can be used for many samples simultaneously.

One of the possible disadvantages of the CVD method is the nonuniformity of the carbon deposited e.g. the isothermal method can lead to surface deposition of carbon which blocks pores and reduces possible access to the interior. Deviney and O'Grady (1976) suggest occasional removal of the outer layer and slow infiltration to reduce blockages. The thermal gradient method results in more carbon deposited in the interior, which may be satisfactory for small specimens, but not for large ones, where turbulence can also be a problem. The temperatures and pressures used need fine adjustment to achieve a uniform carbon deposition.

The microstructure of the deposited carbon can take various forms namely isotropic, smooth or rough laminar

and columnar depending on the pressure and the temperature and the percentage of hydrocarbon in the gas fig 2.18, Oh and Lee (1988). The different microstructural forms have different crystalline sizes and densities, fig 2.19. Jortner (1986) found much porosity caused by carbon deposited on the surface sealing off the interior. Thermal mismatches on cooling can cause circumferential cracks in the matrix according to Oh et.al. (1988) and the carbon basal planes are aligned parallel to the fibre axis, Thomas and Walker (1986).

The gas concentration gradient is the driving force for the deposition process, however hydrogen generated migrates to the exterior, where the concentration is lower, and acts to suppress deposition. Marinkovic and Dimitrijevic (1986) have postulated many formulae for the deposition rate of carbon. They suggested that carbon deposition is a linear function of time, if considered for a short duration, and is related to the mass of the substrate. Dimitrijevic and Marinkovic (1987) used a formula based on initial open porosity and density of deposited carbon with some success, although they found the initial period did not fit the formula, possibly due to closed pores being formed. A model, based on empirical constants, was found to be more satisfactory especially when the rate of change of open and closed porosity was taken into account.

PORES AND CRACKS

Pores and cracks are important microstructural features because they act as pathways for gas or liquids to penetrate in oxidising environments. Strength is also reduced by pores and cracks as they have no load bearing capacity, and they influence fracture by facilitating further cracking. Pores and cracks in carbon/carbon composites, especially low density materials, can form an extensive network throughout the material.

Cracks are defined as having an aspect ratio of more than 5, all other voids are pores. Pores can be further classified by size, i.e. macro pores >50nm, meso pores between 2 and 50nm and micro pores <2nm, Sing et.al. (1985). There are two classes of pores, either closed or open, open pores have access to the surface of the material whereas closed pores are totally enclosed by the material.

Cracks in carbon/carbon composites can be formed either by shrinkage on carbonisation, these are permanent irreversible cracks, or by cooling from the final heat treatment temperature due to the differential thermal expansion coefficient of the matrix and fibre materials; these cracks, termed Mrozowski cracks, are reversible, i.e. they open and close on heating and cooling. Bradshaw and Vidoz (1978) suggest thermal, Mrozowski, cracking is reduced if char yield is

increased and that cracks widened not lengthened on carbonisation. Pores are formed from either bubbles of gases evolved during manufacture or from regions blocked by impregnation or from shrinkage on carbonisation. Rand and McEnaney (1985) suggest the extent of porosity is different in graphitic and non graphitic materials.

Cracks may occur round fibre/matrix interfaces if the bonding is not strong, these may be either Mrozowski or shrinkage cracks. Manocha and Bahl (1988) suggest that ungraphitised fibres have a higher surface energy leading to better fibre/matrix adhesion and less shrinkage gaps than for graphitised carbon fibres. Pitch, resin and CVD matrices have shrinkage and thermal cracks, sometimes regular stress relief cracking is observed. Bradshaw et.al. (1977) suggest that graphitic fillers can be added to liquid impregnation precursors to reduce shrinkage on carbonisation. Resin carbon matrices are solid before and after carbonisation and have large porosity caused by the volatiles evolved on curing which can not escape. Pitch, however, changes from a liquid to a solid on carbonisation allowing most of the gas time to escape through the fluid. CVD matrices often have large pores due to regions being blocked by deposited carbon. Some weaves are inherently porous, e.g. 3D, where the space between the fibre tows is large and difficult to fill totally.

d) HEAT TREATMENT

The fully impregnated/carbonised composite can be subjected to further heat treatment at temperatures in excess of 2000^{o}C . This will improve the structural integrity of the composite, i.e. remove voids, defects and will also remove some impurities. Pitch carbon matrices and CVD matrices readily graphitise at elevated temperatures, however resin carbon matrices do not. The density of pitch carbon matrices are improved up to 2000^{o}C with heat treatment, fig 2.20, whereas the density of the resin matrix initially improves then decreases. A greater increase in density is achieved if heat treatment is applied between each impregnation/carbonisation cycle according to Manocha et.al. (1989). If graphitised fibres are used, rather than carbonised fibres the structure will be improved, as pores and cracks, which would otherwise have been blocked, will be exposed to further impregnation.

e) APPLICATIONS

Carbon/carbon composites find many fields of applications, in medicine, in industry, in aerospace and as brake linings. In medical surgery carbon/carbon composites are used for dental implants, bone implants, heart valves and hip joints, e.g. Jenkins and Carvalho (1977). Hip joints require the material to be biocompatable and not break up during surgery, and, being a ball and socket joint, the material used must

have a low coefficient of friction, low wear, low density and ability to resist high loads. Carbon/carbon composites meet all these requirements according to Heuttner and Keuscher (1983), however silicon carbide/carbon composites have better wear resistance and are used in the joints. Hip joints have been manufactured to meet specific local stress requirements using a variety of different fibre layups at different points of the joint, Fitzer (1987). However carbon/carbon composites are very expensive and cheaper carbon fibre reinforced plastic and metals are more commonly used in these applications.

High temperature fastners e.g. nuts and bolts, can be made from carbon/carbon composites as the material is easily machinable, has zero coefficient of thermal expansion, high stiffness and strength at high temperatures, chemical inertness and thermal shock resistance, Heuttner (1989). 3D cylindrically wound carbon/carbon composites are used for nuts and bolts according to Heuttner (1989), where other material could not be used as they do not meet the desired specifications. In glass making, dies, and furnaces carbon/carbon composites are used, Fitzer (1987). The main requirements are for the material to be non toxic, non melting, corrosion resistant, thermal shock resistant and have a low thermal expansion coefficient. As no stress requirements need to be met 2D plates, or

moulded shapes for dies, of low density carbon/carbon composites are used, Weiss (1990).

2D cylindrically woven carbon/carbon composites often with CVD matrix impregnated to a high density are used as disc brakes for aircraft and racing cars, Jenkins and Kawamura (1976). The material is non-toxic, unlike the asbestos it replaces, and has suitable properties of wear resistance, self lubrication, low density, low coefficient of thermal expansion and high strength and stiffness at high temperatures, Weiss (1990).

The space shuttle uses carbon/carbon composites in many parts. The wing leading edge and nose cone make use of the low density, zero thermal expansion coefficient properties of moulded 2D or 3D materials, which readily conduct heat away from the region. The rocket nozzles and nozzles of the exhaust are made of 3D woven preforms, Fitzer (1987).

There are however two disadvantages to the use of carbon/carbon composites, they oxidise easily and are expensive. Many of the high temperature high strength applications use materials with coatings or inhibitors to reduce destruction of the material by oxidation. The high temperatures and number of impregnation cycles required in manufacture lead to a costly material, hence most applications have been found in the military aerospace areas. Until these two problems are resolved carbon/carbon composites can not fully realise their

potential as a high temperature high specific strength composite.

2.3.3 MECHANICAL PROPERTIES

As a result of the variety of manufacturing conditions and precursor materials carbon/carbon composites have a large range of mechanical properties: for example flexural strengths can range from 50-800MPa, table 2.1 Some models that have been used to calculate the properties of these composites are described in section a) and the effect of various manufacturing conditions on the mechanical properties are detailed in section b). Carbon/carbon composites can fail in several modes from brittle fracture with flat failure surfaces to tough fracture with extensive fibre pullout, these failure modes are described in section c).

a) THEORETICAL CALCULATIONS OF MECHANICAL PROPERTIES

The modulus of a unidirectional composite, E_C, can be estimated from the rule of mixtures on the assumption that the phases are well bonded and that the fibres and matrix although of similar moduli, have similar Poisson's ratios. The rule of mixtures derived from

conditions of constant strain in fibres and matrix, gives:

$$E_c = E_m V_m + E_f V_f,$$

where E_c is the Young's modulus of the composite, E_m, E_f are the moduli of the matrix and the fibre, and V_m, V_f are the volume fractions of the matrix and the fibre.

The rule of mixtures can also be used to estimate the strength of a unidirectional composite. The stress on the composite is distributed in proportion to the relative quantities of the phases and their elastic moduli, so that if there is good bonding the fibres and matrix both fracture at the same strain:

$$\sigma_c = \sigma_f V_f + \sigma_m V_m.$$

The rule of mixtures equations can only give an approximation of strength values because factors such as the influences of porosity are not taken into account. Many carbon/carbon composites are made from woven materials with complex stress patterns that are outside the scope of the rule of mixtures and more complicated analyses are needed to evaluate the properties theoretically.

However, other empirical equations have been proposed for the calculation of the properties of carbon/carbon

composites. To take account of porosity Dimitrijevic and Kaludjerovic (1986) suggested

$$X = X_o \ e^{-bP}$$

where P is porosity, b is a constant, X_o is the nominal value of mechanical property for zero porosity and X is the mechanical property. This equation has also been found to describe the effect of porosity on mechanical properties of two nuclear graphites, Pickup et al (1986). For a 1D/CVD carbon/carbon composite with non-surface-treated fibres, Marinkovic and Dimitrijevic (1985) found that the effect of porosity on mechanical properties fitted the following equation

$$Y = a \ d^b$$

where Y is the mechanical property, d is apparent density and a, b are constants for one set of conditions and composite types. However this equation was not successful when surface treated fibres were used.

The strength and modulus of composites are important properties. However it is also useful to know the fracture energy, i.e. how much energy is required to propagate a crack to failure, and the fracture toughness, which is a measure of the ability of the material to resist crack propagation. The fracture

energy of an isotropic, homogeneous material may be calculated from the Griffith equation,

$$\sigma_f = \sqrt{(2\ E\ \gamma\ /\ c\ \pi)} \quad \ldots\ldots\ldots (1)$$

where c is the critical crack length and γ is the fracture energy. The equation is based on energy balance considerations i.e. the potential energy in the material is equated to the energy required to create two new surfaces when the crack extends. The fracture energy is a material constant. Equation (1) assumes that the material is isotropic, homogeneous and deforms elastically. As a consequence the applicability of the Griffith equation to fracture of composites has been questioned, Sakai et al (1991). The fracture toughness is calculated from

$$K = \sigma\ Y\ \sqrt{(\pi\ c)} \quad \ldots\ldots\ldots (2)$$

where Y is a geometrical factor. As with surface energy, the fracture toughness, K, is a material property. The material is assumed to be isotropic, homogeneous and to deform elastically for the toughness calculations. Therefore equation (2) is subjected to the same uncertanities as equation (1) when applied to the fracture of composites.

b) FACTORS AFFECTING MECHANICAL PROPERTIES

The mechanical properties of carbon/carbon composites are influenced by many factors including fibre layup and volume fraction of the fibre bundles and by the microstructure, i.e. fibre type, cloth weave, matrix type, fibre/matrix adhesion and heat-treatment temperature. The fibre layup characteristics, i.e. 1D, 2D or 3D etc., also influence the properties. 1D carbon/carbon composites are almost twice as strong as 2D woven carbon/carbon composite, fig 2.21, but only in the direction of the fibres, since the strength in the other directions is very low. 3D composites have a more isotropic strength.

For 2D composites there are differences in strength between layered and woven materials and the strength can also vary with different weave patterns. Close weaves, such as plain weaves, are weaker than open weaves such as harness satin weaves, fig 2.22, as there are more fibre bundle cross-over points in close weaves. High stresses occur at bundle cross-over sites and cause microcracks which may be the initiation sites for fracture cracks. Manocha and Bahl (1988) found that plain weave carbon/carbon composites have lower flexural strengths than 8-harness satin weave materials, fig 2.23.

The fibre volume fraction influences properties since a higher volume fraction means more fibres are available to support the applied stresses. However, Chang and Okura (1986) found that there was an optimum fibre volume fraction, between about 0.2 and 0.4, with some variation for different types of composites, where the flexural strength and modulus were a maximum, fig 2.24. However, after an initial rise to 0.1 fibre volume fraction the density remained constant in these materials.

Fibre and matrix precursors lead to carbon materials with different properties. For example, PAN fibres can attain higher strengths than rayon or pitch carbon fibres, table 2.2. Different combinations of fibre and matrix will therefore lead to different composite properties. Fitzer et al (1980a) suggest that pitch-derived matrices only supplement the elastic modulus of a carbon/carbon composite if the graphitic layer planes are oriented tangentially or axially with respect to the fibres, fig 2.25. Bradshaw et al (1977) found that for a composite made from random chopped PAN carbon fibres and resin carbon matrix the flexural strength and strain to failure increased with matrix volume fraction up to 0.6.

CVD matrices have a variety of structural forms, e.g. isotropic or columnar, which have different properties

resulting in composites with different properties. Oh and Lee (1988) found that CVD deposition temperature affects the properties because different microstructures are formed. They found that isotropic and columnar matrices gave lower flexural strengths and moduli than did transitional microstructures. They attributed this to the lower density of the isotropic material and to the presence of large quantities of microcracks in the columnar material.

Fibre/matrix interfaces are important in determining the mechanical properties. According to classical composite theory because strong adherence leads to brittle fracture and lower strength, while weaker fibre/matrix bonding will facilitate delamination which will absorb energy and give improved toughness. Oh et al (1988) cooled two carbon/carbon composites, one slowly and the other quickly. They found that the tensile strength and strain to failure of the slowly cooled composite were greater than for the rapidly cooled material, although their elastic moduli were similar. The slow-cooled material had a terraced fracture path, caused by deviation of the crack path a result of the presence of to pre-existing microcracks, whereas the rapidly cooled material had a flat fracture surface, indicates that microcracks did not form during cooling. Surface treated carbon fibres produce carbon/carbon composites with higher interlaminar shear strength because of improved fibre/matrix adhesion,

according to Ismail and Vangness (1988). Kowbel and Shan (1990) suggest that the strength of a carbon/carbon composite can be tailored by fibre surface oxidation treatment followed by argon plasma etching. Fibre oxidation treatment causes surface crenellations which aid mechanical bonding and reduce composite strength. Argon plasma etching of the fibres reduces fibre surface damage and improves the strength of the composite. Sheaffer (1989), however, suggests that the use of different fibres leads to different fibre/matrix interface characteristics as a result of different bonding mechanisms. PAN based carbon fibres have non frictional bonding, whereas pitch based carbon fibres have high frictional bonding.

Pores and cracks have no load bearing capacity and lead to a reduction in mechanical properties. Many different shapes, sizes and distributions of cracks and pores can occur which will have different influences on the strength and modulus of composites. The stresses at pores and cracks are often very high, especially if the aspect ratio of the void is high. Microcracks can often occur in these high stress regions and hence these voids help to reduce strength and can initiate fracture cracks.

Mechanical properties are affected by the final heat treatment temperature of the composite as this improves the structural integrity of the matrix, Chang and Okura

(1986) show, fig 2.26, how the flexural strength first falls with heat-treatment temperature and then reaches a plateau after about 800^{o}C. The strength of carbon/carbon composites is also dependent on test temperature. Fitzer and Terwiesch (1972), found that the flexural strength of their carbon/carbon composite fell very slightly as the test temperature was increased to 1000^{o}C then it increased again at higher temperatures, fig 2.27. On the other hand Thomas and Walker (1986) found that the modulus decreased substantially beyond a test temperature of 1000^{o}C where the flexural strength was a maximum, fig 2.28.

c) FAILURE MECHANISMS

Carbon/carbon composites can fail in a variety of ways since they are pre-cracked bodies with high levels of residual stresses. Consequently crack propagation to failure is complicated. One of the main influences on crack propagation is fibre/matrix adhesion which can result either from mechanical or chemical bonding. Chemical bonding involves adsorption of matrix molecules on the surface of the fibre and mechanical bonding occurs where physical features of the fibre and matrix interlock. When a force is applied to the composite a shear stress develops along the fibre/matrix interface which enables stress transfer between fibre and matrix so that both parts of the composite react to the applied force.

The effect of the interfacial bond may be seen by considering the situation where the tip of a crack growing in the material approaches the fibre/matrix interface. If the adhesion is poor the fibre may become debonded from the matrix, and this debonding absorbs energy and so inhibits crack growth. Conversely, if the fibre/matrix adhesion is strong the crack may propagate straight across the fibre and the load supported by the fibre must then be transferred to the matrix. The tensile load supported by the fibres builds up again as the distance from the fracture increases, and, at locations remote from the break, the fibre will still support the load. The composite finally fails, either as a result of a gradual increase in the number of broken fibres, to the point where catastrophic failure of the whole composite occurs, which would result in a flat fracture surface, or as a result of multiple debonding with the crack running through the matrix until the matrix can support no more load. This process is called "dusting out". Another mechanism which can hinder crack propagation by absorbing energy is delamination of the layers or plies of the composite.

Ideally the composite should make use of all the available strength of the fibres, but to achieve this the strain to failure of the composite must equal the strain to failure of the fibre. The matrix may fail at a lower strain than the fibre, however, causing the

composite to fail before the full fibre strength is utilised. Fitzer et al (1980b) found that for carbon/carbon composites reinforced with type I fibres the composite failure strain was approximately equal to the fibre failure strain, fig 2.29, leading to a "dusting out" fracture with no matrix at the fracture surface. For a composite with type II fibres failure occurred at a slightly higher strain than the matrix failure strain, leading to some fibre pull-out on the fracture surface. Composites which contained surface treated type II fibres failed at a lower strain than the normal failure strain of either the matrix or the fibre and resulted in a flat fracture surface.

Stress/strain curves for carbon/carbon composites show evidence of very strong fibre/matrix adhesion, fig 2.30, curve E. As the stress increases the material deforms until a limit is reached when it fails in a brittle manner. In curve C, fig 2.30, the stress/strain curve shows evidence of poor adhesion, leading to a tougher material. There is much fibre/matrix debonding which absorbs energy as the crack propagates through the material.

Carbon/carbon composites often have stress/strain curves which contain a mixture of types of failure. Kowbel and Shan(1990) found that surface oxidation treatment of carbon fibres led to a catastrophic mode of failure with flat fracture surfaces and occasional

fibre pullout. Subsequent argon plasma etching of the surface treated fibres introduced a progressive mode of failure, fig 2.30, with much fibre pullout. Fracture is not only influenced by fibre/matrix adhesion. Pores and cracks will also affect the crack mode and path and some regions may be matrix-rich or fibre-rich with no interfaces. The nonlinear part of the stress/strain curve before failure is caused by subcritical cracking which reduces the strength but does not lead to failure.

Many types of cracking can occur in composites, but some depend on the test involved, e.g. shear cracking, and weak interply strength may lead to delamination of the whole ply which is different from fibre/matrix debonding. The toughness or mode of failure of carbon/carbon composites may be influenced by many factors, such as heat-treatment temperature, and these may have resultant effects on the fibre/matrix interface. For example, Oh and Lee (1989) found that as the CVD deposition temperature increased the mode of failure changed from tough behaviour, with fibre pull out at high temperature, to delaminating flat fracture surfaces at low temperature. They suggest that mechanical locking at the fibre/matrix interface is stronger at low temperatures because of better infiltration. Kevans et al (1989) also found that the nature of the fibre/matrix interface changes with CVD deposition temperature.

Williams and Impresca (1975) found that the fibre type influenced the fracture for a composite with a coal tar pitch carbon matrix heat-treated to 3000°C. In tensile tests pitch carbon fibres caused no fibre pull out, whereas PAN carbon fibres resulted in long random distribution of fibre pullout and rayon carbon fibres caused short uniform pullout. They concluded that PAN carbon fibres increase toughness more than rayon and pitch. Manocha et al (1988) suggest that fracture behaviour of graphitised composites depends on the shear properties of the graphitic matrix.

2.3.4. OXIDATION

a) INTRODUCTION

Carbon/carbon composites readily oxidise in air at temperatures above about 450°C with the following reactions occurring,

$$C + O_2 = CO_2$$
$$2C + O_2 = 2CO$$
$$O_2 + 2CO = 2CO_2,$$

so forming either carbon monoxide or carbon dioxide. The rate of oxidation, i.e. the rate of weight loss, is dependant on the temperature. At low temperatures oxidation occurs slowly, then around 750°C there is a

rapid increase in the rate of weight loss until around 900°C when the oxidation rate approaches a plateau.

An Arrhenius plot of oxidation of a porous carbon, fig 2.31, shows three regions of oxidation, commonly referred to as zones I, II and III. At low temperatures, i.e. zone I, the oxidation rate is chemically controlled, that is, it is determined by chemical surface reactions of the composite. Highly active sites, such as catalysts and structural defects, influence the oxidation rate in this regime and the attack is highly selective of the microstructure. Zone I oxidation can penetrate through the thickness of the material.

As the temperature is increased beyond about 800°C the oxidation moves to zone II, where the rate controlling step is in-pore diffusion. A boundary layer of reaction products, i.e. CO and CO_2, is formed, at higher temperatures above 1000°C, on the surface of the specimen and the rate at which oxygen can penetrate this layer determines the oxidation rate in zone III. Attack in this regime is not selective and is confined to surface oxidation.

Oxidation can also be achieved by chemical etching with, for example, chromic acid at 100°C. The oxidation is less rapid than for air oxidation but leads to etching because the acid selectively attacks parts of

the microstructure. The following sections discuss only gaseous oxidation of carbon with the kinetics of oxidation reviewed in section b). The effects of oxidation on the microstructure are reviewed in section c), effects of catalysts in section d), effects of oxidation on mechanical properties in section e) and methods of reducing the effects of oxidation in section f).

b) MECHANISMS AND KINETICS

The carbon oxidation process involves five steps, namely, diffusion of reactant gases to the carbon surface, adsorption of gases into the solid, chemical reaction with carbon, desorption of gaseous products of the reaction and diffusion of product gases away from the surface. The rate at which oxidation occurs is determined by the rate determining step, (RDS) i.e. the slowest step. The RDS depends on many factors e.g. temperature, pressure, porosity, active site concentration and catalysts. The rate of reaction may be complex, i.e., surface oxidation may be controlled by chemical reaction with interior oxidation being controlled by diffusion. This sort of mixed mode can occur in zone II oxidation, where the RDS is in-pore diffusion. The reactivity, i.e. reaction rate, of oxidation is defined by

$$R = - 1/w_o \; dw/dt \ldots\ldots\ldots\ldots (1)$$

where w_o is the initial weight of the specimen. This equation can also be expressed as an Arrhenius equation to give an activation energy. Dacic and Marinkovic (1986) found agreement with equation (1) up to 70% burn off. At higher burn off they used

$$\Delta w \; / \; w_o = 1 - e^{-k_3 t},$$

where k_3 is a constant, to calculate the weight loss with time at 440-530^{o}C for a unidirectional composite derived from CVD and phenolic resin and PAN carbon fibres.

c) EFFECTS OF OXIDATION ON MICROSTRUCTURE OF CARBON/CARBON COMPOSITES

In zone I oxidation occurs more readily at positions in the microstructure where there are weak bonds or high stresses called active sites. Pores and cracks influence the reactivity of the composite as they increase the surface area exposed to potential oxidative attack. The active surface area of the composite increases greatly with only a small percentage burnoff as cracks and pores are enlarged and further regions of the interior are exposed.

The fibre/matrix interface is commonly attacked preferentially as it is often cracked, providing channels for gases, and there are stressed matrix regions in this area. Goto et al (1986) found that for oxidation between 650-800^{o}C of a carbon fibre/glassy carbon composite the fibre/matrix interface was oxidised first, then the graphitic matrix, then the optically isotropic matrix which they attributed to the structural defects and stress concentrations.

At low temperatures oxidation will be uniform throughout the composite with reduction in density but not necessarily volume. Zhao et al (1985) reported uniform oxidation throughout a composite made from random chopped PAN carbon fibres in a matrix of CVD carbon and phenol furfuryl carbon, at 873K. Ehrburger et al (1981b) found, for random chopped PAN fibres in a CVD matrix, the bulk volume changed after 20% weight loss with a CVD matrix heated treated to 3300K but found an immediate volume change when heat treatment of 2870K was used, because of the larger amount of open porosity in the composite with higher heat treatment temperature.

Heat treatment can cause structural changes in carbon/carbon composites which can influence where selective attack occurs in the microstructure, and can also alter the temperature at which oxidation starts.

Bahl et al (1989) found when composites were heat treated to 2700°C the initial temperature of oxidation was 150-200°C higher than when heat treated to 1000°C. For heat treatment at 1100°C Lahaye et al (1989) found the matrix, not the fibre or the interface, oxidised preferentially for a 3D carbon/carbon composite made with PAN carbon fibres and a CVD matrix. However with a heat treatment temperature of 2000°C oxidation of both fibre and matrix at fibre/matrix interface occurred preferentially.

The temperature of oxidation has an influence on what features of the microstructure are attacked. In zones II and III there is more surface attack of all of the microstructure, unlike the selective attack throughout the thickness of the material which is found in zone I. Markovic et al (1981) reported for PAN carbon fibres in a phenol formaldehyde matrix, with both fibre and matrix carbonised at the same time, that below 573K the fibre and sheath were oxidised preferentially. Below 973K the matrix and the fibre but not the sheath were oxidised preferentially and below 1173K the matrix and the interface and the surface were etched.

d) EFFECTS OF CATALYSTS

All carbon/carbon composites have small amounts of impurities, for example Fe 100ppm, Ca 100ppm and Si 200ppm found by Jones et al (1986). Metallic impurities

can act as catalysts in the carbon oxidation reaction, not only affecting the rate of oxidation, but also lowering the temperature at which oxidation first occurs. It is well known that transition metals, such as Fe, Co, Ni, promote the carbon oxidation reaction. For example fig 2.32 shows how an increased content of iron can increase the burn off rate for oxidation of a graphite. The activity of catalysts varies with Ni being more reactive than Co than Fe at around 700^{o}C, however this order is reversed at higher temperatures, Walker(1968). Co reduces the ignition temperature more significantly than Ni or Fe.

Heat treatment can reduce catalytic activity as more impurities are expelled. The number of catalysts on the surface increases with burn off, however their catalytic effect depends on the concentration of the catalyst, the state of the catalyst and the catalyst carbon contact area. Mobility of the catalyst is also an important factor as an immobile catalyst will soon lose contact with the edges of the carbon basal planes and will no longer act as a catalyst. Catalysts become less reactive with time, but some can have their activity restored. For example Fe catalysts lose their activity as they are progressively oxidised to FeO in CO gas Catalytic activity can be restored by reduction of FeO to Fe., Thomas (1965). The concentration of the catalyst is important; Walker et al (1968) found saturation amounts of 130ppm for Ba and 150ppm for Na,

beyond which there was no further effect on the $C-CO_2$ reaction. No saturation point was found in the case of Fe catalysis of the C-CO reaction.

e) EFFECTS OF OXIDATION ON MECHANICAL PROPERTIES OF CARBON/CARBON COMPOSITES

Oxidation has a devastating effect on the mechanical properties of carbon/carbon composites. Cracks and pores are enlarged and inner regions are oxidised destroying substantial parts of the structure of the composite. Zhao et al (1985), fig 2.33, found that 20 % burnoff produced a 75% reduction in Young's modulus and a 64% reduction in flexural strength, for random chopped PAN fibres in a phenolic furfuryl resin and CVD matrix, at 873K. This is similar to the effects of oxidation on graphite as found by Pickup et al (1986) and others.

f) OXIDATION CONTROL

To realise fully the potential of carbon/carbon composites, some form of oxidation inhibitor needs to be used to protect the material from oxidative attack. Carbon/carbon composites can be protected by either coating the whole sample, to provide a diffusion barrier, or by doping the composite with impurities that will slow down the reaction. Much research has been and is being carried out in this area and it has

emerged that different inhibitor schemes are needed for different temperatures and durations.

For low temperature applications, below 1000^{o}C, doping with inhibitors is most useful according to Ehrburger (1989), whereas at high temperatures coatings are more helpful. Additives, such as phosphorous and boron and some of their compounds, slow down the reaction rate of carbon with oxygen. These inhibitors can easily be introduced during manufacture. McKee et al (1984) reports 3wt% boron oxide impregnated into graphite reduced the oxidation resistance by a factor of about 5 at 800^{o}C.

Coatings for higher temperatures act as diffusion barriers and hence need to be impermeable to oxygen. Silicon carbide, SiC, is often used to coat carbon/carbon composites either by reacting silicon with the surface of the carbon or by coating using techniques such as sol-gel or CVD; in all cases the SiC is formed at high temperatures. Silicon carbide is useful as a diffusion barrier and has a low density, however, because of thermal mismatches on cooling, cracks form in the coating which render it useless as even very small cracks can allow rapid oxygen diffusion, Luthra (1988).

Many glassy coatings, such as boron oxide, have been used with SiC to fill in the thermal mismatch cracks,

as they melt into the cracks at suitable temperatures. The SiC/B_2O_3 combination is only useful up to 800-1200^oC, depending on the duration of oxidation, according to Luthra (1988), as the boron oxide volatilises. All high temperature coatings must be thermally suitable as the coating and the composite may experience many high temperature cycles and the coatings must not interfere with the strength or weight of the components.

2.4 OBJECTIVES

The literature survey shows that there have been few published works on the effects of oxidation on the microstructure and mechanical properties of carbon/carbon composites. Many of the applications of these materials are at high temperatures in oxidising environments, therefore a thorough understanding of how oxidation affects these composites is required in order for suitable components to be designed.

The aims of this work were to identify microstructural features that are important for mechanical properties and fracture mechanisms when the material is subjected to air oxidation. Two different composites were used for microstructural and mechanical experiments before and after oxidation; a small amount of work was preformed on a third material. The mechanical properties investigated were: elastic modulus, flexural

strength, impact energy and tensile strength. Fracture mechanisms and microstructural changes, at various stages of oxidation, were monitored using microscopy.

The structure of the rest of the thesis is as follows: Chapter 3 describes the experimental details of the microstructural and mechanical tests performed. The results of experimental work on the unoxidised and oxidised materials are detailed in Chapter 4 and interpreted and discussed in Chapter 5. In Chapter 6 the conclusions reached are listed and areas of useful continuation of this work are identified.

CHAPTER 3 EXPERIMENTAL DETAILS

The research involved familiarisation and characterisation of a variety of carbon/carbon composites using microscopy. Further work was performed on two materials, with limited work on a third material investigating the microstructure and mechanical properties, before and after oxidation .

3.1 MICROSCOPY

Both optical and scanning electron microscopy were used in this research to look at general microstructures, oxidised microstructures and fracture surfaces.

3.1.1 OPTICAL MICROSCOPY

Bulk microstructures and fractured impact and tensile specimens were examined by eye and using a Wild Heebrugg M3Z optical microscope used at x6.5 magnification. No specimen preparation was necessary

The microstructure of specimens, before and after oxidation, and impact and flexural fracture surfaces were examined under higher magnification with polished samples.

Specimens were cut using a diamond saw, mounted in Struers Epofix HQ epoxy resin and left to cure over

night. A vacuum was applied to the uncured mounted specimen to remove air and fill pores. The cured specimens were polished using a Pedamax-2 Planar-2 automatic plane polishing machine using the routine outlined in table 3.1.

Polished samples were examined using a Zeiss MC63 optical microscope capable of magnifying x80. The matrix and fibre have similar reflectivity making it difficult to distinguish between them, to help with this polarised light microscopy was used for microstructural characterisation.

The Zeiss MC63 microscope was used for polarised light microscopy with cross polarised light sources and a full wave quartz plate, this technique highlights regions with strong basal plane orientation. The angle the basal plane makes with the optical system will determine the colour seen, when the basal plane is parallel to the optical system purple will be the colour seen. If the basal planes are at an angle to the optical system they will be blue or yellow, on 90^{o} rotation a blue region will change to a yellow region, fig 3.1.

3.1.2 SCANNING ELECTRON MICROSCOPY

For more detailed examination of the unoxidised and oxidised microstructures and some fracture surfaces

scanning electron microscopy was used. A Joel JSM T330 scanning microscope was used at magnification from x30 to x3000. Carbon is reasonably conductive, therefore no gold coating or other sample preparation was needed.

3.2. MICROSTRUCTURE

Manufacturers of carbon/carbon composites supply little or no detail of their products, table 3.2. Therefore it was necessary to study samples of several materials to characterise the microstructures in order to identify features which may be important in oxidation or fracture

3.2.1. MATERIALS

Two carbon/carbon composite materials were used for detailed studies for both mechanical and oxidation experiments, namely KKarb Type A and SIGRI CC1501G.

KKarb Type A, fig 3.2, is a commercially produced material with rayon carbon fibres and a blended pitch and resin carbon matrix. It is a 2D woven material with a 5 harness satin weave, table 3.3 . Specimens were cut in the plane of the weave and in the warp direction, fig 3.2, although some data is available for specimens in the fill direction.

SIGRI CC1501G, fig 3.3, is also a commercially available material which has PAN carbon fibres and a resin based carbon matrix. The material has a 2D hopsack weave and specimens were cut in the plane of the weave, the fill and warp directions are identical for hopsack weaves. The material is very different from KKarb, i.e. it has different matrix and fibre precursors, different weave patterns and different fibre bundle sizes and so provides a good comparison.

The FMI material, which has rayon carbon fibres in a plain weave and a blended resin and pitch matrix, was used for some mechanical tests, microstructural examination and oxidised tests, fig 3.4.

3.2.2 CHARACTERISATION

Fibre types were identified using optical microscopy and SEM as the cross sections of the fibres are different. Pitch carbon fibres are round, PAN fibres are almost round and Rayon fibres have an irregular cross section, although some special shape pitch and PAN fibres are also available.

Matrix types were identified by using polarised light optical microscopy. Resin matrices are optically isotropic and appear purple and uniform under polarised light, Pitch and graphitic matrices appear speckled blue, yellow and purple, as the crystallites are not

very large, and are oriented at different directions. CVD matrices have a spoke like appearance, the spokes are normally oriented at different angles giving a maltese cross structure of blue and yellow under polarised light, fig 3.5.

The weave patterns were distinguished by examination of the bulk microstructures using optical microscopy and the bundle size per tow was estimated by counting the number of fibres in each bundle

Fibre volume fraction was determined using the linear intersection technique i.e. photographs of the sides of samples were taken on the Zeiss optical microscope and a line was drawn in a random direction. The fibre volume fraction was calculated by measuring the distance of the line which the fibre ends are covering relative to the total length of the line. This was repeated ten times on one photograph to give an average estimate.

The linear intersection method was also used to estimate porosity. There are many flaws with this technique, i.e. only one photograph per specimen was used and photographs are only two dimensional images of three dimensional objects, though this method is useful as a rough guide. Therefore changes in porosity with oxidation were also measured using Image Analysis.

A Joyce Loebl magiscan image analyser with a Leitz microscope, on a x32 magnification was used. The technique involves high contrast images of mounted polished specimens being digitised by a computer from a microscope image passed through a camera. The required parameters of the bright areas, e.g. length, area, are calculated, recorded and analysed by the computer. There is large contrast between the composite and pores, however there is little contrast between fibres and matrix hence this technique is more useful for porosity calculations.

Bulk density for unoxidised and oxidised samples was calculated from the weight and physical dimensions of specimens in air.

3.3. MECHANICAL TESTING

Specimens for the various mechanical experiments were cut with a diamond saw to the relevant dimensions. The dimensions used were to some extent determined by the materials available, as the Sigri and KKarb carbon/carbon composites were supplied in 2.9mm and 3.2mm thick plates respectively. This corresponds to about 7 plies for the KKarb material and about 10 plies for the Sigri material and about 20 plies for the 6.4mm thick FMI material. Notches for the tensile, impact and notched beam specimens were milled to give 1mm wide cracks. Samples were weighed before and after oxidation

to calculate the percentage weight loss and there were no changes in the test procedures for oxidised samples.

3.3.1 FLEXURAL PROPERTIES

Flexural strengths were measured using an Instron 1122 testing machine with a cross head speed of 0.5mm/min. The specimens were loaded in three point bend with rollers of 4mm radius with varying span to depth ratios, fig 3.6.

Specimens of ammx5mmx2.9mm and ammx5mmx3.2mm for the Sigri and KKarb materials respectively were used, where a = 50, 55, 70, 100, 130, 160 mm as the span to depth ratio was varied from 5:1 to 50:1.

The load and cross head displacement were recorded, the deflection of the specimen was assumed to be the cross head displacement, i.e. the testing machine was assumed to be infinitely stiff compared with the sample. Flexural strength was calculated from

$$\text{Flexural Strength} = 1.5\ F\ L/w\ d^2$$

where F is the maximum force in N and L is the span in m and w and d are the width and depth in m. The fractured specimens were mounted, fig 3.6, prepared and examined using the Zeiss optical microscope as described in section 3.1.1.

Samples of 70mmx5mmx3.2mm, 90mmx5mmx2.9mm and 70mmx5mmx3.1mm for KKarb, Sigri and FMI respectively were tested at span to depth ratios of 19:1, 25:1 and 19:1 respectively. The samples were oxidised to various percentage weight loss and tested, analysed and examined as described above. In addition the fracture initiation energy of the KKarb oxidised samples was calculated from

$$\gamma = U / 2 w d$$

where U is the area under the force deflection curve for forces less than the maximum, in J, and w and d are the width and depth in m. The stress intensity factor is calculated from

$$K^2 = 2 \gamma E$$

where γ is the fracture energy described above and E is the elastic modulus, in Pa.

3.3.2 ELASTIC MODULUS

DYNAMIC ELASTIC MODULUS

To determine the modulus the non-destructive sonic resonance method was used, ASTM C747-74(79). In this method the fundamental frequency of a beam is obtained. The rectangular beams of the oxidised and unoxidised

flexural strength KKarb, Sigri and FMI specimens were used, in both in-plane and out-of-plane directions, and were supported on triangular pivots at a distance 0.224L from each end, i.e. at the nodal point for the fundamental frequency. A stylus was placed on one end of the specimen the other end was struck with some sharp instrument, thus inducing the beam to vibrate at its natural frequency. The frequency was recorded by the stylus via an oscilloscope and was printed onto a chart recorder, fig 3.7.

The elastic modulus can be calculated from the frequency by using the following equation

$$E = Ar\ M\ f^2\ /\ w$$

where w = width of bar in metres, m = mass in kilogrammes, f = frequency in cycles/second and Ar = constant related to the length to depth ratio of the bar. The values for Ar are tabulated in ASTM C747.

CALCULATED ELASTIC MODULUS

The gradient from the linear part of the force/deflection curves from the flexural strength tests of oxidised samples was used to calculate elastic modulus from

$$E = F\ L^3\ /\ d\ I$$

where $I = w\ d^3 / 12$

3.3.3. TENSILE PROPERTIES

Tensile specimens of KKarb and Sigri were cut to 14mmx3.2mmx70mm and 14mmx2.9mmx120mm respectively with notch depth ratios ranging from 0 to 0.5. The Sigri material has a low shear strength and required long specimens in order for a sufficient area to be gripped on testing to fracture the sample in tension and not shear. The samples were end tabbed with 1mm shot peened aluminium sheet and glued on under pressure, with Ciba Geigy Araldite 2001 glue, fig 3.8.

The specimens were tested on an Instron 1195 machine with vice grips at a cross head speed of 0.5mm/min. The load and displacement were monitored and the displacement of cross head was assumed to be the deflection of the specimen. The stress was calculated from

$$\sigma = F / d\ (w - a)$$

where F is maximum force in N and d,w,a in m as described in fig 3.8. The stress intensity factor was calculated from

$$K = \sigma\ Y \sqrt{(\pi\ a)}$$

where

$$Y = 1.12 - .23\ a/w + 10.6\ (a/w)^2 - 21.7\ (a/w)^3 + 30.4\ (a/w)^4.$$

The fracture energy was calculated from

$$\text{elastic energy release rate} = - dU / dA \,|_{\delta}$$

and, as there are two surfaces to the crack, the

$$\text{Fracture energy} = - dU / 2\ dA \,|_{\delta}$$

where U is the area under the force deflection curve up to maximum load, in J, and A is the crack area, in m^2. U was plotted against A and the fracture energy was found from the gradient. For all A the deflection at maximum load did not vary much and was considered to be constant for these calculations.

Specimens of fixed notch depth ratio of 0.2 were oxidised, end tabbed and tested in same way. Stress and stress intensity factor were calculated in the same way. However work of fracture was calculated from

$$\gamma = U / 2\ d\ (\ w - a\ )$$

where U = area under force deflection curve(in J) and d,w,a as described in fig 3.8.

The fracture surfaces were examined and fibre pull out length estimated using the M3Z optical microscope. Four KKarb samples of different oxidation weight losses were examined in the SEM and rotated through 45^{o} where fibre pullout length was measured and averaged.

3.3.4. IMPACT ENERGY

A Tensometer Hounsfield Plastic Impact machine was used to perform Charpy impact experiments, fig 3.9. A hammer is suspended from a pivot and released, the hammer hits the sample and swings past after impact. The height the hammer rises after impact compared with the original height is an indication of the energy absorbed by the specimen on fracture. the energy absorbed was recorded on a dial which was turned by a pointer on the hammer. The fracture energy was calculated from

γ = Energy from dial(in J)/ 2 cross sectional area(in m^2)

1/2lb to 1/4lb hammers were used for Sigri and KKarb specimens of dimensions 2.9mmx2.9mmx55mm and 3.2mmx3.2mmx55mm respectively, for notch depth ratios varying from 0 to 0.5. Samples were tested in-plane and out-of-plane directions.

Some FMI samples of dimension of 70mmx100mmx70mm were tested on a Avery Dension impact machine, which operates in the same manner as described for the Hounsfield impact machine.

Further sets of Sigri and KKarb samples with notch depth ratio of 0.25 were oxidised to various amount of weight loss and the work of fracture was calculated, however hammers of weight ranging from 1/16lb to 1/2lb were required as the samples were weakened by oxidation and the scale on the dial was only calibrated for the mid range of energy absorption.

The fracture surfaces of all samples were examined using the MZ40 optical microscope and selected specimens were mounted and examined in the Zeiss optical microscope.

3.4 OXIDATION

Specimens were oxidised in air in a horizontal furnace in the zone I oxidation regime, to ensure uniform oxidation throughout the cross section. To determine the temperature of this region preliminary thermogravimetric studies were performed.

A Stanton Redcroft TG750 thermobalance with powdered samples of 125-150μm was used with a heating rate of 20^{o}C/min to 1000^{o}C to determine the temperature range

required for oxidation. Further investigations were performed, on Sigri specimens of 2.9mmx2.9mmx6mm and KKarb specimens of 3.2mmx3.2mmx6mm at a ramping temperature as before using a Setaram TG-DTA-92 thermobalance.

3.4.1. HORIZONTAL FURNACE

Oxidised of mechanical test samples and microstructural samples was performed in a Carbolite horizontal furnace. Samples were placed in an alumina tube and surrounded with charcoal.

Air flowing at 50-100l/hr and dried with silica gel was passed through the end of the furnace. The furnace was heated at 10^{o}/min to between 500-700^{o}C which was maintained for varying lengths of time to give different weight losses, then cooled to room temperature at about 20^{o}C/min.

The specimens were tested and examined as described in previous sections. The wider tensile specimens were found to oxidise non uniformly and were later placed on a holder, 6 at a time, in the furnace with air fed from a pipe directly above the specimens.

3.4.2. CHEMICAL ETCHING

Mounted and unmounted specimens of a variety of carbon/carbon composites were polished by hand, using wet and dry silicon carbide paper down to 1000 grade, and etched using chromic acid. The specimens were put in a beaker containing freshly made chromic acid, which was kept at 100^{o}C by a water bath. The chromic acid was freshly made from 10g potassium dichromate and 50cc orthophosphoric acid. The samples remained in the bath for 1 hour and were washed ultrasonically for 2 minutes and examined in the SEM. Mounted samples needed to be gold coated before examination in the SEM.

CHAPTER 4 RESULTS

The results obtained from the experiments described in the previous section are presented in this chapter. A preliminary study of the microstructure of nine carbon/carbon composites and the effects of air oxidation on the microstructures are presented in section 4.1. Three of these composites were selected for detailed studies. The mechanical properties and fracture mechanisms of these materials in the unoxidised state are discussed in section 4.2 and the effects of oxidation on these properties are presented in section 4.3.

4.1. MICROSTRUCTURE

The microstructures of several materials, both unoxidised and oxidised, were studied for familiarisation and characterisation by means of the techniques described in Chapter 3. This work was done to gain insights into the characteristic microstructural features of carbon/carbon composites. The microstructure of the unoxidised materials is described in section 4.1.1 and the effects of oxidation are described in section 4.1.2.

4.1.1. CHARACTERISATION OF VARIOUS COMPOSITES

Table 3.2 contains general characteristics of the composites. All of the composites studied have a 2D layup, with most being woven; they also have low density, low fibre volume fraction and high porosity. The majority of the materials have PAN carbon fibres and a resin carbon matrix, in some cases combined with other precursors.

The KKarb and FMI materials are very similar, having rayon carbon fibres in a 5 harness/satin weave and plain weave respectively, table 3.3. The matrix is formed from a blended mixture of pitch and resin and is graphitised. The pitch carbon matrix, when graphitised, has a speckled mosaic appearance, fig 4.1 (a) and the resin carbon matrix leads to stress-graphitised regions round fibre edges, fig 4.1 (b). There are many regularly-spaced intrabundle cracks some of which extend across the whole width of the bundle, for the KKarb material, fig 4.1 (c), and for the FMI material the cracks are larger and extend along as well as across fibre bundles, fig 4.2 (a). Some fibre/matrix interfaces have cracks fig 4.1 (d) and fig 4.2 (b), however there is little porosity at the fibre/matrix interfaces.

The Dunlop and Aerolor 05 and 05BT materials have a CVD matrix and PAN carbon fibres. Large, predominantly

closed, pores, typical of CVD matrix composites, can be seen, fig 4.3 (a), in the Dunlop composite and, fig 4.4 (a), in the Aerolor material. The Dunlop material is a layered composite and has regions of fibres held together very closely with CVD only deposited on outside of bundles and other regions which have carbon deposited round individual fibres or a few fibres, as is also found for the Aerolor composite, fig 4.4 (b). Circumferential and longitudinal microcracks, also characteristic of CVD matrices, can be seen clearly in the Aerolor material, fig 4.4 (c) but are not observed in the Dunlop material. Polarised light micrographs show the rough columnar structure of the Dunlop matrix radiating out from the fibres, fig 4.3. The Aerolor matrix has a smoother laminar matrix structure with the carbon layer plane orientation in the matrix clearly seen, fig 4.4

All three Sigri materials and the Aerolor 223 material have a resin carbon matrix and PAN carbon fibres; the Aerolor composite also has some CVD matrix. The Sigri CC1501G and CC1001G materials are very similar with very large pores, mainly at bundle/bundle interfaces, fig 4.5 (a), where the resin has shrunk on carbonisation and bubbles of volatiles have been trapped on curing. Sigri CC1506G composite does not have such large pores, fig 4.6 (a) because it has a plain weave with more curved fibre bundles than is the case for the other Sigri composites which have hopsack

weaves, table 3.3. Sigri CC1506G has only small amounts of intrabundle cracking, fig 4.6 (b), whereas the other Sigri materials have regular intrabundle cracks across the whole width of the bundle, fig 4.5 (b). The microstructure under polarised light fig 4.7, which is representative of all three Sigri composites, shows small pores in the matrix often at fibre/matrix interfaces (a), but there is very little cracking at the interface. The matrix material is stress-graphitised around fibre edges and carbon layer planes become oriented. This is seen clearly by the blue and yellow regions on the polarised light micrograph, fig 4.7 (b), where large regions of bulk matrix can be seen, especially at bundle/bundle interfaces.

The Aerolor 223 material has a weave pattern that is unclear but it has many long cracks at bundle/bundle fig 4.8 (a), and has some small pores at fibre/matrix interfaces, fig 4.8 (b). The matrix regions around the fibre edges are CVD, fig 4.8 (c), whereas the bulk of the matrix is resin carbon with large resin rich regions. The fibre/matrix interfaces are well bonded and the CVD structure can be clearly seen, fig 4.8, under polarised light.

Although these composites have widely differing microstructures and constituents, some general features are observed. The composites containing graphitised carbon matrix made from a blend of pitch and resin and

rayon carbon fibres, e.g. KKarb, have more interface cracking than the other carbon/carbon composites examined, indicative of poorer adhesion. However, the resin matrix composites, have some small pores at these interfaces. By contrast the composites with CVD and resin carbon matrix have large pores, many of which are closed. Regular intrabundle cracks are seen with the liquid-infiltrated matrix composites where stresses are relieved during volumetric shrinkage on carbonisation and on cooling from final heat treatment temperature.

4.1.2. OXIDATION

THERMOGRAVIMETRY

Powdered samples, 125-150μm, of four materials were oxidised in the Stanton Redcroft TGA-750, fig 4.9. The Dunlop and Sigri CC1001G materials commenced oxidation around 450°C, whereas the KKarb and Sigri CC1501G composites started oxidising at around 650°C. However, at high temperatures it is clear that the Dunlop and KKarb materials are more resistant to oxidation than the Sigri composites. As expected, in each case, the rate of oxidation increases progressively with increasing temperature. In an attempt to establish the oxidation regime of bulk samples of the composites used for mechanical testing, Sigri and KKarb materials in the form of blocks, dimensions given in section 3.4, were oxidised in the Setaram TGA, fig 4.10. In this case both materials started oxidising at about 650°C

and the oxidation rate for both materials was constant between 800°C and 1600°C. The rate of oxidation for the Sigri composite in this region was 0.2 wt%/min which is similar to the 0.22 wt%/min rate found for the KKarb composite. This suggests that the oxidation rate is controlled by mass transfer to the external surface of the composites at temperatures above 800°C. Samples prepared for detailed studies of the effects of oxidation on the microstructure of the materials were oxidised slowly in the temperature range 550°C-700°C in an attempt to ensure uniform, zone I, oxidation throughout the specimens.

MICROSTRUCTURAL OBSERVATIONS

Detailed studies of the effects of oxidation on microstructure were performed on the Sigri CC1501G, KKarb and FMI composites. Fig 4.11 shows the unoxidised KKarb material with the fibre and matrix clearly identified. As oxidation progresses to 1.7% weight loss the matrix starts to be oxidised at the interfaces and the fibre edges are slightly attacked. Further oxidation to 5% weight loss leads to most of the matrix being oxidised and the fibres are severely attacked, and at 9% weight loss the matrix material remains only in bulk regions and the fibres have been severely eroded leaving only needle like ends. The bulk microstructure of the KKarb composite, fig 4.12 shows that as oxidation progresses fibre/matrix interfaces are attacked and individual fibres can be seen, (a), at

5% weight loss and more clearly at 9% weight loss which are not visible in the unoxidised composite. The bundle/bundle interfaces do not appear to be significantly attacked and the intrabundle cracks do not appear to have been enlarged significantly with oxidation.

Fig 4.13 shows that porosity in the KKarb material, as measured by image analysis, increases progressively with oxidation, but with considerable scatter. For example, on oxidation to 5% weight loss porosity increases from about 8% in the unoxidised material to about 12% in the oxidised sample. From the microscopical studies, fig 4.11, 4.12, the major part of this increase is created at fibre/matrix interfaces.

On the unoxidised Sigri material, fig 4.14, the fibre and matrix can be clearly seen and the small pores in the matrix are easily identifiable. As oxidation progresses to 3% and 4% weight loss the matrix material is removed from the fibre matrix interface and only bulk matrix regions are left. The fibres are virtually unaffected, with only slight pitting at the edges. At 17% weight loss, the matrix has been totally eroded and the fibres have been reduced in diameter, fig 4.14, although not as severely as the KKarb material, and extreme pitting is seen on the fibre sides. Fig 4.15, shows the bulk microstructure of the Sigri composite at various stages of oxidation. As oxidation progresses

individual fibres can be seen, fig 4.15 (a), at about 3.5% weight loss and more clearly at higher weight losses; this is similar to the KKarb composite. The bulk resin and bundle/bundle interfaces are not noticeably attacked and the inherent pores in the material are not enlarged to any great extent on oxidation. The porosity, as measured by image analysis, increased from about 20% in the unoxidised material to about 27% after 5% weight loss, fig 4.16, though there is a great deal of scatter. This increase is comparable with that for KKarb.

The matrix and fibre and some interface cracking can be seen on the unoxidised FMI composite, fig 4.17 After oxidation to 2 and 3% weight loss the matrix material is slightly oxidised at the fibre/matrix interface, but the fibres are unaffected. At 5.8% burnoff most of the matrix material has been oxidised, except in bulk regions, and the fibres are slightly attacked. This is very different from the KKarb material where the fibres are severely attacked at 5% weight loss. As with the Sigri and KKarb composites the oxidation at the fibre/matrix interfaces reveals individual fibres in the bulk microstructure, fig 4.18 at 3.3% weight loss, with most fibres identifiable at 7.6% burnoff. As with the Sigri material, the pores and cracks and bundle/bundle interfaces are not oxidised noticeably.

Although efforts were made to ensure uniform oxidation throughout specimens, the whole length and width of every specimen was not uniformly oxidised. However, most of the specimens examined did have uniform oxidation throughout the sample cross sections and there was no change in the overall dimensions of the specimens.

CHEMICAL ETCHING

Chemical etching, with chromic acid, attacked the KKarb material in the same way as air oxidation, i.e. the matrix material at the fibre/matrix interfaces was attacked preferentially. Small pores in the matrix, not located at the fibre/matrix interface, appear to be where the oxidation is initiated in the Sigri material, fig 4.19 (a). The carbon layer planes alignment in the resin carbon matrix is along and around the fibres, fig 4.19 (b). Alignment of carbon layer planes concentrically with the fibres is very evident after chemical etching of the Aerolor 05 composite, fig 4.20, where several distinct layers of CVD deposition are visible. Smooth platelets of CVD crystals can be seen. In contrast, the Dunlop composite has very rough CVD platlets, fig 4.21, although in common with the Aerolor 05 material, concentric layers of matrix around fibres can be seen after chemical etching. The fibre/matrix interface has been attacked in the Dunlop material, but this is not so evident for the Aerolor composite.

SUMMARY

Air oxidation in zone I attacks the matrix at the fibre/matrix interfaces preferentially for the KKarb, Sigri CC1501G and FMI materials. The fibre edges are also oxidised, the fibres of the KKarb material are attacked more readily than for the other composites.

4.2 MECHANICAL PROPERTIES

The results for the unoxidised specimens are given in this section; the flexural properties are detailed in section 4.2.1, the impact energy in section 4.2.2 and the tensile properties in section 4.2.3.

4.2.1 FLEXURAL PROPERTIES

The mechanical properties of the three composites are given in table 4.1

KKARB COMPOSITE

The flexural strength of the KKarb material, tested in the warp direction, increases with span-to-depth ratio up to a ratio of 10:1. For greater span-to-depth ratios the strength remains constant at about 200MPa, fig 4.22, though there is up to about ±20% scatter. Although the flexural strength remains constant for span-to-depth ratios greater than 10:1, the fracture mechanisms change progressively as shown in fig 4.23. Changes in fracture mode are also accompanied by

changes in the load/deflection curves. To show these changes clearly and concisely the failure modes are represented by simple sketches. Example micrographs of the main failure modes observed are shown in fig 4.24. At a span-to-depth ratio of 5:1 the composite fails with several short parallel cracks along bundle/bundle interfaces and small quantities of shear cracking from the compressive face, fig 4.23. The corresponding force/deflection curve shows a linearly increasing load until near peak load when the rate of increase is non linear, as a result of subcritical cracking, and a smooth decrease in load after the maximum, with the rate decreasing as the deflection increases, fig 4.23. Large delaminating cracks occur along the neutral axis for specimens tested at a span-to-depth ratio of 10:1. These cracks are sometimes connected to the compressive face by shear cracking at 45^{o} or to the tensile face by stepped cracks, fig 4.23, and occasionally both. The force/deflection curve for this span-to-depth ratio has a jagged peak at maximum load and then the load decreases in a series of steps, typically one or two large steps with several small steps in between, fig 4.23.

Failure of the KKarb composite, for a span-to-depth ratio of 19:1, as used for oxidation experiments, is by a longitudinal ply/ply interface delamination crack on the tensile side of the specimen, connected to the tensile face by a tensile crack, often with part of the

tensile face having pulled away, fig 4.23. The accompanying force/deflection curve has an increasing load up to a single peak then the load falls catastrophically, often in two steps. At 30:1 span-to-depth ratio there are two or three very prominent ply delamination cracks in the tensile region of the specimen which are connected to the tensile face. The force/deflection curve falls catastrophically in one, or possibly two steps. As the span-to-depth ratio increases to 40:1 and 50:1 the specimens fail by a large delaminating crack in the tensile region, which for most of the 50:1 ratio samples causes the specimens to split into two pieces. The cracks in some samples are connected to the tensile face, fig 4.23. The force/deflection curves are the same as for 30:1 ratio with one catastrophic drop in load reducing it to almost zero load.

The fracture energy, calculated from the force/deflection curves, for the KKarb composite in the warp direction is 2.77kJ/m^2 and the fracture toughness is 10MPa$\sqrt{m}$.

In the fill direction KKarb was tested at a span-to-depth ratio of 19:1 and the specimens failed by cross bundle cracking with some steps, fig 4.25. The force/deflection curve rises to a maximum with a rounded peak then falls in a series of non catastrophic steps.

SIGRI COMPOSITE

The flexural strength of the Sigri CC1501G material increases with span-to-depth ratio up to a ratio of about 20:1. At higher span-to-depth ratios the strength remains constant at about 185MPa, although the mean value reaches a maximum at 30:1, fig 4.26 and there is about ±13% scatter on these values. The fracture mechanisms of the Sigri material are not as easily identifiable, under optical microscopy, as those for the KKarb material, because of the large inherent defects in the Sigri microstructure. At a span-to-depth ratio of 5:1 the fracture path is not distinguishable under optical microscopy, though there is some shear and some longitudinal cracking between pores for some samples, fig 4.27. The force/deflection curves increase linearly until close to the maximum load then curve to a peak. The load then falls quickly to about 80% of the peak load after which it falls slowly, fig 4.27. At a span-to-depth ratio of 10:1 there are many prominent longitudinal cracks between pores along ply interfaces and there is some shear cracking and some cross bundle cracking. The force/deflection curves are similar to those for a ratio of 5:1, but the load decreases quickly to about 50% of peak load before reducing more slowly, fig 4.27.

Failure of specimens tested at a span-to-depth ratio of 20:1 occurs by cracking along ply interfaces, between

pores, connected by shear cracking at 45° to the compressive face. The force/deflection curves have multiple peaks, indicative of subcritical cracking, and reduction of load on failure is by a multi-step process, some steps of which are catastrophic, fig 4.27. For oxidation studies a span-to-depth ratio of 25:1 was used. The fracture surface and force/deflection curves at this span-to-depth ratio are similar to those found at a 20:1 span-to-depth ratio, fig 4.28. Where cracking is by a combination of delamination, shear and cross bundle cracks running between pores. At 30:1 span-to-depth ratio the longitudinal cracks become more dominant with several large cracks running between pores. The force/deflection curves fall by a series of catastrophic steps until about 30% of peak load when the load decreases more slowly. As the span-to-depth ratio increases to 40:1 and 50:1 the longitudinal cracks become longer with a reduction in the shear cracking, fig 4.27. The force/deflection curves fall catastrophically in one or two steps with the load decreasing by about 25% of maximum load before falling at a slower rate.

FMI COMPOSITE

The FMI material, tested at a span-to-depth ratio of 19:1, failed either by delaminating several plies or by shear cracking at 45° to the compressive face. There are some inherent cracks in the FMI material which lead

to delaminating samples splitting into two pieces on failure and the accompanying force/deflection curve increases to a maximum load with a rounded peak, then falls catastrophically to about 30% of maximum after which it falls more slowly, fig 4.28. The shear failure mode samples sometimes have cross bundle cracking in the tensile region as well as shear cracking in the compressive region. The corresponding force/deflection curve has a rounded peak with the load remaining at the maximum then decreasing slowly.

The mean flexural strength for all specimens of the FMI material is 70±18MPa, table 4.2, but the strength of the specimens which failed by shear (85±5MPa) were significantly higher than those which failed by delamination (56±10MPa).

ELASTIC MODULUS

The elastic modulus values for the unoxidised composites determined by the sonic resonance method and also from the load/deflection curves of the flexural tests are presented in table 4.1.

The elastic modulus of the KKarb material, obtained from the sonic resonance method, was 19.4±1.2GPa in the warp direction and 9.5±1GPa in the fill direction and when calculated from flexural strength curves was 24.4±1.9GPa in the warp direction. These values are comparable with the manufacturer's figures. The modulus

of the Sigri material, obtained by the sonic resonance method, is 11.5±0.7GPa which is much lower than the manufacturer's value. From the flexural strength curves the modulus of the Sigri specimens is 42.3±10GPa, which is nearer the manufacturer's quoted value; this suggests that the resonance method is not suitable for this material. The mean value of the elastic modulus for all specimens of the FMI material obtained from the sonic resonance method and from the flexural data were 10±7GPa and 15±8GPa respectively, table 4.1. As with flexural strength data, the elastic modulus for specimens which failed by shear were higher than those for specimens which failed by delamination. Samples of the FMI material which failed in delamination have a modulus of about 7GPa determined by both methods and the specimens which sheared have moduli of 14GPa and 21GPa, from the resonance method and flexural curve methods respectively. Although these are only estimated values they are similar to each other.

4.2.2 IMPACT ENERGY

The flexural impact energy of the KKarb material in the warp direction increases with notch/depth ratio to about 9kJ/m^2 at 0.2 notch ratio, fig 4.30. The fracture surface has a stepped path consisting of a combination of longitudinal and cross bundle cracks, fig 4.31, with large pulled out regions. Almost all of the specimens broke into two pieces. In the fill direction the KKarb

fracture energy increases with notch/depth ratio to 4.5kJ/m^2 at 0.2 notch/depth ratio, fig 4.30. Failure is mainly by cracking straight across the specimen with each transverse bundle pulled out, and virtually all specimens broke into two pieces.

The Sigri material failed in one of three modes: (i) by cracking straight across the specimen, which was accompanied by long fibre pullout; (ii) by delamination along one half of the specimen connected to the notch by shear cracks; (iii) by a mixed stepped mode with some delamination and some cross bundle cracking, fig 4.31. Many of the Sigri samples did not break into two. Unlike the KKarb specimens, the fracture energy decreases with notch/depth ratio for the Sigri material to about 15 kJ/m^2 for 0.2 notch/depth ratio, fig 4.32.

The FMI material failed with a semicircular crack running across the specimens and some fibre pullout, fig 4.31. The FMI specimens broke into two pieces on impact and the fracture energy increases to 17kJ/m^2 for notch/depth ratio of 0.2, fig 4.33. For all the materials there was a large amount of scatter in the impact energy, on average about ±20%. The fracture energy of the unnotched samples estimated from the impact experiments are 10kJ/m^2 for the Sigri composite and 3.24kJ/m^2 for the KKarb composite in the warp direction.

The tensile impact fracture energy was 3.3kJ/m^2 for the KKarb material and 10kJ/m^2 for the Sigri material. The KKarb composite broke into two pieces on tensile impact and fractured in a brittle like manner with little fibre pullout, similar to the fracture of the tensile test specimens. Some of the Sigri samples broke into two pieces and again the fracture was similar to that found for tensile experiments except there was less fibre pullout of about 2-3mm.

4.2.3 TENSILE PROPERTIES

Properties obtained from tensile testing are presented in table 4.2.

KKARB COMPOSITE

The KKarb material, tested in tension in the warp direction, failed with some fibre pullout, often in terraced layers, fig 4.34. The fibre pullout length was about 1 or 2mm. The fracture toughness, calculated from fracture mechanics described in section 3.3.3, increases and the strength decreases with notch/depth ratio giving a toughness of about 12MPa$\sqrt{m}$ and tensile strength of about 95MPa for a notch/depth ratio of 0.2, fig 4.35. The tensile fracture energy, calculated from the toughness as described in section 3.3.3, is 3.06kJ/m^2 for a notch/depth ratio of 0.2 and calculated from the gradient of the energy/area plot, fig 4.36 (a), is 2.7kJ/m^2. The scatter for the data is about

±15%, which is less than for the tensile impact experimental results.

In the fill direction KKarb specimens failed at transverse bundle interfaces with no fibre pullout. The tensile strength, toughness and fracture energy, determined from the toughness and modulus, in this direction were 25MPa, 2MPa$\sqrt{m}$ and 12.6kJ/m^2 respectively, table 4.2.

SIGRI COMPOSITE

The Sigri material fails with long uniform fibre pull out with an average length of 5-10mm, fig 4.34. At the edge of the Sigri samples away from the notch there is often fibre pullout of 14mm or more. The Sigri material does not break into two pieces after maximum load is reached. Separation occurs on further displacement but most of the KKarb specimens break into two pieces on failure. The Sigri tensile strength decreases and fracture toughness increases with notch/depth ratio, giving a tensile strength of 280MPa and a fracture toughness of 40MPa$\sqrt{m}$ at a ratio of 0.2, fig 4.37. The scatter is about ±17% for the strength data and about ±13% for the toughness data, which is less than for the impact and flexure experiments. The fracture energy, calculated from the fracture toughness at a span-to-depth ratio of 0.2, is 20.8kJ/m^2 and from the compliance calculation plot, fig 4.36, is 20kJ/m^2. The

latter value is unreliable, however, as there is a large scatter of data on the energy/area curve.

The force/deflection curves, for all materials tested in tension, rise linearly to a knee, caused by transverse cracking in the matrix, after which the load increases again linearly but at a slower rate. Subcritical cracking causes non linearity near the peak load and, in the case of Sigri, results in some false summits. The load decreases catastrophically to almost zero when failure occurs.

4.3 EFFECT OF OXIDATION ON MECHANICAL PROPERTIES

The mechanical properties of the samples when subjected to oxidation at various percentage weight losses are given in this section. The changes in flexural properties are given in section 4.3.1, the changes in impact energy in section 4.3.2 and the changes in tensile properties in section 4.3.3.

4.3.1 FLEXURAL PROPERTIES

Flexural properties for 10% weight loss are listed in table 4.3

KKARB COMPOSITE

The flexural modulus of the KKarb material, in the warp direction, obtained by the resonance method decreases

from 19.4GPa to 14.2 GPa, i.e. by 27%, for 10% weight loss, table 4.3. The flexural strength, tested at a span-to-depth ratio of 19:1, decreases from 200MPa to 115MPa, i.e. by 43%, for 10% weight loss. The modulus falls uniformly with weight loss, whereas the flexural strength falls sharply at first and then more slowly after about 10% weight loss, fig 4.38. The scatter is about ±25% for the flexural strength data, and about ±12% for the elastic modulus data. The fracture toughness and fracture energy, determined from force/deflection curves, also decrease sharply in the initial stages of oxidation and then more slowly after about 10% oxidation. The fracture energy and the fracture toughness obtained from the flexural data reduce from 2.77kJ/m^2 to 0.67kJ/m^2, i.e. by 76%, and from 10MPa$\sqrt{m}$ to 4.3MPa$\sqrt{m}$, i.e. by 57%, respectively for 10% weight loss, fig 4.39.

The fracture energy is less than that found from tensile experiments, table 4.2, and only represents the energy required to initiate the failure crack, as only the area under the elastic region of the force/deflection curve is used to calculate the fracture energy.

The force/deflection curve for the unoxidised material falls catastrophically after reaching maximum load, fig 4.40. At 1.7% weight loss the force/deflection curve falls, after peak load, in a series of catastrophic

steps, the number of steps increasing as weight loss increases, fig 4.40. At 5% weight loss the load decreases in a series of smaller steps which are smaller still for 9% weight loss. The maximum load decreases and there is a smoother peak at maximum load with progressive oxidation.

The unoxidised KKarb specimens fail with longitudinal ply delamination cracks connected to the tensile surface, fig 4.40, 4.41. However as oxidation progresses, e.g. to 1.7% weight loss, the longitudinal cracks become less dominant and some cross bundle cracking occurs, fig 4.41. Further oxidation results in more cross bundle cracking connecting small delamination cracks leading to a stepped fracture surface, still with bundle pull-off on the tensile face. At 9% burnoff fracture is straight across the specimen with only small steps.

A significant feature of the fracture behaviour of carbon/carbon composites is that there is a wide variation in fracture mode for specimens showing the same strength or for specimens subjected to the same amount of oxidation. Specimens at points A and B on fig 4.38 have the same flexural strength but different weight losses. Point A fails by delamination, as described for unoxidised samples fig 4.40, 4.41, and point B fails straight across the specimens with very small steps, as described for samples with 9% weight

loss fig 4.40. Points C and D on fig 4.38 have the same weight loss but different flexural strengths, C fails with delamination and some cross bundle cracking, as described for samples with 1.7% weight loss, fig 4.40, and D fails with a stepped fracture surface, as described for samples of 5% weight loss. This type of behaviour goes some way to explain the scattered fracture data obtained for carbon/carbon composites.

SIGRI COMPOSITE

The elastic modulus of the Sigri material, obtained by means of the resonance method, increases with weight loss fig 4.42, again suggesting this method is unsuitable for this material. However, the value of elastic modulus, calculated from the flexural strength results, decreases smoothly with burnoff with a reduction from about 42GPa to about 36GPa, i.e. of 14%, for 10% weight loss, fig 4.43, with a scatter of about ±28%. The elastic modulus, calculated from the flexural strength results, for the KKarb material decreases from about 24GPa to about 17GPa, i.e. by 30%, for 10% weight loss, fig 4.43, this is a similar reduction to that found for the elastic modulus calculated from the resonance method. The flexural strength of the Sigri composite, tested at a span-to-depth ratio of 25:1, decreases smoothly with weight loss from about 183MPa to 141MPa, i.e. by 23%, for 10% weight loss, fig 4.42, with only a small amount of scatter of about ±10%.

After reaching the peak load the force/deflection curves for the unoxidised Sigri samples have a multi-stepped reduction in load with a mixture of large and small steps, fig 4.28. On oxidation, which was studied to almost 15% weight loss, no change was observed in the force/deflection curves. The fracture surface is a mixture of bundle interface cracks connecting pores and some shear cracking, fig 4.28. Again there appears to be no change of fracture mode on oxidation.

FMI COMPOSITE

For the FMI material flexural strength values fall into two clear bands, corresponding to the delaminating and shear modes of failure, fig 4.44. For both types of failure modes, flexural strength decreases gradually and smoothly with weight loss; from about 56MPa to about 25MPa, i.e. by 55%, for 10% burnoff for the delaminating mode and from 86MPa to about 5MPa, i.e. by almost 100%, for 10% weight loss for the shear mode, table 4.3. These are estimates as only a limited range of weight losses were tested. The scatter of the shear mode is about ±50%, whereas for the delamination mode it is about ±17%.

The elastic modulus determined from the resonance method decrease from about 14GPa to about 3GPa, i.e. by 79%, for 10% weight loss for the shear mode and from 7.5GPa to about 3GPa, i.e. by 60%, for 10% weight loss for the delaminating mode, fig 4.44. The scatter of

elastic modulus for specimens that fail in the shear mode is ±35%, however, the scatter of data for samples which fail in the delaminating mode is much smaller. The elastic modulus values obtained from the flexural strength load/deflection curves for the FMI material also separate into two distinct groups, fig 4.45. For both groups the elastic modulus falls smoothly with increasing weight loss and, if extrapolated, the modulus for specimens which fail in the delaminating mode falls from 7GPa to 1GPa, i.e. by 86%, for 10% weight loss, whereas the modulus of specimens which fail in the shear mode falls to zero before 10% weight loss, however the curves are likely to reduce more slowly than a linear extrapolation. The data for both modes of failure have a scatter of about ±50%. The fracture surfaces and force/deflection curves for both modes of failure were described in fig 4.28 and on oxidation there was no observable change in fracture or of force/deflection curves.

4.3.2. IMPACT ENERGY

The flexural impact fracture energy for the KKarb material in the warp direction decreases from about $9kJ/m^2$ to about $5.2kJ/m^2$, i.e. by 42%, for 10% weight loss with up to ±30% scatter. The fracture energy decreases more slowly with further weight loss, fig 4.46. Fracture for the unoxidised material, under impact conditions, is characterised, fig 4.30, by a

stepped fracture path with a combination of longitudinal delamination type cracking which extends along the specimen and cross bundle cracking. As oxidation increases, e.g. to 3% burnoff, the longitudinal cracks become less prominent and the length of pulled out regions reduces, fig 4.47. At higher weight losses, e.g. 9% weight loss, the cross bundle cracking becomes more dominant and specimens fail with a crack straight across with very little longitudinal cracking, fig 4.47. This change in fracture mode is similar to that found for flexural strength experiments.

Some variations in fracture mechanisms for specimens subjected to similar conditions was noted for impact fracture of the KKarb composite. Samples A and B, fig 4.46 have the same weight loss but different fracture energies. Specimen A fails with a stepped crack with some longitudinal delamination cracking, as for 3% burnoff specimens; fig 4.47, but specimen B fails straight across, as for 9% burnoff samples fig 4.47. Samples B and C have the same fracture energy but different weight losses. Sample C fails with much longitudinal cracking, more than for 3% weight loss samples, but less than for unoxidised specimens. When tested in the same mode as the tensile experiments the impact fracture energy falls smoothly from 3.3kJ/m^2 to about 2.7kJ/m^2, i.e. by 18%, for 10% weight loss with

no obvious change in fracture mode on oxidation, fig 4.48.

The flexural impact fracture energy of the Sigri material decreases from about 15kJ/m^2 to 5.7kJ/m^2, i.e. by 62%, for 10% burnoff. The impact fracture energy falls more slowly with further weight loss, fig 4.49, with up to ±50% scatter. The tensile impact fracture energy decreases more smoothly from 10kJ/m^2 to about 6.5kJ/m^2, i.e. by 35%, for 10% weight loss, fig 4.48. The scatter of data for the Sigri and KKarb materials in this mode is about ±15%. The three modes of flexural impact fracture for the Sigri composite, as described in fig 4.30, occur at all weight losses investigated with no single mode dominating. The samples A, B and C in fig 4.49 all have the same weight loss but different fracture energies. Specimens A and C failed with a crack straight across the specimen, while sample B failed in a delaminating mode, fig 4.30. Samples D and E have the same fracture energy but different weight losses; specimen E failed with a crack across the sample, whereas sample F failed by a delamination crack. The tensile impact fracture mode did not change with oxidation for either the KKarb or the SIgri composites.

4.3.3 TENSILE PROPERTIES

The tensile properties for the oxidised materials are given in table 4.4.

KKARB COMPOSITE

For the KKarb material in the warp direction the tensile fracture energy falls steadily from 2.9kJ/m^2 to about 1.9kJ/m^2, i.e. by 34%, for 10% weight loss for a fixed span-to-depth ratio of 0.2, table 4.4, but there is a large amount of scatter, about ±50%, fig 4.50. The tensile strength and fracture toughness fall steadily with 29% reduction for 10% weight loss and with a scatter of data of ±15%, fig 4.50, as fracture toughness is related to strength it decreases in the same manner. The fracture surface, as shown in fig 4.33, does not change with oxidation. The fibre pullout length, as examined by SEM for four samples with several regions of the fracture surface investigated, shows little variation on oxidation, fig 4.51. There are small variations across the specimen width but there is a normal distribution of pullout lengths in each region.

SIGRI COMPOSITE

The tensile fracture energy of the Sigri material decreases sharply in the initial stages of oxidation and then falls more slowly as weight loss increases. The fracture energy decreases from about 20kJ/m^2 to

about 5.7kJ/m^2, i.e. by 71%, for 10% weight loss. The fracture toughness and tensile strength, however, fall slowly and smoothly with weight loss giving about 37% reduction for 10% burnoff, fig 4.52. The scatter for all the data was about ±10%. No change of fracture mode on oxidation was observed and the fibre pullout length, calculated form micrographs, showed no change in pullout length with oxidation, fig 4.51.

CHAPTER 5 DISCUSSION

The microstructural features of several carbon/carbon composites are discussed in section 5.1. The mechanics of failure and the mechanical properties of three carbon/carbon composites are discussed in sections 5.2 and 5.3 respectively. In section 5.4 the influence of oxidation on the microstructure of these composites is evaluated. The fracture mechanisms of oxidised composites are discussed in section 5.5 and the reduction in strength and other mechanical properties with weight loss is described in section 5.6. The chapter is summarised in section 5.7. Unless otherwise stated references to the properties of the KKarb material relate to the warp direction and it should be remembered that because of the symmetric weaves of the FMI and Sigri materials they have no warp and fill directions.

5.1 MICROSTRUCTURE OF UNOXIDISED COMPOSITES

One of the microstructural features that is common to liquid impregnated carbon/carbon composites is intrabundle cracking, formed by stresses from volumetric shrinkage on carbonisation and from contraction on cooling. Uniformly spaced intrabundle cracks are seen in the KKarb material, fig 4.1, and in the Sigri CC1501G and CC1001G materials, fig 4.5. Kohno et al (1991) also found regularly spaced intrabundle

cracks for layered composites with a variety of PAN carbon fibre bundle widths and a resin matrix. In the FMI material these stresses lead to cracking along bundles as well as intrabundle cracks, fig 4.2. In the Sigri CC1506G and the Aerolor 223 materials only small amounts of intrabundle cracking are evident and the Aerolor 223 composite has extensive cracking of bundle/bundle interfaces, fig 4.8. The porosity of liquid impregnated carbon/carbon composites depends on the matrix precursor. For resin carbon matrices, such as those found in the Sigri composite, large quantities of volatiles are given off during curing and carbonisation which cannot escape. Hence they have large pores between about 100μm and 600μm long for the Sigri CC1506G and CC1501G materials respectively. This is similar to CVD porosity where many pores occur through regions being blocked off by deposition of carbon at constrictions in the pore network.

The porosity in CVD matrices can be of the same size as that for resin carbon matrices, e.g. 100μm fig 4.3. Although large numbers of smaller pores, as seen in the Aerolor 05 material, fig 4.4, are more common for CVD matrices. The structure of the carbon matrix of carbon/carbon composites depends on the precursor used, e.g. spoke-like carbon layers are seen for a CVD matrix, fig 4.3, and stress graphitised regions occur round fibre edges, as also found by McAllister and Taverna (1971). Fig 4.6 shows an example for a resin

matrix. The fibre/matrix adhesion appears, from micrographs, to be good for CVD matrix composites such as the Dunlop and Aerolor 05 materials, fig 4.3,4.4. Ehrburger and Lahaye (1981a) also found good fibre/matrix and matrix/matrix adhesion from microstructural studies of composites with rayon carbon fibres and a CVD matrix. Small pores are seen at the fibre/matrix interfaces in the Sigri material, fig 4.7, and the KKarb and FMI materials have many small cracks, suggesting weaker adhesion at these interfaces than for the CVD matrix materials.

5.2 FRACTURE MICROMECHANICS

A characteristic feature of the fracture of carbon/carbon composites revealed by this study is the variability in the fracture mechanisms. Such variations result from the heterogeneous nature of these materials with large localised variations in microstructure. This aspect of the fracture of carbon/carbon composites also contributes to the large degree of scatter in the mechanical properties values. The features of the fracture processes described in this section are typical and relate to the majority of specimens tested.

TENSILE FAILURE

In tension the Sigri material failed with extensive fibre pullout of about 7.5mm, whereas the KKarb material failed with small length, l, of pullout of

only 1.5mm, fig 4.34. The expected fibre pullout lengths can be calculated from the work required to pullout a fibre, as described by Cottrell (1964);

$$2\,\gamma = V_f\,\sigma\,l\,/\,12$$

where γ is the fracture energy, V_f is the fibre volume fraction and σ is the tensile strength. Rearranging the equation gives

$$l = 24\,\gamma\,/\,\sigma\,V_f.$$

Substituting the values of tensile strength of 95MPa and γ = 2.9kJ/m^2 from table 4.2 and V_f = 0.45 from table 3.2 for the KKarb material in the above equation gives a pullout length of 1.6mm which is within the range of fibre pullout lengths found in this work of about 1-2mm. Substituting the values of tensile strength of 274MPa and γ = 20kJ/m^2 from table 4.2 and V_f = 0.38 from table 3.2 for the Sigri material in the above equation gives a pullout length of 4.6mm which is also within the range of fibre pullout lengths found in this work of about 5-10mm. The greater pullout length for the Sigri material suggests that the fibre/matrix adhesion for the Sigri composite is not as strong as that for the KKarb composite. There are contradictory findings in the literature on the influence of fibre strength on fibre/matrix adhesion in carbon/carbon composites. Williams and Impresca (1975) found that the

tensile fracture mode was dependent upon fibre type for a pitch carbon matrix composite. PAN carbon fibres led to long, randomly-distributed fibre pullouts and rayon carbon fibres led to short uniform fibre pullouts because of their different bonding mechanisms. This is also found in this work where rayon carbon fibres in the KKarb material lead to short fibre pullout and PAN carbon fibres in the Sigri material lead to long pullouts. However, Sheaffer (1989) who found that single filaments of PAN carbon fibres in resin carbon matrices failed with no fibre pullout because there was good fibre/matrix bonding. Surface treatment or detreatment of carbon fibres changes the mechanisms of bonding and according to Kowbel and Shan (1990) leads to different types of fracture. However, in the present work there is no conclusive microstructural evidence of the existence or absence of fibre surface treatment, fig 4.1,4.2,4.7.

Pollock (1990) attributes the different tensile failure fracture surfaces of 2D woven carbon/carbon composites to the average crimp angle, with more crimped samples exhibiting a more brittle failure. The average crimp angle is found from schematic representations of the weave patterns as segments of fibre as shown in fig 5.1. A weighted average gives the crimp angle, Θ, as

$$\Theta = \Sigma L \theta / \Sigma L$$

where L is the length and θ is the angle of the element. For the materials studied the average crimp angles were found to be 3.9^{o} and 12.3^{o} for the KKarb material in the warp and fill direction respectively, 5^{o} for the Sigri material and 31^{o} for the FMI composite. The KKarb and Sigri composite have crimp angles that are approximately the same, i.e. 3.9^{o} and 5^{o} respectively, but have different fracture surfaces, therefore the crimp angle cannot account for the different amounts of fibre pullout observed. The Sigri material has an increase of fibre pullout length further away from the notch, fig 4.34. Phillips (1972) also found, for a carbon fibre reinforced glass composite, that the pullout length was increased further away from the notch. This was attributed to fast crack initiation at the notch followed by slower propagation of the crack, and hence the material was sensitive to strain rate. This suggests that the fracture mechanisms of the Sigri material could also be strain rate dependent.

The first matrix cracking was thought to be the most important feature of the tensile fracture process of carbon/carbon composites according to Sakai et al (1991), and Pollock (1990) also suggests that tensile fracture is initiated in the matrix. Fracture surfaces of the KKarb and Sigri materials reported here are post mortem examinations and it is therefore difficult to comment on this theory. The matrix may, however,

influence the amount of fibre pullout because, according to Savage (1988), polymer resin carbon matrices in carbon/carbon composites lead to poor fibre/matrix bonding, as was the case for the resin carbon matrix Sigri material. Notches, used in tensile specimens, should not cause failure and hence should be smaller than the critical crack length, which Sato and Kurumada (1989) calculated to be 1.2 and 2.2mm for their coal tar pitch and PAN or pitch carbon fibre composites. They used a modified Griffith equation as described in section 2.3.3;

$$c = 1 / \pi \times (K / \sigma)^2,$$

where σ is the tensile strength, K is the fracture toughness and c is the critical crack length, this assumes a central crack in an infinite plate, which is not the case for these composites, but it gives a rough guide to the critical crack length. Values of K = 12MPa$\sqrt{m}$ and σ = 95MPa from table 4.2 for the KKarb material when substituted in the above equation give a critical crack length of 5mm. Substituting values of K = 37.6MPa$\sqrt{m}$ and σ = 274MPa, from table 4.2, for the Sigri material in the above equation gives a critical crack length of 6mm. The notches used in this work, of about 2.8mm long, were shorter than the critical crack lengths of 5 and 6mm calculated for the KKarb and Sigri composites respectivley, therefore the notches did not

cause failure: they only acted as crack initiation sites.

In summary, this work has shown that the fibre type influences the fracture mechanisms with PAN carbon fibres leading to weaker fibre/matrix bonding and possibly the resin matrix also leads to reduced interface adhesion. This explains the long fibre pullout found in tensile tests for the Sigri material which contains PAN carbon fibres in a resin carbon matrix. Conversly, there is strong adhesion between the rayon carbon fibres and the pitch/resin carbon matrix in the KKarb composite leading to short fibre pullout in tensile tests.

FLEXURAL FAILURE

The flexural failure mode of the KKarb material, fig 4.23, becomes more delaminating and the force/deflection curves change from a controlled slow reduction to a more catastrophic reduction in load as the span to depth ratio increases. The same trend is seen in flexural failure of the Sigri material, fig 4.27, but the delamination cracks are not so long. These cracks are blunted and deviated by pores; also compressive shear cracking occurs even at higher span to depth ratios.

In a similar study of flexural failure of a 3D carbon/carbon composite Tanamura et al (1990) found an

increase in brittleness with increasing span to depth ratio, but in this case the third dimension plays an important role in restricting crack propagation. Several workers, e.g. Kowbel and Shan (1990), have found that a catastrophic reduction in load on a force/deflection curve is related to brittle failure across the specimen. It might therefore be expected that a more brittle type of failure would occur as span to depth ratio increases. Ply/ply delamination dominates the failure, as the span to depth ratio increases, of the KKarb and Sigri composites. However, delamination is an energy absorbing process, like cross specimen cracking, and also results in drastic reductions in load on force/deflection curves. These materials do not fail across the specimens because, as span to depth ratio increases, the tensile stresses between the bundles increase, eventually pulling them apart in a delaminating fashion. These interfaces are weaker than the transverse fibre bundle strength, and it is therefore easier for cracks to delaminate plies than to propagate across bundles, as was the case in the work of Kowbel and Shan (1990).

The KKarb composite in the fill direction fails in flexure with small stepped cracks containing cross bundle and along bundle cracking, fig 4.25. Cross-bundle cracking is often initiated by high stresses in fibre bundles at cross-over points. But, in the case of the KKarb composite, the ply interfaces are weak and so

cause some additional longitudinal cracks. The cross bundle cracking due to the close weave pattern accounts for the more stepped cracking found for the fill direction compared with the warp direction of the KKarb material. Manocha and Bahl (1988) also found a more brittle type of fracture for a closer woven material. Their plain weave carbon/carbon composite failed in a brittle manner, whereas their 8 harness satin weave composite failed in a mixed mode. After reaching the peak load the force/deflection curves for the KKarb material in the fill direction fall steadily in a series of steps as the crack propagates across bundles, this is similar to the "Alternation" cracking described by Tanamura et al (1990) in their study of 3D carbon/carbon composites.

Flexural failure in the FMI composite occurs either by delamination or by a shear failure mode, fig 4.29. The specimens which fail by delamination have large inherent delaminating cracks which determine the fracture mode. The initial drastic fall in load on the force/deflection curves for this mode of failure suggests that delamination is a fast energy absorbing process. The shear mode of failure of the FMI specimens is influenced by the lack of resistance to shear of the inherent cracks and the bundle cross-over cracks. The force/deflection curves, for the shear mode of failure, imply that shear cracking is a gradual process.

IMPACT FAILURE

On flexural impact testing there was little change in the work of fracture with notch depth, fig 4.30,4.32,4.33, for all materials tested. Therefore, as with tensile tests, the materials were not notch sensitive. The KKarb material failed in steps with some large delamination cracks and some fibre pullout, fig 4.31. This is similar to the features of fracture surfaces from the flexural strength experiments, fig 4.23. However the increased strain rate enabled cracks to propagate across specimens which therefore broke into two pieces, whereas this did not occur in flexural failure at slow strain rate.

In the fill direction the appearance of a KKarb composite flexural impact fracture, fig 4.31, is similar to that for slow strain rate flexural fracture. However there is a marked change in the failure mode of the FMI material under impact conditions. The FMI composite fails under flexural impact loading with circular bundle pullout, fig 4.31, rather than by the delaminating or shear failure modes found for slow strain rate flexural failure, fig 4.29. As in the case of the KKarb material in the fill direction, microcracks at fibre bundle cross-over points in the FMI composite, which has a plain weave pattern, lead to the cross bundle cracking seen in the flexural impact fracture of the FMI composite. This is not seen at slower strain rates, perhaps because at a span to depth

ratio of 19:1 failure is not strictly in flexure but has a large shear component leading to a shear failure.

The modes of failure of the Sigri composite under flexural impact, fig 4.31, are very different from those in the normal flexural tests, fig 4.27, and hence strain rate is important. This corroborates the finding for tensile experiments. In flexural tests the failure occurs mainly by short delaminating cracks between pores with some shear and cross bundle cracking. However, for the flexural impact tests there are two cracking mechanisms, cross bundle and delamination cracking. There appears to be no dominant mechanism, suggesting that the energy required for delamination cracking is the same as that required to propagate a crack across the sample. Hence, either of the modes or a mixture of modes is observed, fig 4.31. For slow strain rates, however, pores dominate the fracture by blunting and deflecting cracks, leading to a mixed mode of failure, but pores have no effect on impact failure.

5.3 MECHANICAL PROPERTIES

There are many factors which influence the mechanical properties of carbon/carbon composites. In the following section we try to identify and explain the effect of some of these factors on various composite mechanical properties.

ELASTIC MODULUS

The elastic moduli of the KKarb and Sigri materials determined by the sonic resonance method (19 and 11 GPa respectively) were lower than those determined from the load/deflection curves in flexural tests (24 and 42 GPa respectively), table 4.1. These differences can be attributed to the limitations of the sonic resonance method when applied to carbon/carbon composites. This method is based on the resonant properties of an isotropic, homogeneous continuum model beam. Carbon/carbon composites are anisotropic and heterogeneous materials with a significant amount of porosity. The discrepancy is greater for the Sigri material, possibly because of the presence of large pores, fig 4.5. For this reason only the elastic moduli calculated from the load/deflection curves will be considered in the following discussion.

Influence of Fibre Type

The range of elastic modulus values of the three composites (15GPa to 42GPa) can be partially attributed to the fibres used. The Sigri composite has PAN carbon fibres whereas the KKarb and FMI materials have rayon carbon fibres, table 3.2. Although no exact information is available on the elastic modulus of the carbon fibres used, PAN carbon fibres have, in general, a higher stiffness than rayon carbon fibres (the average value from table 2.2 are 350GPa and 250GPa for PAN and rayon carbon fibres respectively) thus leading to a

composite of higher elastic modulus. However, the FMI material contains the same fibres as the KKarb material but has a lower modulus of 15GPa compared with 24GPa for the KKarb material, and therefore other factors must contribute to the differences in modulus of these composites.

It might be expected that a large fibre volume fraction would lead to a higher modulus. The Sigri composite has a smaller fibre volume fraction (0.38) than the KKarb and FMI materials (0.45 and 0.50 respectively), table 3.2, though it has a higher modulus. It would seem therefore that fibre volume fraction is not a contributor to the differences in modulus between these materials.

Application of the Rule of Mixtures

A more quantitative consideration of these factors may be had by applying the rule of mixtures to calculate the elastic modulus of the three composites. The rule of mixtures, described in Hull (1981), is given by the equation

$$E_c = E_f V_f + E_m V_m,$$

where E_c, E_f and E_m are the moduli for the composite, fibres and matrix respectively and V_f and V_m are the fibre and matrix volume fractions respectively. The rule of mixtures is derived for a unidirectional

composite, with well bonded fibre/matrix interfaces, with fibres and matrix having similar strains. This does not describe the carbon/carbon composites studied, but it gives a rough estimate of the moduli.

The exact moduli of the fibres and matrix of the KKarb, Sigri and FMI materials are not known, therefore values of modulus of fibres and matrix found from the literature in table 2.2 will be used for rule of mixtures calculations. For the KKarb material the average value of fibre modulus, E_f, from table 2.2 is 250GPa. The exact blend of pitch and resin in the matrix for the KKarb material is unknown but an average value from table 2.2 gives a value of the matrix modulus, E_m, as 20GPa. The fibre volume fraction, V_f, is 0.45 from table 3.2 and the matrix volume fraction, V_m, is $0.38 = 1 - V_f - P$, where P is the porosity. Substituting these values for the KKarb material in the rule of mixtures equation gives the modulus of the KKarb material, E_{KKarb}, as 119GPa, table 5.1, however a value of E_{KKarb} = 24GPa was found in this work. If the worst fibre modulus from table 2.2, i.e. E_f=28GPa, is assumed and substituted in the rule of mixtures equation a modulus of E_{KKarb} = 19GPa results, which is much closer to the value found in these results, table 5.1.

The FMI composite has the same fibres and matrix precursors as the KKarb composite, therefore, the same

moduli values as for the KKarb material are assumed. V_f = 0.5 and V_m = 0.31, from table 3.2, for the FMI material are sustituted in the rule of mixtures equation giving E_{FMI} = 20GPa which is also similar to the value, of 12.5 GPa, found in these results, table 5.1.

For the Sigri material the average value of fibre modulus, E_f, from table 2.2 is 350GPa and of matrix modulus, E_m, is 24GPa. The fibre volume fraction, V_f, is 0.38 from table 3.2 and the matrix volume fraction, V_m, = 0.51. Substituting these values for the Sigri material in the rule of mixtures equation gives E_{Sigri} = 145GPa, table 5.1, however a value of E_{Sigri} = 42GPa was found in this work. If the worst fibre modulus from table 2.2, i.e. E_f=200GPa, is assumed and substituted in the rule of mixtures equation a modulus of E_{Sigri} = 88GPa results, which is two times the value found in this work, table 5.1.

The higher values of elastic modulus calculated from the rule of mixtures when using the average fibre moduli compared to those found experimentally in this work, table 5.1, can be attributed to various factors. Fibre degradation or fracture during manufacture leads to lower fibre moduli than used in the equation which would result in a lower composite modulus. The fibres and matrix are not well bonded and the materials studied are 2D woven composites whereas the rule of

mixtures is for a unidirectional composite with good fibre/matrix adhesion, these differences could lead to a higher calculated value of modulus. There are many microstructural variations between these materials, such as porosity, weave etc, which may contribute to the differences in modulus.

The moduli of the resin and pitch carbon matrix materials are similar at about 20GPa, table 2.2, so that differences in matrices between the composites cannot account for the differences in elastic modulus. Therefore, although the matrix contributes to the composite modulus, as seen in table 5.1, its contribution is similar for all three materials.

Influence of Weave Pattern

Other factors, such as weave pattern, may also influence the modulus. The influence of weave pattern can be represented by a simple model comprising a series of springs as in fig 5.2a. This model applies strictly to a comparison of different textile weave patterns and in the present context assumes the composite has no matrix. The examples used in the comparison are a plain weave, as found in the FMI material, and an 5 harness satin structure, as found in the KKarb material. If a curved and a straight fibre both of length L experience a load F the straight fibre extends by δ whereas the curved fibre extends by $(\pi/2 - 1)\ L + \delta$, fig 5.2b. Hooke's law, i.e. $F = k\ \delta$, where F

is the force applied and δ is the deflection gives a relationship between stiffness and elongation for constant force applied as $k \alpha 1/\delta$. If the curved fibre springs have a stiffness of k_1 and the straight fibre springs have a stiffness of k_2, then

$$k_2/k_1 = \delta_1/\delta_2 = (\pi/2 - 1)\ L + \delta\ /\ \delta$$

and if $L/\delta = 0.02$ is assumed then

$$k_2/k_1 = 30.$$

This can be related to the stiffness of the weave patterns by incorporating Hooke's law into the definition for the modulus giving

$$E = \sigma\ /\varepsilon = F\ L\ /\ A\ \delta = F\ L\ k\ /\ A\ Fm,$$

and for a fixed length and area

$$E\ \alpha\ k.$$

Hence the ratios of the moduli for the weave patterns becomes

$$E_{5H/S}\ /\ E_{plain} = 2\ k_1 + 4\ k_2\ /\ 6\ k_1 = 20,$$

indicating that more tightly woven layups would be expected to have lower moduli, which is found to be the

case in this study, table 4.1. However from the examples in this model the modulus of the KKarb material might be expected to be 20 times that for the FMI material, but the FMI composite has a modulus of 15GPa and the KKarb material has a modulus of 24GPa. The type of deformation of the fibre bundles of this simple model does not account for the surrounding matrix material which resists deformation reducing the effect of weave pattern on the calculated modulus.

If the spring model is extended to include the matrix as an extra spring in parallel with the fibres, fig 5.2c, then the composite modulus can be expressed by

$$1 / E_c = 1 / E_m + 1 / E_f = E_f + E_m / E_f E_m.$$

Therefore the ratio of the moduli becomes

$$E_{5H/S}/E_{plain} = (E_f+E_m/E_f E_m)_{plain} \times (E_f E_m/E_f+E_m)_{5H/S}$$

E_m is assumed constant for both the weave patterns and from table 5.1 E_f/E_m = 1.4 for the KKarb and FMI materials which have 5 harness satin and plain weaves respectively. However the values of E_c for the two materials were too low and too high respectively compared with the experimental results, table 5.1. Therefore an increased value of E_f/E_m = 2 is assumed for the KKarb (5 harness satin weave) material and a reduce value of E_f/E_m = 1 is assumed for the FMI (plain

weave) material. Substituting these values in the above equation gives the ratio of the moduli as

$$E_{5H/S}/E_{plain} = 13,$$

which is higher than the ratio of $E_{KKarb}/E_{FMI} = 1.6$ found from the results in table 4.1.

However the weave pattern could be a contributing factor to the difference in modulus of the tightly woven FMI and KKarb materials in the fill direction to those of the more open weave KKarb material in the warp direction and the Sigri material. Pollock (1990) also attributed a lower elastic modulus in the fill direction, compared with the warp direction, to weave pattern.

Influence of Porosity

The large pores of the Sigri composite compared with those of the KKarb and FMI composites suggests that the Sigri material might have a lower modulus because the pores do not add to the stiffness of the material. However, the numerous intrabundle cracks of the KKarb and FMI materials lead to a lower density (1.36g/cm^3 and 1.28g/cm^3 for the KKarb and FMI materials respectively compared with the 1.4g/cm^3 of the Sigri material) and hence to a lower modulus. Oh and Lee (1989b) also attribute the lower moduli and flexural strengths of some carbon/carbon composites to lower

density. This suggests that shape and size of the porosity is not as important as the amount of porosity.

Summary

In summary, fibre modulus appears to be the most important factor affecting differences in modulus of the three composites studied with density also having an effect. The weave pattern also influences the modulus and is possibly the principal reason for the differences in modulus between the KKarb material in the fill and warp directions.

TENSILE AND FLEXURAL STRENGTHS

The flexural strengths of the Sigri and KKarb composites (183MPa and 200MPa) respectively, are greater than the flexural strengths of the KKarb material in the fill direction (105MPa) and of the FMI material (70MPa), table 4.1. However, the tensile strength of the Sigri composite (274MPa) is about three times that of the KKarb composite of (95MPa), table 4.2. The tensile strength of the KKarb material in the fill direction (25MPa) is lower than that in the warp direction.

Influence of Fibre Type

Weisshaus and Kenig (1990) suggested that the tensile strength of a resin and pitch matrix composite reinforced with PAN carbon fibres is dominated by fibre strength. PAN carbon fibres are, in general stronger

than rayon carbon fibres, table 2.2, and this suggests that the Sigri material reinforced with PAN carbon fibres should be stronger than the KKarb and FMI materials reinforced with rayon carbon fibres. This is found to be the case when the tensile strengths of KKarb and Sigri are compared (95 and 274MPa, table 4.2), but the flexural strengths of these materials are comparable (about 190MPa) and that of the FMI material is much lower (56-85MPa). Of course, differences in fibre strength cannot explain the differences in flexural strength of the KKarb material in the warp and fill directions (95 and 25MPa respectively, table 4.2). Thus fibre strength has an influence on the tensile strength of the composites, but other factors appear to be more important in controlling flexural strength. However, flexural strength of the composites involves the transverse strength of fibres which may not be much different for the PAN and rayon carbon fibres.

Variations in fibre volume fraction and bundle size, which may have an influence on fibre/matrix interactions and the cracking process, may offset the effect of fibre strength on the composite strength. Some insight into the possible effect of these factors on the strength of composites may be had by comparing KKarb and FMI materials. These materials are both reinforced with rayon carbon fibres so that complications caused by differences in fibre strength are minimised. Table 3.2 shows that the fibre volume

fraction and bundle size of the FMI material (0.5 and 3000 respectively) are greater than for the KKarb material (0.45 and 1000 respectively) although the flexural strength of the FMI material (56-85MPa, table 4.1) is much less than that of the KKarb material (200MPa). This comparison suggests that fibre volume fraction and fibre bundle size are not important in controlling the flexural strength of these materials. However, Granoff et al (1973) found an increase in flexural strength and tensile strength with fibre volume fraction for a rayon carbon fibre and CVD matrix composite which they attributed to a reduction in porosity and restructuring of the matrix. This suggests perhaps that fibre volume fraction for liquid impregnated composites does not influence the matrix structure and hence does not affect the strengths.

Application of the Rule of Mixtures

Values of strength may be calculated from the rule of mixtures equation for strength, Hull (1981), i.e

$$\sigma_c = \sigma_f \ V_f + \sigma_m \ V_m,$$

where σ_c, σ_f and σ_m are the strengths for the composite, fibres and matrix respectively and V_f and V_m are the fibre and matrix volume fractions respectively. The same constraints apply as for the rule of mixtures calculation of elastic modulus. For all the materials half the fibre volume fraction was used as only half

the fibres are in the direction of the tensile load and contribute to the strength. The other half of the fibres are in a direction perpendicular to the load and contribute nothing to the strength. The exact strengths of the fibres and matrix of the KKarb and Sigri materials are not known, therefore values of strength of fibres and matrix found from the literature in table 2.2 will be used for rule of mixtures calculations and the lowest fibre strength values from table 2.2 will be assumed, as for the modulus calculations. For the KKarb material the lowest value of fibre strength, σ_f, from table 2.2 is 620MPa. The exact blend of pitch and resin in the matrix is unknown but an average, from table 2.2, gives the value of matrix strength, σ_m, as 66MPa. Half the fibre volume fraction, V_f, is 0.225 from table 3.2 and the matrix volume fraction, V_m, = 0.38. Substituting these values for the KKarb material in the rule of mixtures equation gives the strength of the KKarb material, σ_{KKarb}, as 165MPa, table 5.2, however a value of σ_{KKarb} = 95MPa, i.e. about half the calculated value, was found in this work.

For the Sigri material the lowest value of fibre strength, σ_f, from table 2.2 is 1600MPa and the average value of matrix strength, σ_m, is 100MPa. Half the fibre volume fraction, V_f, is 0.19 from table 3.2 and V_m = 0.51. Substituting these values for the Sigri material in the rule of mixtures equation gives the strength of the Sigri material, σ_{Sigri}, as 355MPa,

table 5.2, however a value of σ_{Sigri} = 274MPa, i.e. about two thirds the calculated value, was found in this work.

The lower experimental values compared with those from the calculations, table 5.2, can be attributed to poor fibre/matrix bonding, fibre degradation and also to dissimilar strain to failures of the fibre and matrix, Thomas and Walker (1986) state that the strain to failure of resin carbon matrices are 2-3% and for carbon fibres are 0.5-1.4%. There must, however, be other factors not included in the model to account for differences in tensile strength between the warp and fill directions of the KKarb material. Many microstructural features influence strength and one single feature cannot be identified to account for these differences, but several are discussed here.

The graphitised pitch and resin matrix of the KKarb and FMI materials have better alignment and hence higher strengths than the resin matrix of the Sigri material. This might suggest that the KKarb and FMI composites should be stronger than the Sigri composite. However, the reverse is true in practice, and therefore it would seem that the matrix has no influence on strength. If the matrix volume fraction is increased by 0.1 for the KKarb and Sigri materials then the rule of mixtures calculation gives an increase in strength of only 5 and 3.9% respectively. This supports the fact that the

matrix has little influence on the strength of these composites. Fitzer et al (1980a) also found no influence of matrix orientation on bulk strength for a pitch matrix carbon/carbon composite.

Influence of Weave Pattern

An important influence on the strength, which may account for the differences between the KKarb warp and fill directions, is the weave pattern. In a plain weave composite, such as FMI, there is a higher density of stressed bundle cross-over regions compared with composites with satin or hopsack weaves, such as Sigri. It would therefore be expected that plain weaves lead to lower strengths because of the more severe bending of the fibre bundles. Manocha and Bahl (1988) found that the flexural strength of a plain weave carbon/carbon composite was less than for an 8 harness satin-weave carbon/carbon composite. They attributed this to the presence of microcracks at fibre bundle cross over points. Applying this principle to the materials studied here would lead to a predicted ranking for strength, of: KKarb warp direction (satin weave) >Sigri (hopsack weave) >FMI (plain weave). In practice, although the FMI material has the lowest flexural strength, the KKarb and Sigri materials have similar flexural strengths.

Pollock (1990) qualifies the relationship between strength and weave pattern by saying that tensile

strength is a function of the average crimp angle and therefore a possible explanation of this anomaly is that the hopsack weave and 5 harness satin weaves of the Sigri and KKarb materials respectively have similar average fibre curvatures of 4-5°, which were calculated in section 5.2, hence, the materials have similar microcracking, resulting in composites of similar strength. The Krenchel model (Krenchel (1964)) gives a simple method for calculating the effect of weave pattern on strength by modifying the rule of mixtures as follows;

$$\sigma_c = \eta \quad \sigma_f \quad V_f + \sigma_m \quad V_m,$$

and $\eta = \Sigma\ a \cos^4\theta$ where a is the proportion of fibres at angle θ to the load direction. From the schematic representation of the weave patterns in fig 5.1 the KKarb material in the warp direction has about 21% of fibres at 75°, 42% of fibres at 2° and 37% of fibres at 4° which gives a Krenchel factor for the KKarb material in the warp direction, η_{Kw}, of 0.99. The KKarb material in the fill direction has about 61% of fibres at 3.25°, 37% of fibres at 28° and 2% of fibres at 8° which gives a value of η_{Kf} = 0.85. The Sigri material has about 78% of fibres at 6° and 22% of fibres at 1.5° which gives a value of η_S = 0.98. The FMI material when averaged over all parts has about 100% of fibres at 30.1° which gives a value of η_F = 0.56, table 5.3.

Substituting the strength and volume fraction values used in table 5.2 and values of η for the KKarb material into the modified rule of mixtures equation gives σ_{Kw} = 163MPa and σ_{Kf} = 144MPa, table 5.3. The FMI material has the same fibre and matrix precursors as the KKarb material but has V_f = 0.25 and V_m = 0.31 which when substituted into the above equation gives σ_F = 103MPa, table 5.3. Substituting the strength and volume fraction values used in table 5.2 and the value of η for the Sigri material into the equation gives σ_S = 349MPa, table 5.3. This is the same ranking as found in the experimental results, table 5.3, showing that higher crimp angles can account, to some extent, for the KKarb fill and warp directions having different strengths.

Influence of Porosity

The three materials studied have different pore structures and different densities which may have some influence on the strength. According to Oh and Lee (1989) density influences the flexural strength and according to Pollock (1990) it also influences the tensile strength of carbon/carbon composites. For the three materials studied tensile strength increases with density whereas flexural strength does not, tables 4.1, 4.2, 3.2. To a large extent variations in density of these materials reflect variations in total porosity. Pickup et al (1986), and others, used the equation, based on empirical data,

$$X = X_0 \ e^{-bP}$$

to relate a mechanical property X to a nominal value at zero porosity X_0 and to porosity P, where b is a constant related to the pore shape, this equation can equally apply to the strength as to the modulus. If one nominal zero porosity strength value for the KKarb and FMI carbon/carbon composites and a single b value are assumed, as they have the same fibre and matrix precursors, then $X \ \alpha \ e^{-P}$. This leads to a ranking of $X_{KKarb} > X_{FMI}$ which agrees with the ranking found in tables 4.1 and 4.2 for the elastic modulus and flexural strength, possibly suggesting some dependence between total porosity or density and strength.

However a simple dependency of flexural or tensile strength on density seems unlikely as the shape and size of voids determines the stress concentrations in these materials. For example, the major part of the porosity in the Sigri material is in the form of rounded pores, fig 4.5, whereas in the KKarb material porosity is in the form of sharp intrabundle cracks, fig 4.1. This would imply that $b_{KKarb} > b_{Sigri}$ as this is a shape dependent factor and if all other factors are equal this would give a ranking of $X_{Sigri} > X_{KKarb}$ which is true for tensile strength and modulus in tables 4.1 and 4.2 but not for flexural strength in table 4.1. These differences in microstructure lead to

different microcracking mechanisms for flexural fracture, as illustrated in figs 4.23 and 4.27. However, the flexural strengths of KKarb and Sigri materials are comparable, and it appears, therefore, that differences in microstructural porosity do not have a strong influence on flexural strength but it may influence tensile strength. Manocha et al (1988) also concluded that porosity had little or no effect in controlling the flexural strength of resin matrix composites.

In summary, the greater tensile strength of the Sigri material relative to that of the KKarb material in the warp direction, can be attributed mainly to greater fibre strength and density. The difference in flexural and tensile strengths between warp and fill directions for the KKarb material is attributed to the different weave patterns. The closer weaves of the FMI and KKarb materials, in the fill direction, result in microcracking at fibre bundle cross over points, so reducing the composite flexural strength. The lower value of flexural strength for delaminating mode failure of FMI material, compared to shear mode failure, may not be significant in view of the fact that these are estimated values.

FRACTURE MECHANICAL PROPERTIES

The fracture toughness of the Sigri material is 37.6MPa$\sqrt{m}$ and that of the KKarb material is 12MPa$\sqrt{m}$ and

2MPa$\sqrt{m}$ in the warp and fill directions respectively, table 4.2. The values for the KKarb material are similar to those obtained by Sato and Kawamuda (1990), 3-4MPa$\sqrt{m}$, for rayon or PAN carbon fibres in a pitch matrix. The value for the Sigri material is much higher, however. This suggests that the Sigri composite is a tougher material and this is reflected in the tensile fracture surfaces where the Sigri material has longer fibre pullouts compared with the KKarb material, fig 4.34. The fracture toughness values of the KKarb composite obtained from flexural and tensile tests are similar, tables 4.1 and 4.2, perhaps suggesting that the toughness of the KKarb material is the same for both modes of failure. The fracture surface of the KKarb material in the fill direction is almost straight across the specimen, with only slight deviations caused by the fibre bundles. This more brittle mode of fracture is reflected in the lower value of toughness, 2MPa$\sqrt{m}$.

The fracture energy, γ, may be calculated from the fracture mechanics equation relating it to the fracture toughness, K, as described in Knott (1981);

$$\gamma = K^2 / 2 E.$$

For the KKarb composite using K = 12MPa$\sqrt{m}$ and E = 21GPa, from tables 4.1 and 4.2, gives γ = 3.3kJ/m^2 and for the Sigri composite using K = 37.6MPa$\sqrt{m}$ and E =

42.3GPa, from tables 4.1 and 4.2, gives γ = 16.7kJ/m^2. These values are in good agreement with the measured values of 20kJ/m^2 for the Sigri material and 2.9kJ/m^2 for the KKarb material, table 4.2. This agreement is perhaps surprising since the above equation is based upon linear elastic fracture mechanics in which the strain energy in the specimen is quantitatively converted to surface energy in a purely brittle type fracture. The behaviour of carbon/carbon composites are not linear elastic and the fracture processes are complex and far from brittle.

Other workers found fracture energies similar to those of the KKarb composite, Boad (1990), for example, found that the work of fracture for various CVD matrix composites was 2-9kJ/m^2. The large difference between the values for the Sigri and KKarb materials suggests that the extra separation of fibres and matrix involved longer fibre pullout as more frictional work is involved in pulling out a longer fibre over a greater length.

The fracture toughness values increase with notch depth, fig 4.35,4.37, for both the KKarb and Sigri materials. Sakai et al (1991) obtained a similar result for a CVD matrix carbon/carbon composite. The fracture toughness, therefore, does not appear to be a material constant suggesting that linear elastic fracture mechanics is not strictly applicable to these

materials. It might be expected that the tougher Sigri material would have a longer critical crack length. However thw calculations in section 5.2 showed Sigri had critical crack lengths of 6mm and KKarb material of 5mm, this also suggests the limitations of fracture mechanics when applied to these materials.

Harris et al (1988) found, for a wide range of composite precursors and layups, that the fracture toughness and tensile strength had the same linear relationship for all the materials studied, within a wide band, with K/σ=about $0.064\sqrt{m}$. This lead to all composites studied having a critical defect size of about 1mm. As this seemed unlikely, they therefore concluded that fracture mechanics had no meaning when applied to composites. However, for the Sigri and KKarb materials when toughness was plotted against strength, fig 5.3, for different notch depths no correlation between strength and toughness was found for the Sigri material and only a weak correlation found for the KKarb composite. However, if only values in the range where the geometric coefficient Y, described in section 2.3.3.a, is valid, e.g. a/w = 0.3, are considered then $K/\sigma=0.0603\sqrt{m}$ and $K/\sigma=0.184\sqrt{m}$ for the KKarb and Sigri materials respectively. These results confirm that fracture mechanics is not applicable to these composites, because the fracture is a complex process involving debonding of fibres and matrix and

delamination unlike the smooth brittle fracture assumed for linear elastic fracture.

IMPACT ENERGIES

The work of fracture values measured by tensile impact tests were 3.3kJ/m^2 and 10kJ/m^2 for the KKarb and Sigri materials respectively, table 4.2. The work of fracture for the KKarb material is similar to that found from the tensile tests, suggesting there is little, if any, strain rate dependence of the fracture energy. However the Sigri composite work of fracture obtained from the tensile tests is twice that from tensile impact experiments. This implies that the fracture energy of the Sigri material is strain rate sensitive, as was also found for tensile fracture. In the flexural impact mode the works of fracture are 9kJ/m^2 and 15kJ/m^2 for the KKarb and Sigri materials, respectively. The Sigri material has similar work of fracture values for both modes of impact testing, possibly implying that delamination and fibre pullout require similar amounts of energy. The KKarb composite has more delamination cracking in the flexural impact mode than the tensile impact mode and hence has a higher work of fracture in the flexural mode.

5.4 EFFECTS OF OXIDATION ON MICROSTRUCTURE

Preferential oxidation was observed at fibre/matrix interfaces in the three materials studied, all of which

were liquid impregnated, fig 4.11-fig 4.18. Initially the matrix was attacked, and this was followed by slower oxidation of the fibre edges. This was also observed for the chemically etched KKarb and Sigri materials. The carbon layer plane orientation is clearly seen for the etched Aerolor 225 and Dunlop materials, since if the carbon layer planes are aligned perpendicular to the surface they expose the edge atoms of the layer which are reactive with oxygen and so oxidise easily. There are three factors which could explain preferential oxidation of the matrix at fibre/matrix interface, namely stresses, porosity and impurities.

At fibre/matrix interfaces the matrix is stressed during shrinkage on carbonisation. These stressed regions have better alignment of carbon basal plane layers than the bulk matrix, especially if the composite has been heat treated. Goto et al (1986) attribute preferential oxidation at fibre/matrix interfaces to stressed regions in the matrix. Etching of resin carbon matrices shows alignment of the matrix layer planes around fibres, fig 4.19, and where fibres are close together the structure in the matrix meets and disclinations are formed, according to Ragan and Emmerson (1990). It might be expected that disclinations cause high stresses and would therefore be sites of preferential oxidation, but the stresses are perhaps not as high as at the fibre/matrix

interfaces where the oxidation starts. It is well known that graphite is less reactive than glassy carbon, and this would suggest that the more aligned stressed regions of the matrix would be less reactive.

Another possible explanation for preferential oxidation of fibre/matrix interfaces is the large number of cracks and pores in these regions which enable the oxidising gases to reach a large surface area, fig 4.1. Fig 4.19 suggests that oxidation starts at the pores in the Sigri material, and McKee (1987) also found that penetration of gases at fibre/matrix interfaces results in rapid oxidation within bundles with fibre and matrix being oxidised simultaneously. However, if this were the reason for preferential attack it would also be expected that a rapid expansion of pores and inherent intrabundle cracks would be observed. In the materials studied no such expansion of inherent voids was seen, fig 4.12,4.15.

As discussed in section 2.3.4, impurities can act as catalysts to oxidative attack of carbon. There are many impurities in carbon/carbon composites some of which are removed on heat treatment and some of which migrate to the surface of fibres. Preferential attack at these fibre edges might be expected as a result with subsequent attack of the matrix as gases penetrate the interface. However, the present research suggests that

the that matrix is oxidised first, fig 4.14, and the influence of impurities, if any, is not evident.

It is therefore concluded that preferential attack of the matrix at fibre/matrix interfaces was probably caused by stressed regions in the matrix and enhanced by the accessibility of these interfaces, for oxidising gases, through inherent pores and cracks.

5.5 EFFECT OF OXIDATION ON FRACTURE MICROMECHANICS

TENSILE FAILURE

There was no observable change in fracture with weight loss for the Sigri and KKarb materials. The fibre pullout length calculated from

$$l = 24\ \gamma\ /\ \sigma\ V_f$$

can be calculated at 10% weight loss. Reductions of $\gamma_{10}/\gamma_0 = 0.7$, $V_{f10}/V_{f0} = 0.8$ and $\sigma_{10}/\sigma_0 = 0.7$ are assumed for 10% weight loss, these values are estimated from the data in tables 4.2 and from the oxidised micrographs, figs 4.12, 4.15, 4.18. Substituting these values into the above equation gives a change in pullout length as

$$l_{10}/l_0 = \gamma_{10}\ /\ \sigma_{10}\ V_{f10} \times \sigma_0\ V_{f0}\ /\ \gamma_0$$
$$= 1.25$$

The experimental scatter for carbon/carbon composites was found to be about ±15%, therefore if l_{10}/l_0 is not substantially greater than twice the scatter, i.e. 1.30, changes will not be detectable. These calculations suggest that more than a 10% weight loss is needed before increases in fibre pullout length on oxidation are detectable. Therefore higher weight losses than used in these experiments are needed before increses in pullout length are observable.

In the unoxidised composites the PAN carbon fibres and resin carbon matrix were thought to provide worse fibre/matrix adhesion and hence lead to longer fibre pullout, but for the oxidised materials this is no longer the case as the interfaces are destroyed by oxidation. The pullout length for the oxidised composites is determined by the fibre strength, and hence there is still larger pullout for the Sigri material compared with the KKarb material.

FLEXURAL FAILURE

The mode of flexural failure of the KKarb material changed with oxidation from delamination cracking to stepped cross-bundle cracking, fig 4.40, this change of mode was accompanied by a change in the shape of the force/deflection curves from a drastic decrease from peak load to a stepped reduction.

Oh and Lee (1989), who examined the flexural strength of a carbon/carbon composite with plain woven PAN carbon fibre and of a CVD composite, found similar changes to those found in this work. Decreasing deposition temperature or decreasing partial pressure of gas during CVD modified the matrix microstructure, resulting in a more brittle type of failure, which was attributed to a change from a chemical to stronger mechanical bonding of fibre and matrix. Manocha et al (1991) found that graphitisation of a carbon/carbon composite results in more shear deformation. The force/deflection curves became more stepped as the orientation of the matrix sheath around the fibre changed and the fibres could slip more easily.

These examples illustrate the well proven principal of composite theory that an increase in fibre/matrix bonding, brought about by modifications in the matrix microstructure, can lead to a reduction in toughness. In the case of the KKarb material the changes in fracture behaviour on oxidation (from delaminating mode to cross-bundle mode) are brought about by removal of matrix material rather than by modification of matrix microstructure. These changes are accompanied by a transition from a catastrophic failure mode to a more gentle progressive failure mode of the force/deflection curves.

However, for the KKarb composite the fibre/matrix interfaces are attacked on oxidation decoupling the fibres and matrix hence weakening the bundles, whereas bundle/bundle interfaces are not noticeably attacked by oxidation. Therefore the weakest part of the microstructure changes from ply/ply interfaces to fibre/matrix regions within bundles as oxidation progresses and cracks can propagate more easily across bundles.

There was no change in the mode of flexural failure with oxidation for the Sigri material. High stresses in the compressive faces of the samples tend to caused shear cracking and some delamination occurs in the Sigri material and pores dominate fracture as they blunt and deviate cracks. Even though the fibre bundles are weakened following oxidation, facilitating cross bundle cracking, all the cracks are short as they are blunted by pores, fig 4.28. The pores are unaffected by oxidation and therefore the mode of failure is unchanged by oxidation.

The FMI material also shows no change in flexural failure mode with oxidation because the shear mode of fracture is dominated by shear cracking with cracks at bundle cross-over points, fig 4.29. These cross-over points are unaffected by oxidation and are weaker than fibre/matrix regions within bundles so that there is no change in mode of fracture on oxidation. The

delaminating mode of failure of the FMI material, fig 4.29, is caused by cracks inherent in the materials these cracks are unaffected by oxidation.

IMPACT FAILURE

A change in mode of failure in flexural impact on oxidation was observed for the KKarb material, fig 4.47. The amount of delamination cracking was reduced and the amount of cross bundle cracking was increased as in the flexural tests, fig 4.40, and is also attributed to a weakening within the bundles relative to the bundle/bundle interfaces.

For the Sigri materials the mode of failure did not change with oxidation and there was no dominance of any single type of failure. The oxidative attack of fibre/matrix interfaces resulting in the weakening of bundles might be expected to lead to a dominance of cross bundle failure. The fact that this is not observed suggests that delamination cracking requires little energy under impact testing.

5.6 EFFECT OF OXIDATION ON MECHANICAL PROPERTIES

ELASTIC MODULUS

The elastic modulus of the Sigri material increased from 11.5 to 12.5 GPa on oxidation of 10% weight loss when tested by the sonic resonance method, fig 4.42. This is further evidence for the limitations of the

sonic resonance method when applied to carbon/carbon composites and particularly the Sigri material, section 5.3.

If the rule of mixtures for the modulus is applied to composites oxidised to 10% weight loss assuming decsreases of 20% and 30%, estimates from figs 4.12, 4.15, 4.18, for the V_f and V_m respectively then the moduli reduce to 15GPa, 85GPa and 16GPa for the KKarb, Sigri and FMI materials respectively, table 5.4. This gives for all three materials a moduli reduction of between 3 and 21% for 10% weight loss this is similar to the reduction of 30% found for the KKarb material and the 14% found for the Sigri material, table 5.4.

The density was identified as a feature which contributed to the difference in modulus of the unoxidised KKarb and Sigri composites in section 5.3. The relationship between density, ρ, and porosity, P, is given by

$$\rho = \rho_o (1 - P)$$

where ρ_o is the density of the pore free material. At 10% weight loss the equation can be used to give an indication of the change in density;

$$\Delta\rho = \rho_{10} / \rho_0 = (1 - P_{10}) / (1 - P_0),$$

where subscripts 10 and 0 denote values of properties at 10% and 0% weight loss respectively. From figs 4.13 and 4.16 the porosity for the KKarb material increases from 7.5% to 11% for 10% weight loss and the Sigri material porosity increases from 21% to 26% for 10% weight loss. Therefore in the above equation $\Delta\rho_k = 0.96$ for the KKarb material, i.e. a 4% reduction in density for a 10% weight loss, and $\Delta\rho_s = 0.94$, for the Sigri material, i.e. a 6% reduction in density for a 10% weight loss. Therefore the fall in density cannot account for the greater reduction of modulus of the KKarb than the Sigri material.

Oxidation decouples the fibre and matrix at the fibre/matrix interfaces, e.g. fig 4.11, which perhaps implies that the modulus of the oxidised composites depends to a much greater extent on the fibres. This assumption could account for the greater reduction of modulus in the KKarb composite, 28%, compared with the Sigri composite, 14%, table 5.4, since the modulus of the PAN fibres in the Sigri composite is greater than that of the rayon fibres in the KKarb composite, table 2.2.

The FMI material has the same matrix and fibre precursor materials as the KKarb composite, table 3.2. Therefore a similar reduction in modulus for the KKarb and FMI materials might be expected. However the KKarb material has a reduction in modlus of 28%, table 4.3,

whereas the elastic modulus of the FMI material, determined by both experimental methods, falls substantially to a low value for 10% weight loss, fig 4.44, 4.45, table 4.3. However only a small range of weight losses was examined for the FMI composite, and it is therefore difficult to comment on this estimated decrease of modulus. Zhao et al (1985) found a greater percentage decrease in elastic modulus of about 38% for 10% weight loss for their carbon/carbon composite containing random chopped fibres, but they gave no indication of the changes in microstructure after oxidation.

TENSILE AND FLEXURAL STRENGTH

The KKarb material shows a reduction of flexural strength of 43% for 10% weight loss, table 4.3, which is similar to the findings of Zhao et al (1985) of 44% for 10% weight loss, for carbon/carbon composites and those of Pickup et al (1986) for oxidation of nuclear graphites. However, a smaller reduction of 23% in flexural strength for 10% weight loss was found for the Sigri composite, table 4.3.

As noted above, it is difficult to compare the findings of this work with those of Zhao et al (1985) because they gave no details of the effects of oxidation on microstructure. However, the work on oxidation of graphites by Pickup et al (1986) suggests that slit pores with high aspect ratios developed in the graphite

on oxidation, leading to easier crack initiation and a reduction in flexural strength. Despite the increase in porosity of the KKarb and Sigri composites with oxidation, fig 4.13,4.16, there is no similar development of the inherent pores and cracks, and therefore these features are not the cause of the reduction in strength with weight loss. The larger reduction in flexural strength for the KKarb material can perhaps be attributed to the change in fracture mechanism from a delaminating mode to a cross bundle cracking mode. This change in fracture mode is not seen for the Sigri material.

If the rule of mixtures for the strength is applied to composites oxidised to 10% weight loss again assuming decsreases of 20% and 30%, estimates from figs 4.12, 4.15, 4.18, for the V_f and V_m respectively then the tensile strength reduce to 129MPa and 278MPa for the KKarb and Sigri materials respectively, table 5.4. This gives a reduction in tensile strength of 22% which is similar to the experimental reductions of 29% for the KKarb material and 37% for the Sigri material for a 10% weight loss, table 5.4. The slightly greater decrease of tensile strength for the Sigri materials of 37%, tablke 4.4 compared with the 29% reduction for the KKarb material is perhaps caused by the slightly greater decrease in density of the Sigri material of 6% compared with 4% for the KKarb material, as calculated earlier in this section. Again, the decoupling of the

fibre and matrix on oxidation, e.g. fig 4.14, leads to an increase in the role of fibres in determining the strength.

The fracture toughness of the composites is proportional to the strength, see equation in section 3.3.3, for these materials. Therefore the reduction, for 10% weight loss, in fracture toughness is the same as the reduction in strength i.e. 29% and 37% for the KKarb and Sigri materials respectively, table 4.4. This suggests that oxidation has the same effect on crack growth resistance for both materials. From flexural results, fig 4.39, the toughness of the KKarb composite was reduced by 57% for 10% weight loss. This is higher than the 48% found by Zhao et al (1985), and perhaps the reduction for the KKarb material can again be attributed to the change in fracture mechanism. Although it is more likely that the value from the three pioint bend tests is unreliable as the fracture energy is dificult to determine. For this reason further values of the toughness for the other materials were not calulated.

The work of fracture, from tensile tests, decreases by 71% for 10% weight loss for the Sigri composite whereas it decreases by only 34% for the KKarb compositetable 4.4. This difference can possibly be explained by the reduction in the work required to pullout a fibre as the fibre/matrix bonding is reduced on oxidation. The

unoxidised Sigri material has a larger component of pullout work than the KKarb material leading to a greater reduction in work of fracture for the oxidised Sigri material.

The critical crack length calculated from

$$c = 1 / \pi \times (K / \sigma)^2$$

is 5mm and 6mm for the KKarb and Sigri materials respectively, the same as values calculated in section 5.2. This shows that critical crack length does not change with oxidation since the strength and toughness decrease by similar amounts on oxidation. From three point bend tests the work of fracture of the KKarb composite decreases by 76% for 10% weight loss compared with the 37% found by Zhao et al (1985). However again the suitabilty of these values is questionable and the calculations were not repeated for other materials.

IMPACT ENERGIES

The work of fracture in flexural impact for the Sigri and KKarb composites is reduced by 62% and 42% respectively, table 4.3, for 10% weight loss which is the reverse trend of the 43% and 23% for the KKarb and Sigri material flexural strengths respectively. The reductions for fast strain rate and for slow strain rate tests for the KKarb material are similar to each other, table 4.3. By contrast the Sigri material

reduces by 62% for fast strain rate and by 23% for slow strain rate experiments, tables 4.3.

Tensile impact fracture energy decreases by 18 and 35% with 10% weight loss for KKarb and Sigri respectively, table 4.4. This is much less than the reduction of flexural impact of 42% and 62% for the KKarb and Sigri materials respectively, table 4.3. Again, the interfaces are reduced on oxidation and, as in the tensile tests, energy is not now required to debond the fibre and matrix. The fracture energy falls to the same value around $6kJ/m^2$, table 4.4, for the Sigri material from both tensile and tensile impact samples, suggesting perhaps that the strain rate dependence is removed with oxidation and reduction of fibre/matrix interface adhesion.

5.7 SUMMARY

The fibre properties were found to be a major contributor to the modulus and strength of the composites studied, leading to higher tensile strength and modulus values for the Sigri composite. The importance of fibre properties increased substantially for the oxidised composites. The weave patterns were found to contribute to the lower properties of the tightly woven FMI and KKarb (fill direction) materials, because of the microcracks at the bundle cross over points.

The Sigri material had poor fibre/matrix adhesion, as shown by the long fibre pullout in tensile failure, and it has some strain rate dependence of tensile properties. The flexural impact modes of failure were different from the flexural test fracture for the Sigri and FMI materials because of the greater strain rates on impact. On oxidation the mode of failure did not change for the Sigri and FMI materials, but they did change for the KKarb material for flexural impact and flexural tests. This was attributed to the weakest part of the microstructure changing from ply interfaces to intra-bundle regions. However the Sigri and FMI failure mechanisms are dominated by pores and microcracks respectively which are unaffected by oxidation.

There was a greater reduction of flexural strength with weight loss for the KKarb material compared with the Sigri composite which was attributed to the change in faulure mode. On oxidation the fibre modulus becomes the main contributor to the composite modulus. As the matrix modulus was a larger portion of the fibre modulus for the KKarb material, compared with the Sigri composite, the KKarb composite exhibited a greater reduction in modulus on oxidation.

CHAPTER 6 CONCLUSIONS AND SUGGESTIONS FOR FURTHER WORK

6.1 CONCLUSIONS

The principal findings of this work are summarised in this chapter starting with the findings for the unoxidised materials. The effects of oxidation on the mechanical properties are considered next and the chapter concludes with some suggestions for future work.

UNOXIDISED COMPOSITES

The modulus of the Sigri material was higher than for the KKarb and FMI materials; this is attributed to the greater modulus of the PAN fibres used in the Sigri composite and lower density of the KKarb and FMI materials. The closer weave patterns of the KKarb composite (fill direction) and the FMI composite are a possible further cause for their lower modulus compared with the KKarb material (warp direction).

The flexural strength of the Sigri and KKarb (warp direction) materials were similar and they were greater than that for the KKarb (fill direction) and FMI materials. This can be attributed to the higher strength of the PAN fibres in the Sigri material and the lesser extent of cracking in bundles and the more open weave of the KKarb material in the warp direction. The FMI and KKarb (fill direction) materials have high

stresses and microcracks at fibre cross over points which contribute to their lower strengths.

As the span to depth ratio increases the KKarb (warp direction) and Sigri composites fail with increasing amounts of delamination, although the extent of delamination is less in the Sigri material because cracks are blunted by pores. The accompanying force/deflection curves show a change from a gradual decrease after peak load to a more stepped and catastrophic reduction after peak load. The FMI material fails in one of two modes; either by delamination of a few plies or by shear at 45^{o} to the compressive face.

The tensile strength of the Sigri material was higher than that of the KKarb material. This is attributed to the Sigri composite being a tougher material that the KKarb composite, as demonstrated by the extensive fibre pullout of 5 to 10mm for the Sigri material compared with fibre pullout lengths of about 2mm for the KKarb material. There is also less intrabundle cracking in the Sigri material. Tensile fracture and tensile properties of the Sigri composite were found to be strain rate dependent. Fracture mechanics was found to be inapplicable to the Sigri material and of questionable value when applied to the KKarb material.

OXIDISED COMPOSITES

The matrix of all three carbon/carbon composites investigated was initially oxidised at fibre/matrix interfaces; this is caused by stressed regions in the matrix which were established during carbonisation, and is enhanced by the ability of gases to penetrate through inherent and developed cracks and pores at these interfaces.

Similar reductions in elastic modulus of about 20% were found after oxidation of the Sigri and KKarb composites to 10% weight loss. After oxidation the flexural strength of the KKarb (warp direction) composite fell by 54% for 10% weight loss and the Sigri composite was reduced by only 23% for 10% weight loss. These differences in reduction of flexural strength with oxidation were attributed to different fracture mechanisms for the two composites, which, in the case of the KKarb composite, are affected by oxidation as discussed below.

The flexural mode of failure of the KKarb material changed with oxidation from a delaminating failure to stepped, cross-bundle cracking. This was attributed to the selective oxidation of the fibre/matrix interfaces within bundles on oxidation making this region weaker than ply/ply interfaces and hence facilitating cross bundle cracking as oxidation proceeds. The force/deflection curves changed from catastrophic to

stepped reduction in force. The Sigri and FMI materials showed no change of fracture mechanism on oxidation. For the Sigri material flexural fracture mechanism is dominated by pores and the FMI material fracture is dominated by microcracks at the fibre-bundle cross-over points. Oxidation enhances the effect of these features, resulting in no change in fracture mechanism and therefore no change in force/deflection curves.

The decoupling of the fibre and matrix on oxidation leads to greater influence of the fibres on the tensile strength, resulting in similar reductions of strength on oxidation for the KKarb and SIgri composites.

A number of general conclusions emerge from this study regarding the mechanical properties of woven 2D carbon/carbon composites. First, these materials are highly heterogeneous so that there is a large amount of scatter in the results of mechanical tests. This is linked to the observation that there is often some variation in the failure mode from specimen to specimen when tested under the same conditions. An example is the flexural failure of specimens of the FMI material which divide into two different modes: delaminating failure or shear failure, fig 4.?. Therefore the extreme scatter of results appears to be an inherent feature of mechanical testing of carbon/carbon composites which must be accepted when working with these materials.

Second, although the three materials which were most intensilvely studied in this work fall within the general class of 2D woven carbon/carbon composites, their fracture modes under constant test conditions were often very different from each other. For example, in flexural strength tests the KKarb material fails by delamination of plies whereas the Sigri material fails by a mixture of, delamination, cross-bundle cracking and shear. These differences reflect the different starting materials, composite construction and processing conditions of the composites. The sensitivity of the properties of these composites to these factors makes it difficult to develop generalisations about their structure/property relationships, although some trends have been identified in this work.

The diverse nature of these composites leads to a large scatter of experimental results, this and the reduction in strength observed on oxidation mean that careful consideration must be given to the properties of these materials when designing components

6.2 FUTURE WORK

Weave patterns and fibre properties have been identified as crucial features for mechanical properties. Studies of one material with different

fibre types and different weave patterns could verify, or perhaps qualify, the findings of this thesis.

To complete this work more extensive studies of the FMI material would be useful, as it has some of the same features of the KKarb material, i.e. the same fibre and matrix type and similar, if more extensive, cracking.

On oxidation the pores of the Sigri material and the crimp angle of the FMI material were more important to the fracture process than the effects of oxidation at fibre/matrix interfaces. Studies of liquid-impregnated carbon/carbon composites with various crimp angles and different shapes and sizes of pores could perhaps establish the relative importance of these features for oxidised and unoxidised composites.

Investigations into CVD matrix carbon/carbon composites following the same set of experiments as for this work would be useful to give a further comparison of results.

REFERENCES

Albugues, F. and Grenie, Y. (1985). The fabrication and the process characteristics of high performance multidimensional carbon carbon composites. Proc 15th Biennial Conf. on Carbon, Philadelphia, June 1985, pp. 276-277.

Bacon, R. (1973). Carbon fibres made from rayon precursors. Chemistry and Physics of Carbon, **13**, 2-95. (P.L. Walker Jr and P.A. Thrower eds.) New York: Marcel Dekker.

Bahl, O.P., Dhami, T.L. and Manocha, L.M. (1989). Oxidation behaviour of different carbon carbon composites. Proc 19th Biennial Conf. on Carbon, Philadelphia, June 1989, pp.310-311.

Bashir, K. (1988). The development of phenolic resin based carbons with improved high temperature oxidation resistance. Ph.D. thesis, School of Materials Science, University of Bath.

Bennett, S.C. and Johnson, D.J. (1979). Electron microscopy studies of structural heterogeneity in PAN based carbon fibres. Carbon, **17**, 25-39.

Boad, S. (1990). Private communications.

Bradshaw, W.G., Pindi, P. and Kartak, R.F. (1977). Correlation between structure and properties of chopped fibre carbon carbon composites. Proc. 13th Biennial Conf. on Carbon, Irvine, California, July 1977, pp. 126-127.

Bradshaw, W.G. and Vidoz, A.E. (1978). Fibre/matrix interactions in unidirectional carbon carbon composites. Am. Ceram. Soc. Bull., **57**, 193-198.

Brocklehurst, J.E. (1972). Fracture in polycrystalline graphite. Chemistry and Physics of Carbon, **13**, 145-279. (P.L. Walker Jr and P.A. Thrower eds.) New York: Marcel Dekker.

Chang, T. and Okura, A. (1986). Fabrication method for carbon carbon composites and their properties. Composite '86: Proc 3rd Japan-US Conf. on Composite Materials, Tokyo, pp.425-432.

Cottrell, D. (1964). Proc. Royal Soc., **A282**, pp 2-8.

Crawford, D. (1972). PhD Thesis, Department of Textile Industries, University of Leeds.

Dacic, B. and Marinkovic, S. (1987). Kinetics of air oxidation of unidirectional carbon fibre/CVD carbon composites. Carbon, **25**(3), 409-415.

Deviney, M.L. and O'Grady, T.M. eds. (1976). Petroleum Derived Carbons. Washington DC: Am. Chem. Soc. ACS Symposium Series 21, pp.212-227.

Dimitrijevic, S. and Kaluderovic, B. (1986). Microhardness of carbon fibre/CVD carbon composites. Proc. Carbon '86, Baden-Baden, Germany, June 1986, pp.726-727.

Dimitrijevic, S. and Marinkovic, S.(1987). Description of CVD carbon infiltration of porous substrate. Proc. 18th Biennial Conf on Carbon, Worcester, USA, June 1987, pp. 430-431.

Donnet, J-B. and Bansal, R.C. (1984). Carbon Fibres. New York and Basel: Marcel Dekker. International fibre science and technology series, volume 3.

Dorey, G. (1987). Carbon fibres and their applications. J. Phys. D: Appl. Phys., **20**, 245-256.

Dresselhaus, M.S., Dresselhaus, G., Sugihara, K., Spain, I.L. and Goldberg, H.A. (1988). Graphite Fibres and Filaments. Berlin: Springer-Verlag.

Edie, D.D. (1989). Pitch and mesophase fibres. In Carbon fibres and filaments: Proc of a NATO Advanced Study Institute, Alvor, Portugal, May 1989 (J.L.Figueiredo, C.A. Bernado, R.T.K. Baker and K.J. Huttinger, eds.), pp. 43-72. Dordrecht, Netherlands: Kluwer Academic Publishers.

Ehrburger, P. (1989). Protective layers for special types of composites. In Carbon fibres and filaments: Proc of a NATO Advanced Study Institute, Alvor, Portugal, May 1989 (J.L.Figueiredo, C.A. Bernado, R.T.K. Baker and K.J. Huttinger, eds.), pp. 327-336. Dordrecht, Netherlands: Kluwer Academic Publishers.

Ehrburger, P., Lahaye, J. and Borgeois, C. (1981a). Characterisation of carbon carbon composites :I textural and microstructural properties. Carbon, **19**, 1-5.

Ehrburger, P. and Lahaye, J. (1981b). Characterisation of carbon carbon composites :II oxidation behaviour. Carbon, **19**, 7-10.

Fitzer, E. and Terwiesch, B. (1972). High temperature strength of carbon-carbon composites up to 2000^{o}C. High Temp. High Press., **4**, 359-362.

Fitzer, E., Heuttner, W. and Manocha, L.M. (1980a). Influence of process parameters on the mechanical properties of carbon carbon composites with pitch as matrix precursor. Carbon, **18**, 291-295.

Fitzer, E., Geigl, K.H. and Heuttner, W. (1980b). The influence of carbon fibre surface treatment on the mechanical properites. Carbon, **18**, 265-270.

Fitzer, E. (1987). The future of carbon carbon composites, Carbon, **25**(2), pp.163-196.

Fitzer, E. (1989a). Carbon fibres - present state and future expectations. In Carbon fibres and filaments: Proc of a NATO Advanced Study Institute, Alvor, Portugal, May 1989 (J.L.Figueiredo, C.A. Bernado, R.T.K. Baker and K.J. Huttinger, eds.), pp. 3-42. Dordrecht, Netherlands: Kluwer Academic Publishers.

Fitzer, E. (1989b). Carbon fibres and composites. In Carbon fibres and filaments: Proc of a NATO Advanced Study Institute, Alvor, Portugal, May 1989 (J.L.Figueiredo, C.A. Bernado, R.T.K. Baker and K.J. Huttinger, eds.), pp. 169-219. Dordrecht, Netherlands: Kluwer Academic Publishers.

Forrest, M.A. and Marsh, H. (1982). The effect of carbonisation at high pressure on structure in the matrix carbon of carbon carbon composites. Proc 6th Int. Conf. on Carbon and Graphite, London, Sept 1982, pp.288-290.

Fourdeux, A., Perret, R. and Ruland, W. (1971). General structural features of carbon fibres. Proc. 1st Int. Conf. on Carbon fibres, Plastics Institute, London, pp57-62.

Gill, R.M. (1972). Carbon Fibres for Composite Materials. London: Iliffe books, for the Plastics Institiute.

Granoff, B., Pierson, H.O. and Schuster, D.M. (1973). Dependence of thermal and mechanical properties on fibre volume percent. J. Composite Materials, **7**, 36-52.

Goto, K.S., St Pierre, G.R. and Han, K.H. (1986). A review of oxidation kinetics of carbon fibre/carbon matrix composites at high temperatures. Trans. I.S.I.J., **26**, 597-603.

Harris, B., Dorey, S.E. and Cooke, R.G. (1988). Strength and toughness of fibre composites. Composites Science and Technology, **31**, 121-141.

Heuttner, W. and Keuscher, G. (1983). Carbon/carbon hip joint stems. Proc 16th Bienn. Conf. on Carbon, San Diego, July 1983, pp 486-487.

Heuttner, W. (1989). Potential of carbon/carbon composites as structural materials. Proc of a NATO Advanced Study Institute, Alvor, Portugal, May 1989 (J.L.Figueiredo, C.A. Bernado, R.T.K. Baker and K.J.

Huttinger, eds.), pp. 275-300. Dordrecht, Netherlands: Kluwer Academic Publishers.

Hull, D. (1981). An introduction to composite materials. Cambridge: Cambridge University press.

Hishiyama, Y., Inagaki, M., Kimura, S. and Yamada, S. (1974). Graphitisation of carbon fibre/glassy carbon composites. Carbon, **12**, 249-258.

Ismail, I.K. and Vangness, M.D. (1988). On the improvement of carbon fibre/matrix adhesion. Carbon, **26**(5), 749-751.

Jenkins, G.M. and Kawamura, K. (1976). Polymeric Carbons - Carbon Fibre, Glass and Char. Cambridge: Cambridge university press.

Jenkins, G.M. and Carvalho, F.X. (1977). Biomedical applications of carbon fibre reinforced carbon in implant prothesis. Carbon, **15**, 33-37.

Johnson, D.J. and Tyson, C.N. (1969). The fine structure of graphitised fibres. J. Phys. D: Appl. Phys., **2**, 787-795.

Johnson, D.J. (1987). Structural studies of PAN-based carbon fibres. Chem and Phys of Carbon, **20**, 1-55, (P.A. Thrower ed.) NY:Marcel Dekker.

Jones, L.E., Thrower, P.A. and Walker, P.L. jr. (1986). Reactivity and related microstructure of 3D carbon carbon composites. Carbon, **24**(1), 51-60.

Jortner, J. (1976). Proc. USA Army Symp. on Solid Mechanics, Cape Cod, pp 123-132.

Jortner, J. (1986) Macroporosity and interface cracking. Carbon, **24**, 603-613.

Kasatochkin, V.I., Korshak, V.V., Kubdryavtsov, Y.P., Sladkov, A.M. and Sterenberg, I.E. (1973). On crystalline structure of carbyne. Carbon, **11**, 70-72.

Kevans, R.J., Hay, R.S., Pagano, N.J. and Parthasarathy, T.A. (1989). The fibre-matrix interface in ceramic composites. Am. Ceram. Soc. Bull., **68**(2), 429-435.

Knott, J.F. (1981). Fundamentals of fracture mechanics. London: Butterworths.

Kohno, T., Kurosaki, K. and Herai, T. (1991). Effect of ply thickness on the mechanical properties of 2-dimensional carbon/carbon composites. Proc 20th Biennial Conf. on Carbon, Santa Barbara, USA, June 1991, pp.394-395.

Kowbel, W. and Shan, C.H. (1990). Mechnisms of fibre-matrix interactions in carbon carbon composites. Carbon, **28**, 287-300.

Krenchel, H. (1964). Fibre reinforcement. Copenhagen: Akademisk Forlag.

Kroto, H. (1990). Carbon Particles in Space, Stars and on Earth. Proc. IOP, Engineering Physics Divisional Conf., Coventry, Dec. 1990, pp. 68-69.

Lahaye, J., Lowys, F. and Ehrburger, P. (1989). The reactivity of carbon carbon composites. Carbon, **28**(1), 137-142.

Lewis, R.T. and Bacon, R. (1989). Orientation of mesophase pitch on carbon and ceramic surfaces. Proc 19th Biennial Conf. on Carbon, Philadelphia, June 1989, pp.248-249.

Luthra, K.L. (1988). Oxidation of carbon carbon composites - A theoretical analysis. Carbon, **26**(2), 217-224.

McAllister, L.E. and Taverna, A.R. (1971). Three dimensionally reinforced carbon/carbon composites. Proc 10th Bien. Conf. on Carbon, Bethlehem, PA, June 1971, pp.66-67.

McKee, D.W. (1987). Oxidation behaviour and protection of carbon carbon composites. Carbon, **25**, 551-557.

Manocha, L.M. and Bahl, O.P. (1988). Influence of carbon fibre type and weave pattern on the development of 2D carbon carbon composites. Carbon, **26**(1), 13-21.

Manocha, L.M., Yasuda, E., Tanabe, Y. and Kimura, S. (1988). Effect of carbon fibre surface treatment on mechanical properties of carbon carbon composites. Carbon, **26**(3), 333-334.

Manocha, L.M., Bahl, O.P. and Singh, Y.K. (1989). Carbon carbon composites with different carbon fibres. Proc 19th Biennial Conf. on Carbon, Philadelphia, June 1989, pp.282-283.

Manocha, L.M., Bahl, O.P. and Singh, Y.K. (1991). Abnormal behaviour during graphitisation of carbon/carbon composite made with pitch based carbon fibres. Carbon, **29**(3), 351-360.

Marinkovic, S. and Dimitrijevic, S.(1985). Carbon carbon composities from CVD. Carbon, **23**, pp.691-699.

Marinkovic, S. and Dimitrijevic, S.(1986). The influence of CVD process constraints on the formation of carbon carbon composites. Proc. Carbon '86, Baden-Baden, Germany, June 1986, pp.687-689.

Markovic, V., Marinkovic, S. and Marsh, H. (1981). Aspects of formation of carbon/carbon fibre composites by co-carbonisation of PAN fibres and matrix precursor. Proc 15th Biennial Conf. on Carbon, Philadelphia, June 1985, pp.272-273.

Mochida, I., Itoh, I., Korai, Y., Fujitsu, H. and Takeshita, K. (1985). Catalytic graphitisation of carbon fibres. Proc 15th Biennial Conf. on Carbon, Philadelphia, June 1985, pp.308-309.

Oh, S-M and Lee, J-Y. (1988). Effect of microstructure on the mechanical properites of carbon carbon composites. Carbon, **26**(6), 769-776.

Oh, S-M, Lee, J-Y and Sohn, K-Y. (1988). Failure behaviour of carbon carbon composites prepared by CVD. Carbon, **26**(2), pp.157-162.

Oh, S-M and Lee, J-Y. (1989). Fracture behaviour of 2D carbon carbon composites. Carbon, **27**(3), 423-451 .

Olry, P. Choury, J.J. and Christin, F. (1990). Novoltex: Un nouveau concept de renfort tridimensionnel pour composite carbone carbone. Proc. Carbone '90, Paris, July 1990, pp. 478-479.

Phillips, D.C. (1972). The fracture energy of carbon fibre reinforced glass. J. Mater. Sci., **7**, 1175-1191

Pickup, I.M., McEnaney, B. and Cooke, R.G. (1986). Fracture processes in graphite and the effects of oxidation. Carbon, **24**(5), 535-543.

Pollock, P.B. (1990). Tensile failure of 2D carbon carbon composites. Carbon, **28**(5), 717-723

Ragan, S. and Emmerson, G.T. (1990). Disclinations in the matrix architecture of phenolic based carbon carbon composites. Proc. Carbone '90, Paris, July 1990, pp 484-485.

Rand, B. and McEnaney, B. (1985). Carbon binders from polymeric resins and pitch. Br. Ceram. Trans. J., **85**(5), pp. 157-162

Reynolds, W.N. and Sharp, J.V. (1974). Crystal shear limit to carbon fibre strength, Carbon, **12**, 103-110.

Sakai, M., Miyajima, T. and Inagaki, M. (1991). Fracture toughness and fibre bridging of carbon fibre reinforced carbon composites. Composites Science and Technology, **40**(3), 231-250.

Sato, S. and Kurumuada, A. (1989). Tensile properties and fracture toughness of carbon fibre felt reinforced

carbon carbon composites at high temperatures. Carbon, **27**(6), 791-803.

Savage, G. (1988). Carbon carbon composite materials. Metals and Materials, **4**, 544-548.

Sheaffer, P.M. (1989). Single filament bonding in carbon carbon composites. Proc. 19th Biennial Conf. on Carbon, Philadelphia, June 1989, pp.242-243.

Sing, K.S.W., Everett, D.H., Haul, R.A.W., Moscou, L., Pierotti, R.A., Rouquerol, J. and Siemieniewska, T. (1985). IUPAC. Reporting physorption data for gas/solid systems with special reference to determination of surface area and porosity. Pure and Applied Chemistry, **57**(4), 603-619.

Smith, E.A. (1970). Design engineering series: Carbon Fibres. London: Morgan-Grampian Ltd.

Tanamura, T., Tatsumi, N., Narisawa, M., Shioyama, H., Kea, S., Adachi, M. and Souma, I. (1990). Fracture behaviour of 3D carbon/carbon composite by 3 point bend test with various span to depth ratios. Proc. Carbone '90, Paris, July 1990, pp. 510-511.

Tibbetts, G.G. (1989). Vapour grown carbon fibres. In: Carbon Fibres and Filaments: proc of a NATO Advanced Study Instuitute, Alvor, Portugal, May 1989 (J.L.Figueiredo, C.A. Bernado, R.T.K. Baker and K.J. Huttinger, eds.), pp. 73-94. Dordrecht, Netherlands: Kluwer Academic Publishers.

Thomas, J.M. (1965). Microscopical studies of graphite oxidation. Chem. and Phys. of Carbon, **1**, 122-203. (P.L. Walker jr ed.) NY: Marcel Dekker.

Thomas, C.R. and Walker, E.J. (1986). Carbon carbon composites. Materials in Aerospace: Proc. first Int. conf., London, April 1986, pp. 138-167.

Walker, P.L. jr., Shelef, M. and Anderson, R.A. (1968). Catalysis of carbon gasification. Chemistry and Physics of Carbon, **4**, 287-383. (P.L. Walker Jr and P.A. Thrower eds.) New York: Marcel Dekker.

Ward, P.J. (1986). Microstructural features of carbon carbon composites. M.Sc. thesis, University of Sheffield, Sheffield.w

Watt, W and Johnson, W. (1971). Carbon fibres from 3 denier PAN textile fibres. Proc. 3rd Conf. on Industrial Carbons and Graphite, London, April 1970, pp. 417-426.

Weiss, R. (1990). Carbon/carbon - a family of materials. Proc Int. Symp. on Carbon. Tsukuba, Japan, Nov 1990, pp. 10-14.

Weisshaus, H. and Kenig, S. (1990). Carbon/carbon composite Processing - Microstructure - Property relationships. Proc. Carbone '90, Paris, July 1990, pp. 490-491.

White, J.L., Ng, C.B., Buechler, M. and Watts, E.J. (1985). Microstructure of Mesophase pitch. Proc. 15th Biennial Conf. on Carbon, Philadelphia, June 1985, pp. 310-311.

White, J.L. and Sheaffer, P.M. (1989). Pitch based processing of carbon carbon composites. Carbon, **27**(5), 697-707.

Williams, J.M. and Imprescia, R.J. (1975). Improvemnt in oxidation resistance of the leading edge thermal protection for a space shuttle. J. Spacecraft, **12**(3), 151-157.

Zhao, J.X., Bradt, R.C. and Walker, P.L. jr. (1985). Effect of air oxidation at 873K on the mechanical properties of carbon carbon composites. Carbon, **23**(5), 9-15.

Flexural strength (MPa)	50-800
Interlaminar shear strength (MPa)	8-40
Elastic modulus (GPa)	17-130
Tensile strength (MPa)	35-500

Table 2.1 Mechanical properties for carbon carbon composites from literature and manufacturers.

	Fibre Type			Matrix type		
	Pitch	PAN	Rayon	CVD	Pitch	Resin
Tensile strength (MPa)	1720-2760	1600-3100	620-2520	–	22-42	90-110
Elastic Modulus (GPa)	193-830	200-517	28-517	–	12	23-32

Table 2.2 Mechanical properties of the fibres and matrix materials. from Ward (1986) and Rand and McEnaney (1985)

CLOTH/PAPER	SIZE	TIME	LUBRICANT
Wet and Dry Silicon Carbide paper	320	10 s until flat	Water
	500	20 s	
	1000	30 s	
	4000	1 min until no scratches	
PAN W Cloth	3µm	2 min	Struers DP
DUR 1 Cloth	1µm	2 min	Struers lubricant Red
OPS Cloth		2 min	Struers OP-S Suspension

Table 3.1 Polishing routine for mounted specimens

Manufacturer *	Material	Fibre type	Matrix type	Fibre diameter (μm)	Fibre volume fraction	Porosity (%)	Density (g/cm^3)	Bundle size (fibres/ tow)
KKarb	Type A	Rayon	Resin/pitch	7.6	0.45	17	1.36	1000
FMI		Rayon	Resin/pitch	8.3	0.5	19	1.28	3000
Dunlop		PAN	CVD	8.2	0.25	13	1.8	-
	CC1001G	PAN	Resin	7.6	0.4	18	1.12	3000
Sigri	CC1501G	PAN	Resin	6.3	0.38	11	1.4	5000
	CC1506G	PAN	Resin	6.3	0.23	14	1.22	10000
	05	PAN	CVD	6.8	0.27	20	1.7~	-
Aerolor	05BT	PAN	CVD	6.2	0.25	19	-	-
	223	PAN	Resin/CVD	7.6	0.25	12	1.4~	-

~from manufacturer's data

* manufacturers addresses given in table 3.4

Table 3.2 General Characteristics of the Composites

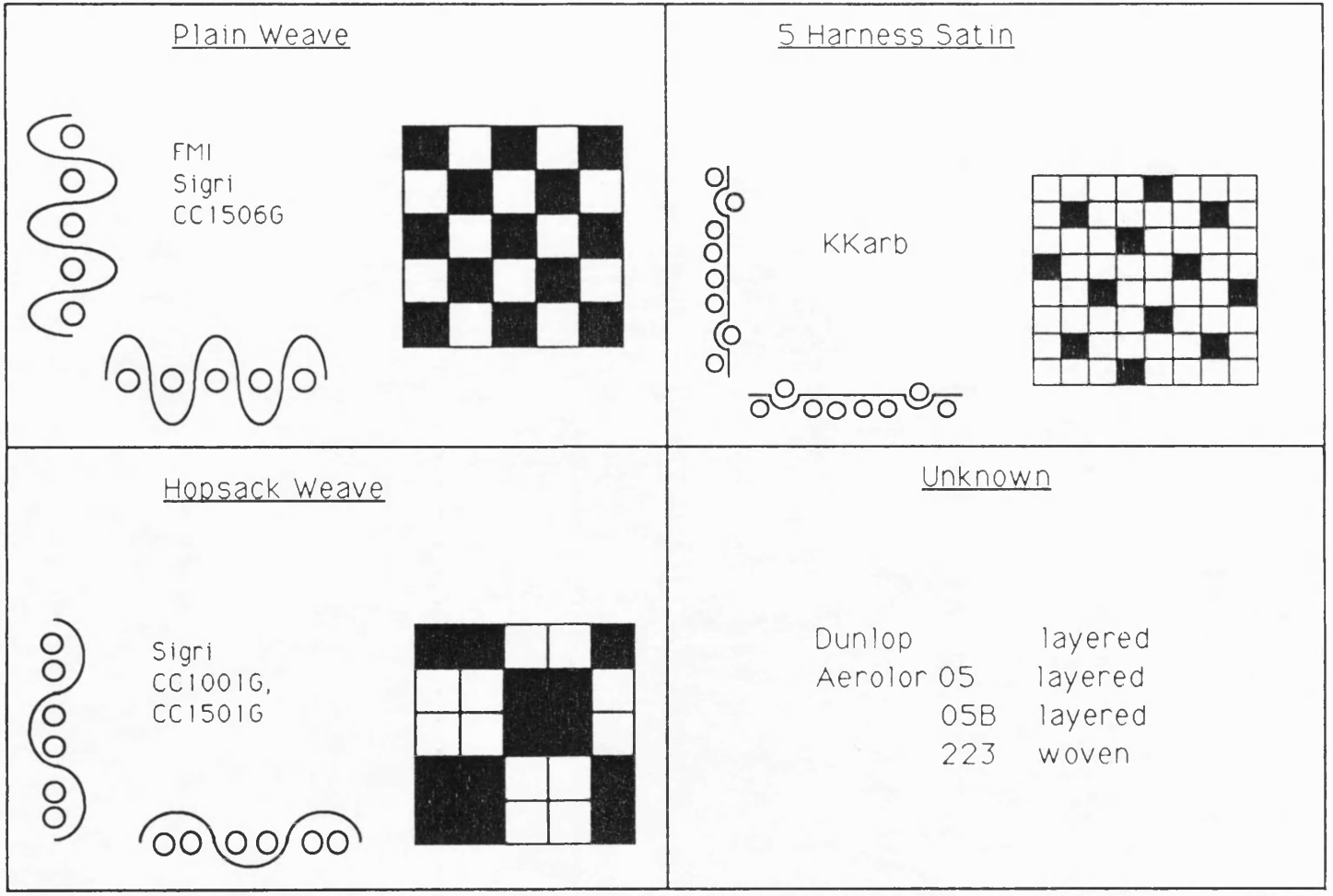

Table 3.3 Weave Patterns of the Composites

Material	Manufacturer	Addresses
KKarb	Kaiser Aerotech	PO Box 1678, San Leandro, California, USA.
FMI	FMI Composites Ltd.	3 Queen St, Galashiels, Selkirkshire.
Dunlop	Dunlop PLc.	Holbrook Lane, Coventry, Warwickshire.
Sigri	Sigri GmbH	Hoechst UK Ltd, Stainland Works, Holywell Green, W. Yorks.
Aerolor	Le Carbone (UK) Ltd.	South St, Portslade, Sussex.

Table 3.4 Manufacturers Addresses

Material	Flexural Strength MPa	Elastic Modulus GPa		Flexural Impact Energy kJ/m²
		resonance method	L/d plot	
KKarb (warp)	200±40	19.4±1.2	24.4±1.9	9±.7
KKarb (fill)	105.2±6	9.5±1	-	4.5±.5
Sigri	182.6±25	11.5±.7	42.3±10	15±3.6
FMI	70*	10*	15*	17.8
delaminating mode	56.3*	7.5*	7*	-
shear mode	85.5±5	14*	21*	-

* estimated values

Table 4.1 Flexural Properties of Unoxidised Composites

Material	Tensile Experiments			Tensile Impact Energy kJ/m^2
	Tensile Strength MPa	Fracture Toughness $MPa\sqrt{m}$	Fracture Energy kJ/m^2	
KKarb (warp)	95±13.1	12±2	2.9±.2	3.3±.4
KKarb (fill)	25	2	12.6	-
Sigri	274±47	37.6±4.9	20±5	10±3.6

Table 4.2 Tensile Properties of Unoxidised Composites

Material		Flexural Strength MPa	Elastic Modulus GPa		Flexural Impact Energy kJ/m^2
			resonance method	L/d plot	
KKarb (warp)		115 (43%)	14.2 (27%)	17 (30%)	5.2 (42%)
Sigri		141 (23%)	12.5	36 (14%)	5.7 (62%)
FMI	delam.	25* (55%)	3* (60%)	1 (86%)	-
	shear	5* (~100%)	3* (79%)	-	-

* estimated values (x%) percentage reduction

Table 4.3 Flexural Properties of Oxidised Composites at 10% Weight loss

Material	Tensile Experiments		Tensile Impact Energy kJ/m^2
	Tensile Strength MPa	Fracture Energy kJ/m^2	
KKarb (warp)	67.5 (29%)	1.9 (34%)	2.7 (18%)
Sigri	173 (37%)	5.7 (71%)	6.5 (35%)

(x%) percentage reduction

Table 4.4 Tensile Properties of Oxidised Composites at 10% weight loss

Material	Fibre volume fraction Vf	Fibre Modulus Ef (GPa)	Matrix volume fraction Vm	Matrix Modulus Em (GPa)	Composite Modulus Ec (GPa)	Experimental Modulus (GPa)
KKarb	0.45	250	0.38	20	119	24
KKarb	0.45	28	0.38	20	19	24
Sigri	0.38	350	0.51	24	145	42
Sigri	0.38	250	0.51	24	88	42
FMI	0.5	28	0.31	20	20	15

Table 5.1 Modulus rule of mixtures values

Material	Fibre volume fraction Vf	Fibre Strength sf (MPa)	Matrix volume fraction Vm	Matrix Strength Em (MPa)	Composite Strength Ec (MPa)	Experimental Strength (MPa)
KKarb	0.225	620	0.38	66	165	95
Sigri	0.19	1600	0.51	100	355	274
FMI	0.25	620	0.31	66	175	-

Table 5.2 Strength rule of mixtures values

Material	Krenchel factor	Tensile strength MPa (Krenchel)	Tensile strength MPa (Experimental)
KKarb (warp)	0.99	163	95
KKarb (fill)	0.85	144	25
Sigri	0.98	349	274
FMI	0.56	103	-

Table 5.3 Krenchel factor effect on composite strength

Material	Rule of mixtures			Exp'tal percentage reduction (%)	Rule of mixtures			Exp'tal percentage reduction (%)
	Elastic modulus (GPa)		Percentage reduction (%)	from table 4.3	Tensile strength (MPa)		Percentage reduction (%)	from table 4.4
	10% weight loss	0% weight loss			10% weight loss	0% weight loss		
KKarb	15	19	21	30	129	165	22	29
Sigri	85	88	3	14	278	355	22	37
FMI	16	20	20	86	138	175	21	-

Table 5.4 Elastic modulus and tensile strength reductions for 10% weight loss

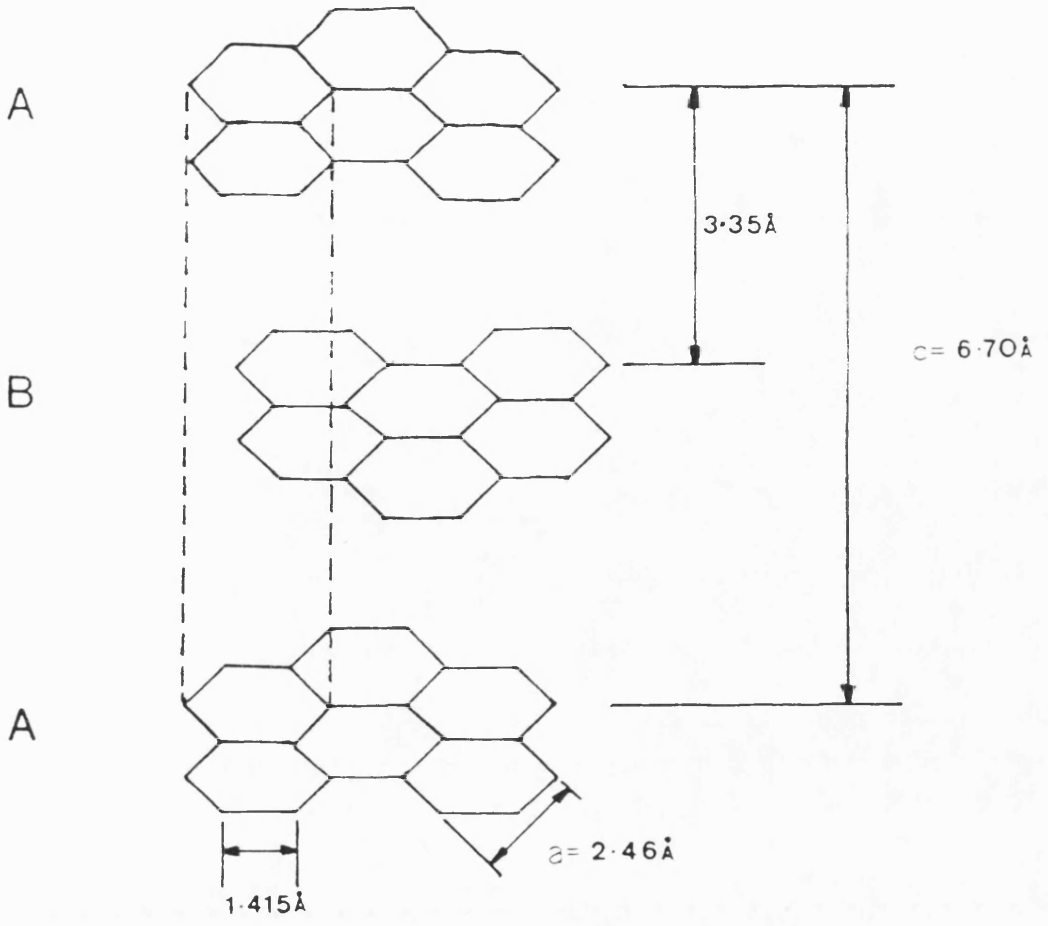

FIG. 2.1 STRUCTURE OF GRAPHITE

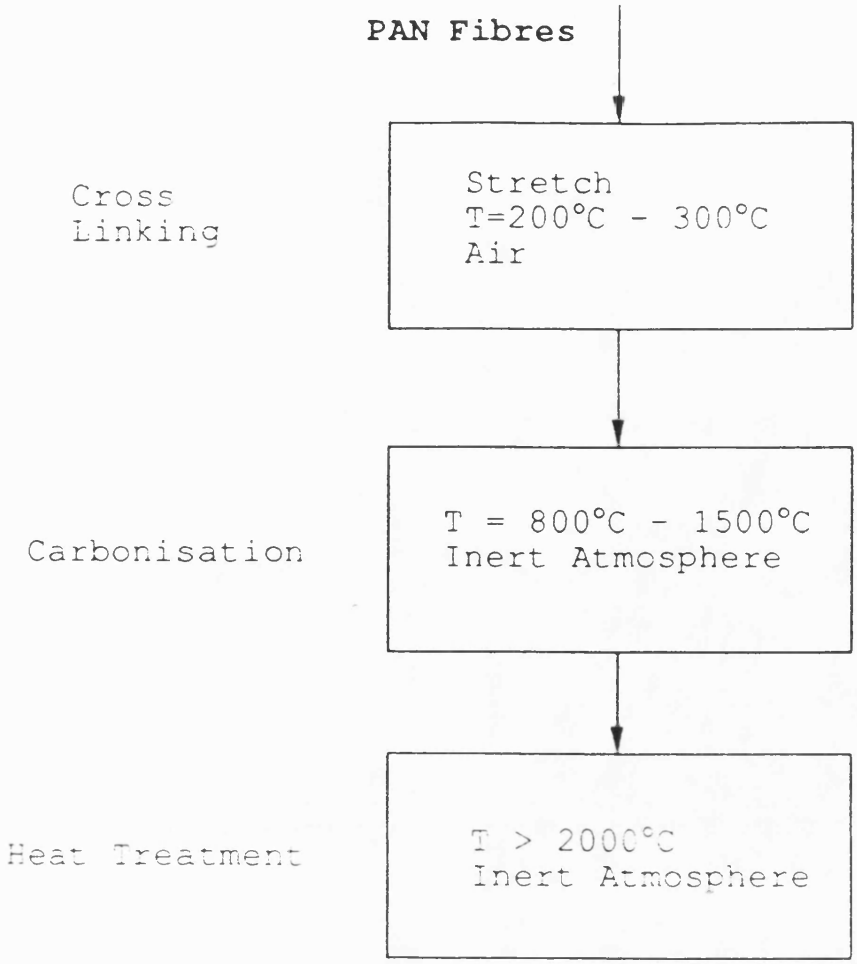

FIG. 2.2 MANUFACTURE OF PAN BASED CARBON FIBRES

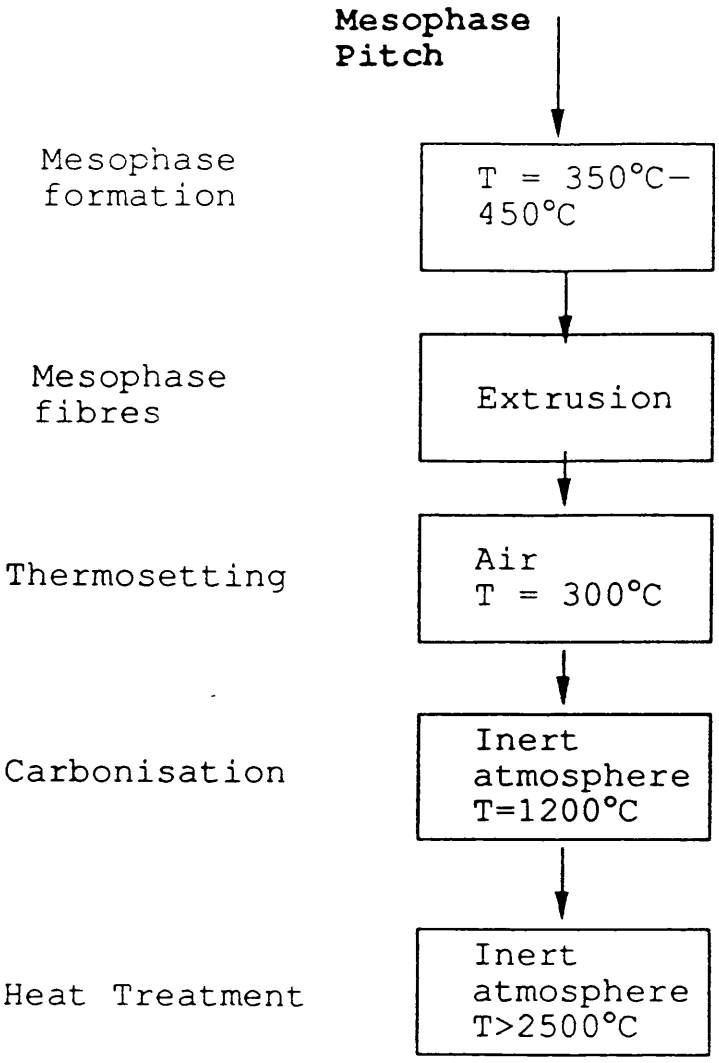

FIG. 2.3 MANUFACTURE OF PITCH BASED CARBON FIBRES

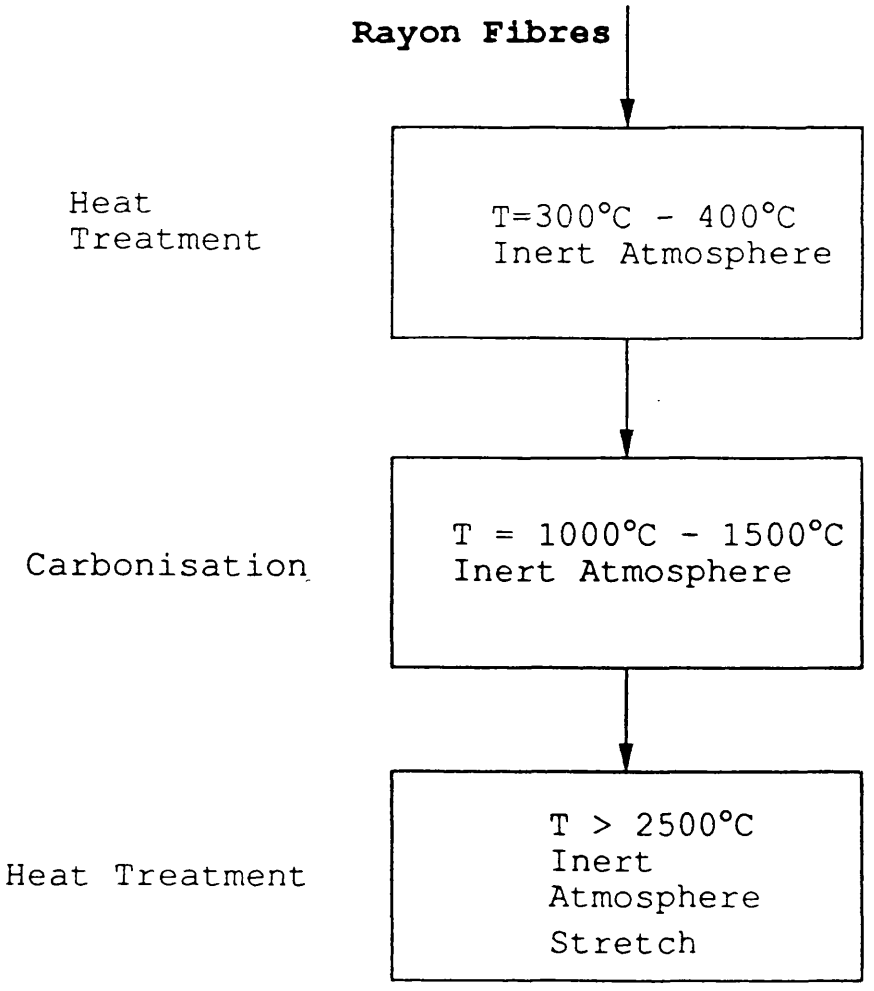

FIG. 2.4 MANUFACTURE OF RAYON BASED CARBON FIBRES

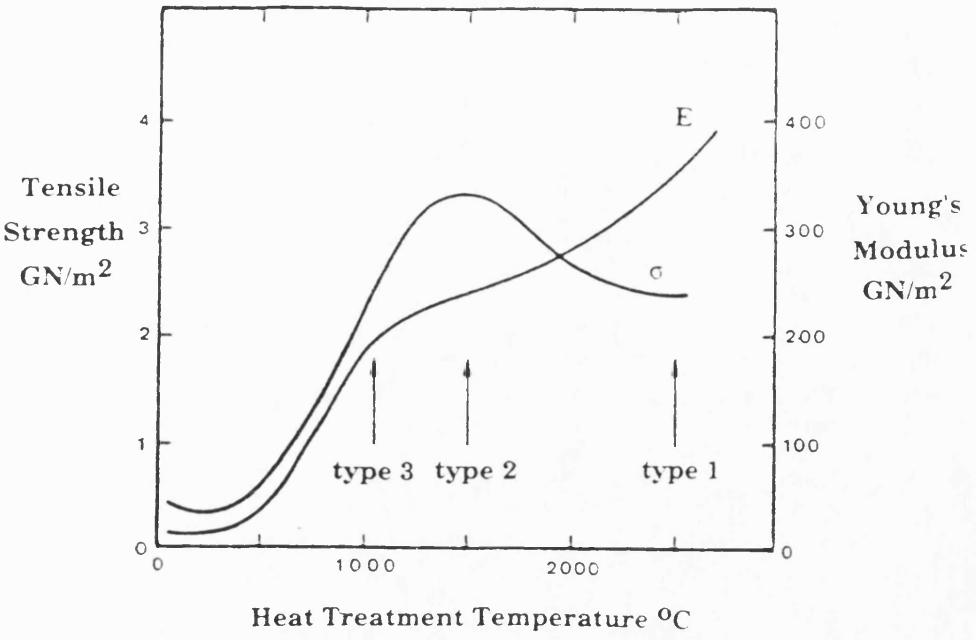

FIG. 2.5 TENSILE STRENGTH AND MODULUS FOR DIFFERENT HEAT TREATMENT TEMPERATURES
from Dorey (1986)

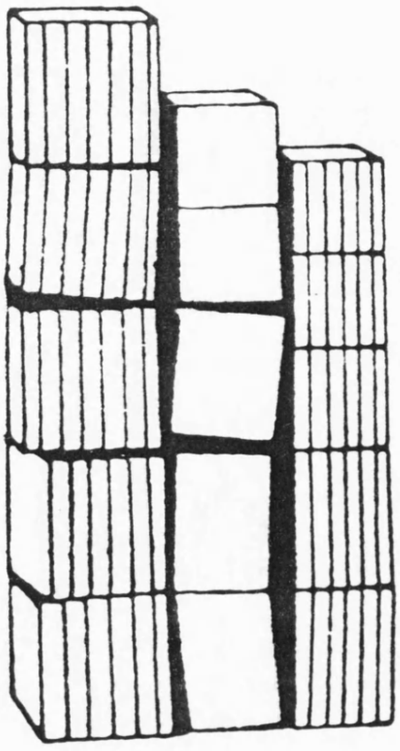

FIG. 2.6 JOHNSON AND TYSON MODEL OF PAN BASED CARBON FIBRES

from Johnson and Tyson (1969)

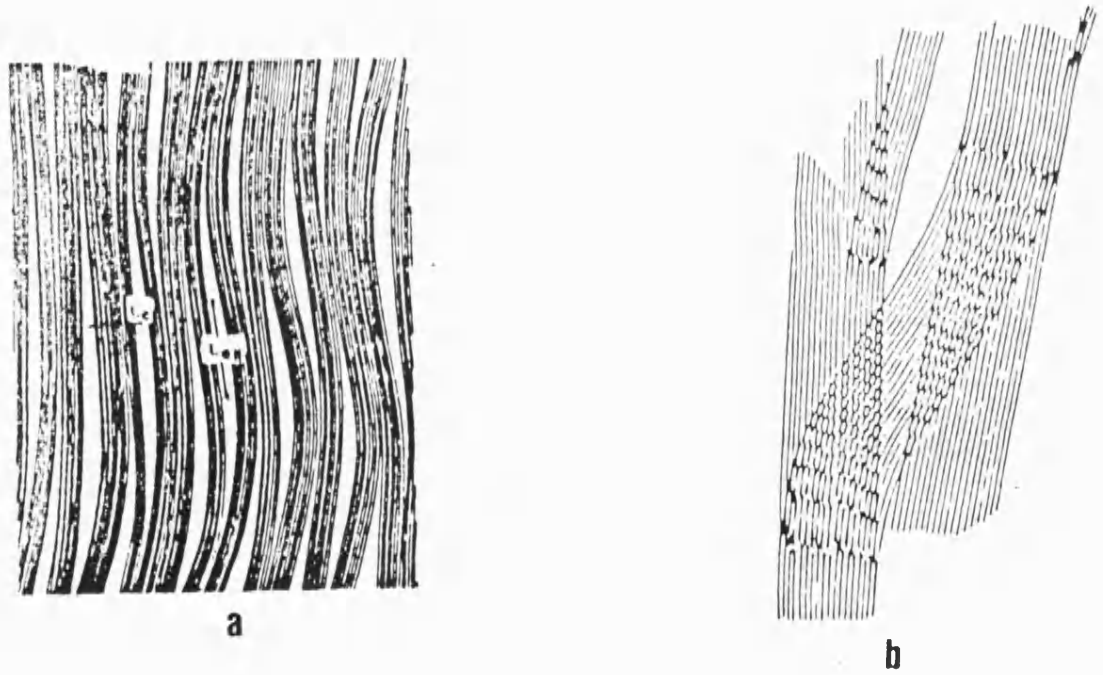

FIG. 2.7 RIBBON LIKE MODEL OF PAN BASED CARBON FIBRES

a) **from Fourdeux et.al. (1971)**
b) **from Crawford (1972)**

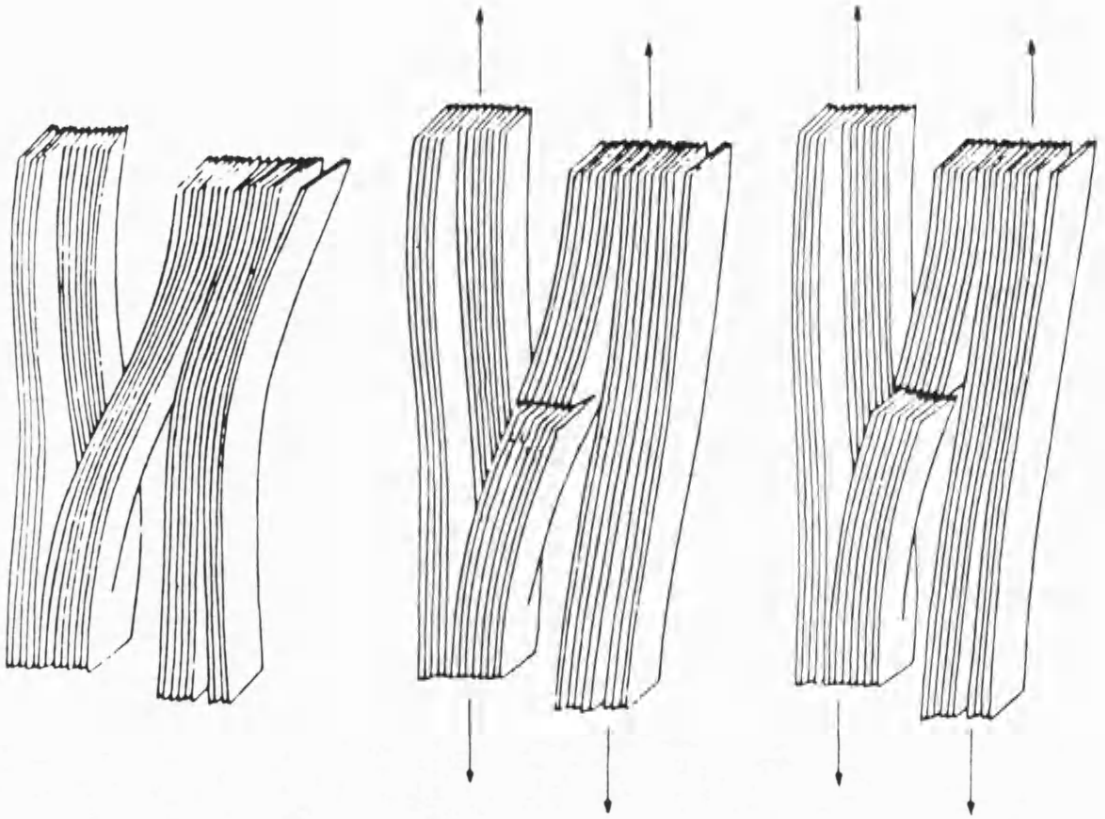

FIG. 2.8 REYNOLDS-SHARP MECHANISM OF TENSILE FAILURE OF CARBON FIBRES depicted by Johnson (1987)

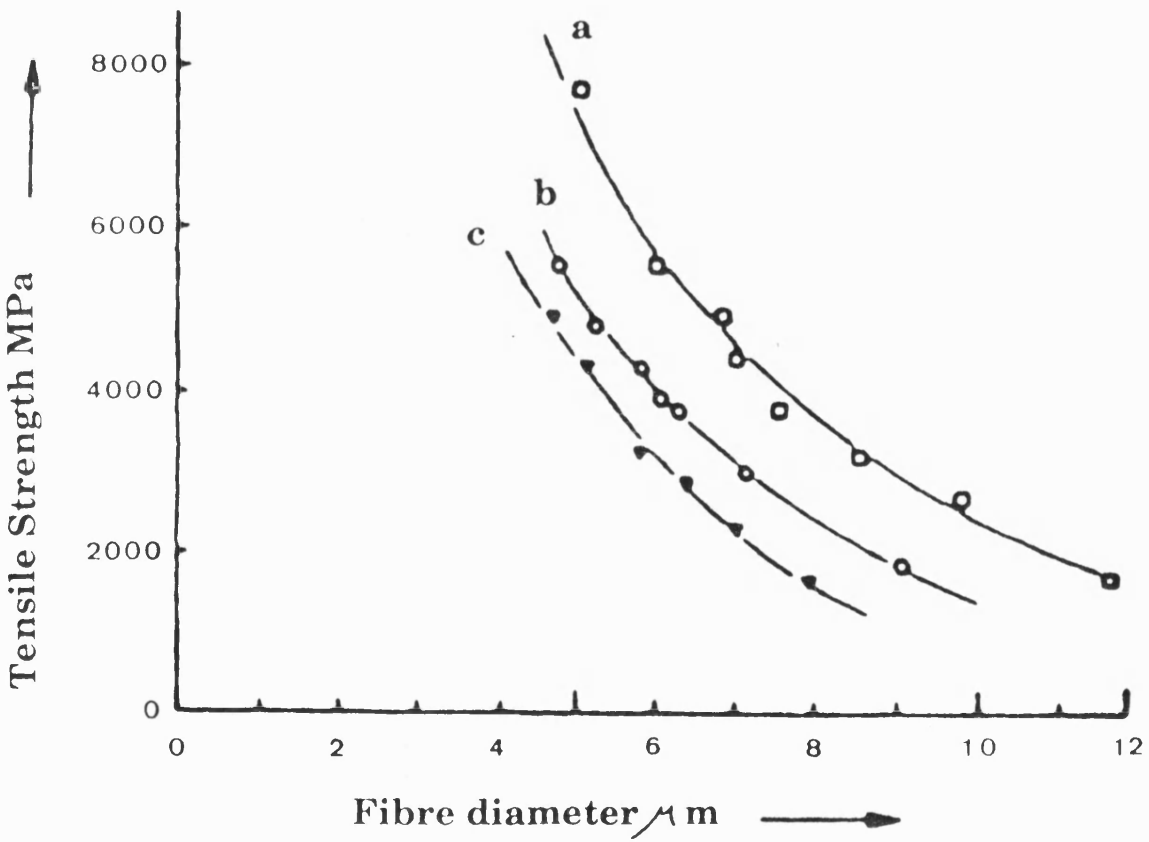

FIG. 2.9 TENSILE STRENGTH AT VARIOUS DIAMETERS FOR a) Hercules A54, b)Torayca T300 and c) Torayco M40 carbon fibres

from Fitzer (1989b)

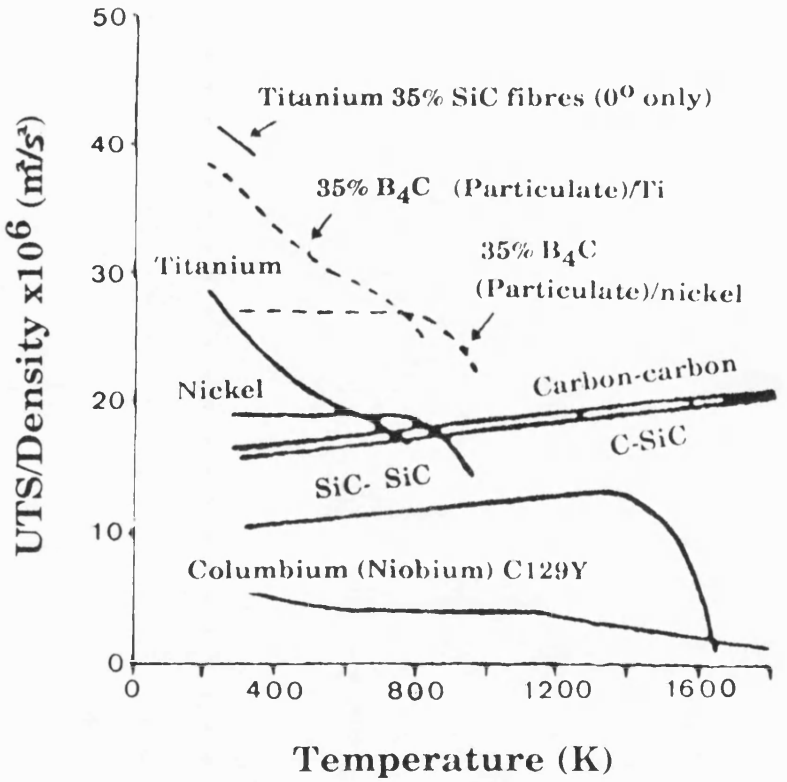

FIG. 2.10 COMPARISON OF SPECIFIC STRENGTHS AT ELEVATED TEMPERATURES.

from Savage (1988)

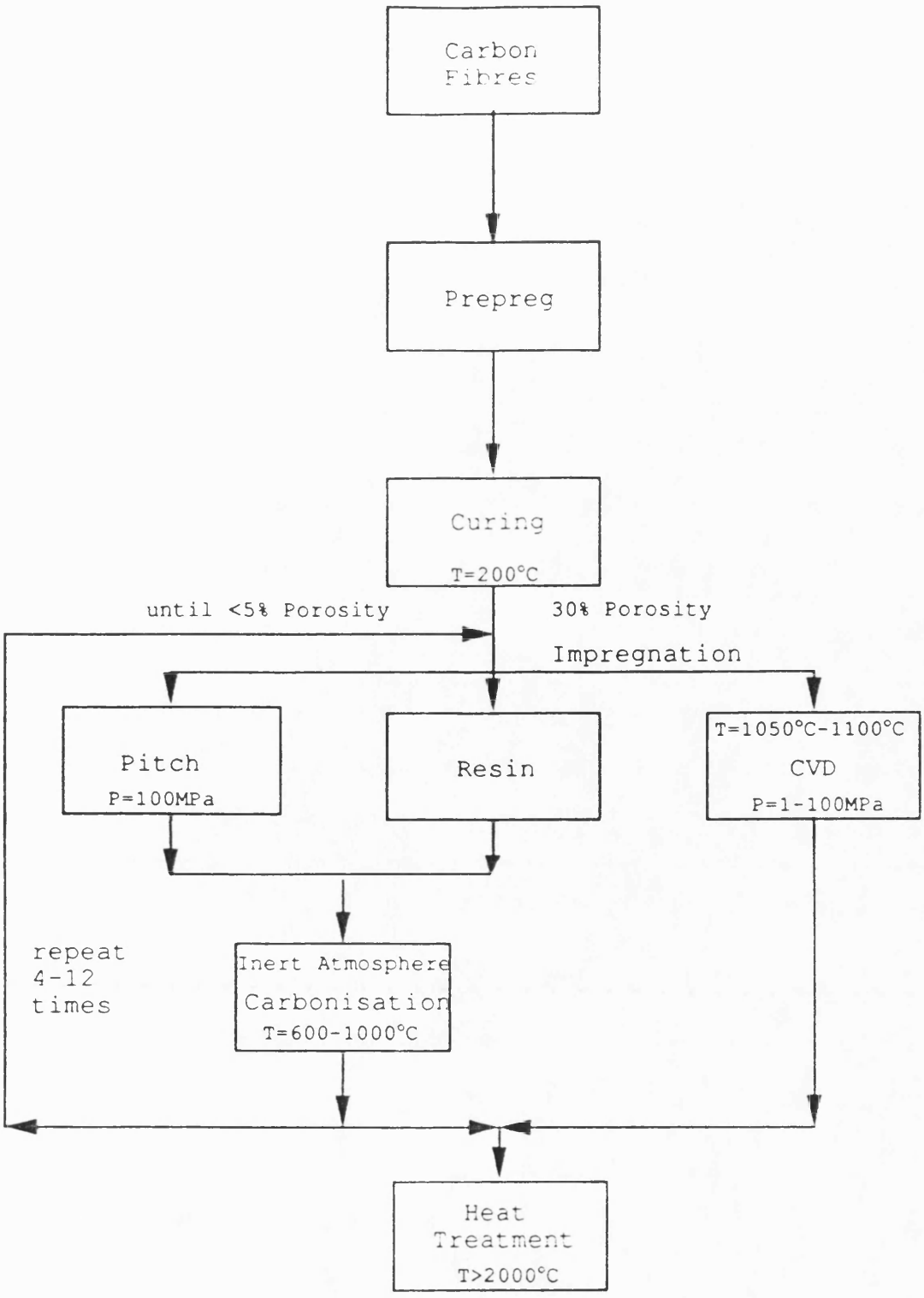

FIG. 2.11 MANUFACTURING PROCESS FOR CARBON CARBON COMPOSITES.

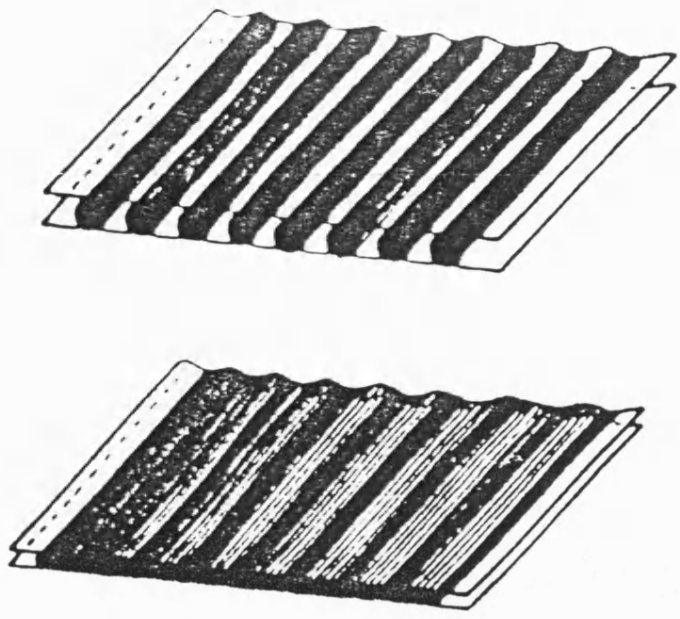

FIG. 2.12 UNIDIRECTIONAL PREPREG MANUFACTURE.
from Gill (1972)

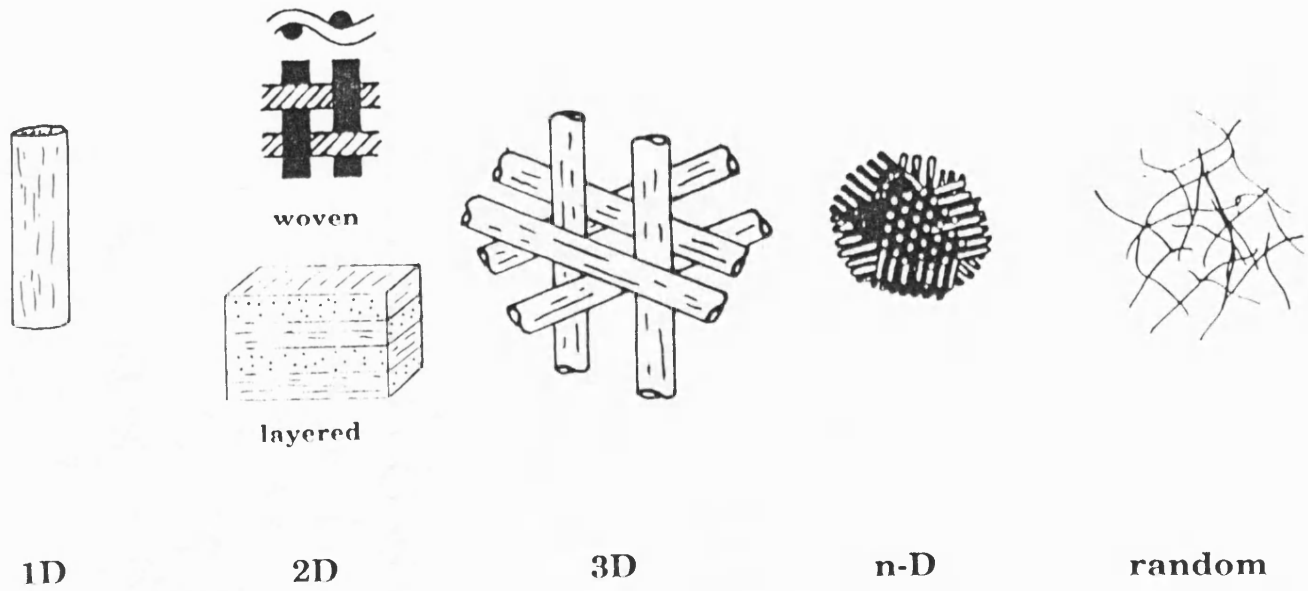

FIG. 2.13 POSSIBLE WEAVE DIMENSIONS.

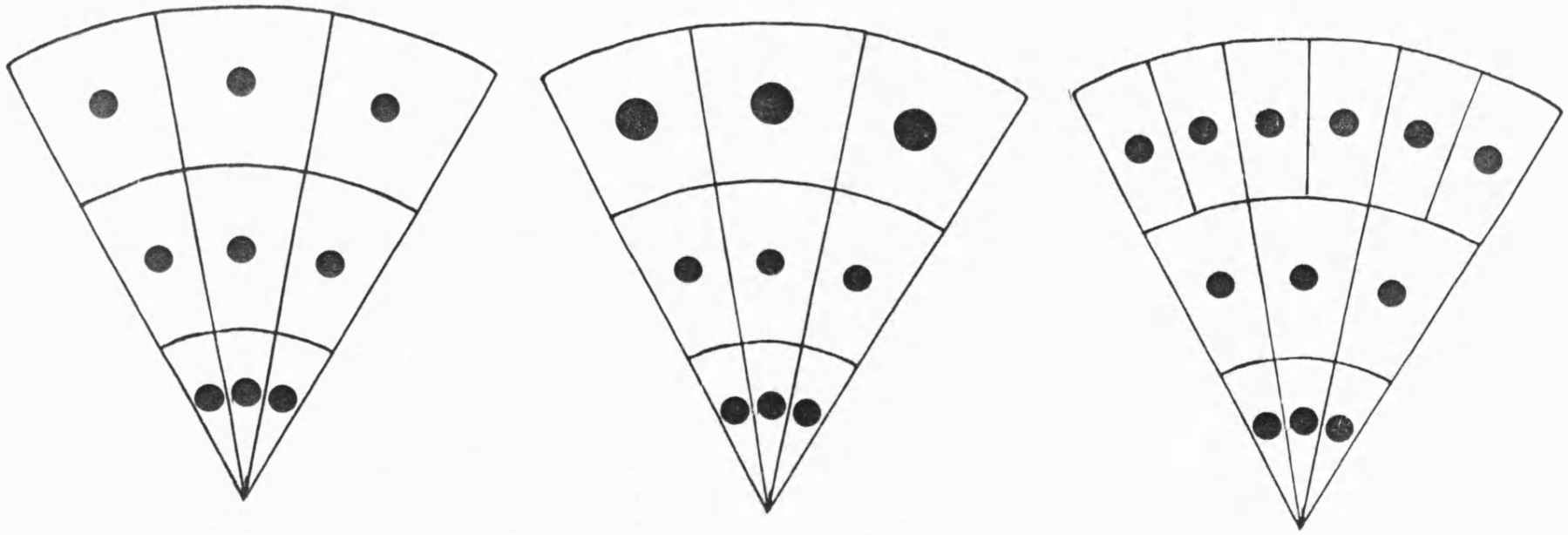

No Compensation

Compensation

FIG. 2.14 3D CYLINDRICAL WEAVES

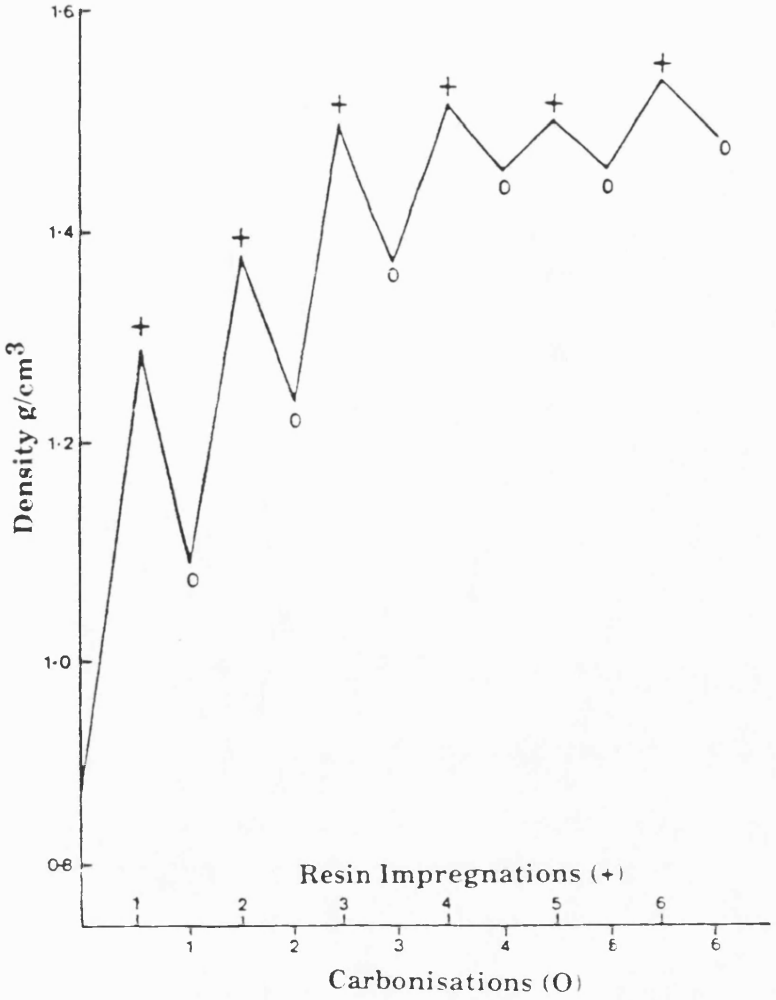

FIG. 2.15 EFFECT OF IMPREGNATION AND CARBONISATION ON DENSITY FOR A RESIN MATRIX.

from Thomas and Walker (1986)

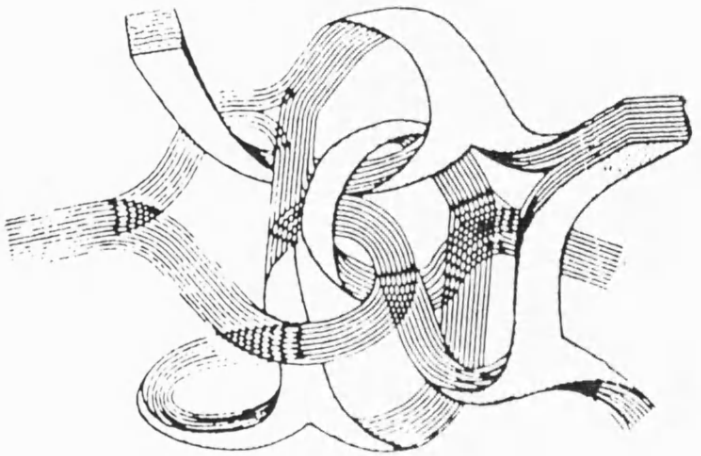

FIG. 2.16 MODEL OF THE STRUCTURE OF A RESIN BASED CARBON.
from Jenkins and Kawamura (1976)

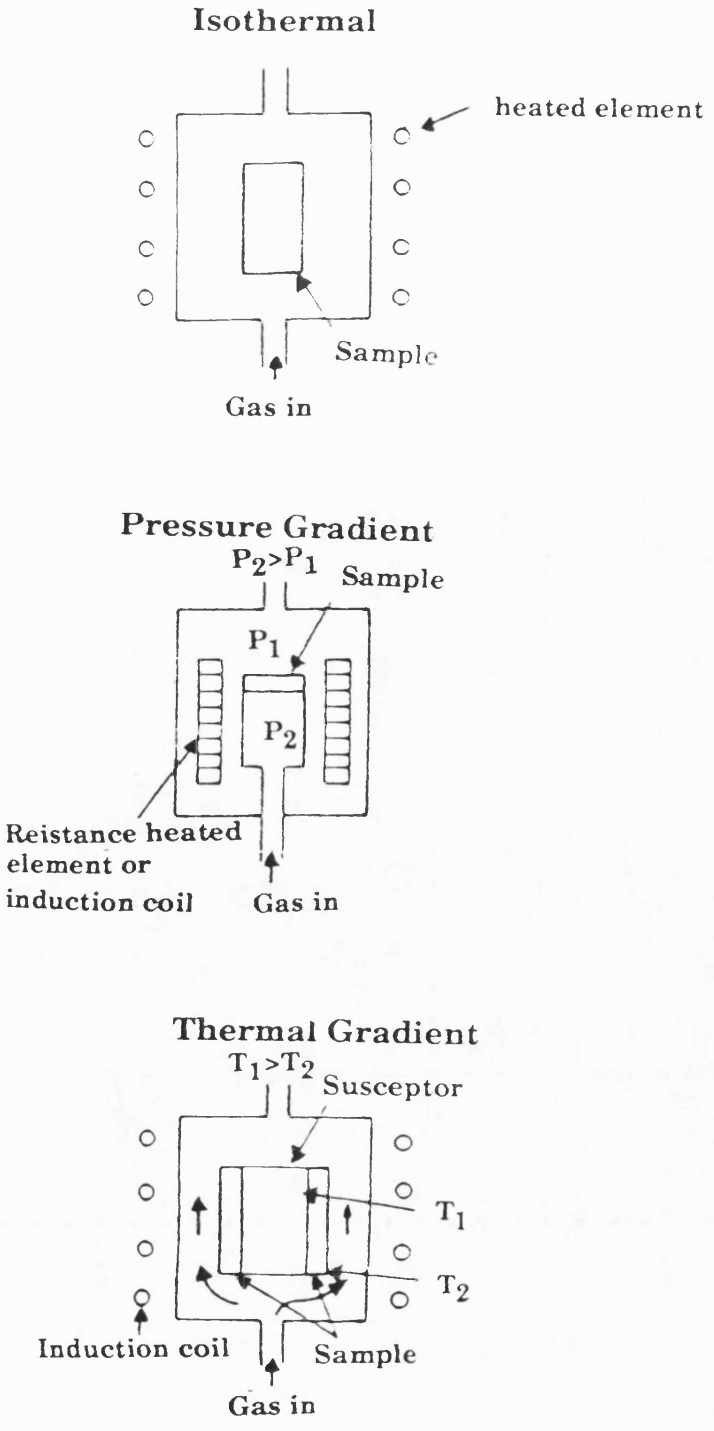

FIG. 2.17 METHODS OF CARBON VAPOUR DEPOSITION IMPREGNATION.

from Savage (1988)

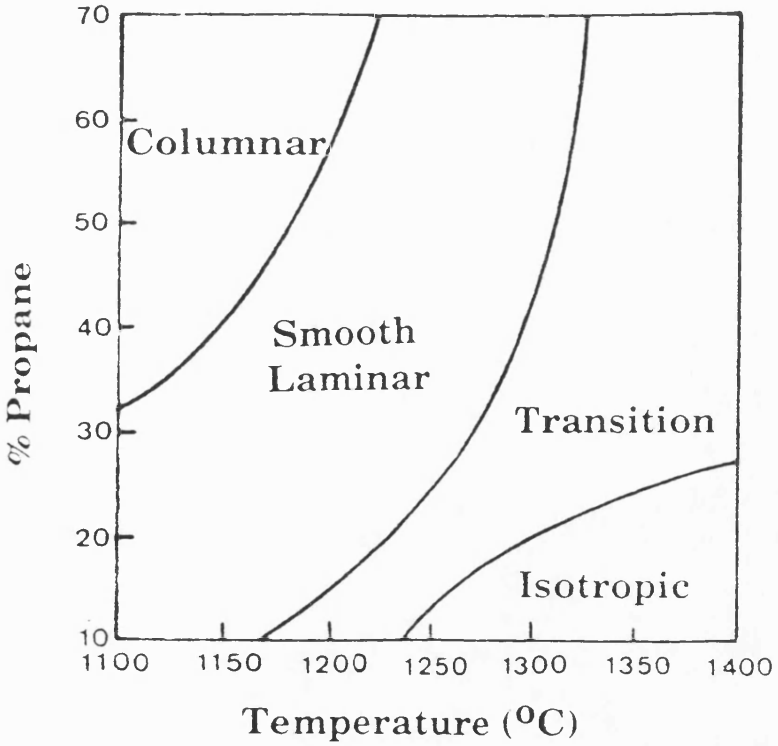

FIG. 2.18 EFFECT OF DEPOSITION CONDITIONS ON THE MICROSTRUCTURE OF CVD CARBON CARBON COMPOSITES.

from Oh and Lee (1988)

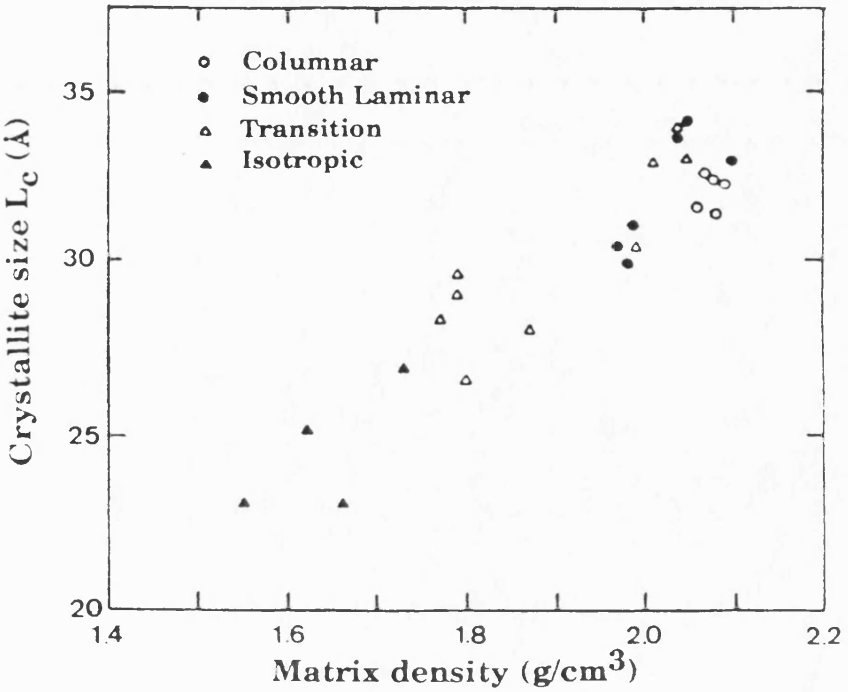

FIG. 2.19 DENSITY AND CRYSTALLITE SIZE FOR VARIOUS CVD MICROSTRUCTURES.

from Oh and Lee (1988)

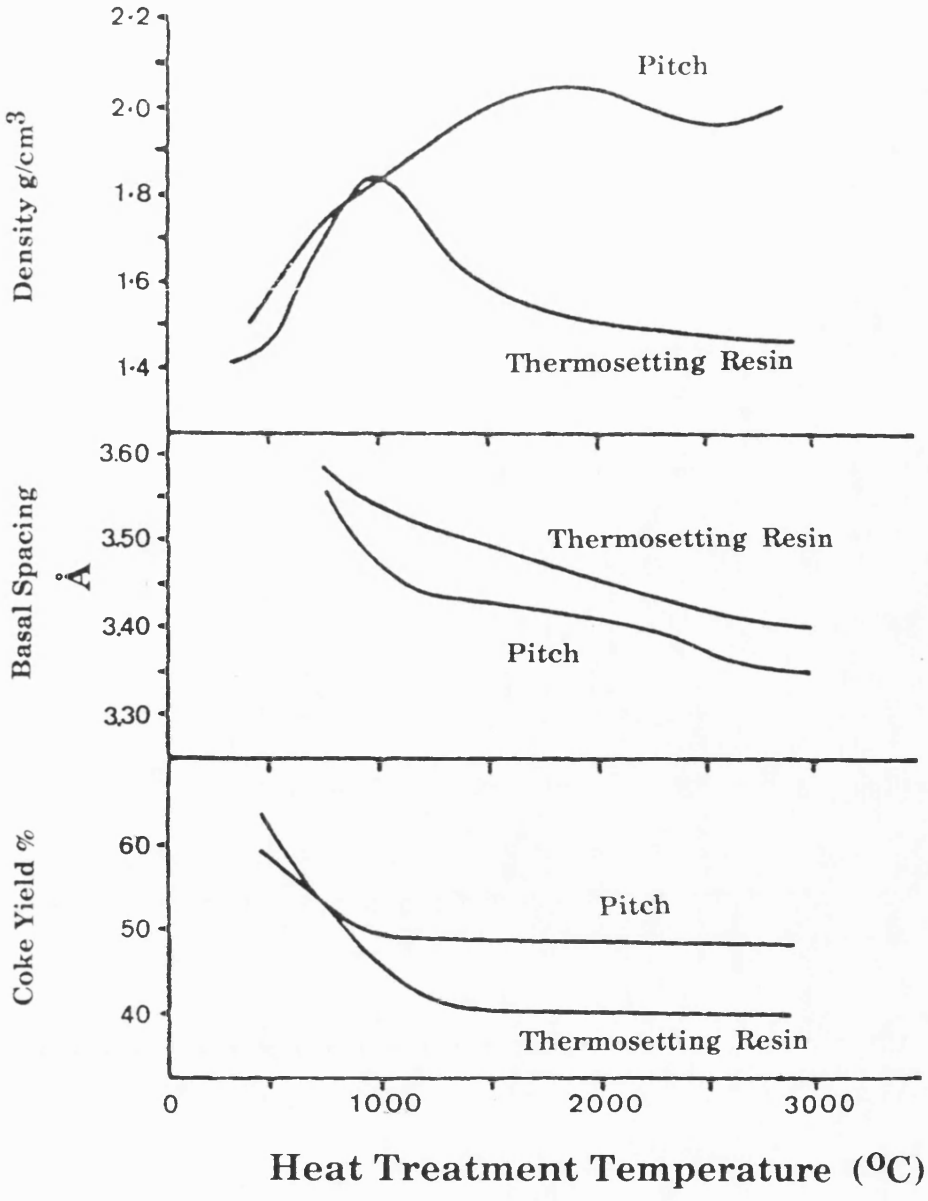

FIG. 2.20 EFFECT OF HEAT TREATMENT TEMPERATURE ON VARIOUS FACTORS FOR PITCH AND RESIN.

from Savage (1988)

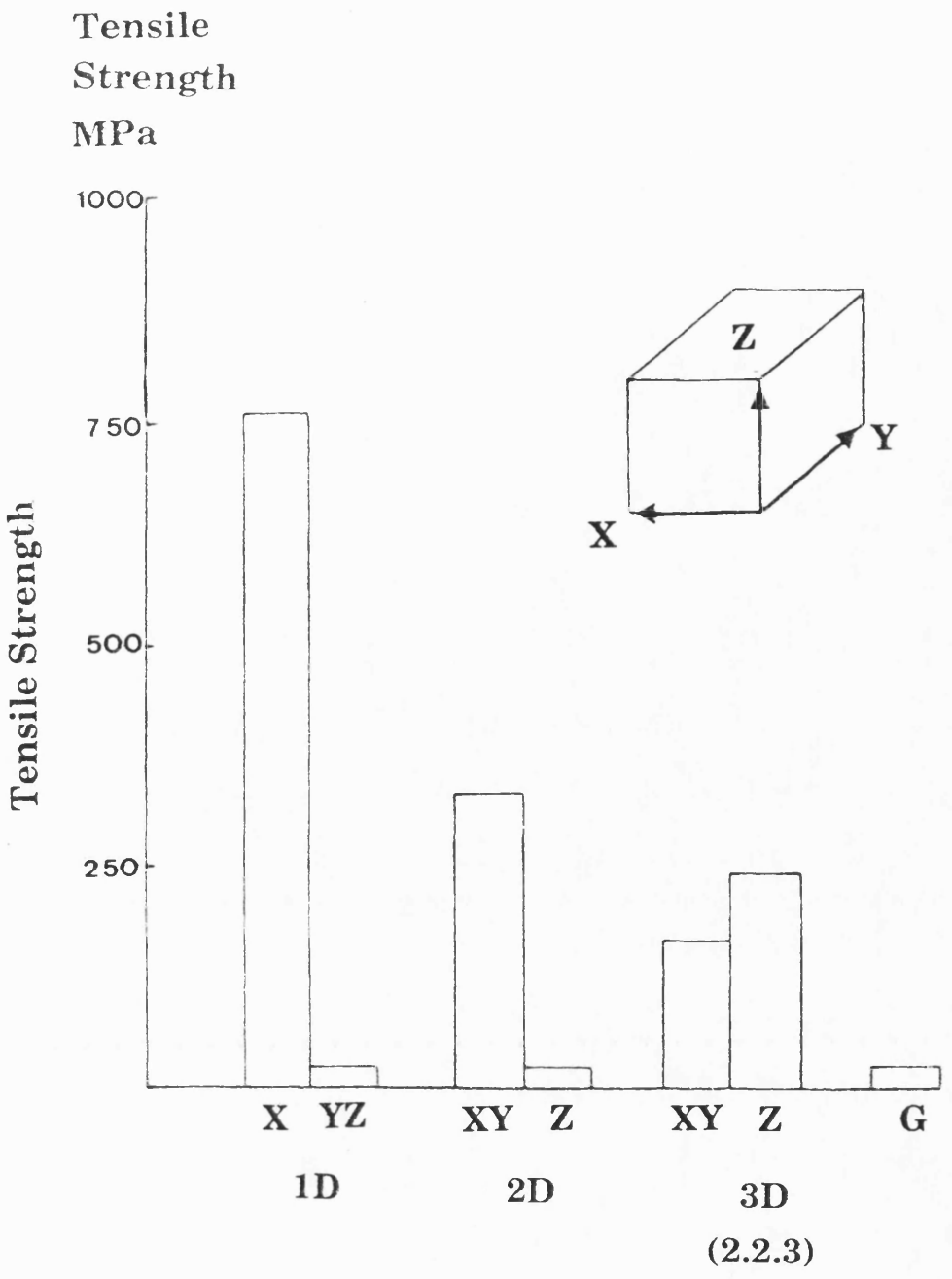

FIG. 2.21 TENSILE STRENGTH WITH DIFFERENT LAYUPS

from Thomas and Walker (1986)

Plain Weave

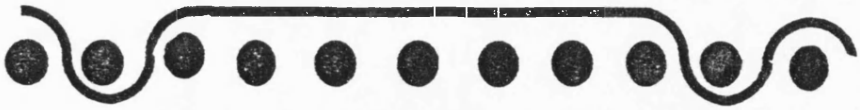

8 Harness Satin Weave

FIG. 2.22 WEAVE PATTERNS

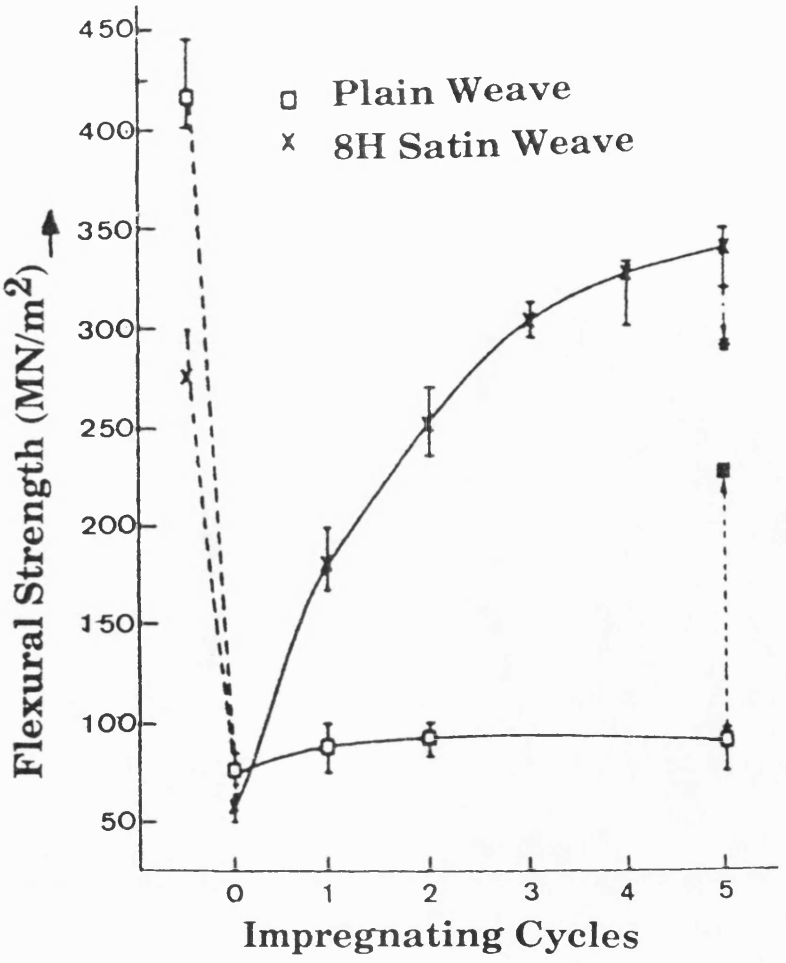

FIG. 2.23 EFFECT OF WEAVE PATTERN ON FLEXURAL STRENGTH AT DIFFERENT STAGES OF IMPREGNATION

from Manocha and Bahl (1988)

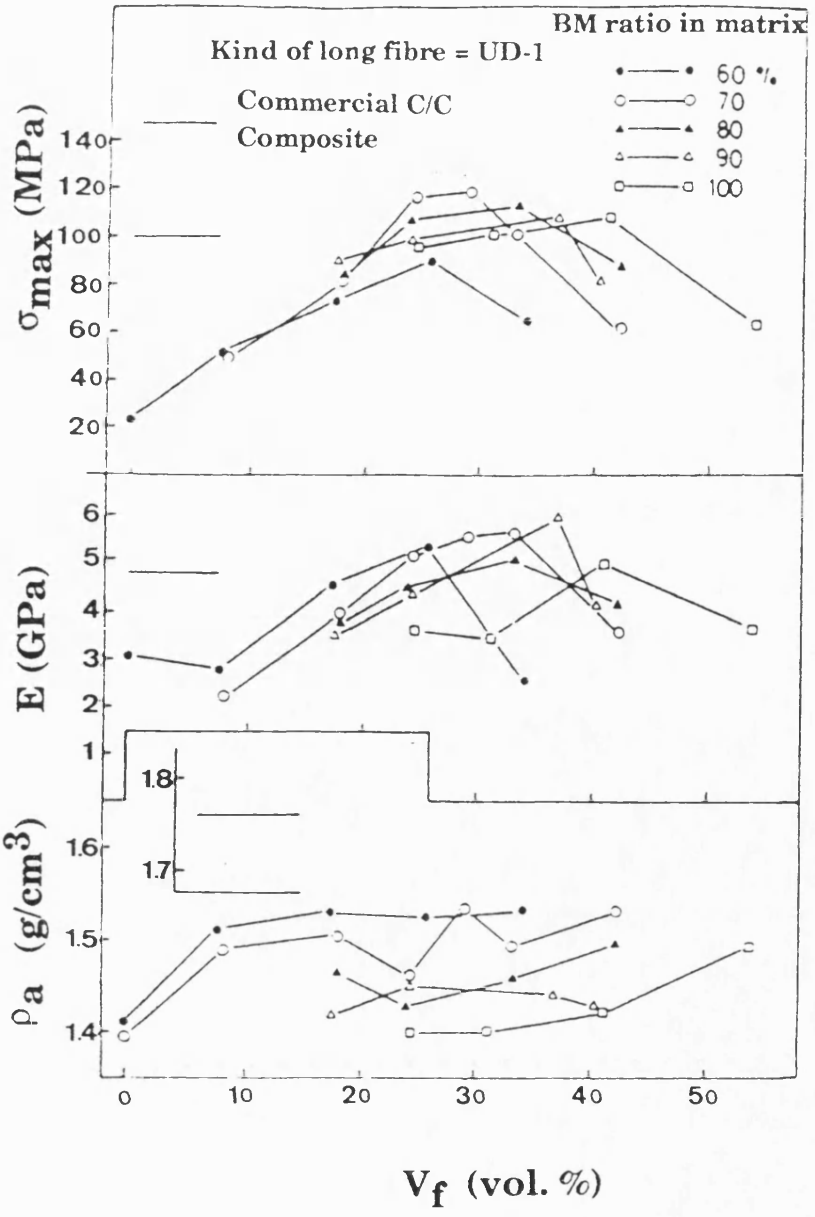

FIG. 2.24 EFFECT OF FIBRE VOLUME FRACTION ON VARIOUS PROPERTIES

from Chang and Okura (1986)

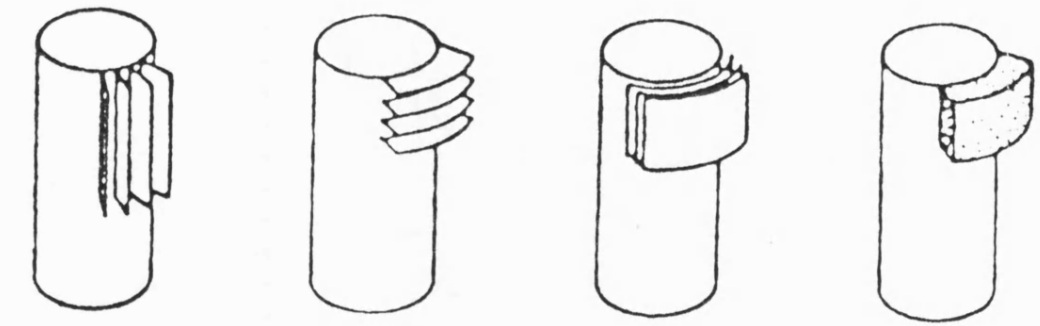

FIG. 2.25 POSSIBLE ARRANGEMENT OF A CARBON MATRIX

from Jortner (1976)

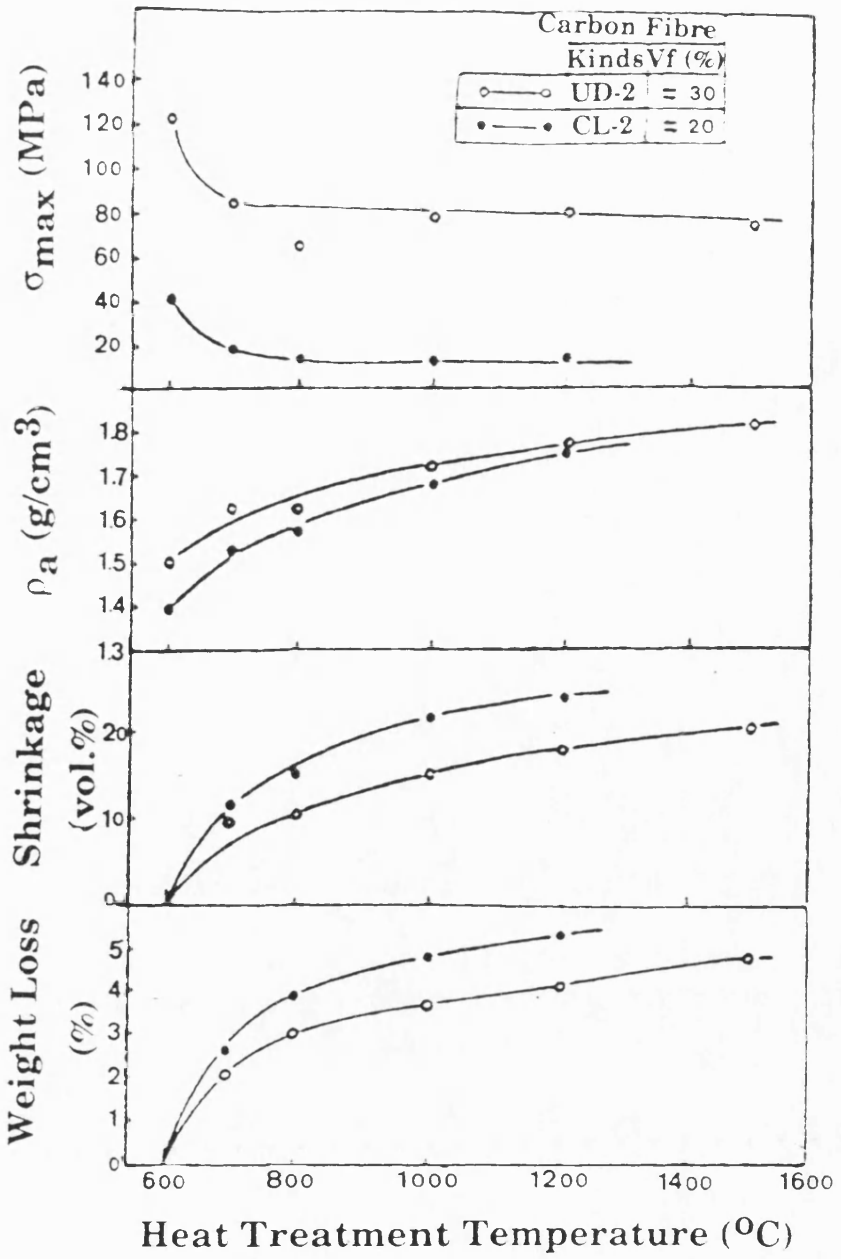

FIG. 2.26 EFFECT OF HEAT TREATMENT TEMPERATURE ON VARIOUS FACTORS
from Chang and Okura (1986)

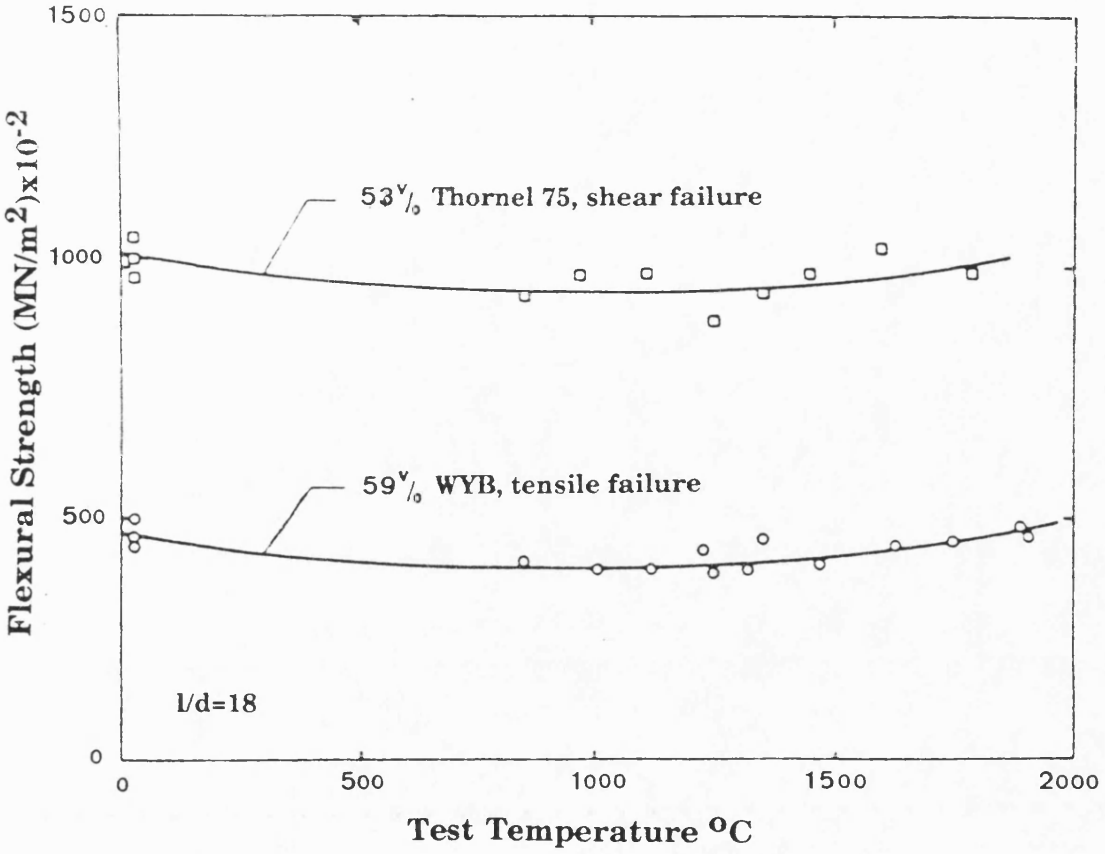

FIG 2.27 EFFECT OF TEST TEMPERATURE ON FLEXURAL STRENGTH

from Fitzer and Terweisch (1972)

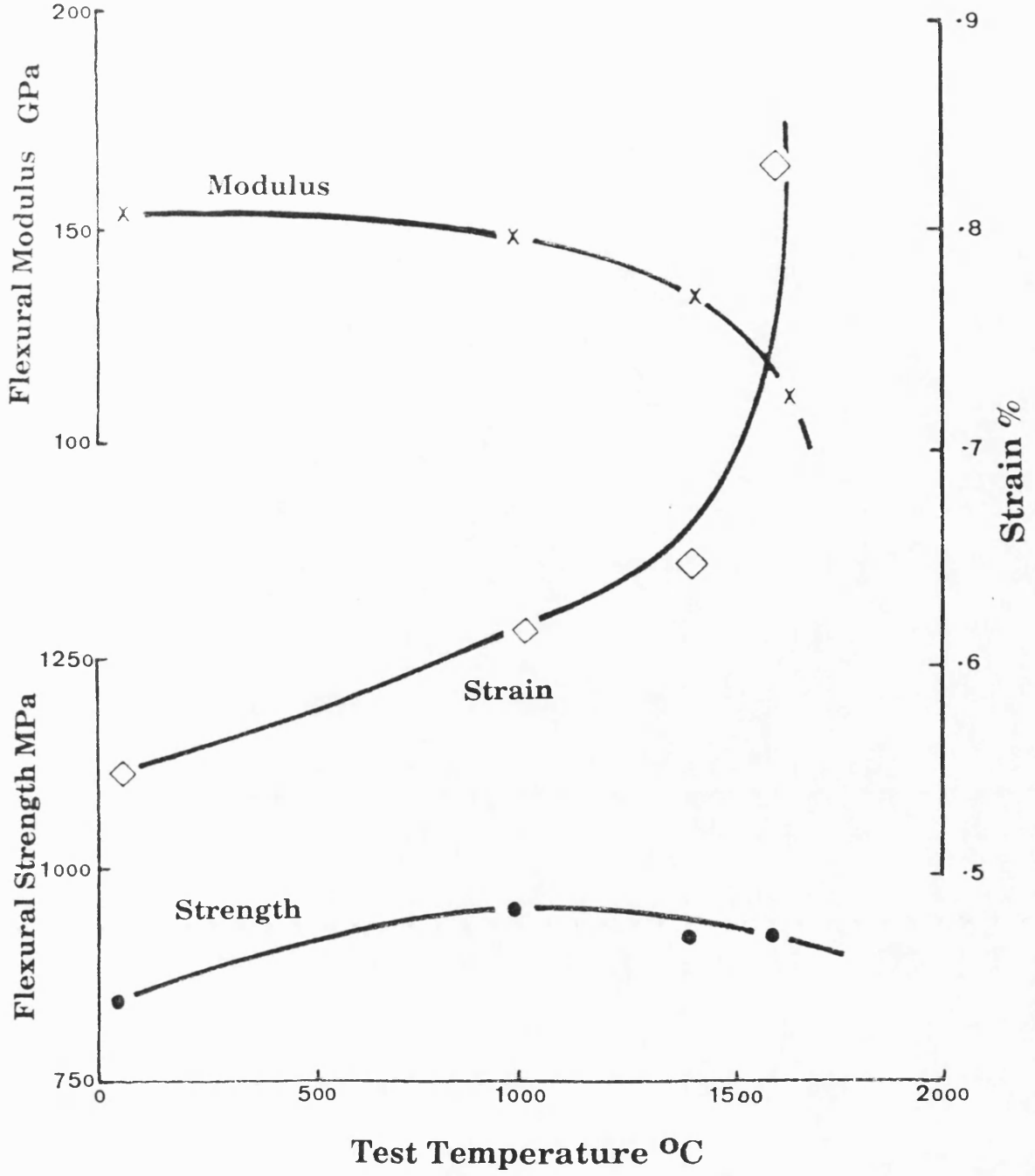

FIG. 2.28 EFFECT OF TEST TEMPERATURE ON FLEXURAL STRENGTH AND MODULUS.

from Thomas and Walker (1986)

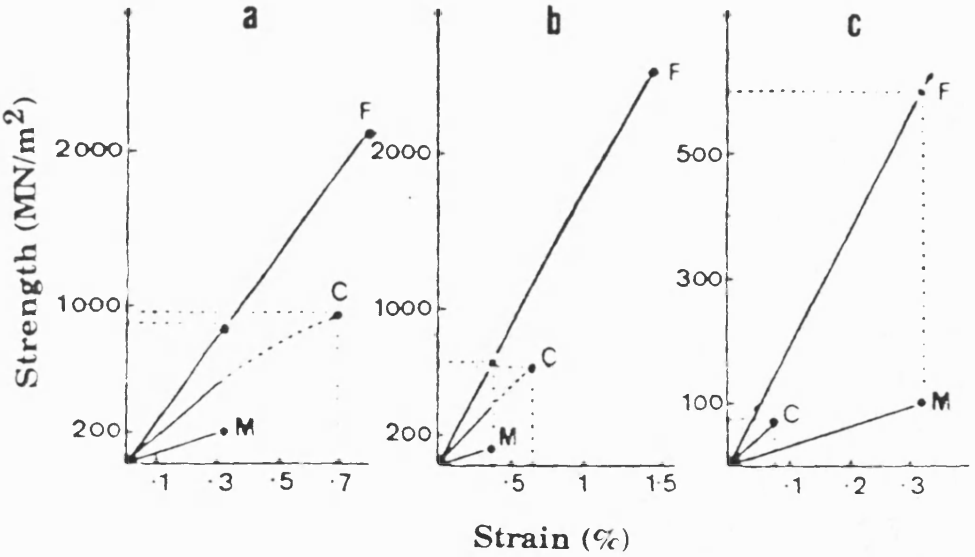

FIG. 2.29 STRESS/STRAIN CURVES FOR CARBON CARBON COMPOSITES WITH PAN FIBRES a)type I fibres, b) type II fibres and c) surface treated type II fibres

from Fitzer et.al. (1980b)

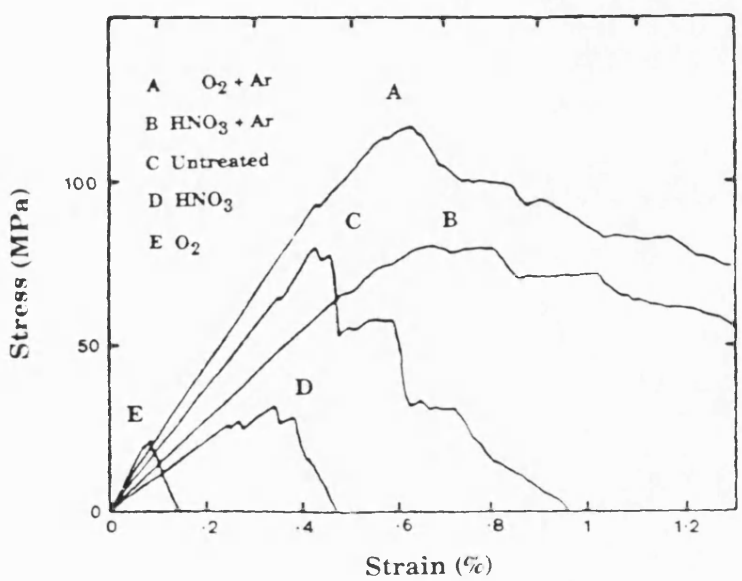

FIG. 2.30 STRESS/STRAIN CURVE FOR 2D CARBON CARBON COMPOSITES

from Kowbel and Shan (1990)

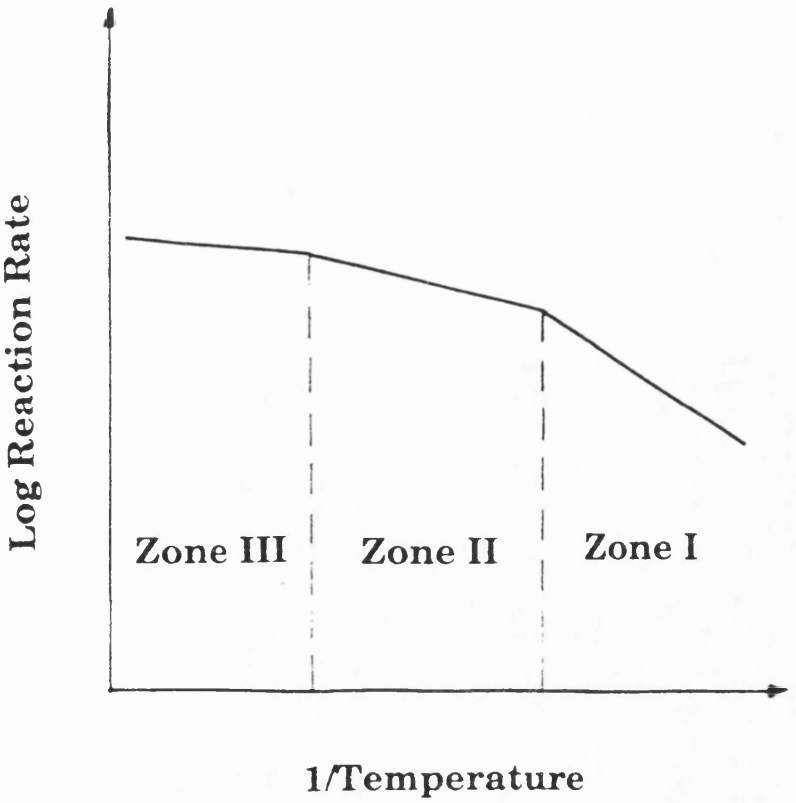

FIG. 2.31 OXIDATION ZONES

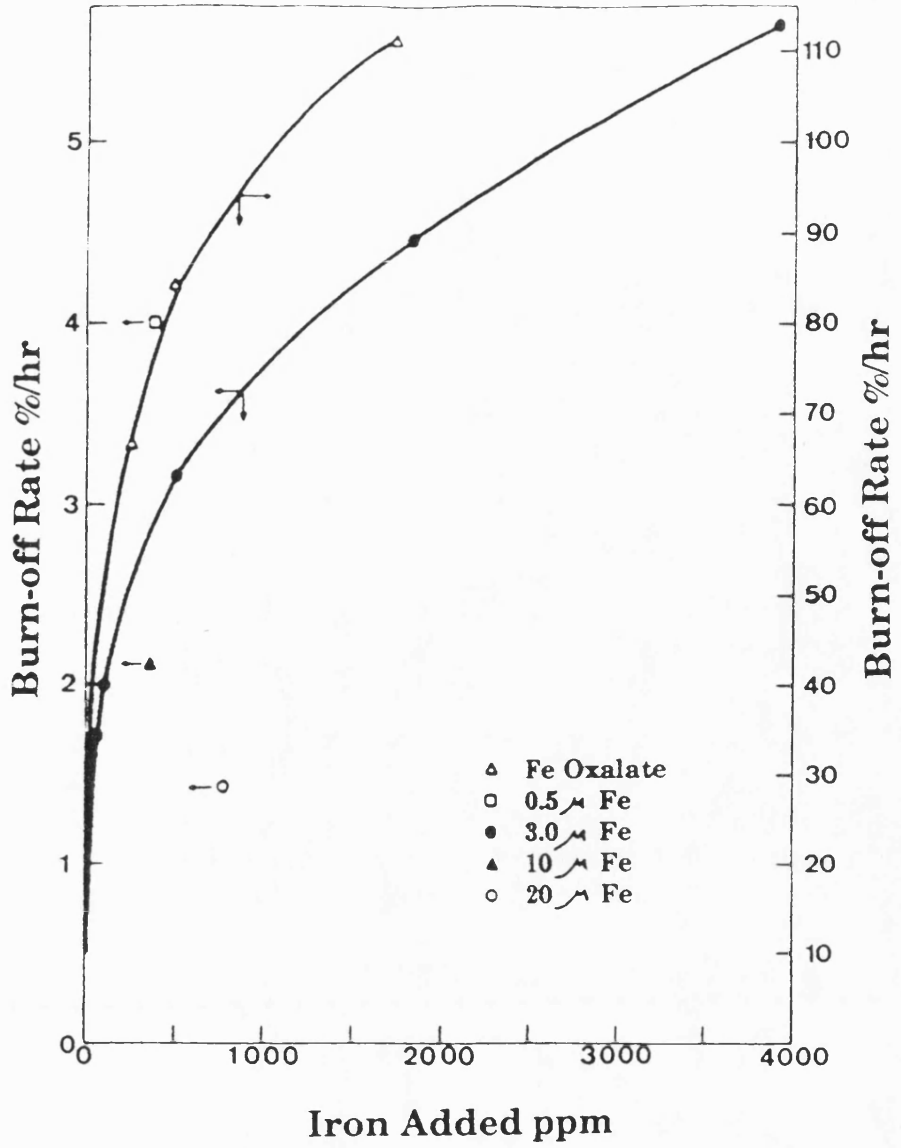

FIG 2.32 EFFECT OF AMOUNT OF IRON ON THE RATE OF GRAPHITE OXIDATION

from Walker (1968)

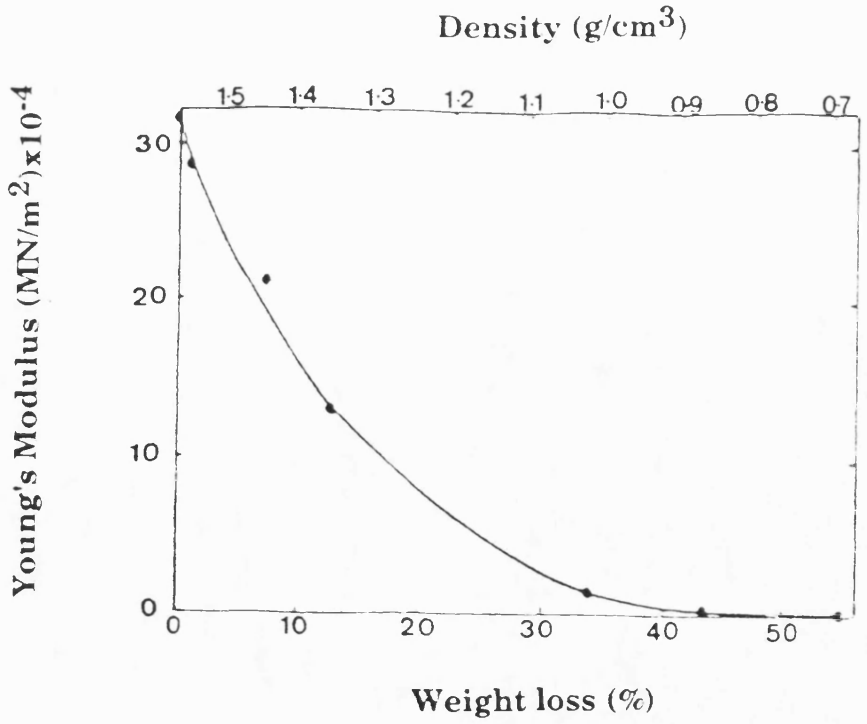

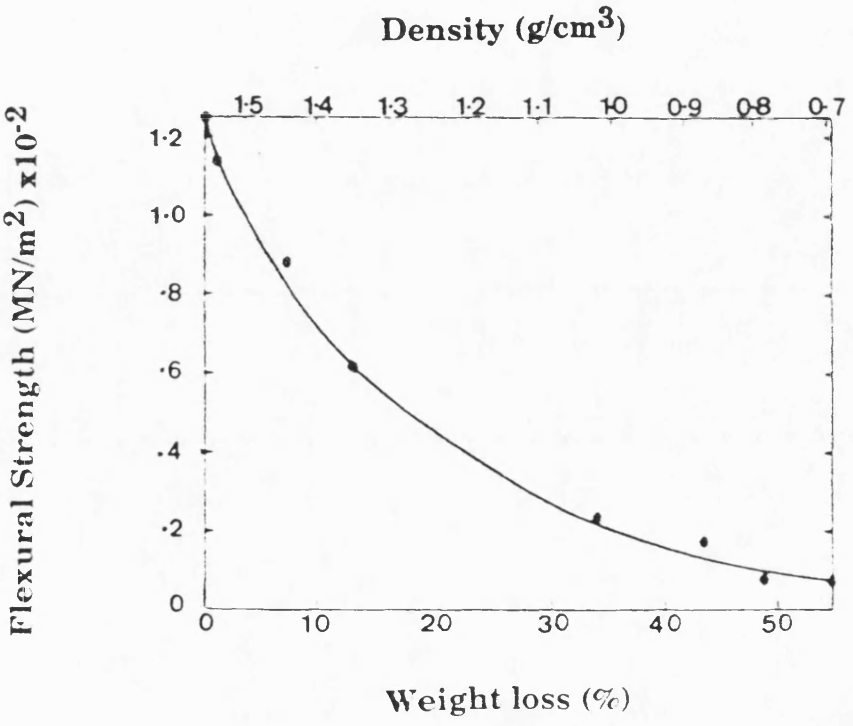

FIG. 2.33 EFFECT OF OXIDATION ON STRENGTH AND MODULUS OF A CARBON CARBON COMPOSITE

from Zhao et.al. (1985)

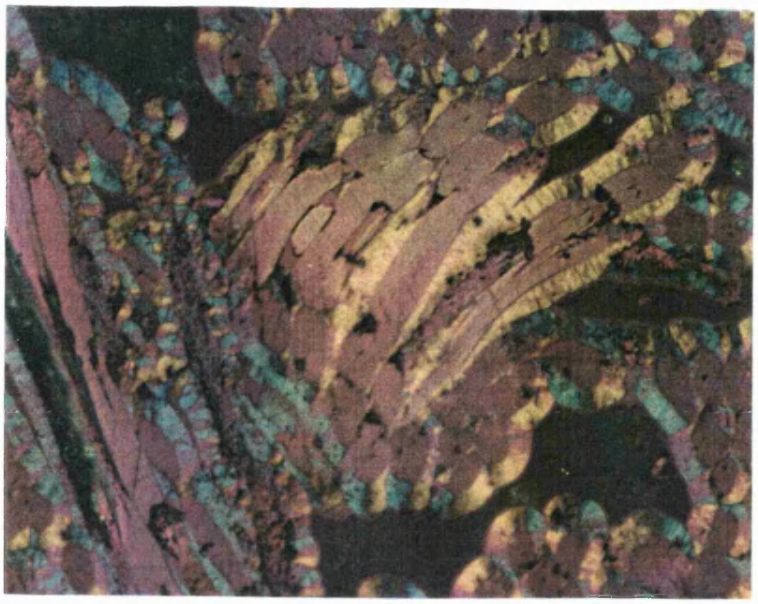

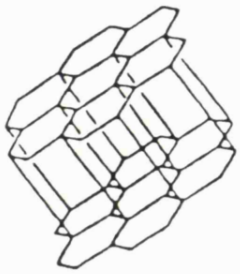

YELLOW

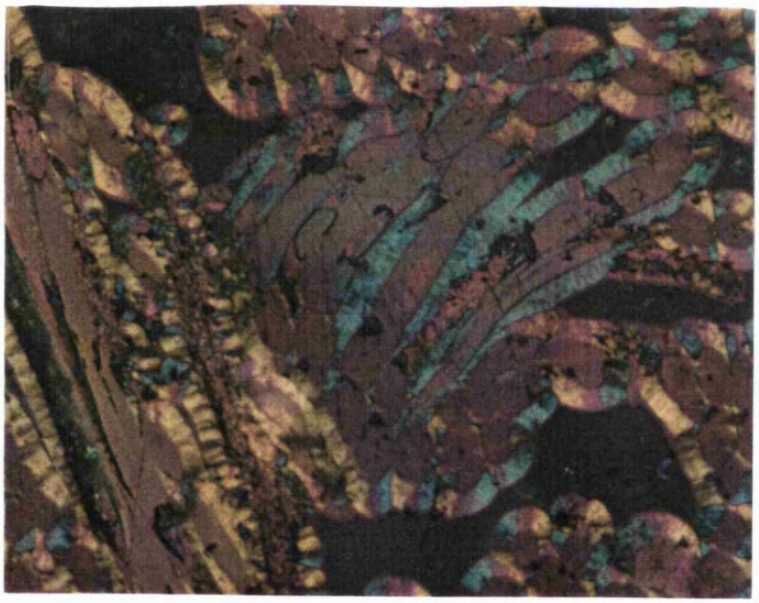

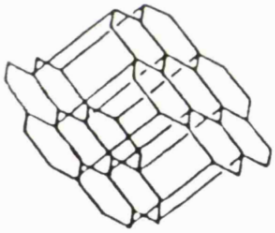

BLUE

FIG 3.1 BASAL PLANE ORIENTATION AND RESULTANT COLOURS IN POLARISED LIGHT MICROSCOPY

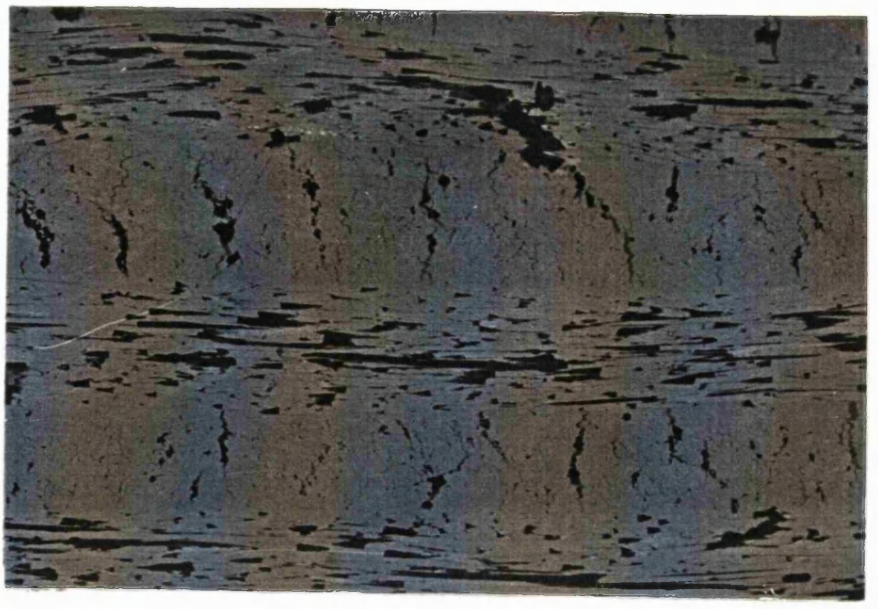

100 μm

a

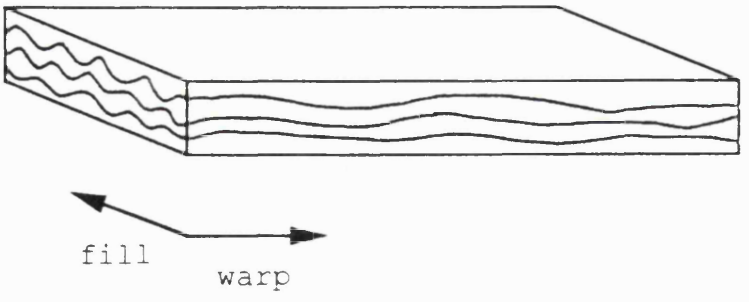

b

FIG 3.2 KKARB MATERIAL SHOWING a) microstructure and b) specimen orientation

FIG 3.3 SIGRI MATERIAL MICROSTRUCTURE

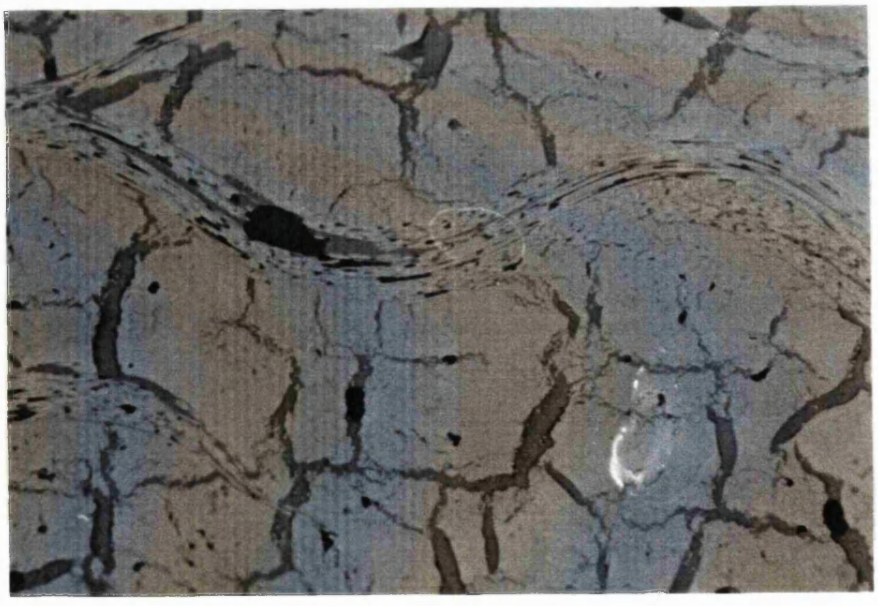

FIG 3.4 FMI MATERIAL MICROSTRUCTURE

RESIN (PURPLE)

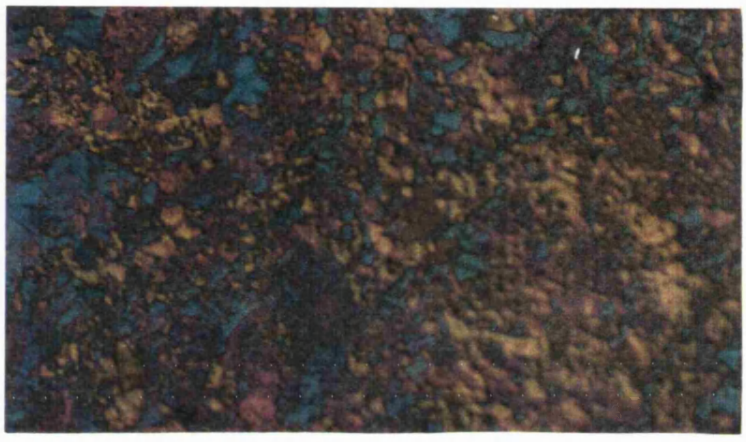

PITCH (SPECKLED)

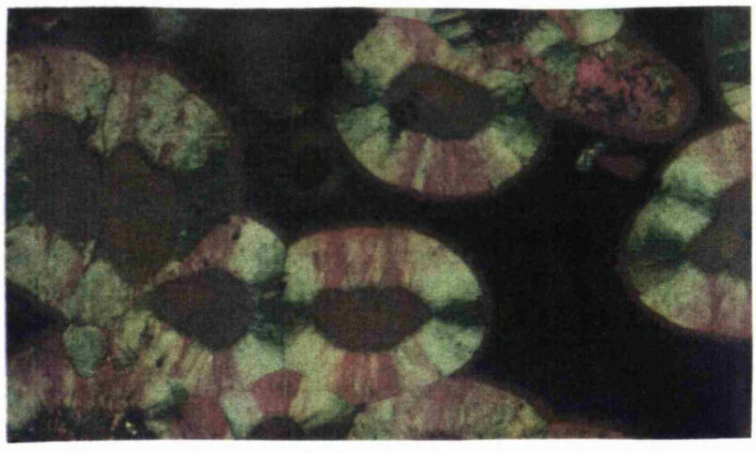

CVD (MALTESE CROSS)

FIG 3.5 MATRIX TYPES UNDER POLARISED LIGHT

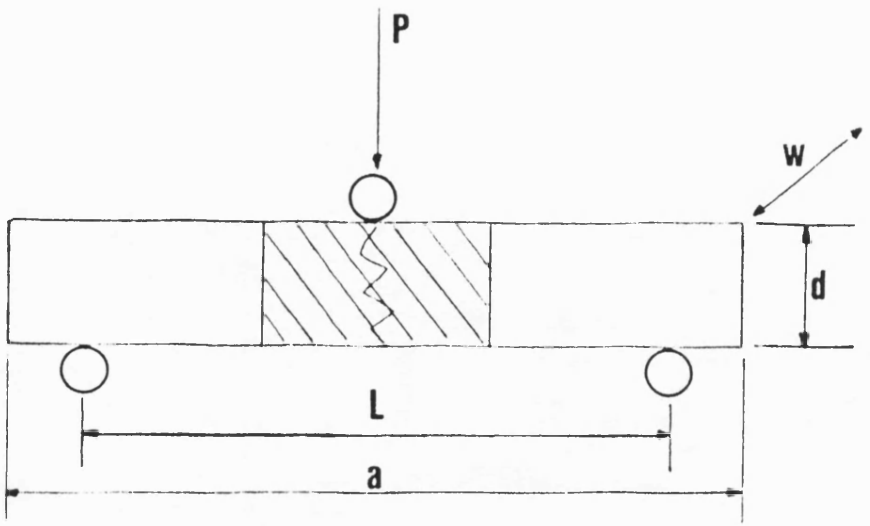

FIG 3.6 FLEXURAL STRENGTH DETERMINATION SHOWING REGION MOUNTED FOR EXAMINATION IN SHADED AREA

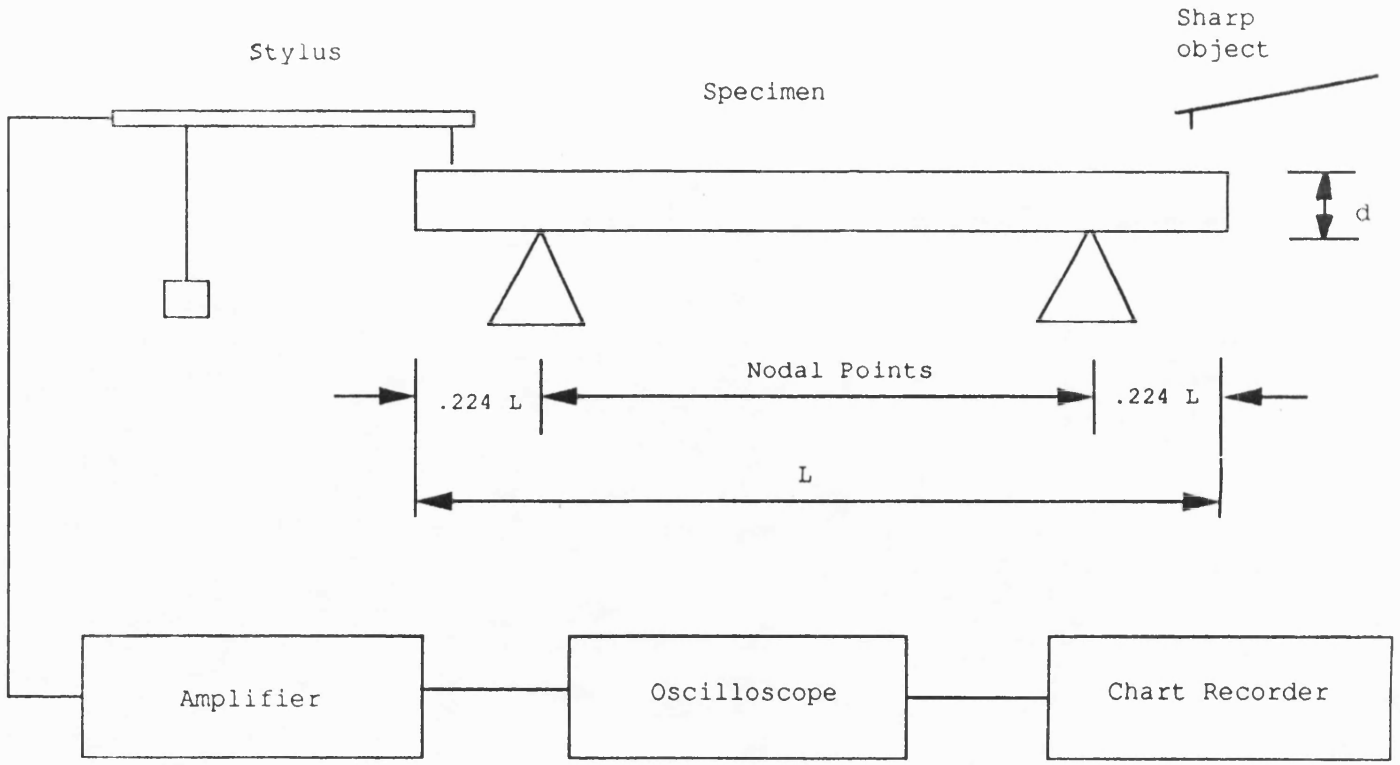

FIG 3.7 DYNAMIC ELASTIC MODULUS APPARATUS

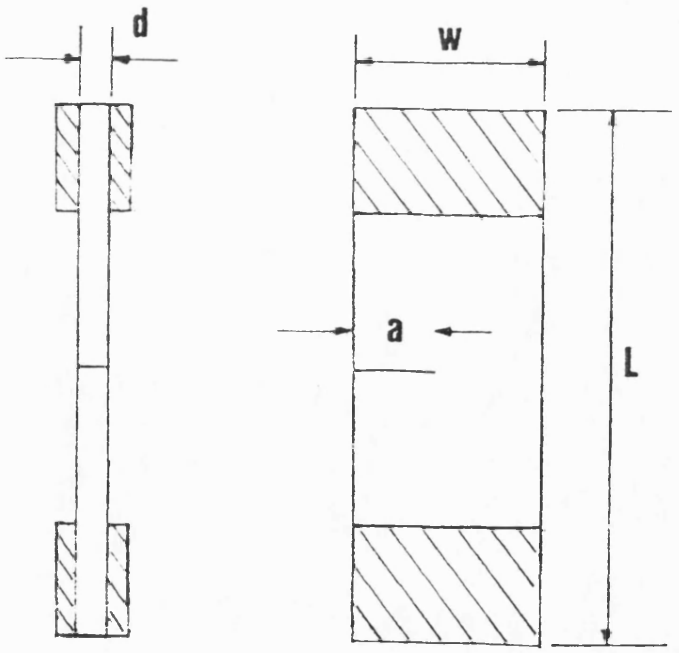

FIG 3.8 TENSILE TEST SPECIMEN

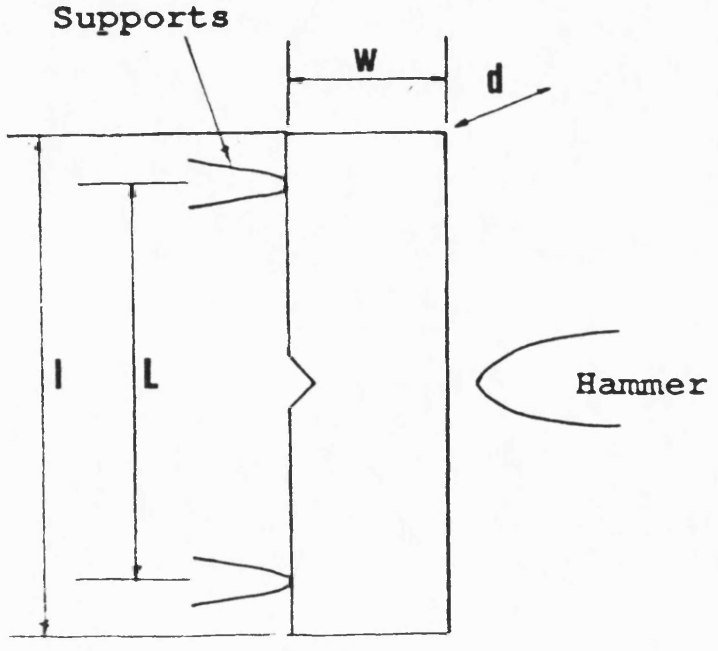

FIG 3.9 IMPACT ENERGY DETERMINATION

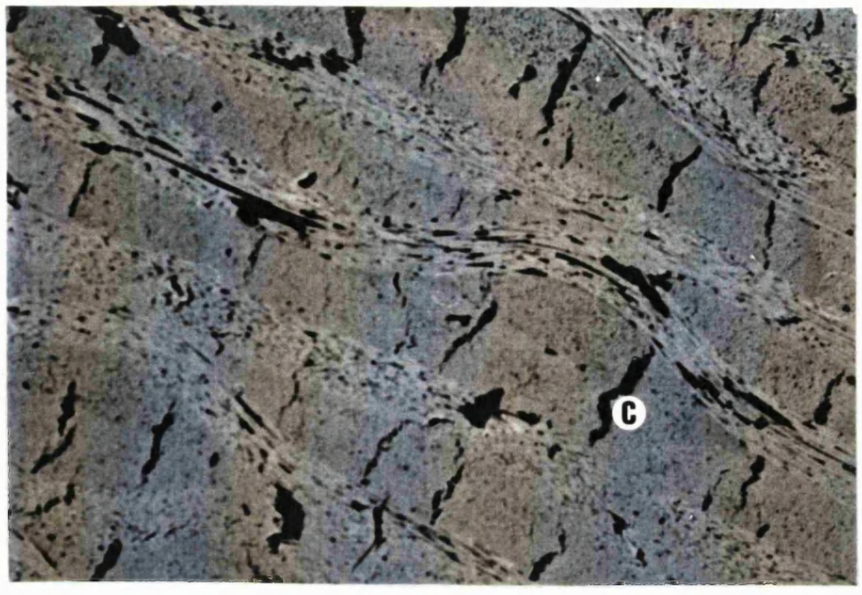

200μm

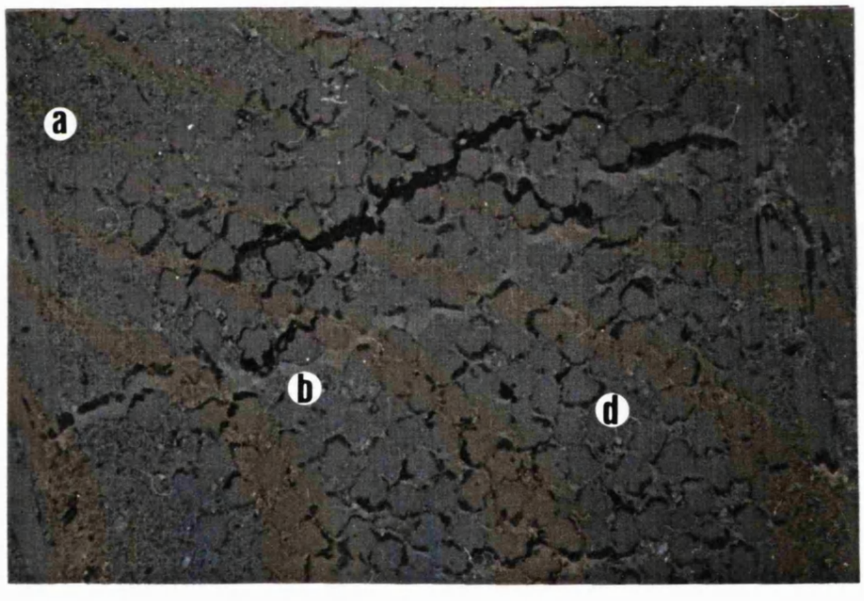

10μm

FIG 4.1 KKARB MICROSTRUCTURE

showing a) pitch influence in matrix, b) resin influence in matrix, c) intrabundle cracking and d) fibre/matrix interface cracks

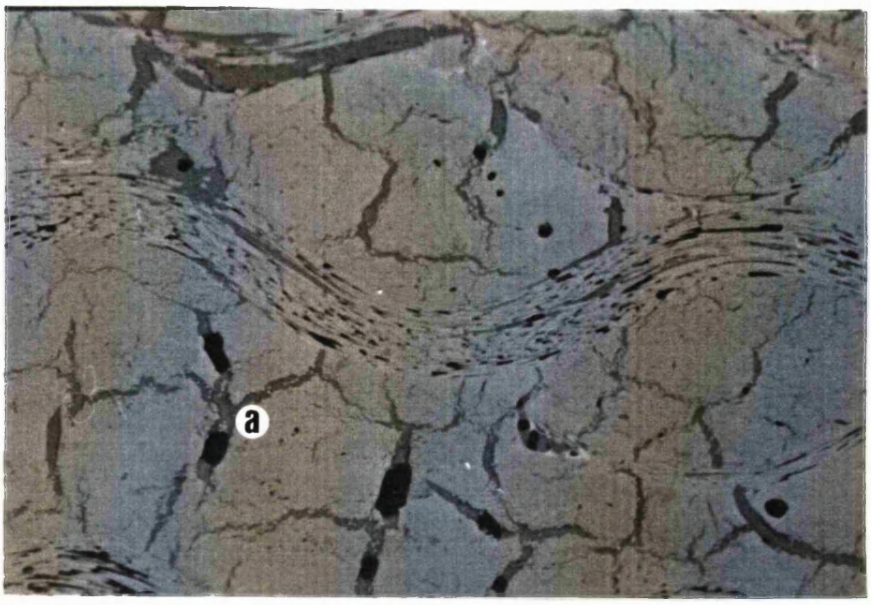

100μm

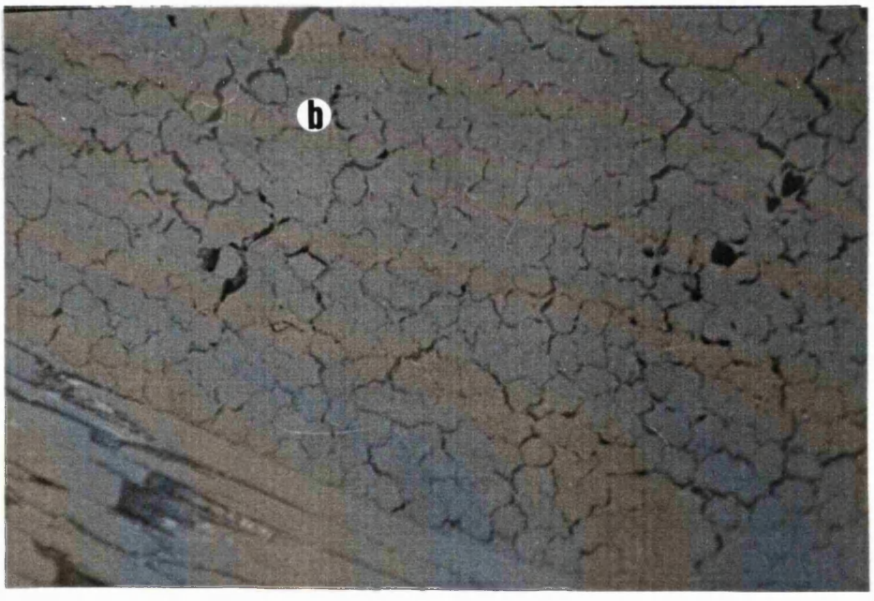

10μm

FIG 4.2 FMI MICROSTRUCTURE

showing a) cracks along and across bundles and b) fibre/matrix interface cracking

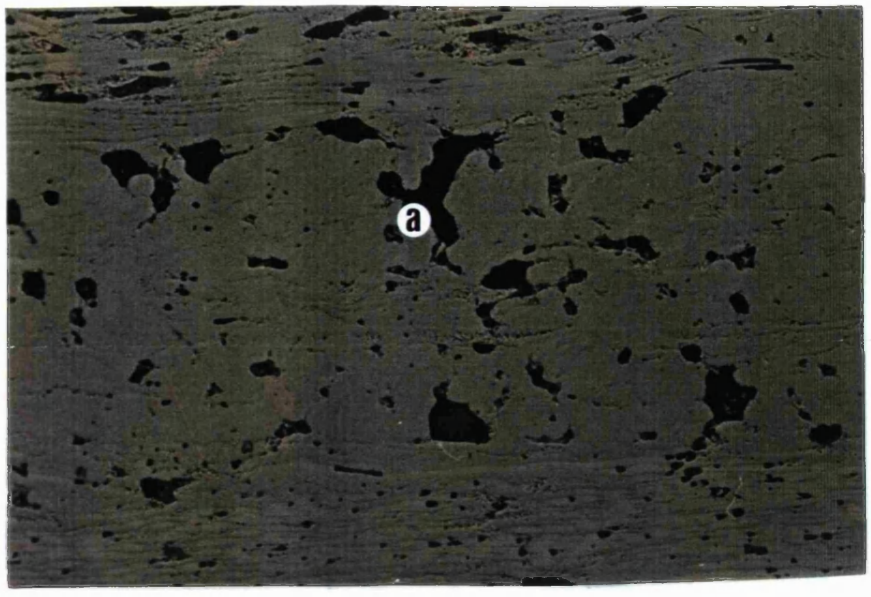

100μm

10μm

FIG 4.3 DUNLOP MICROSTRUCTURE

showing a)porosity

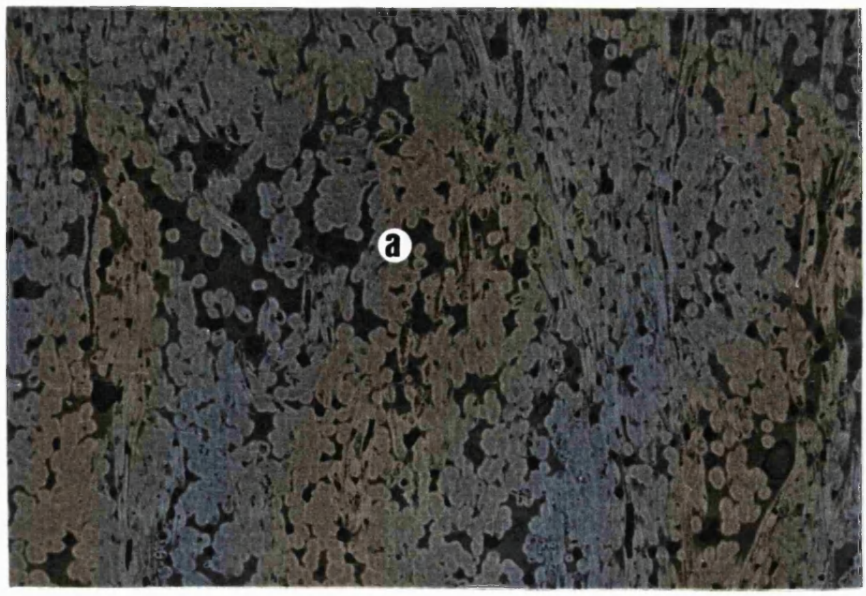

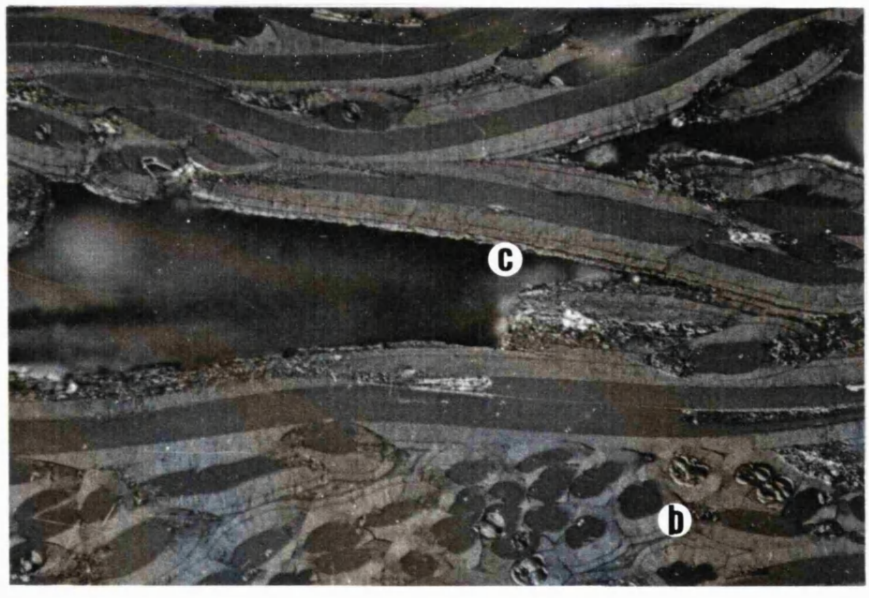

FIG 4.4 AEROLOR 05BT MICROSTRUCTURE showing a) porosity, b) deposition around individual fibres and c) matrix microcracks

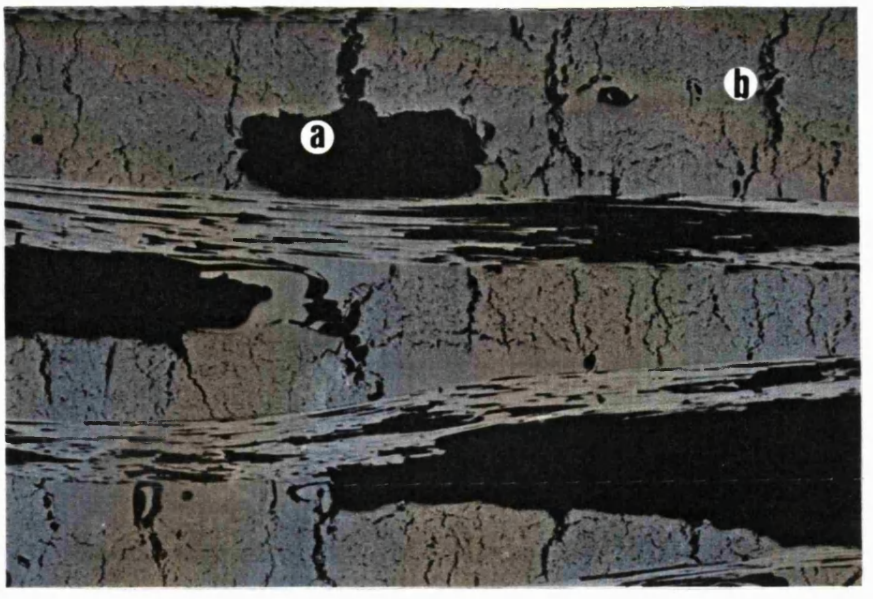

100μm

FIG 4.5 SIGRI CC1501G AND CC1001G MICROSTRUCTURE

showing a) porosity and b) intrabundle cracks

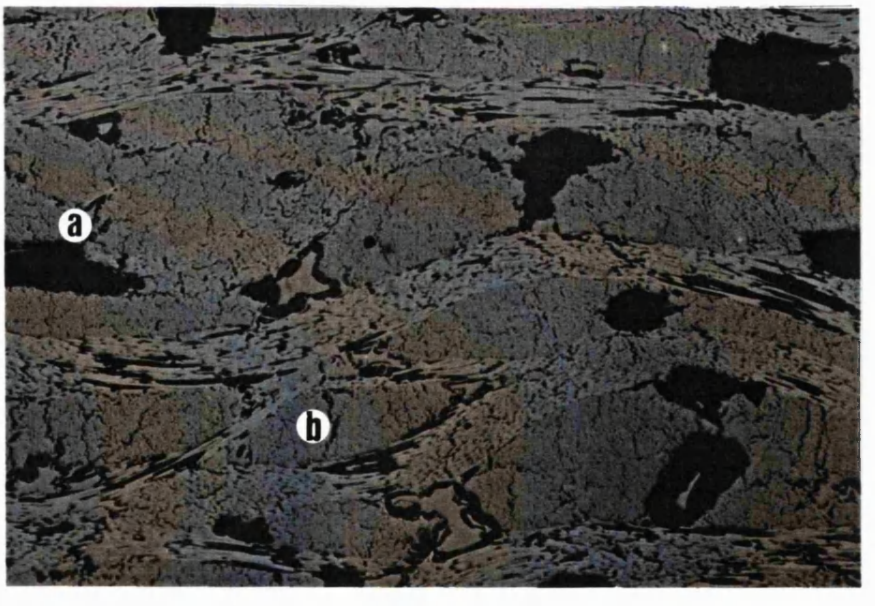

100μm

FIG 4.6 SIGRI CC1506G MICROSTRUCTURE

showing a) porosity and b) intrabundle cracks

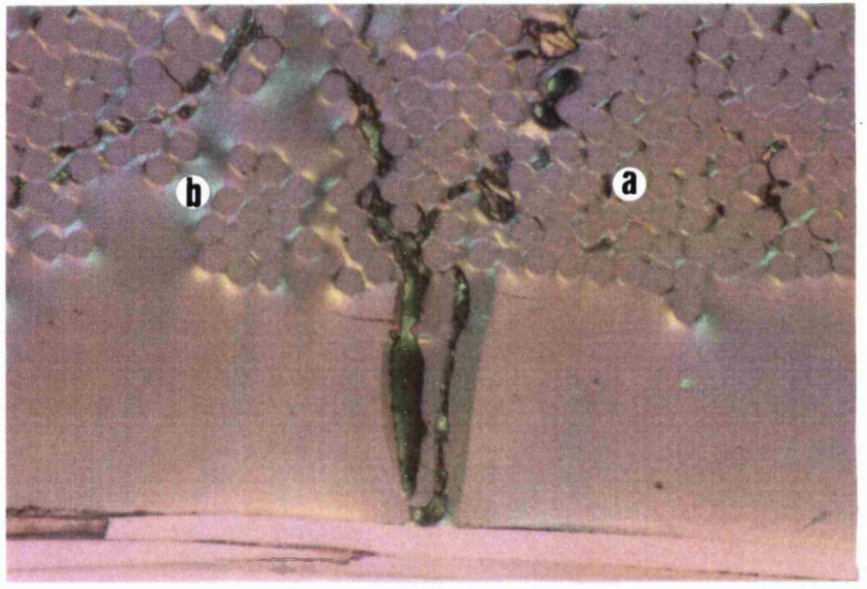

FIG 4.7 SIGRI MICROSTRUCTURE

showing a) small pores at fibre/matrix interfaces and b) orientation of the matrix shown by the blue and yellow regions

100μm

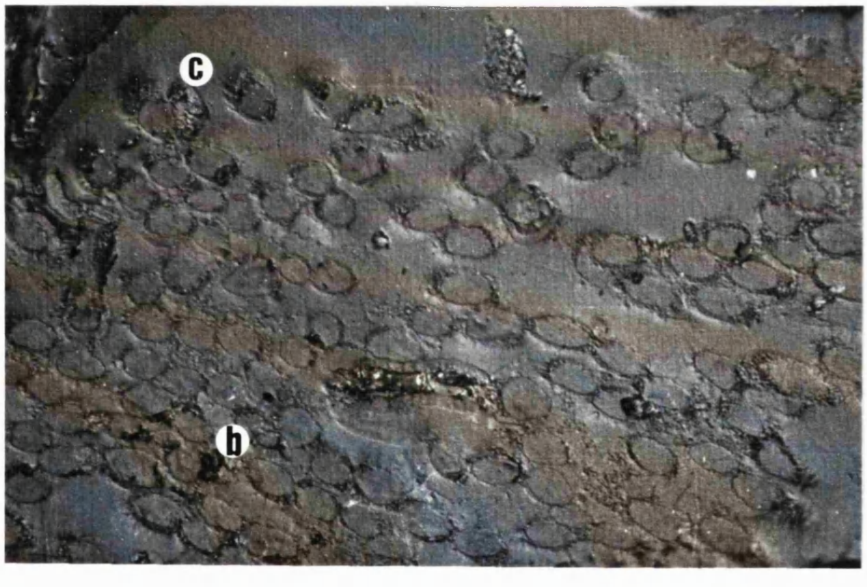

10μm

FIG 4.8 AEROLOR 223 MICROSTRUCTURE showing a) long cracks at bundle/bundle interfaces, b) pores at fibre/matrix interfaces and c) CVD matrix

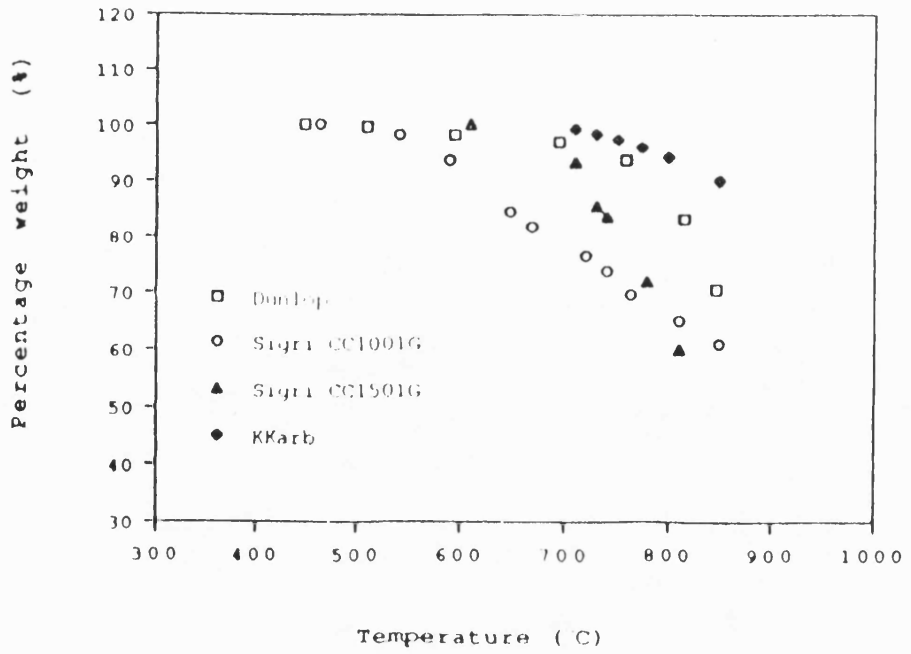

FIG 4.9 MEASUREMENTS OF WEIGHT LOSS AS A FUNCTION OF TEMPERATURE DURING OXIDATION IN A STANTON REDCROFT THERMOBALANCE

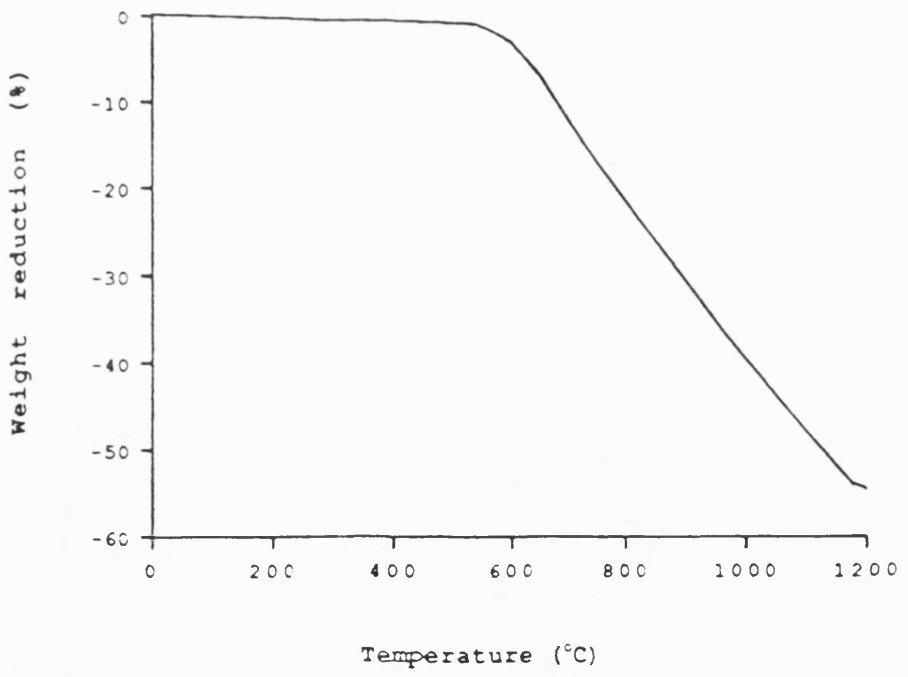

a

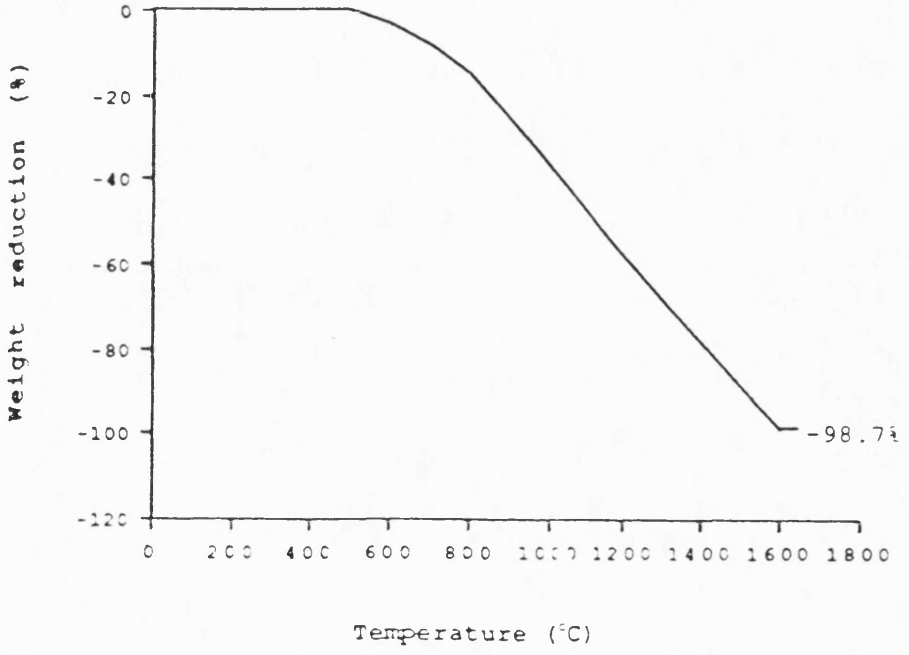

b

FIG 4.10 MEASUREMENTS OF WEIGHT LOSS AS A FUNCTION OF TEMPERATURE DURING OXIDATION IN A SETARAM THERMOBALANCE FOR a) SIGRI AND b) KKARB COMPOSITES

heating rate 20°C/min air flow 50cc/min

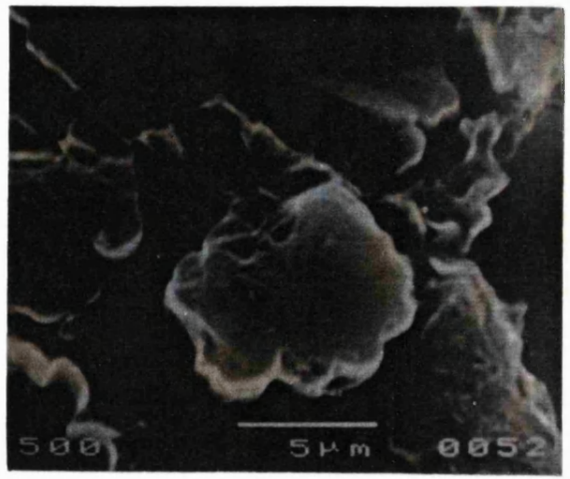

0% weight loss

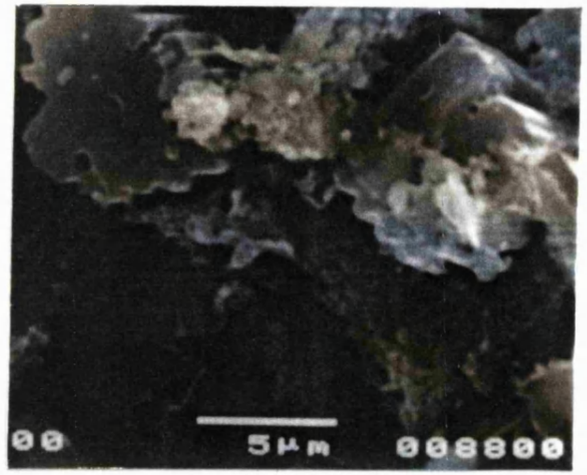

1.7% weight loss

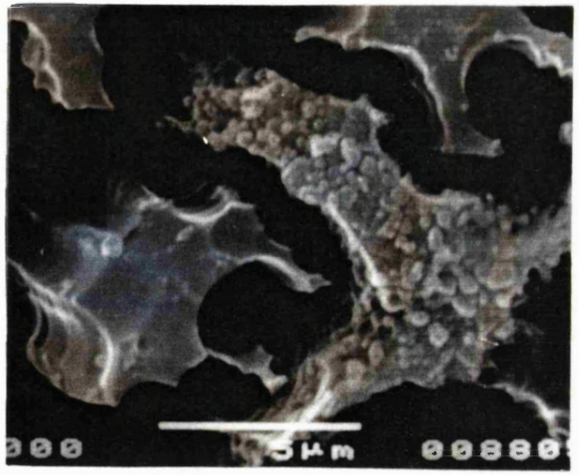

5% weight loss

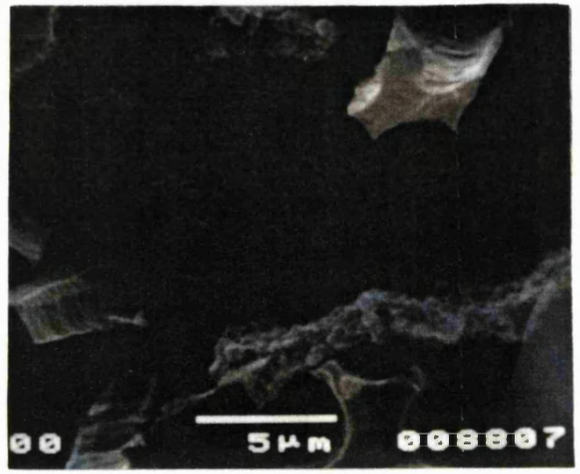

9% weight loss

FIG 4.11 EFFECT OF OXIDATION AT VARIOUS WEIGHT LOSSES ON THE MICROSTRUCTURE OF THE KKARB COMPOSITE

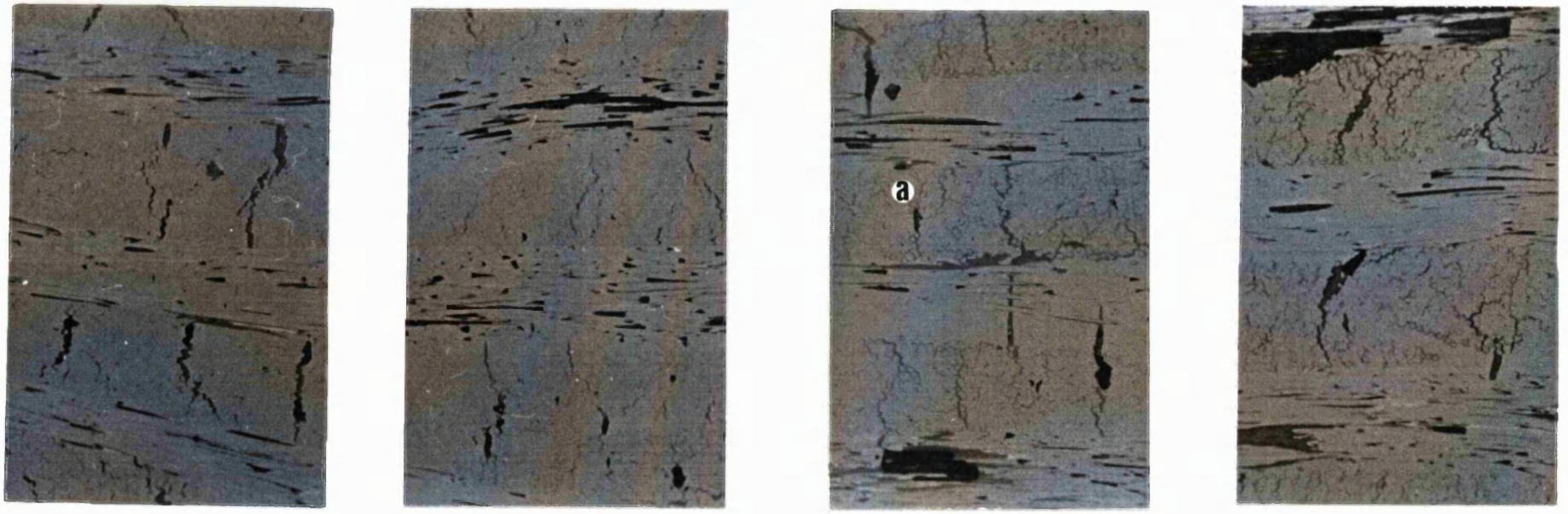

0% weight loss 1.7% weight loss 5% weight loss 9% weight loss

200μm

FIG 4.12 EFFECT OF OXIDATION AT VARIOUS WEIGHT LOSSES ON THE BULK MICROSTRUCTURE FOR THE KKARB COMPOSITE

showing a) individual fibres highlighted by oxidation

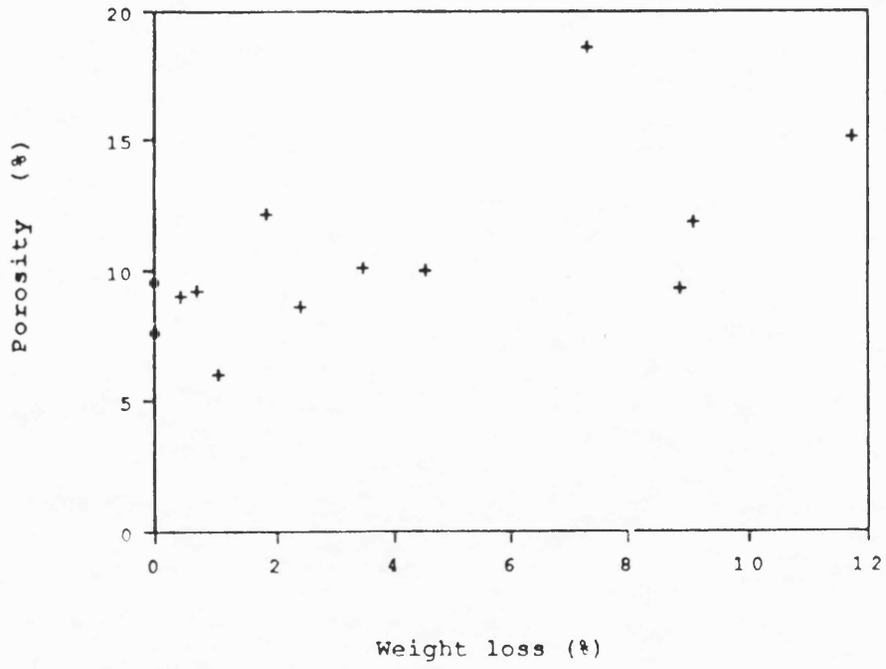

FIG 4.13 POROSITY CHANGE WITH WEIGHT LOSS FOR THE KKARB COMPOSITE

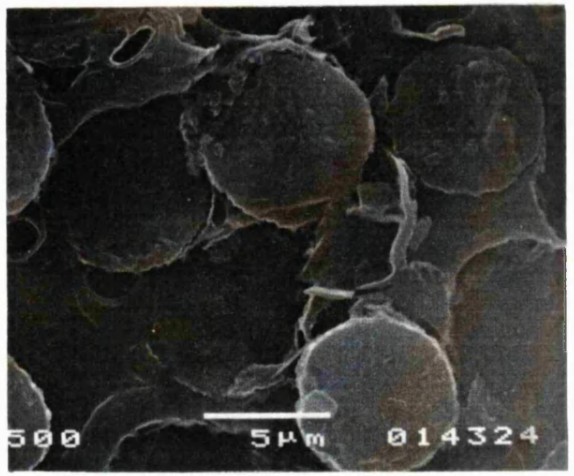

0% weight loss

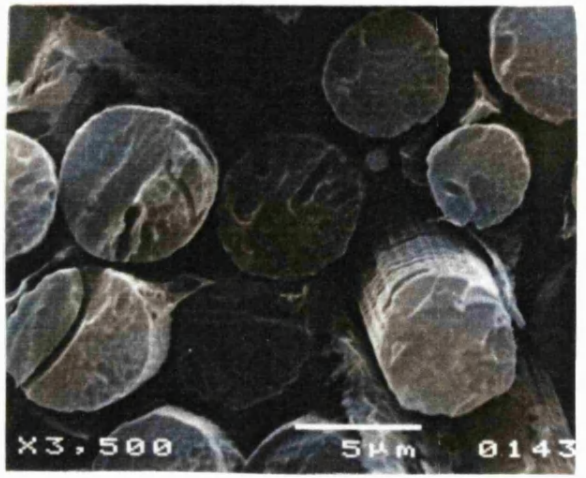

3.4% weight loss

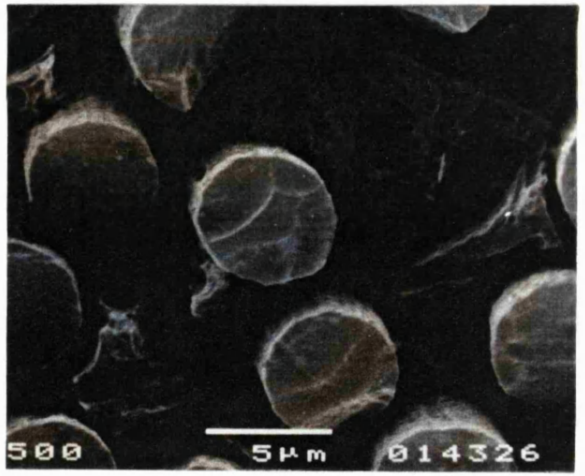

4.4%weight loss

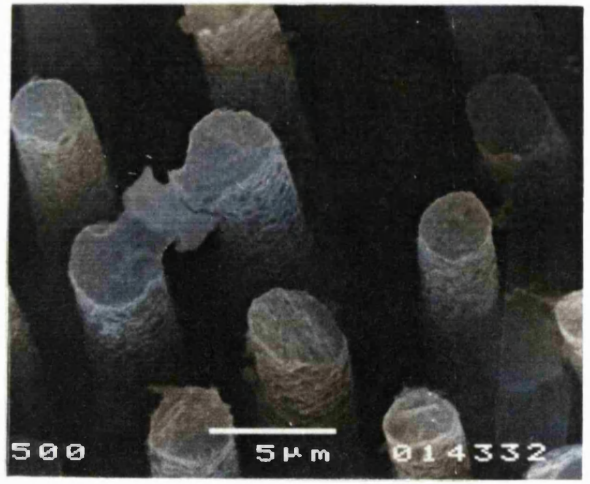

17.1% weight loss

FIG 4.14 EFFECT OF OXIDATION AT VARIOUS WEIGHT LOSSES ON THE MICROSTRUCTURE OF THE SIGRI COMPOSITE

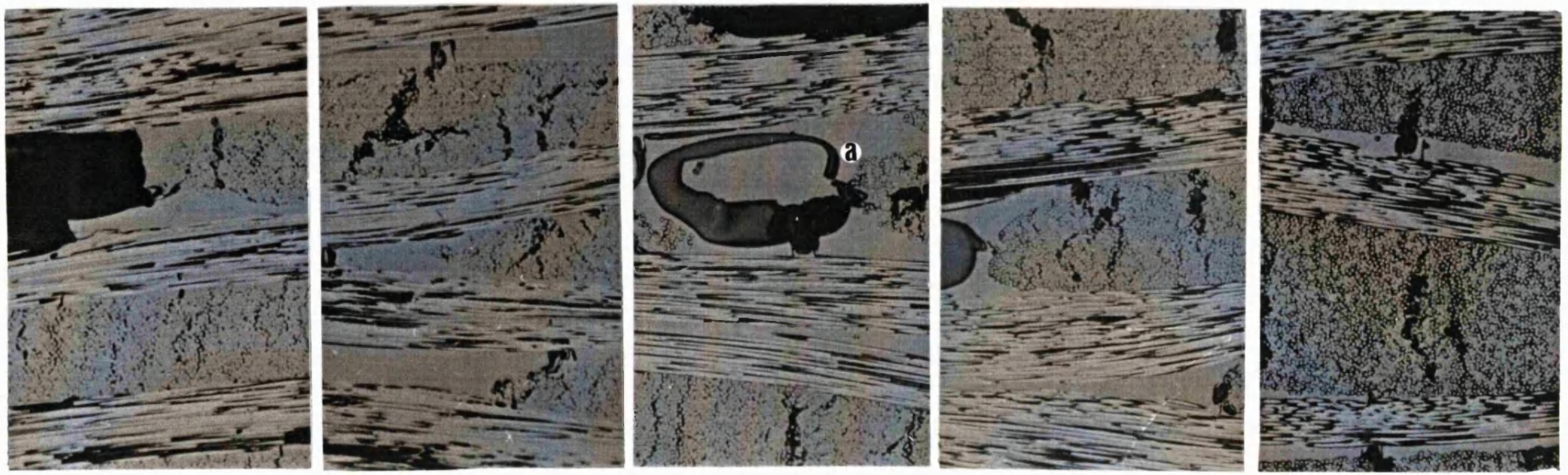

0% weight loss 2.5% weight loss 3.5% weight loss 17.4% weight loss 21% weight loss

200μm

FIG 4.15 EFFECT OF OXIDATION AT VARIOUS WEIGHT LOSSES ON THE BULK MICROSTRUCTURE OF THE SIGRI COMPOSITE

showing a) individual fibres highlighted by oxidation

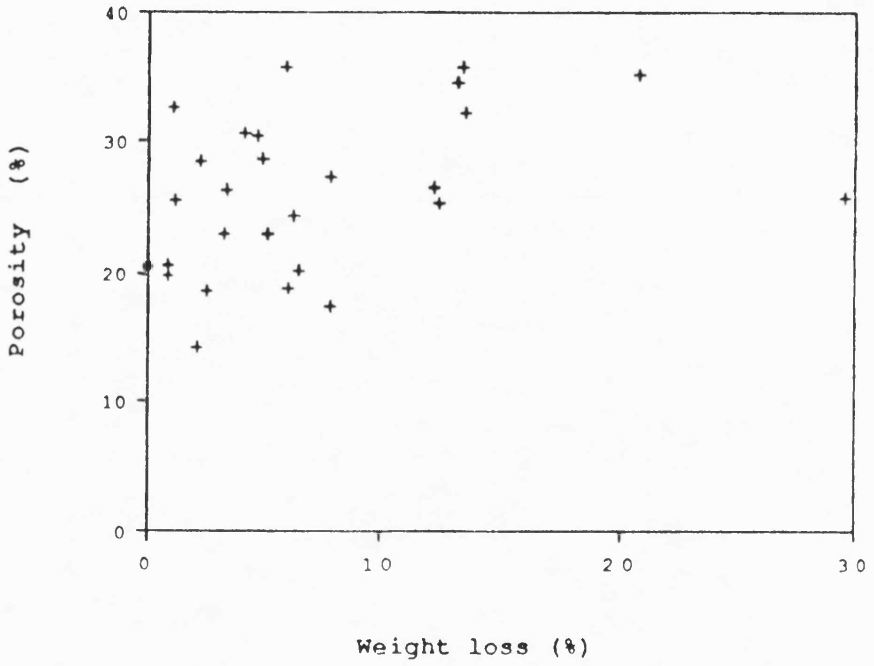

FIG 4.16 POROSITY CHANGE WITH WEIGHT LOSS FOR THE SIGRI COMPOSITE

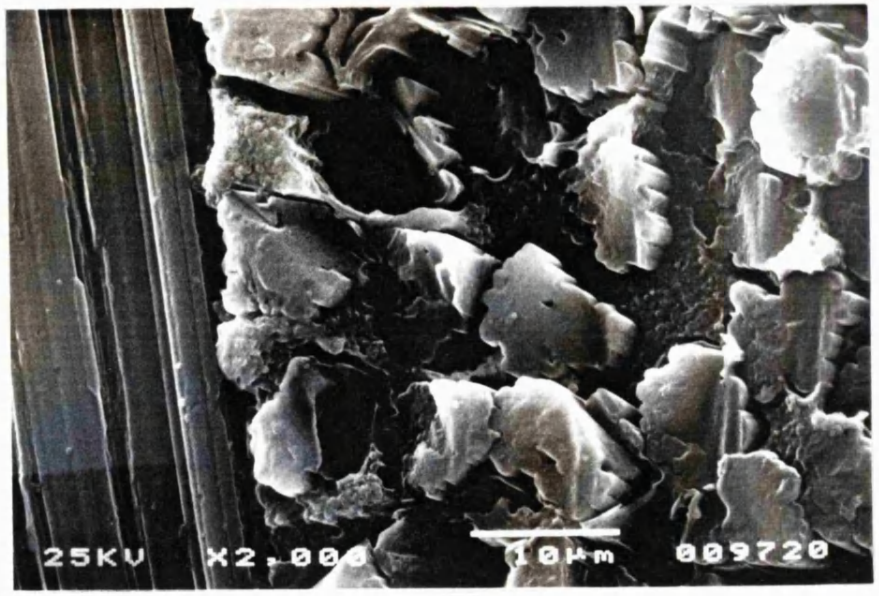

0% weight loss

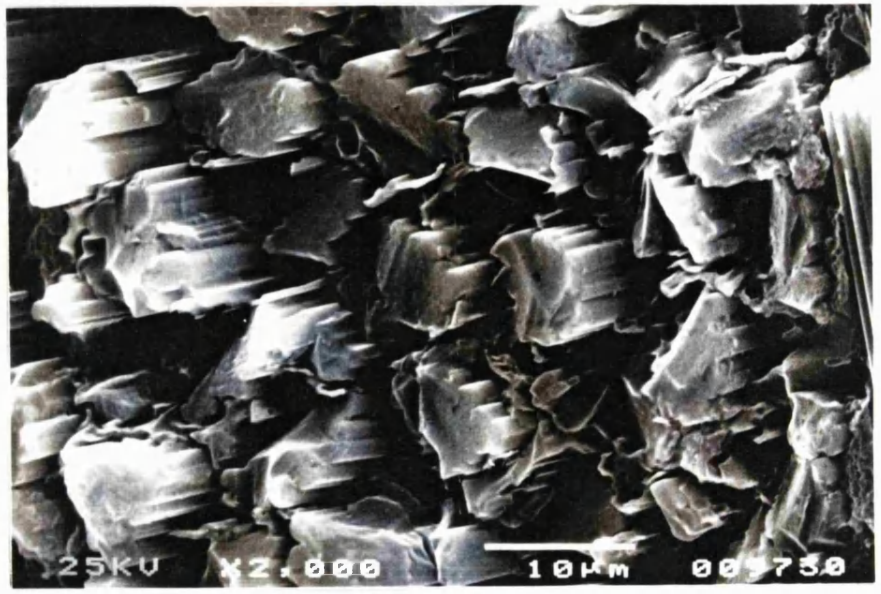

5.8% weight loss

FIG 4.17 EFFECT OF OXIDATION AT VARIOUS WEIGHT LOSSES ON THE MICROSTRUCTURE OF THE FMI COMPOSITE

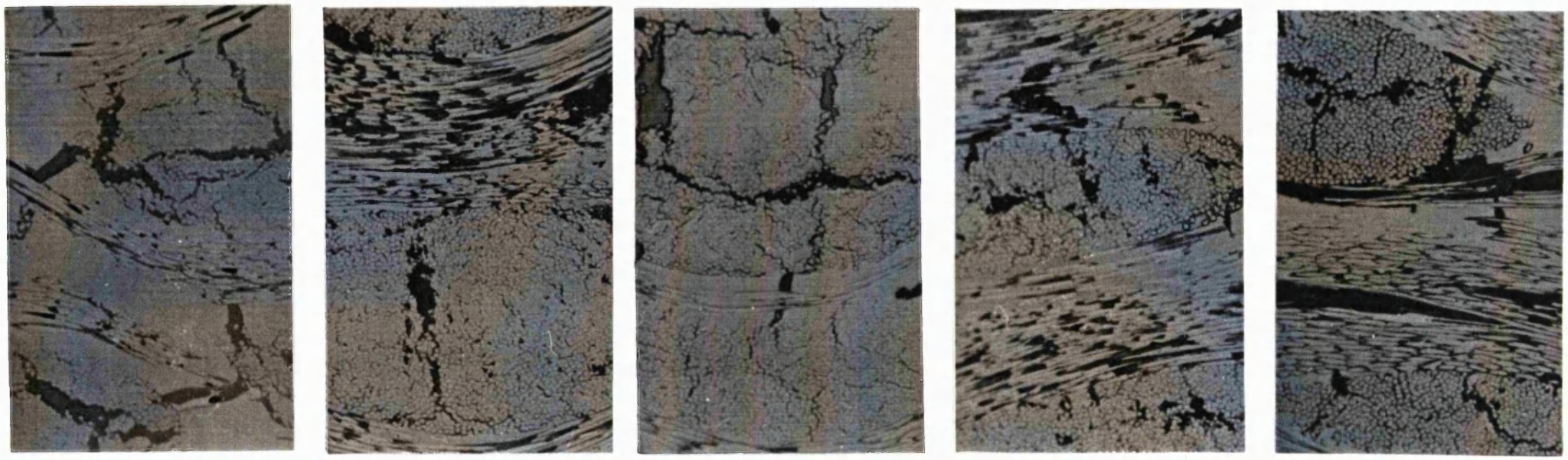

0% weight loss 2.2% weight loss 3.3% weight loss 7.6% weight loss 20.8% weight loss

200μm

FIG 4.18 EFFECT OF OXIDATION AT VARIOUS WEIGHT LOSSES ON THE BULK MICROSTRUCTURE OF THE FMI COMPOSITE

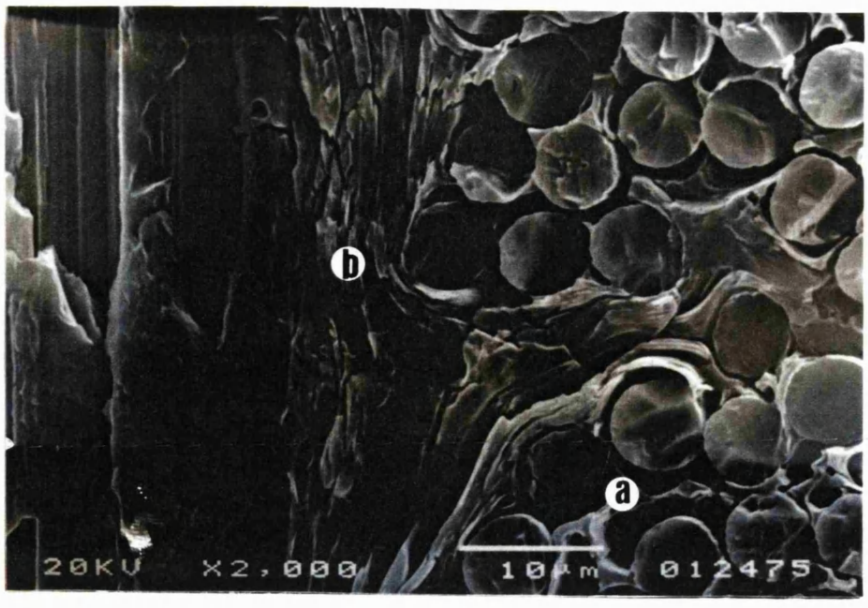

FIG 4.19 SIGRI CHEMICALLY ETCHED MICROSTRUCTURE

showing a) small pores where oxidation starts and carbon matrix alignment

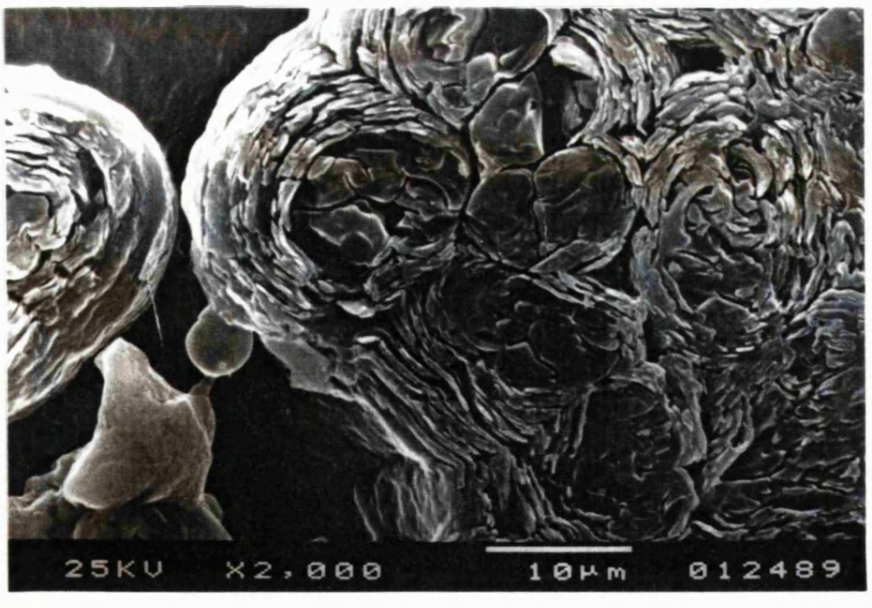

FIG 4.20 AEROLOR 05 CHEMICALLY ETCHED MICROSTRUCTURE

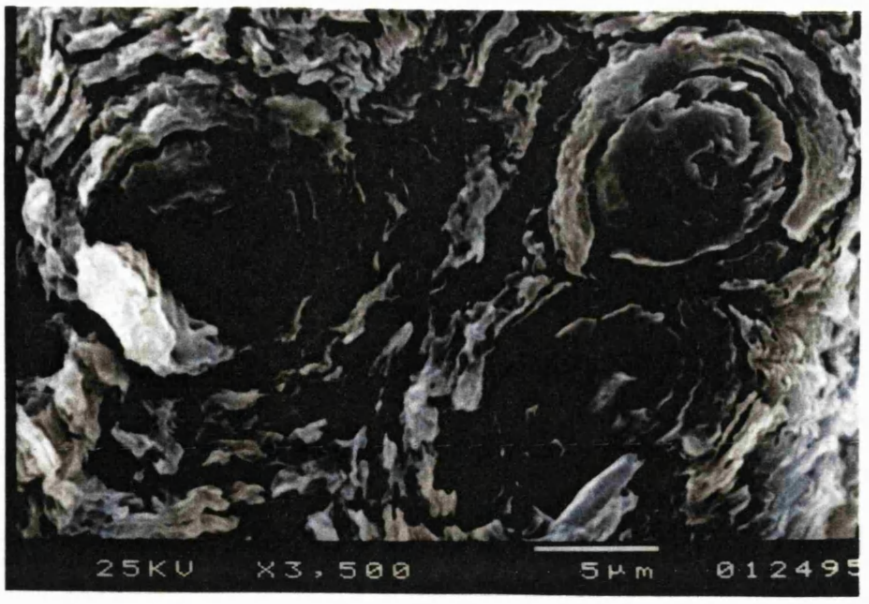

FIG 4.21 DUNLOP CHEMICALLY ETCHED MICROSTRUCTURE

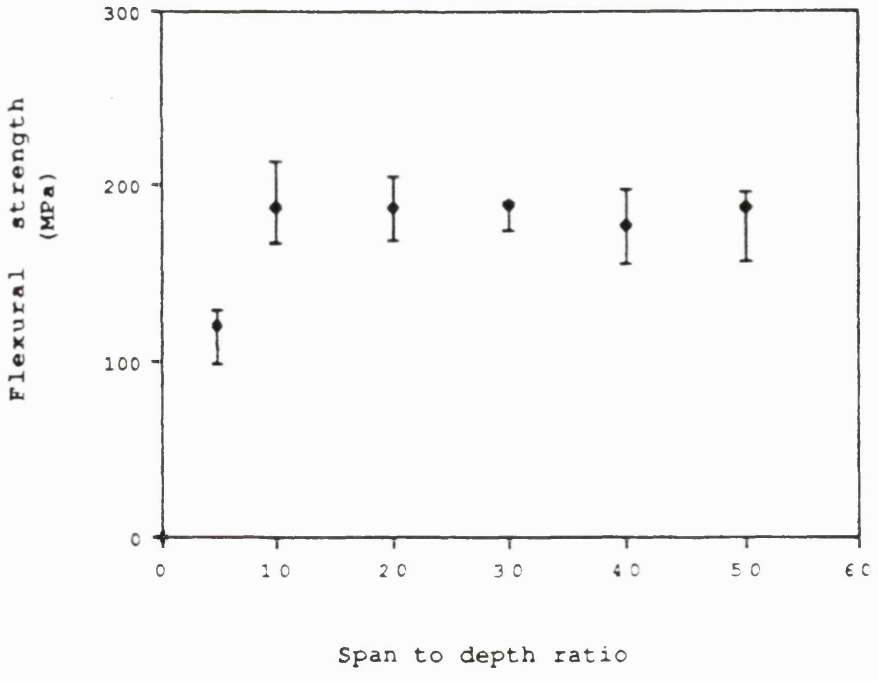

FIG 4.22 FLEXURAL STRENGTH VARIATION WITH SPAN TO DEPTH RATIO FOR THE KKARB COMPOSITE

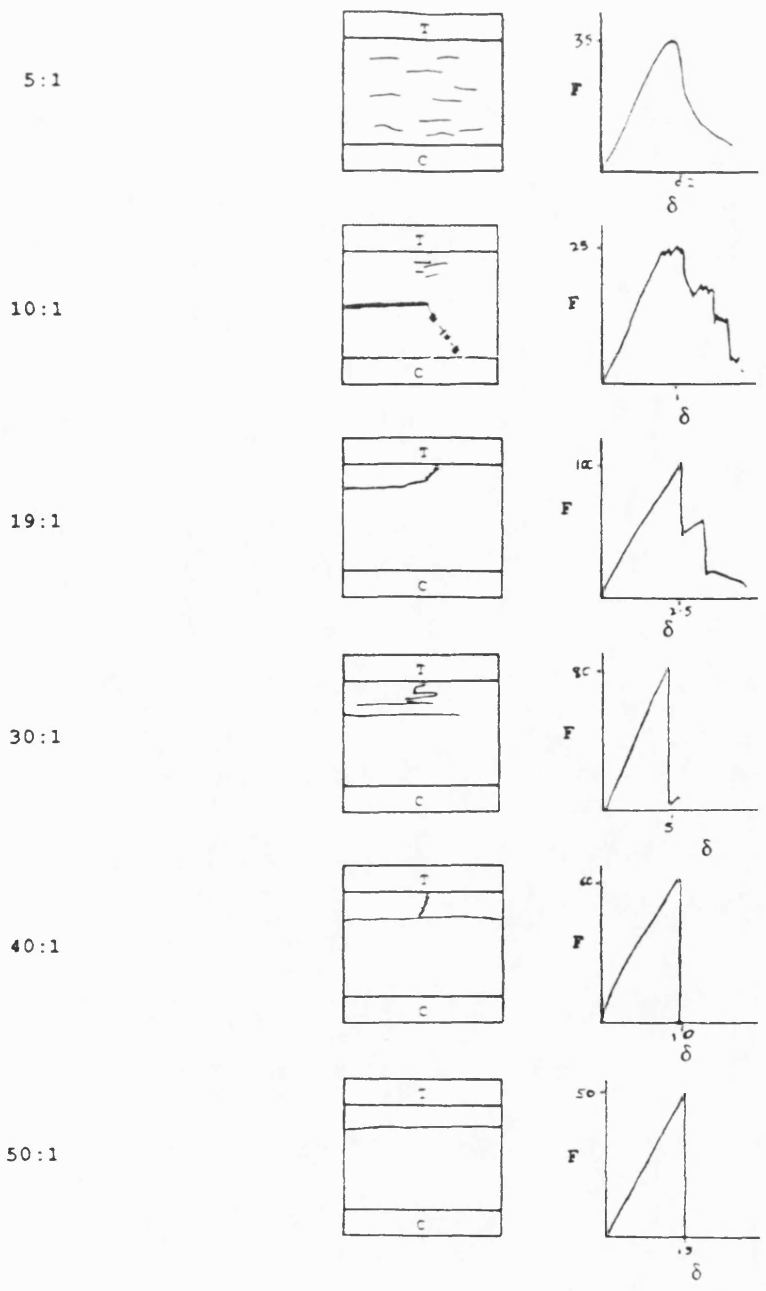

FIG 4.23 KKARB MODES OF FAILURE FOR DIFFERENT SPAN TO DEPTH RATIOS

T=tensile face of composite F=force in N /// =shear crack

C=compressive face of composite δ=deflection in mm

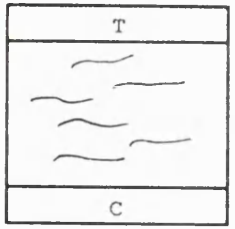

a

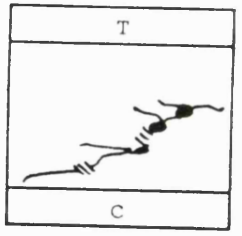

b

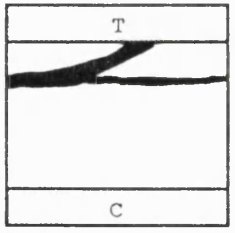

c

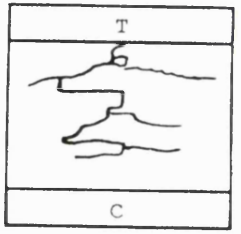

d

FIG 4.24 THE MAIN MODES OF FAILURE OF CARBON/CARBON COMPOSITES SHOWING a) BUNDLE/BUNDLE INTERFACE CRACKING, b) SHEAR CRACKING, c) DELAMINATION CRACKING AND d) STEPPED CRACKING

T=TENSILE FACE OF COMPOSITE C=COMPRESSIVE FACE OF COMPOSITE /// =SHEAR CRACKING

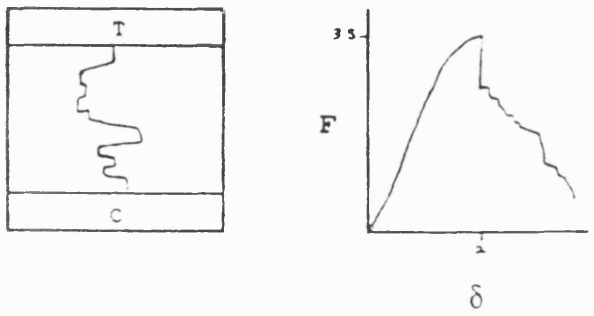

T=tensile face of composite F=force in N

C=compressive face of composite δ=deflection in mm

FIG 4.25 KKARB FILL DIRECTION FAILURE MODE WHEN TESTED IN FLEXURE

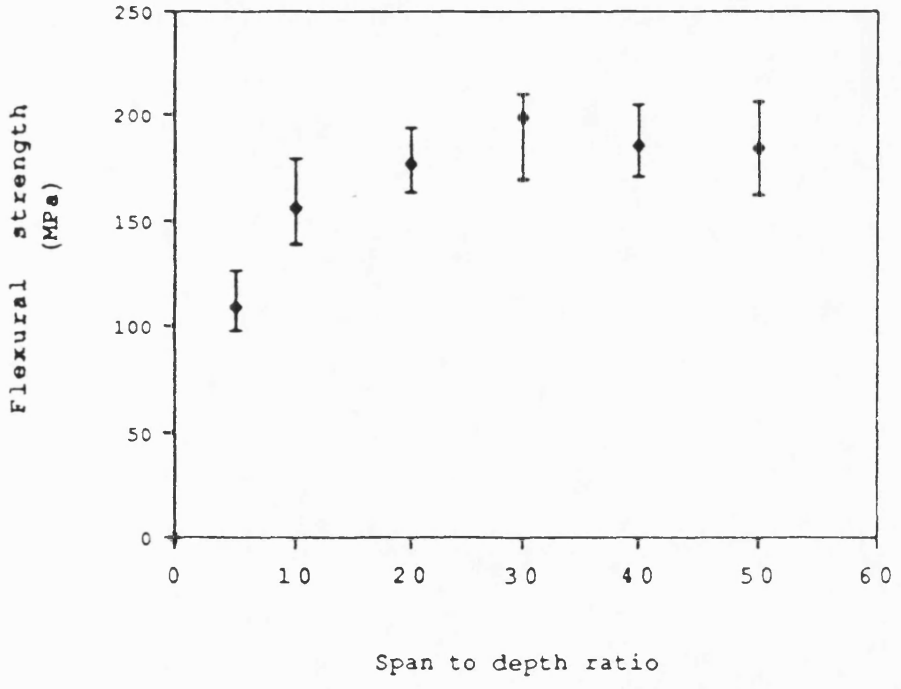

FIG 4.26 FLEXURAL STRENGTH VARIATION WITH SPAN TO DEPTH RATIO FOR THE SIGRI COMPOSITE error bars show variation of actual data

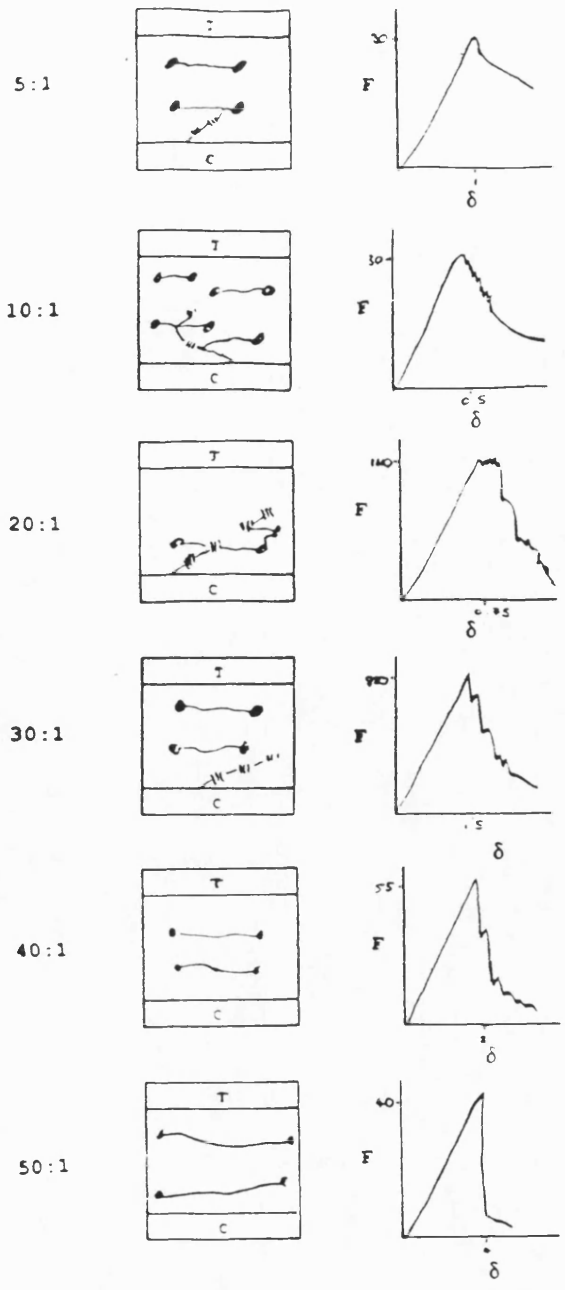

FIG 4.27 SIGRI MODES OF FAILURE FOR DIFFERENT SPAN TO DEPTH RATIOS

T=tensile face of composite F=force in N /// =shear crack

C=compressive face of composite δ=deflection in mm • :pores

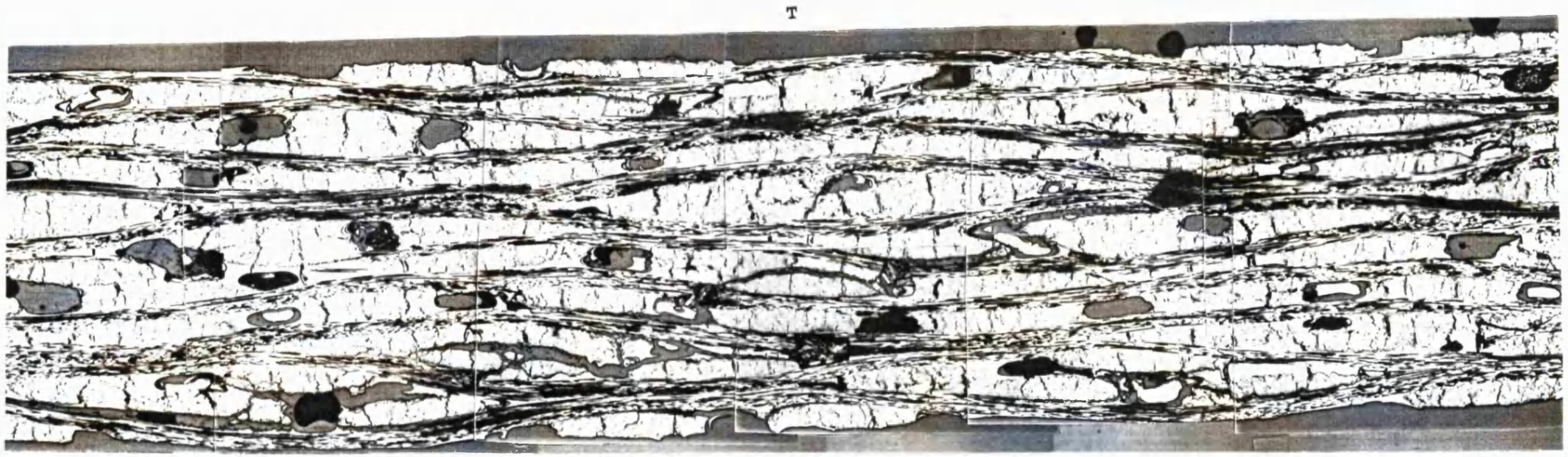

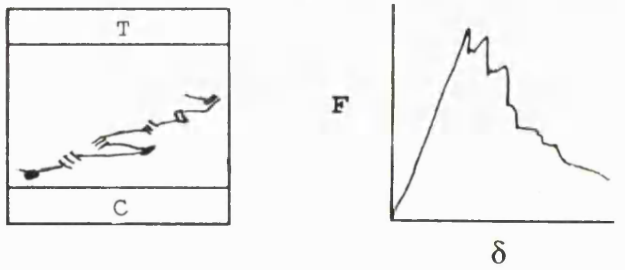

T=tensile face of composite F=force ⫽ =shear crack

C=compressive face of composite δ=deflection ● =pores

FIG 4.28 FORCE/DEFLECTION CURVE AND FRACTURE SURFACE FOR THE SIGRI COMPOSITE

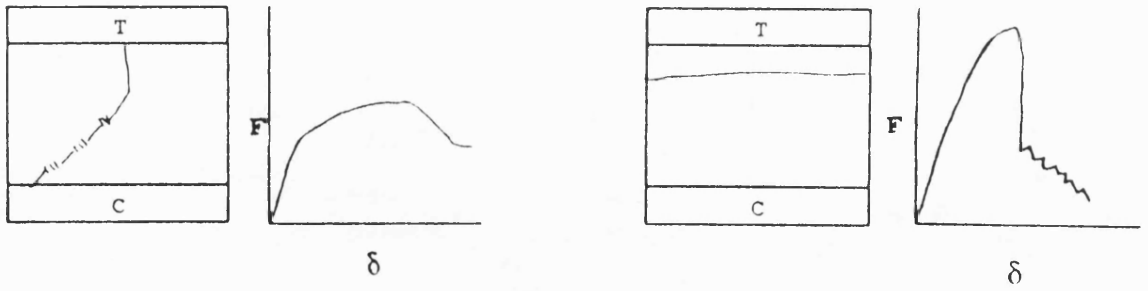

Shear Delaminating

FIG 4.29 FMI FAILURE MODES WHEN TESTED IN FLEXURE

T=tensile face of composite F=force ⸗ =shear crack

C=compressive face of composite δ=deflection

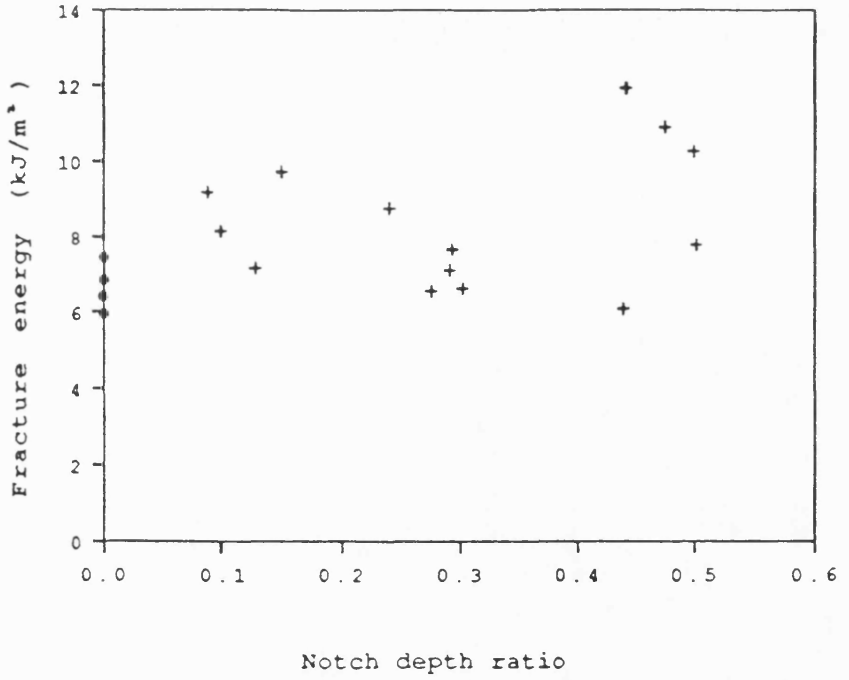

a

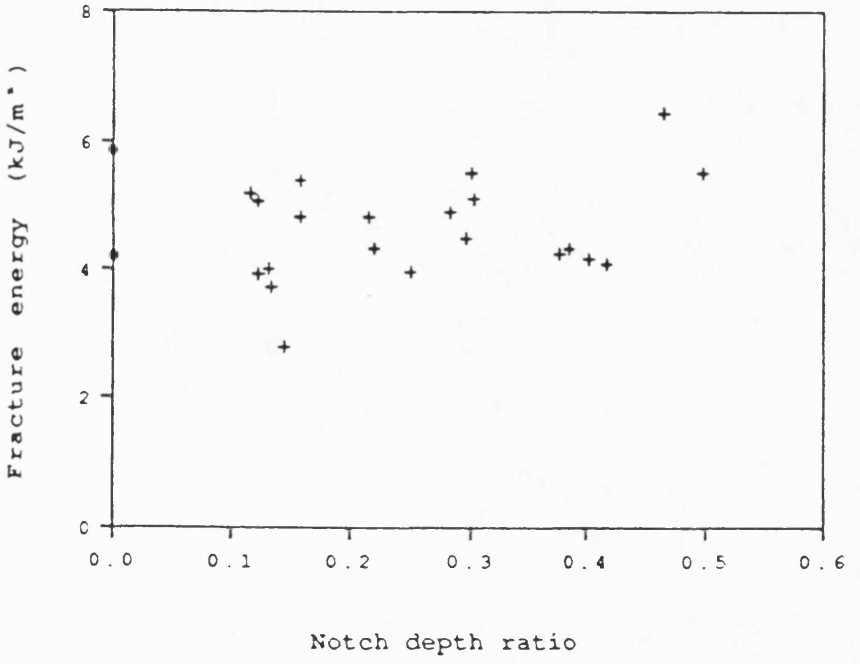

b

FIG 4.30 VARIATION OF FLEXURAL IMPACT ENERGY WITH NOTCH DEPTH FOR THE KKARB COMPOSITE IN a) WARP AND b)FILL DIRECTIONS

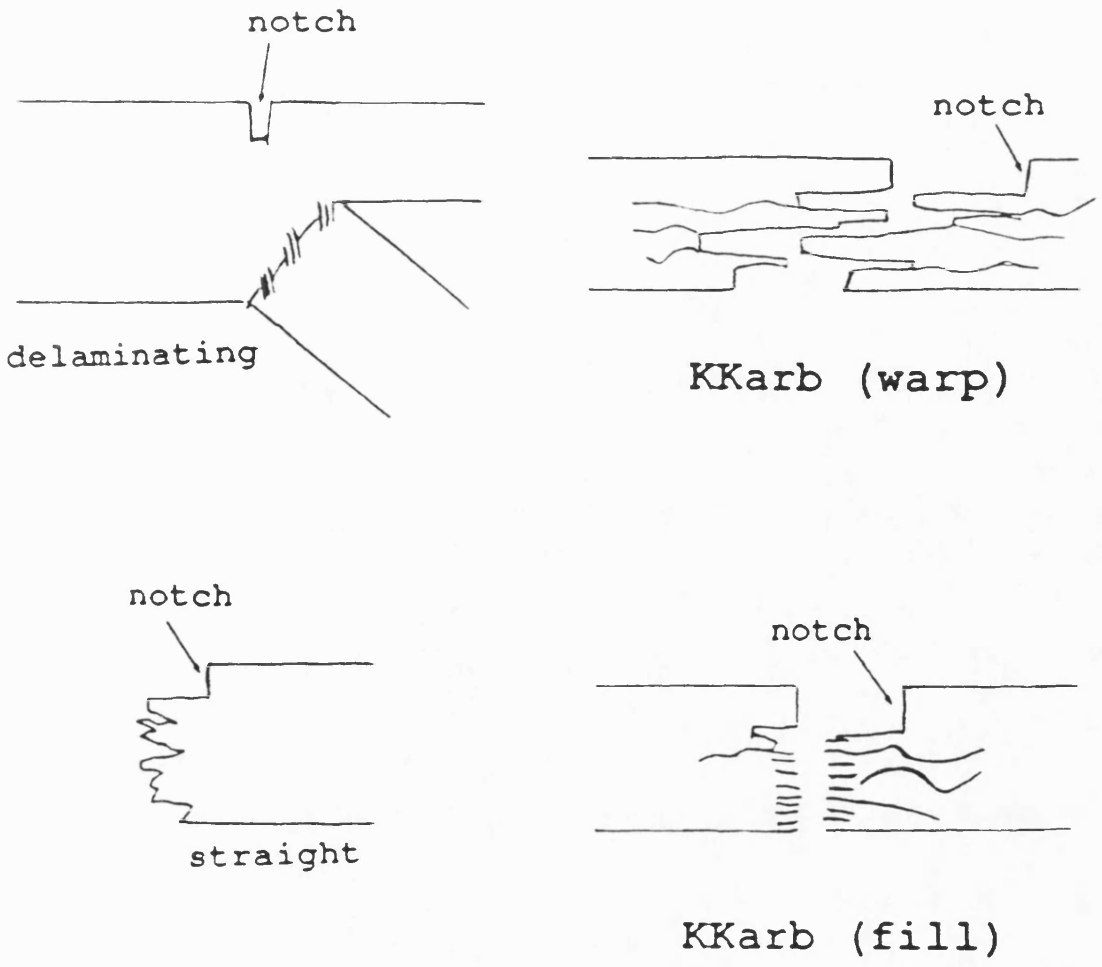

FIG 4.31 MODES OF FAILURE FOR ALL MATERIALS WHEN IMPACT TESTED

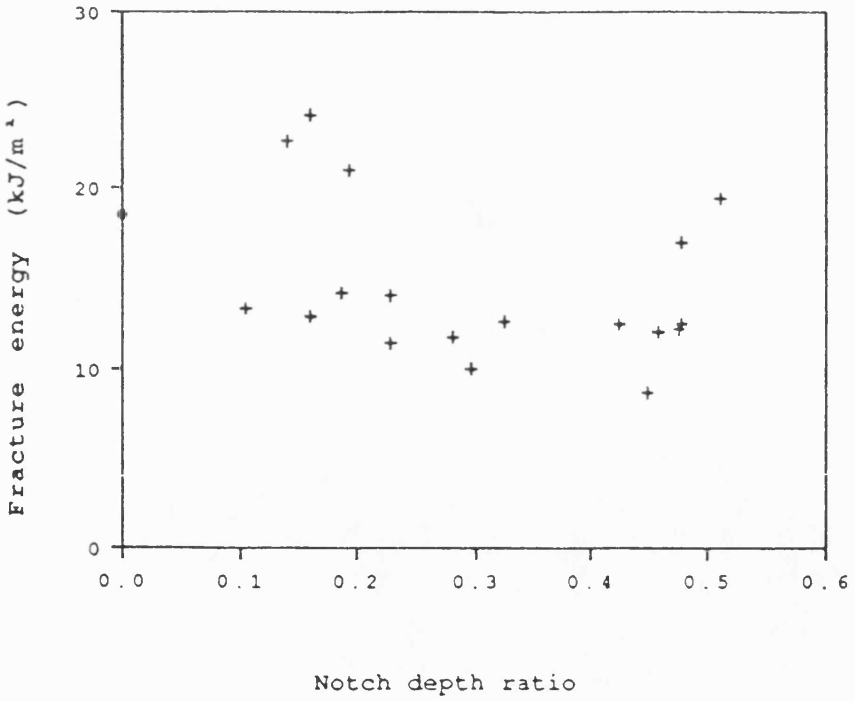

FIG 4.32 VARIATION OF FLEXURAL IMPACT ENERGY WITH NOTCH DEPTH FOR THE SIGRI COMPOSITE

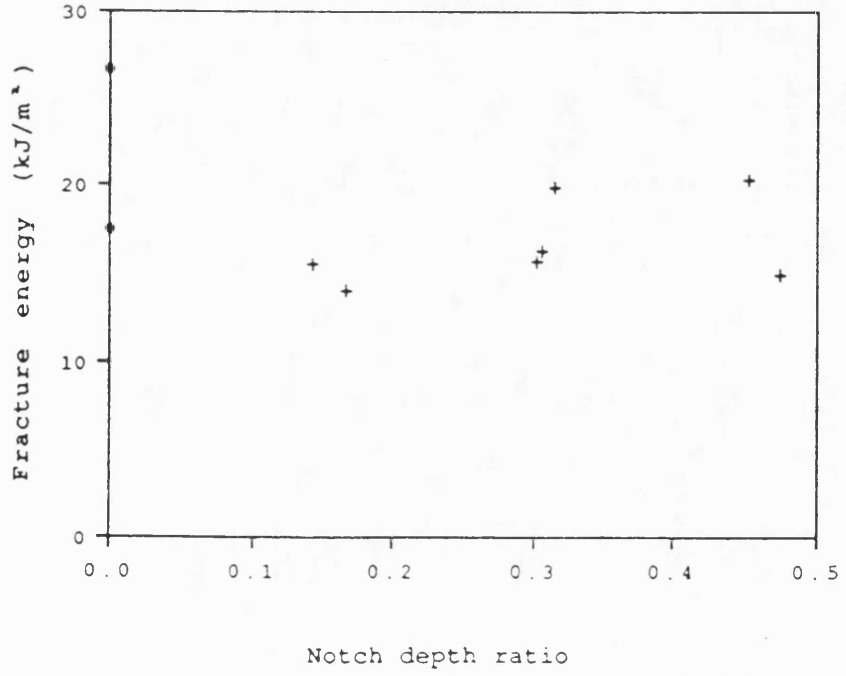

FIG 4.33 VARIATION OF FLEXURAL IMPACT ENERGY WITH NOTCH DEPTH FOR THE FMI COMPOSITE

a

1mm

b

1mm

FIG 4.34 TENSILE FAILURE OF a) SIGRI AND b) KKARB SAMPLES

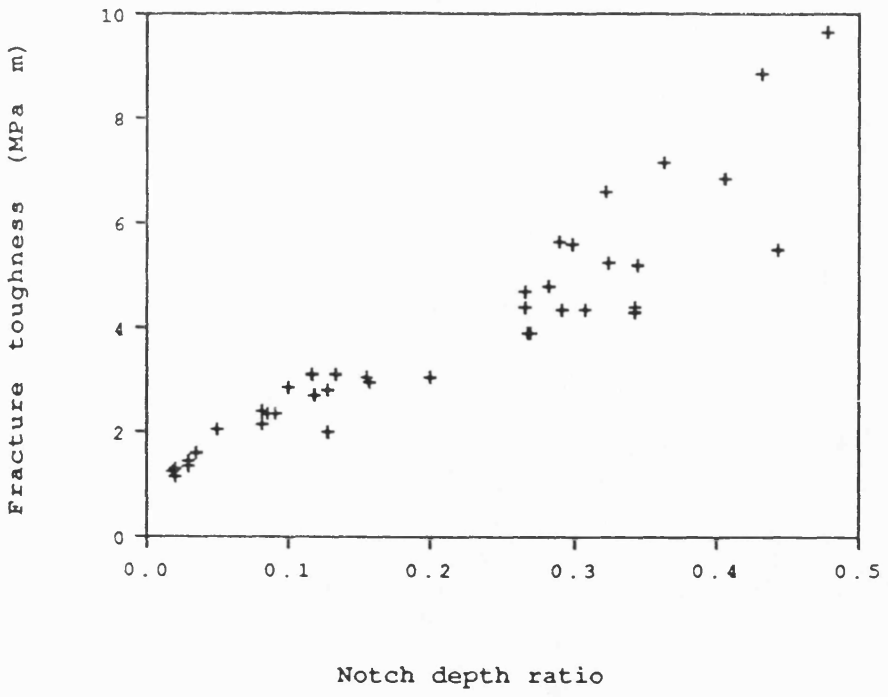

a

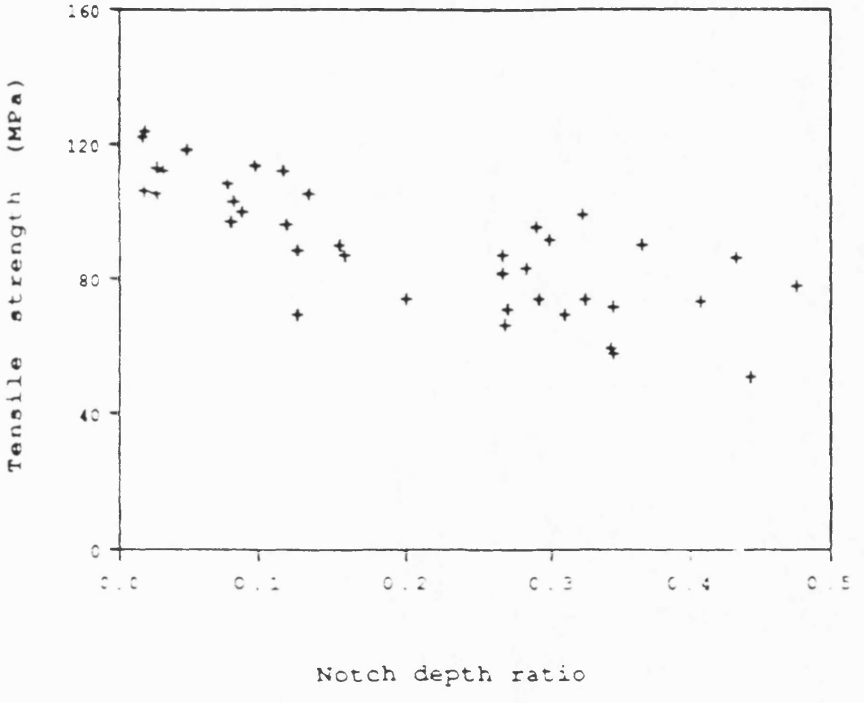

b

FIG 4.35 VARIATION OF a) TOUGHNESS AND b) TENSILE STRENGTH WITH NOTCH DEPTH FOR THE KKARB COMPOSITE

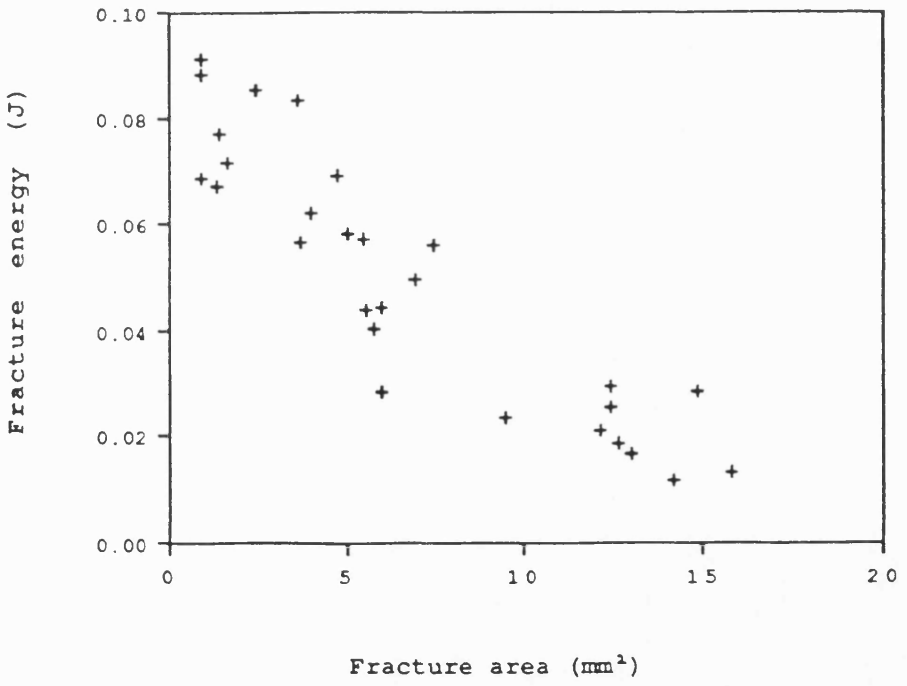

a

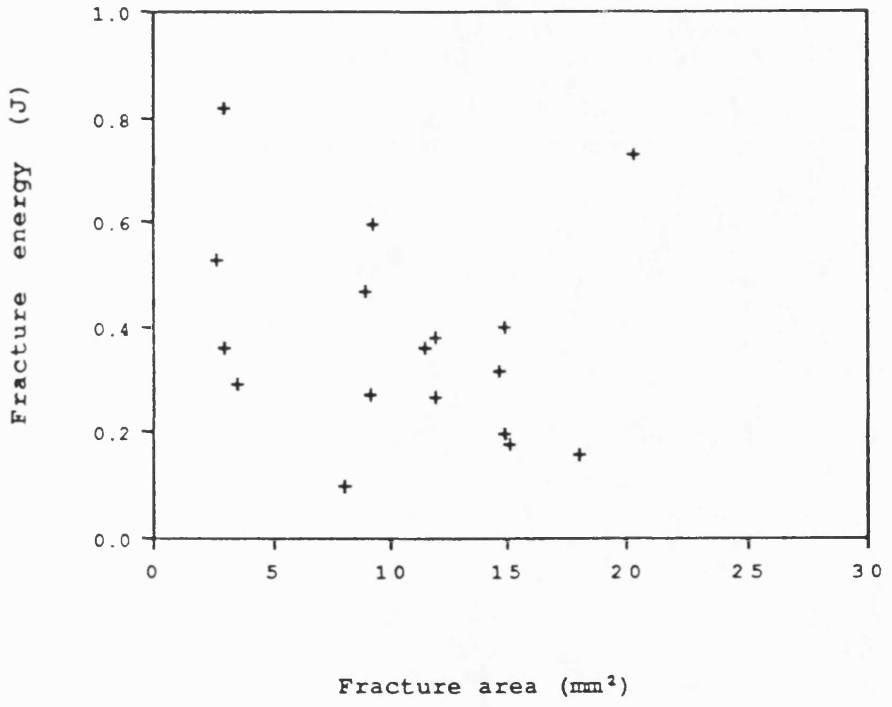

b

FIG 4.36 VARIATION OF FRACTURE ENERGY WITH FRACTURE AREA FOR a) KKARB AND b) SIGRI

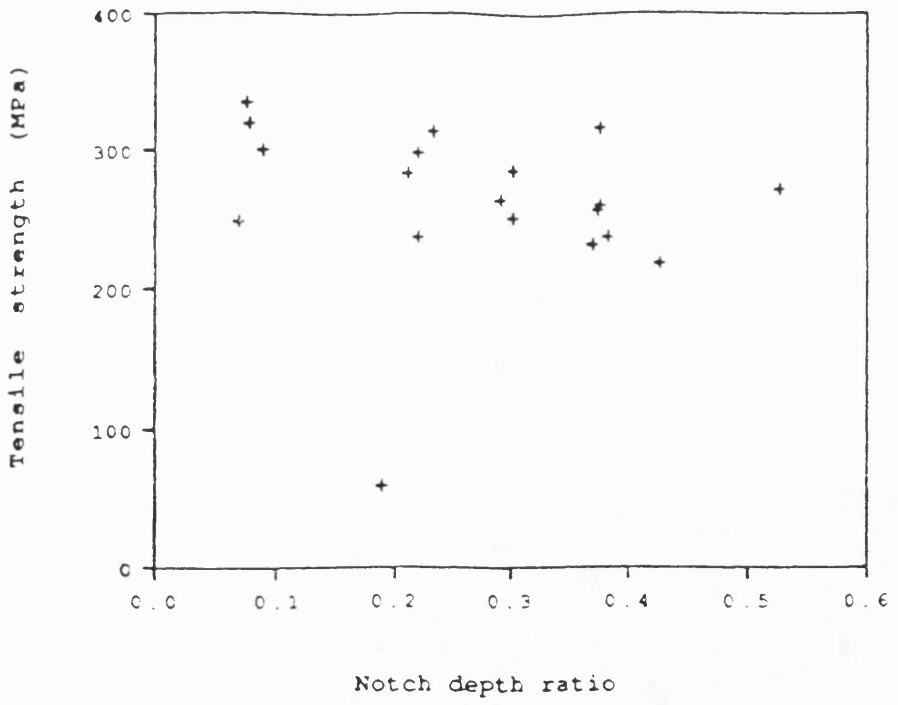

a

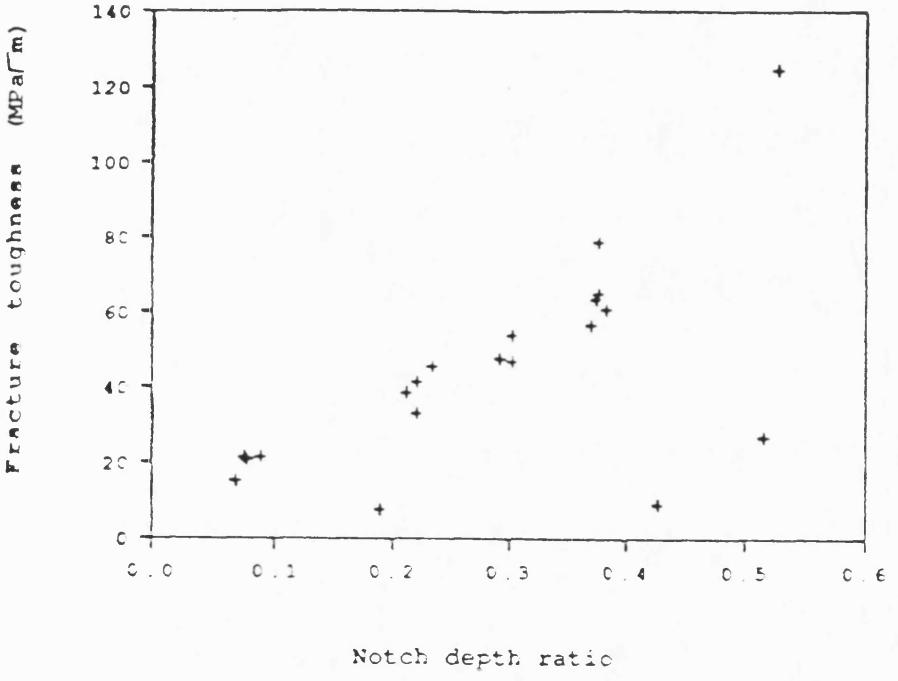

b

FIG 4.37 VARIATION OF a) TENSILE STRENGTH AND b) TOUGHNESS WITH NOTCH DEPTH FOR THE SIGRI COMPOSITE

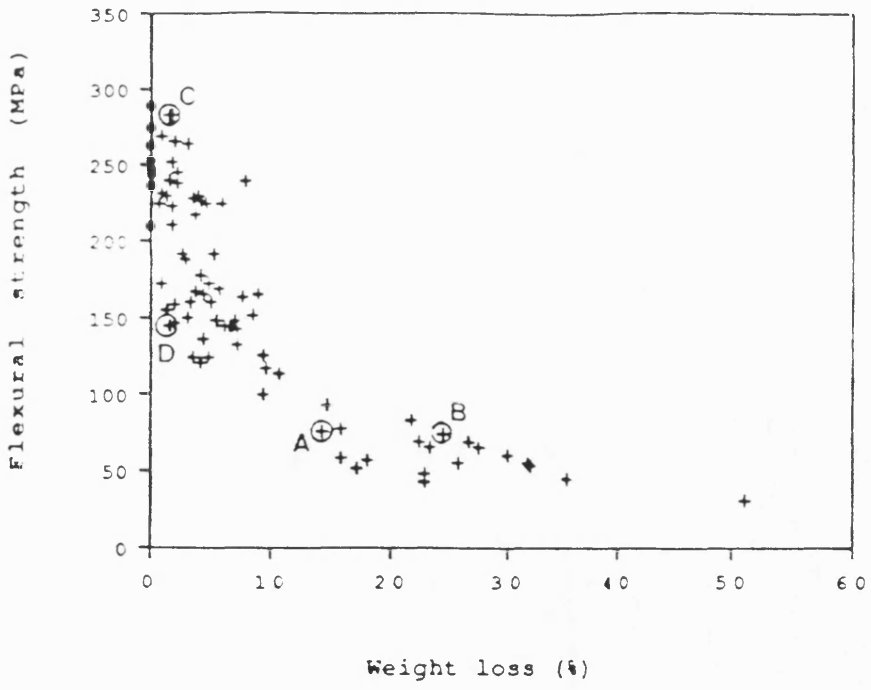

a

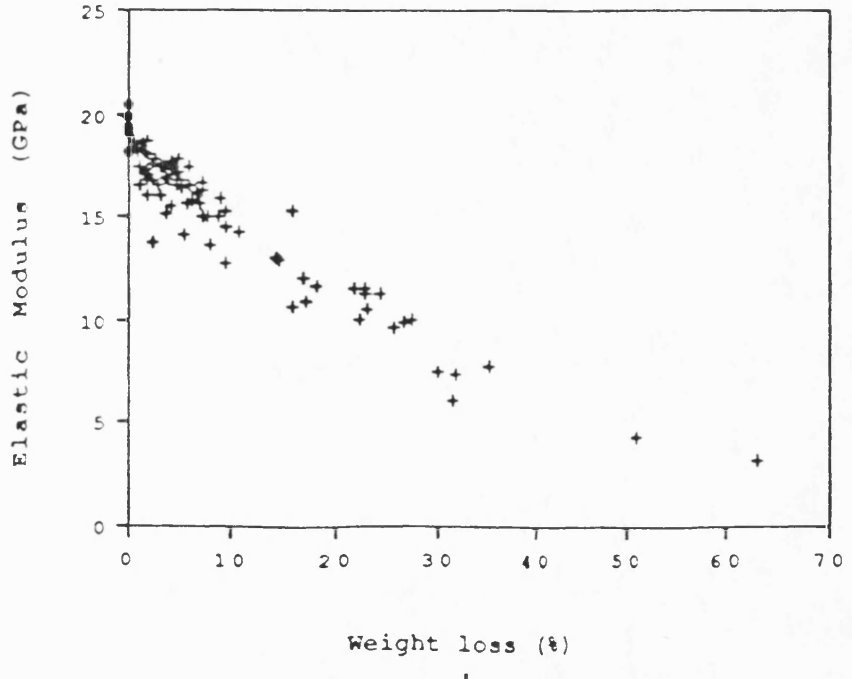

b

FIG 4.38 EFFECT OF WEIGHT LOSS ON a) FLEXURAL STRENGTH AND b) ELASTIC MODULUS OF THE KKARB COMPOSITE

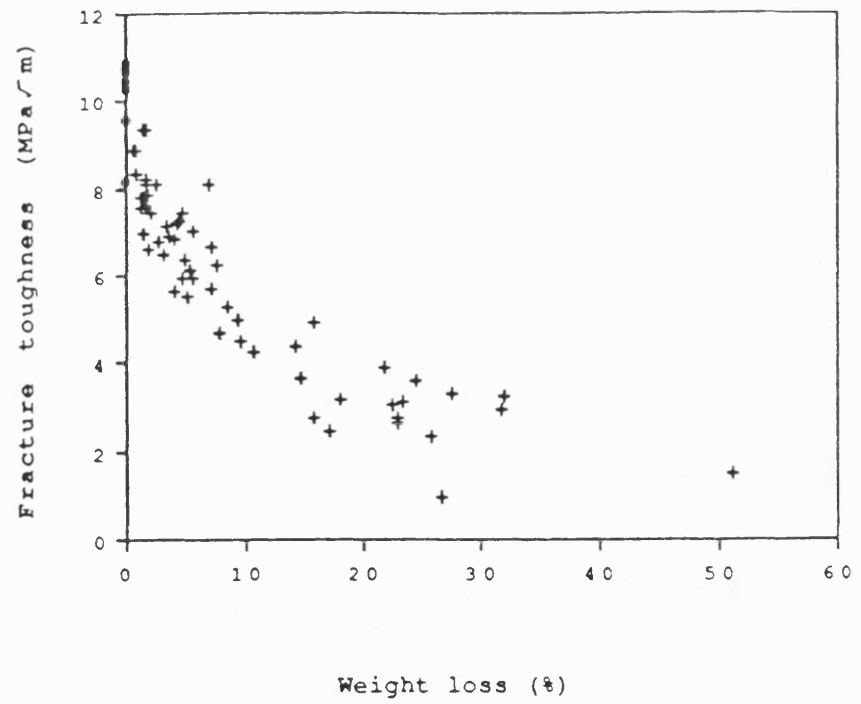

a

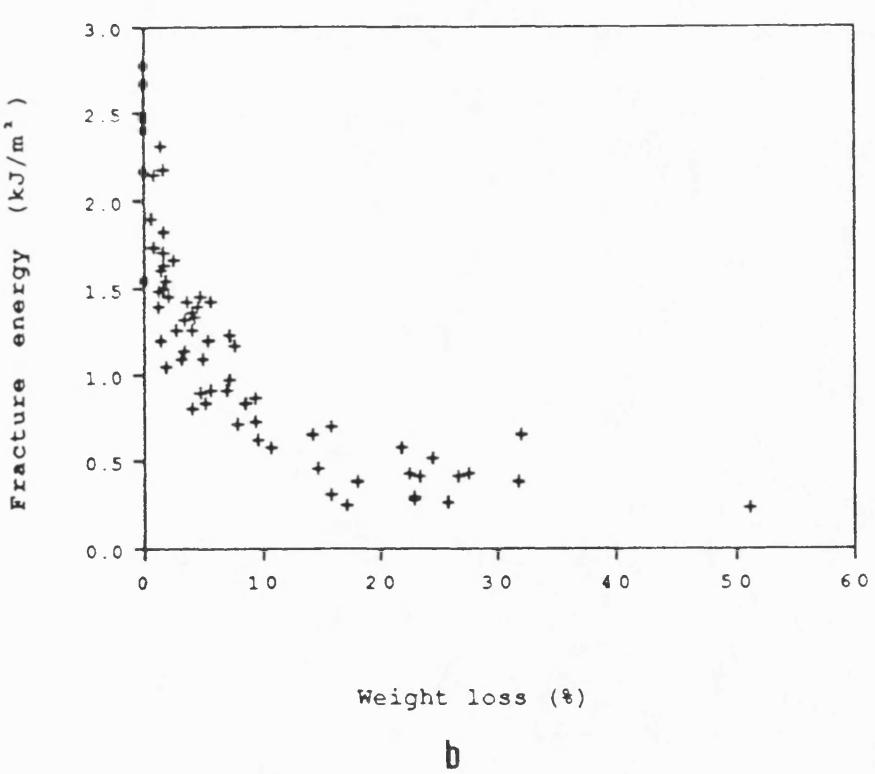

b

FIG 4.39 EFECT OF WEIGHT LOSS ON a) TOUGHNESS AND b) FRACTURE ENERGY FOR THE KKARB COMPOSITE WHEN TESTED IN FLEXURE

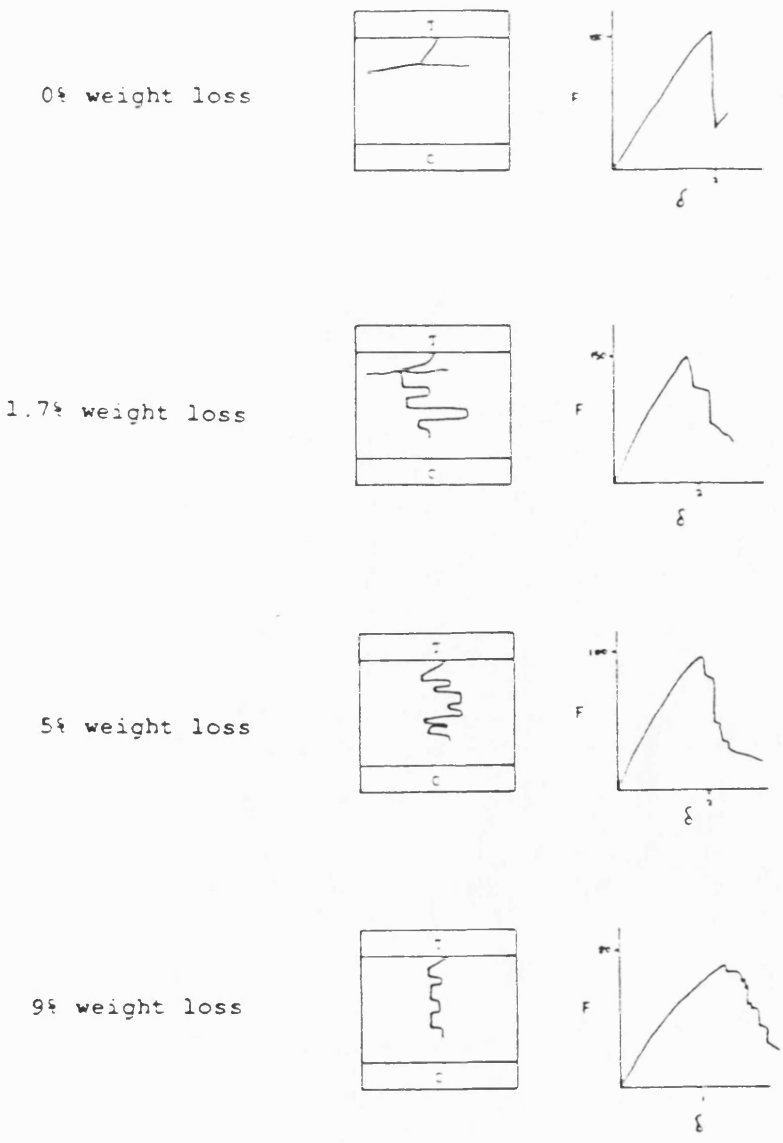

FIG 4.40 KKARB MODES OF FAILURE WITH DIFFERENT AMOUNTS OF WEIGHT LOSS

T=tensile face of composite F=force in N

C=compressive face of composite δ=deflection in mm

0% weight loss

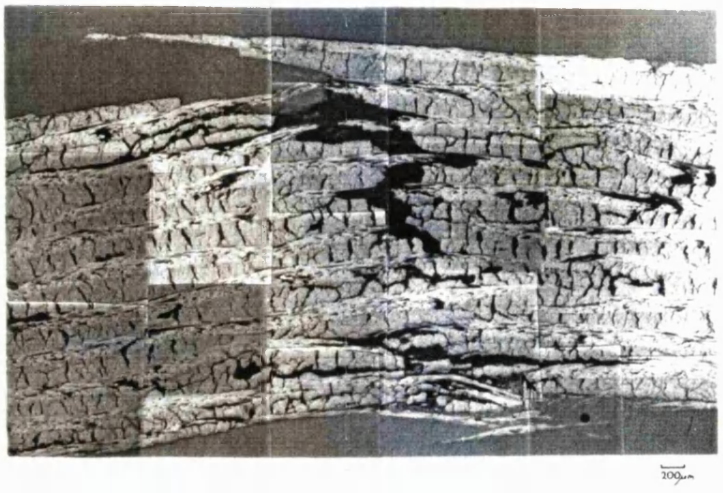

5% weight loss

FIG 4.41 KKARB MODES OF FAILURE WHEN TESTED IN FLEXURE

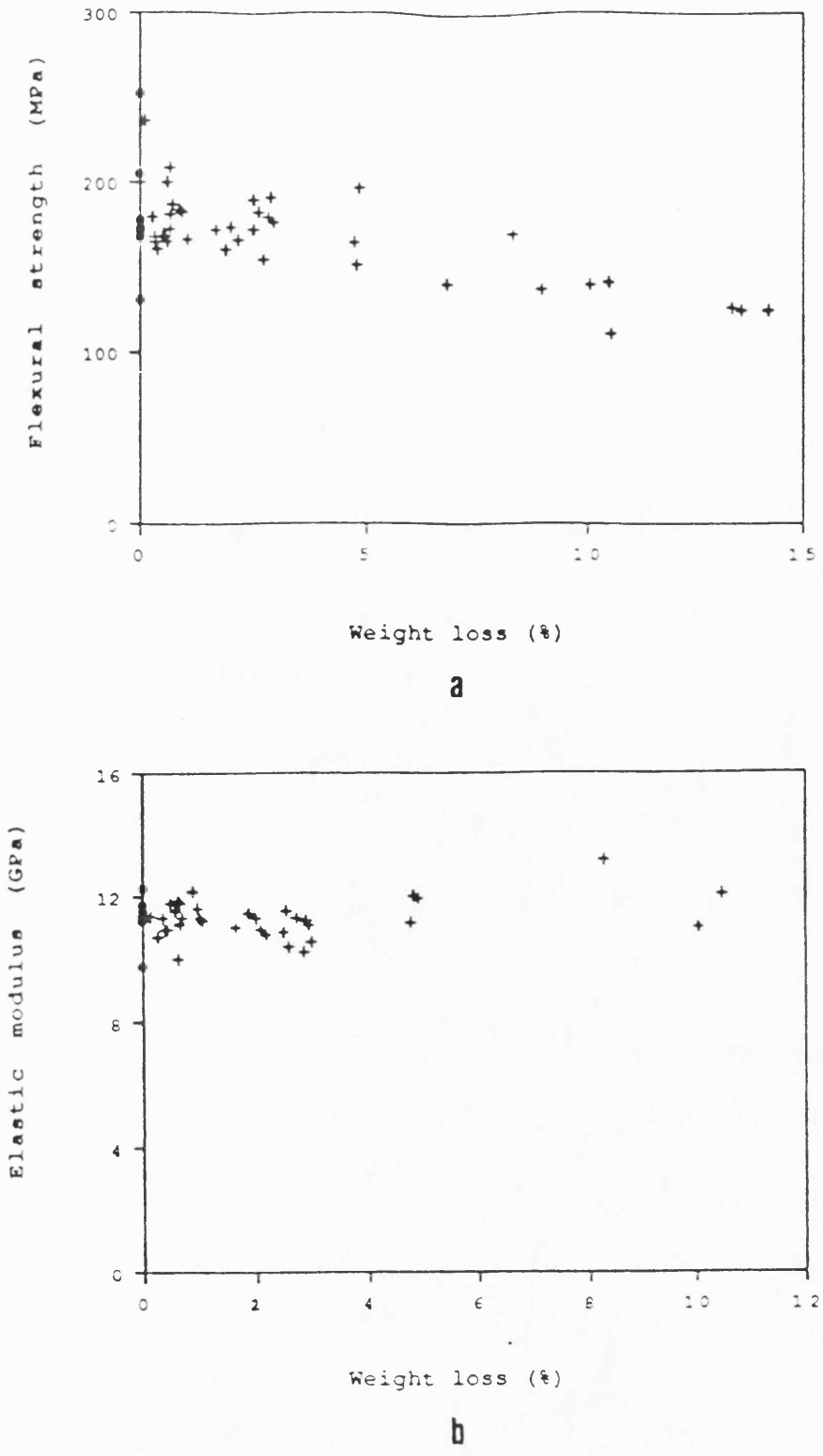

FIG 4.42 EFFECT OF WEIGHT LOSS ON a) FLEXURAL STRENGTH AND b) ELASTIC MODULUS (RESONANCE METHOD) OF THE SIGRI COMPOSITE

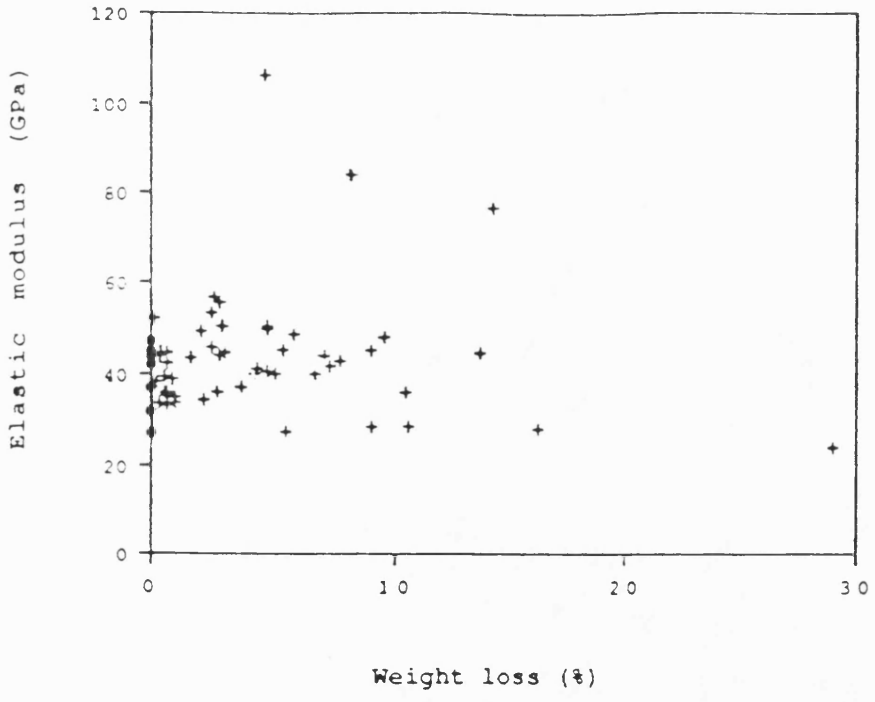

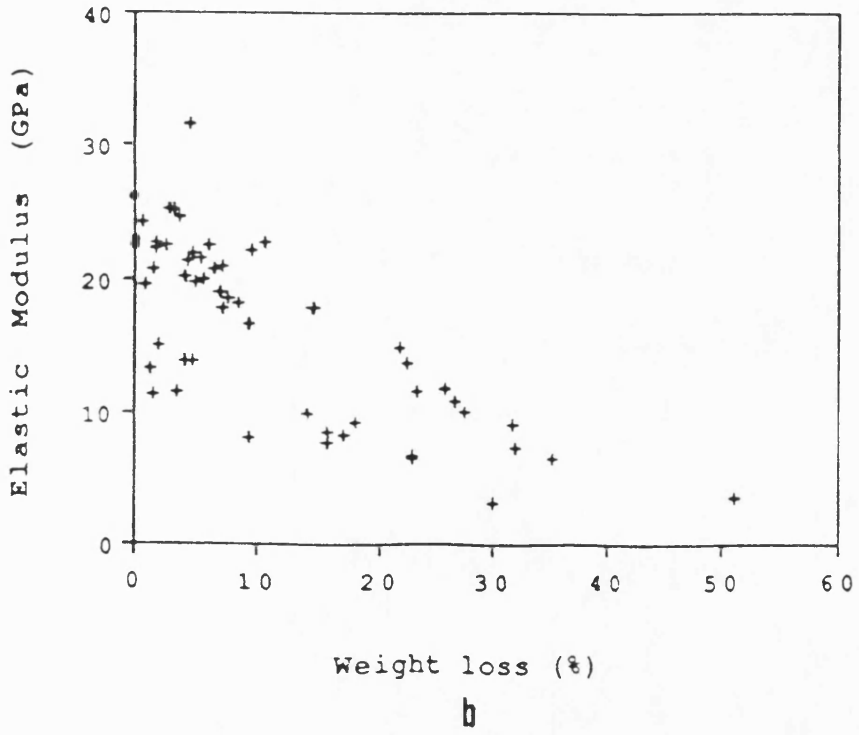

FIG 4.43 EFFECT OF WEIGHT LOSS ON ELASTIC MODULUS OF a) SIGRI AND b) KKARB CALCULATED FROM FLEXURAL TESTS

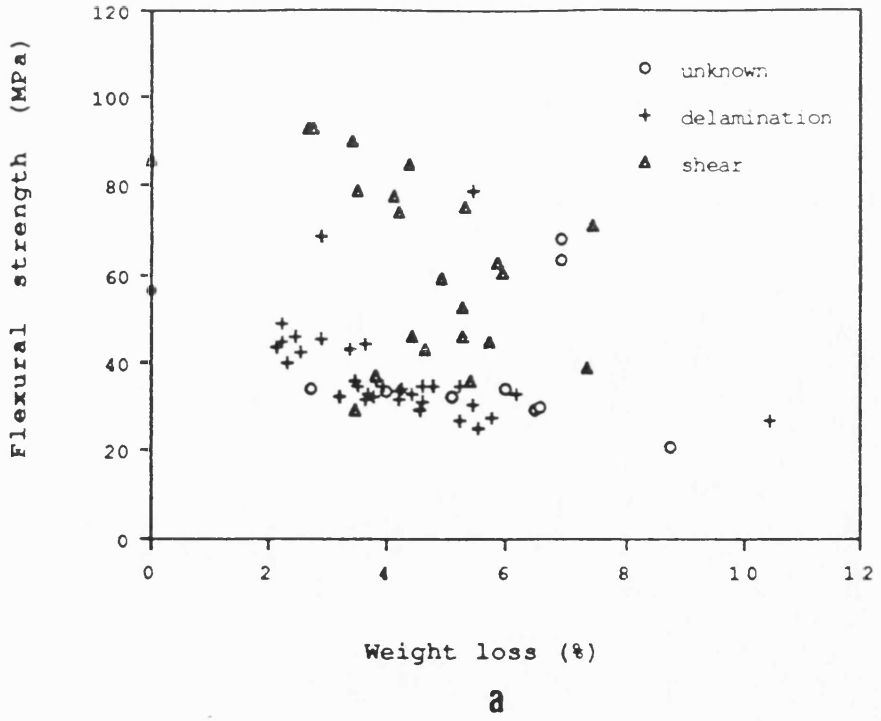

a

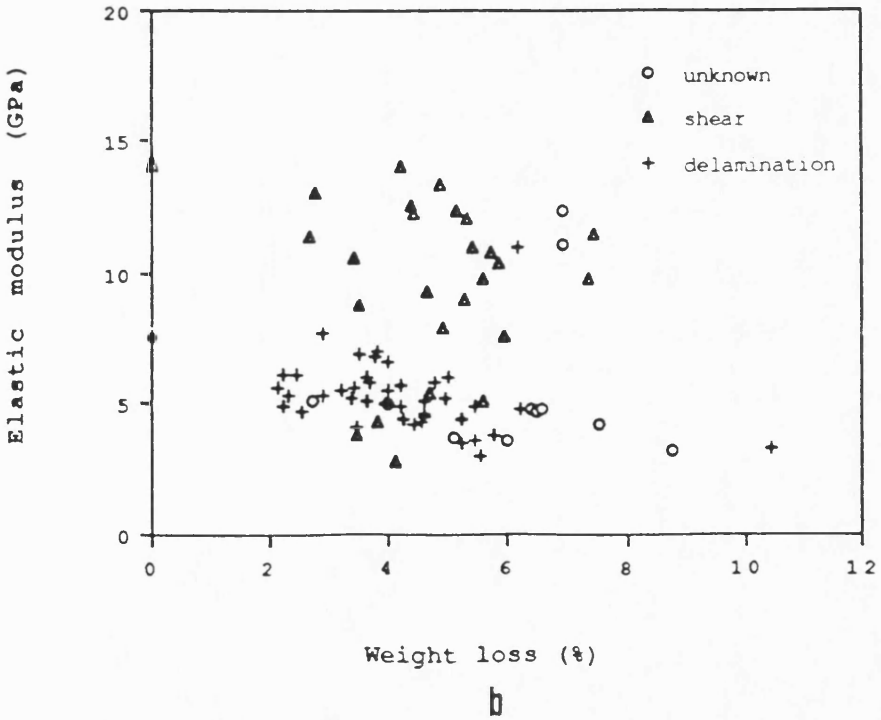

b

FIG 4.44 EFFECT OF OXIDATION ON a) FLEXURAL STRENGTH AND b) ELASTIC MODULUS FOR THE FMI COMPOSITE

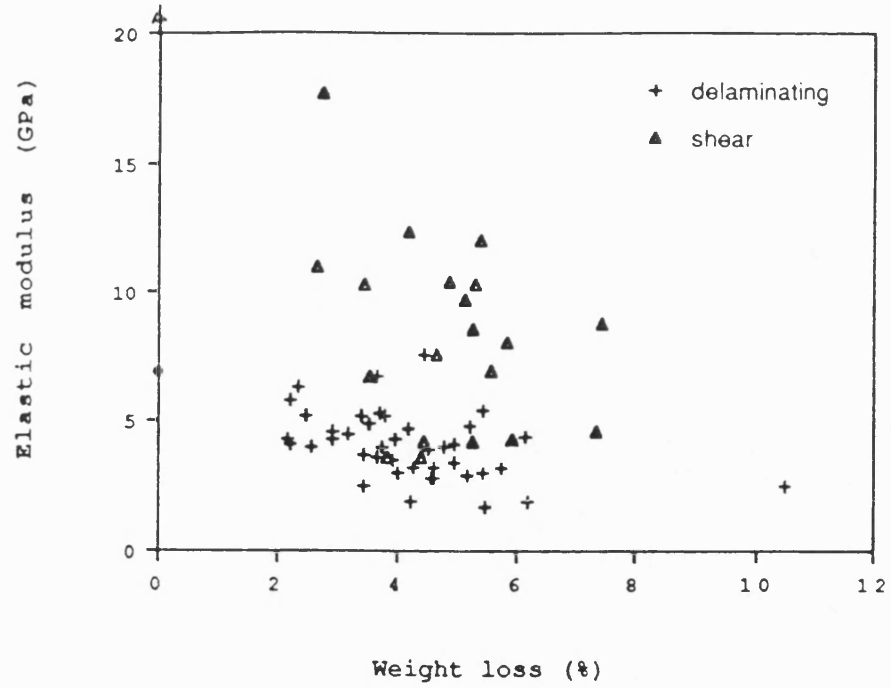

FIG 4.45 EFFECT OF WEIGHT LOSS ON CALCULATED ELASTIC MODULUS OF THE FMI COMPOSITE

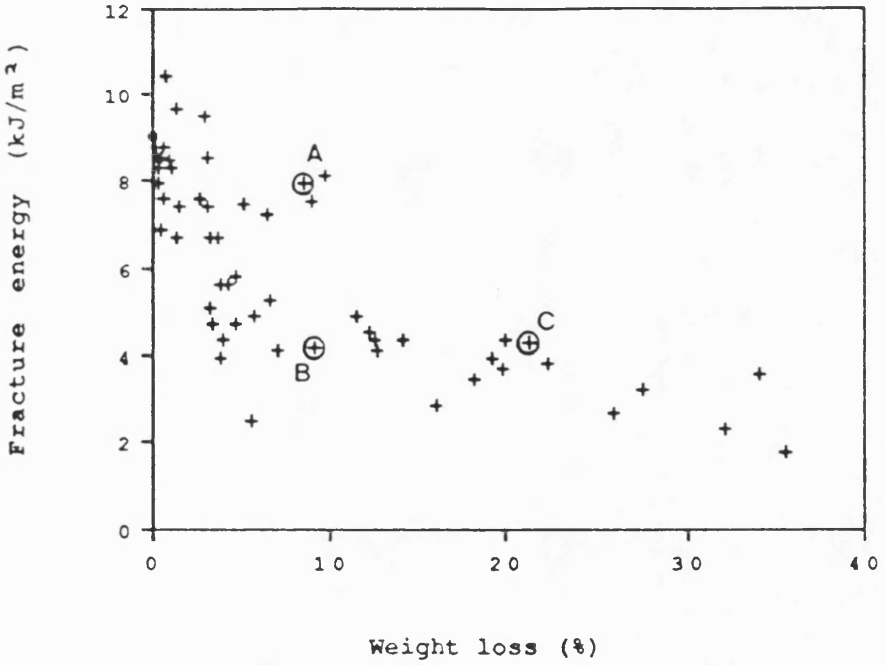

FIG 4.46 EFFECT OF WEIGHT LOSS ON FLEXURAL IMPACT FRACTURE ENERGY FOR THE KKARB COMPOSITE

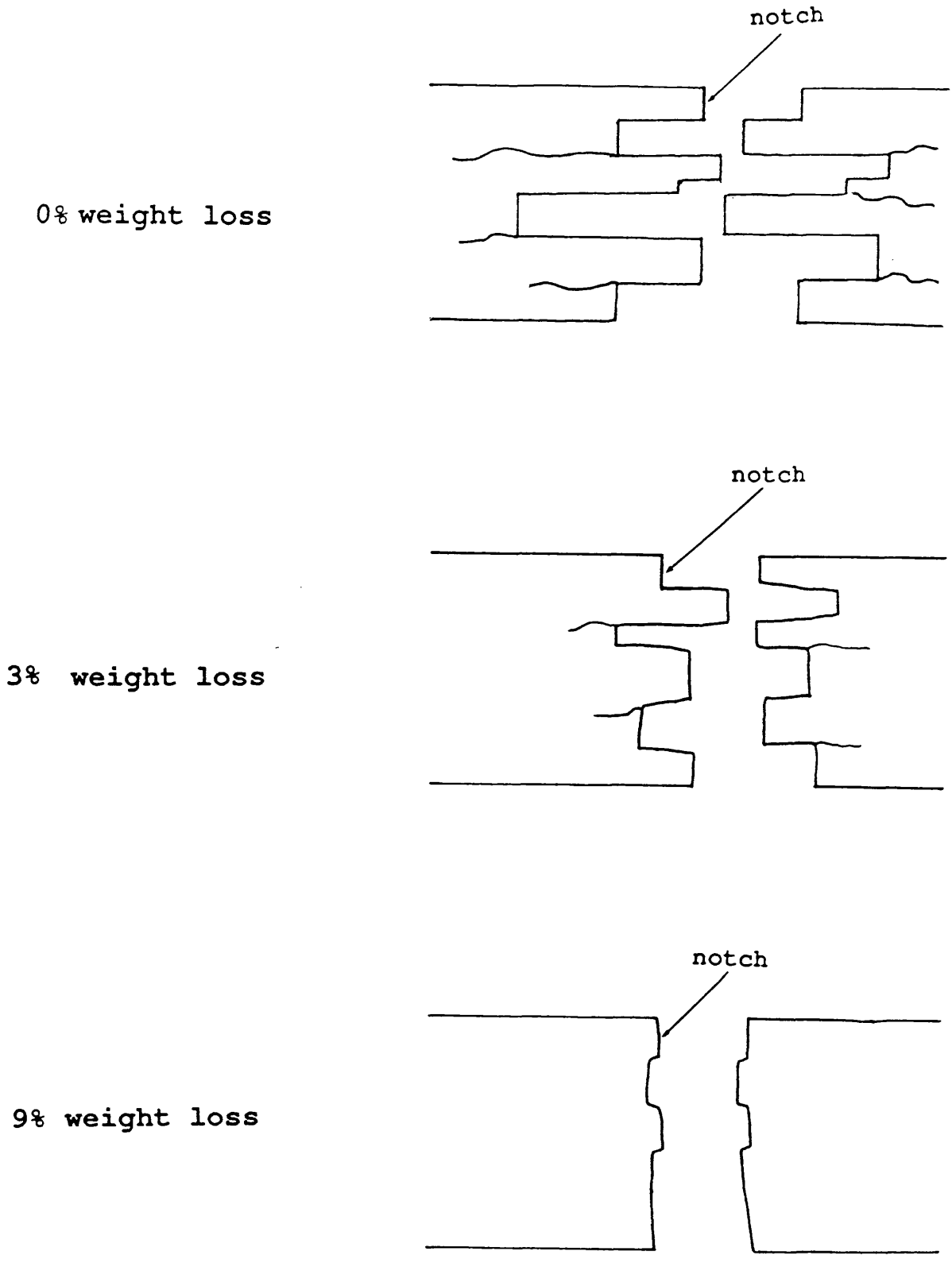

FIG 4.47 KKARB FLEXURAL IMPACT FRACTURE MODE VARIATION WITH OXIDATION

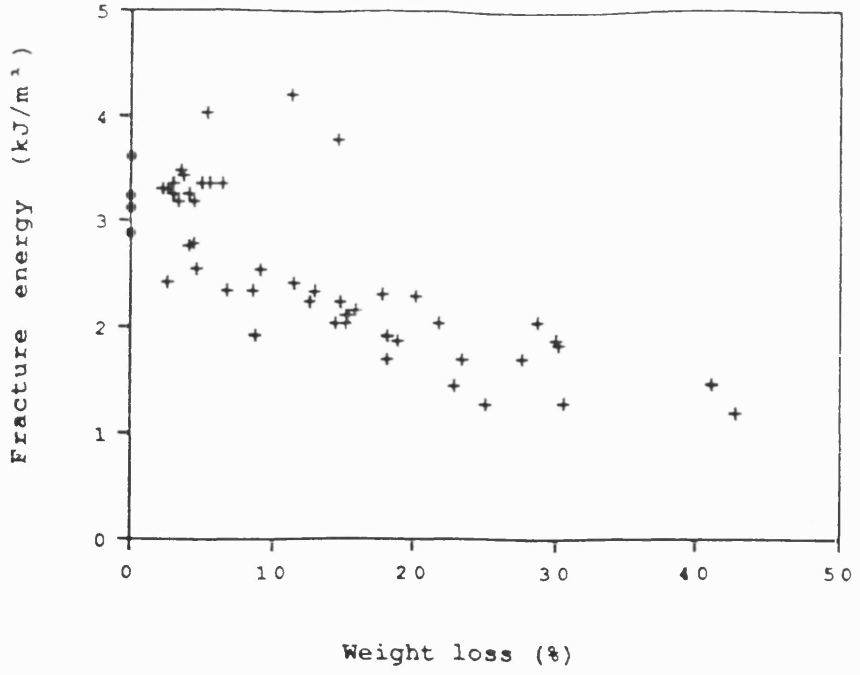

a

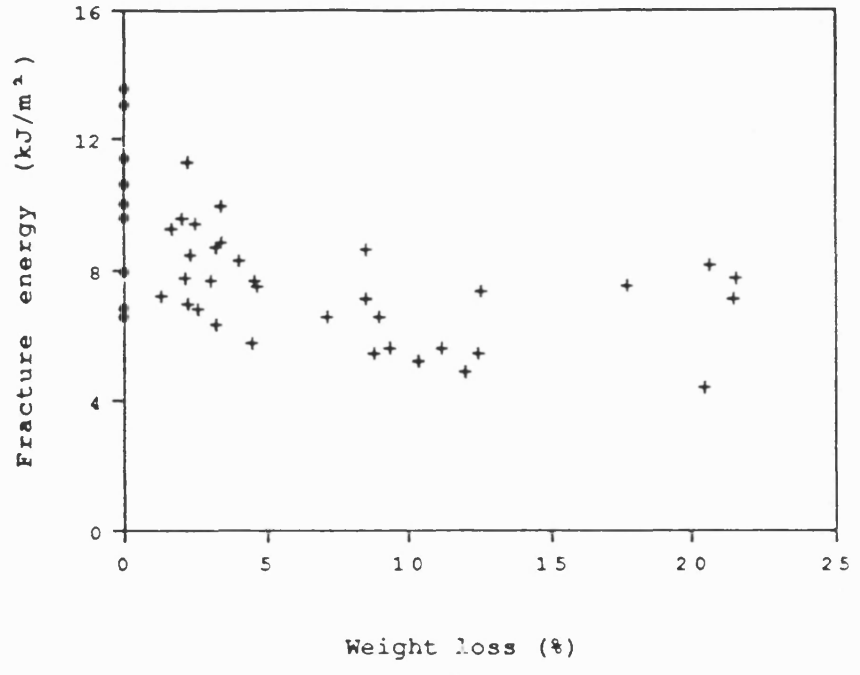

b

FIG 4.48 EFFECT OF WEIGHT LOSS ON THE TENSILE IMPACT FRACTURE ENERGY FOR a) KKARB AND b) SIGRI SPECIMENS

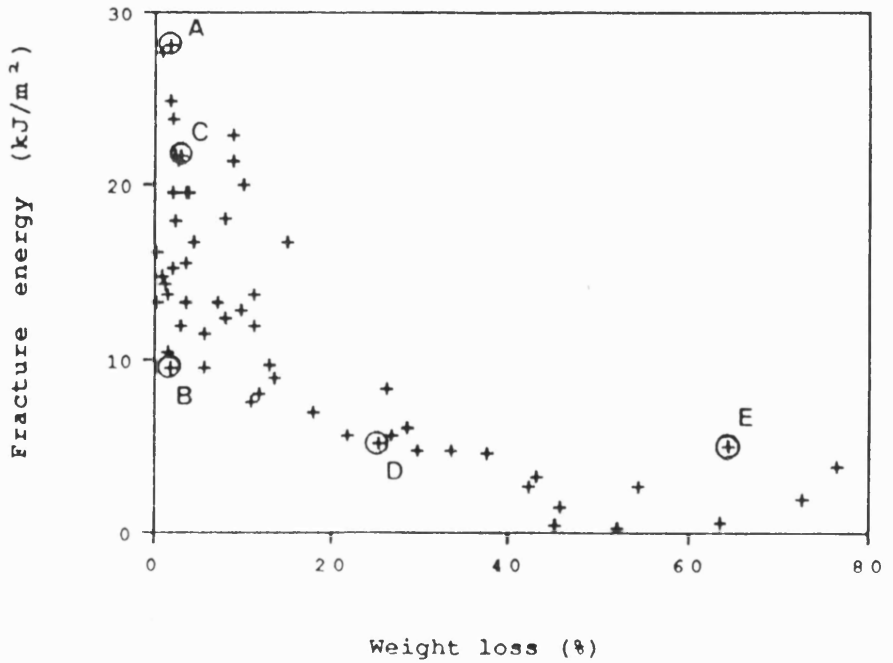

FIG 4.49 EFFECT OF WEIGHT LOSS ON FLEXURAL IMPACT FRACTURE ENERGY FOR THE SIGRI COMPOSITE

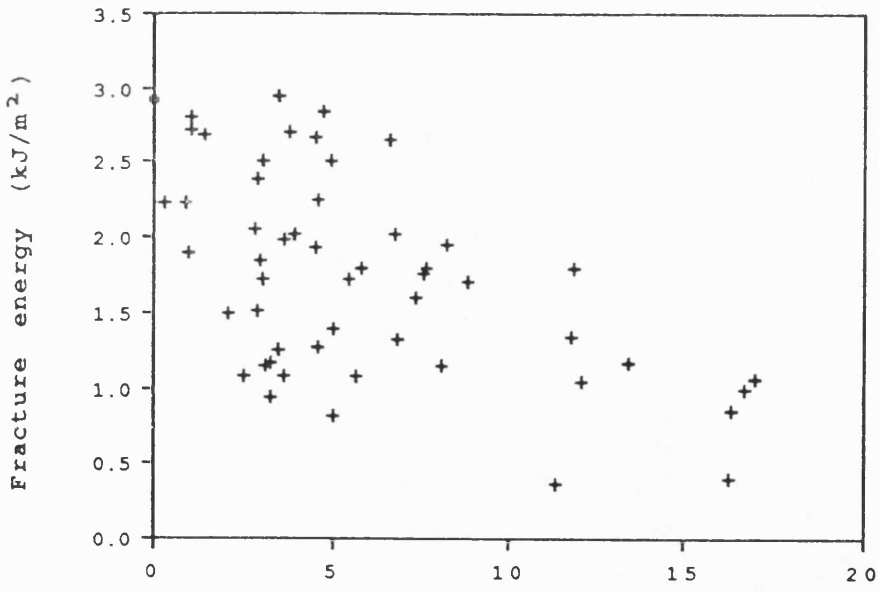

a

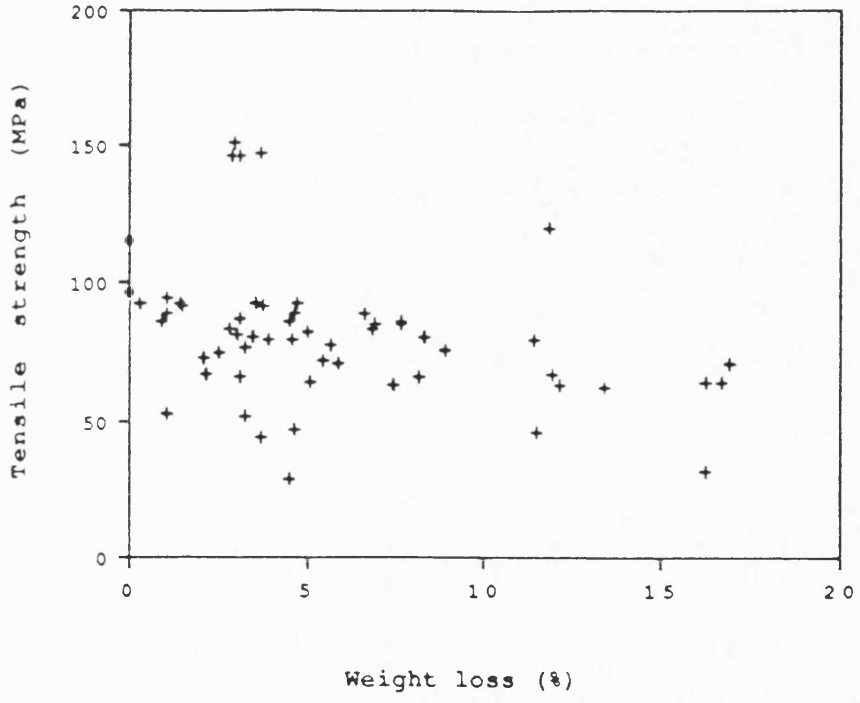

b

FIG 4.50 EFFECT OF WEIGHT LOSS ON a) TENSILE FRACTURE ENERGY AND b) TENSILE STRENGTH OF THE KKARB COMPOSITE

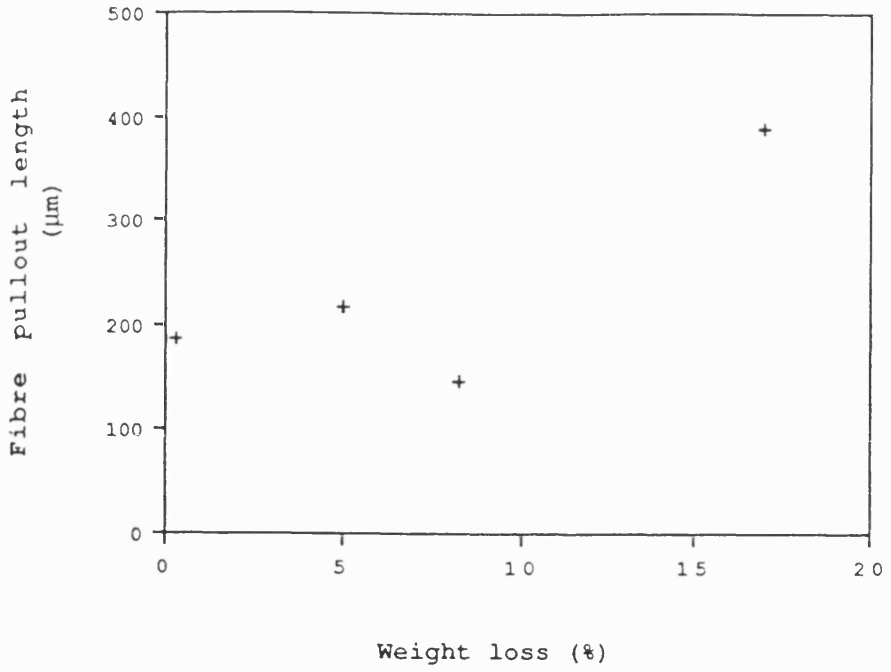

a

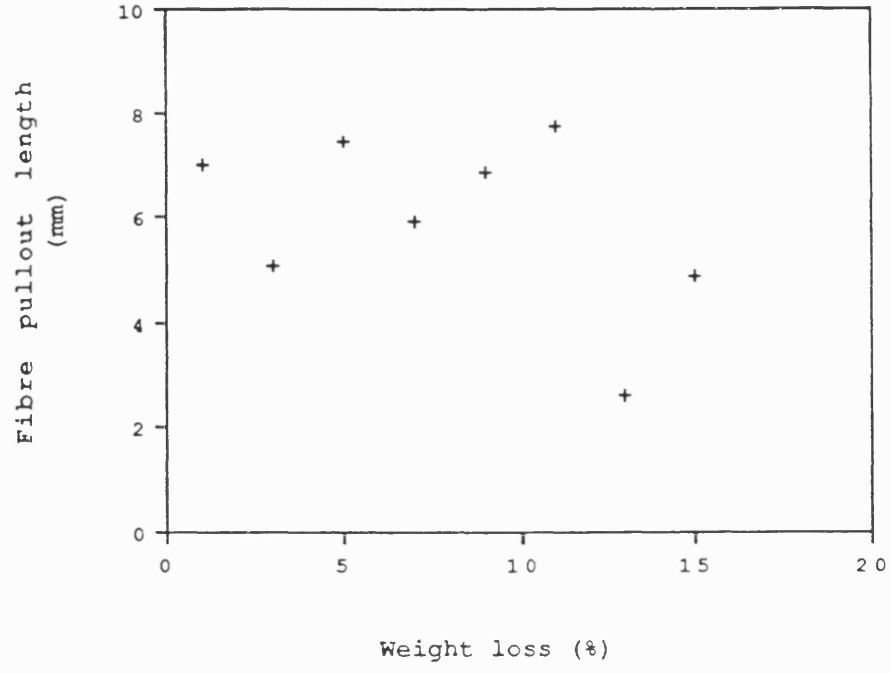

b

FIG 4.51 FIBRE PULLOUT LENGTH FOR a) KKARB AND b) SIGRI

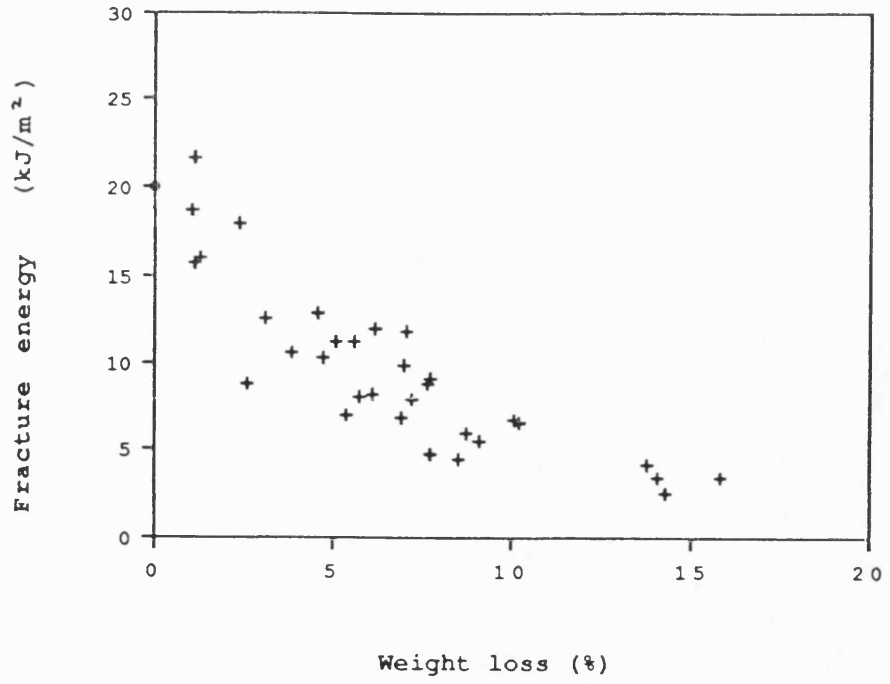

a

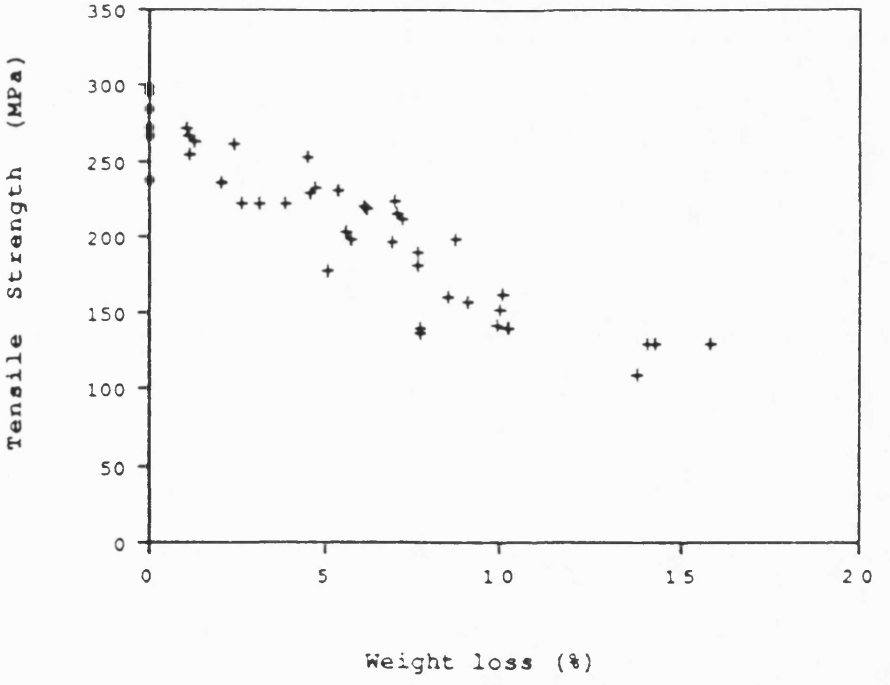

b

FIG 4.52 EFFECT OF WEIGHT LOSS ON a) TENSILE FRACTURE ENERGY AND b) TENSILE STRENGTH OF THE SIGRI COMPOSITE

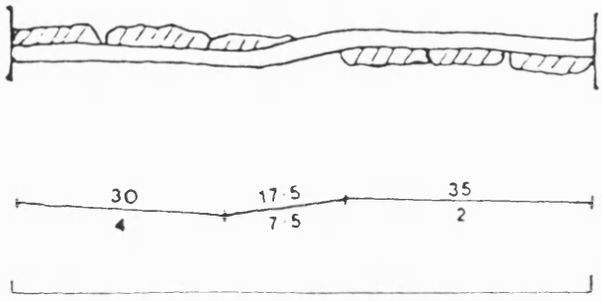

KKarb (warp)

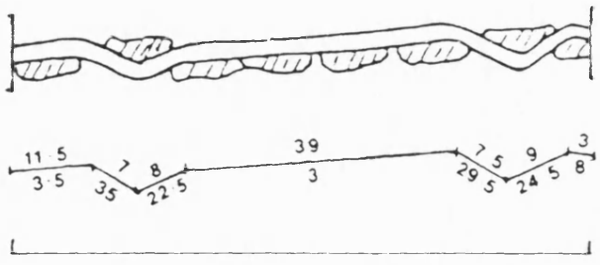

KKarb (fill)

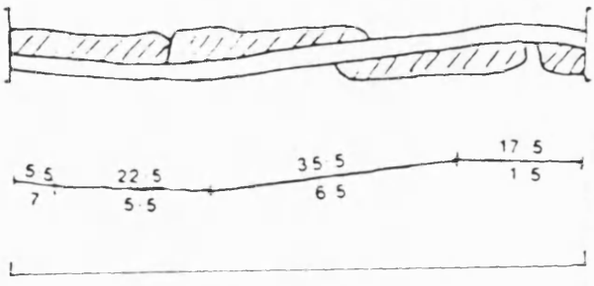

Sigri

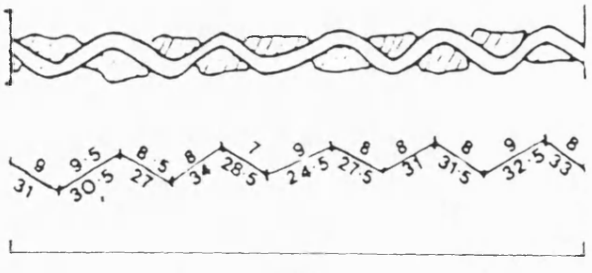

FMI

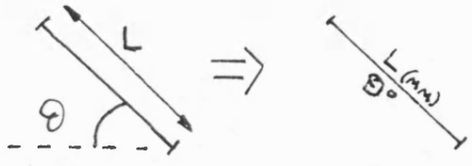

FIG 5.1 ANGLES OF THE WEAVE PATTERNS

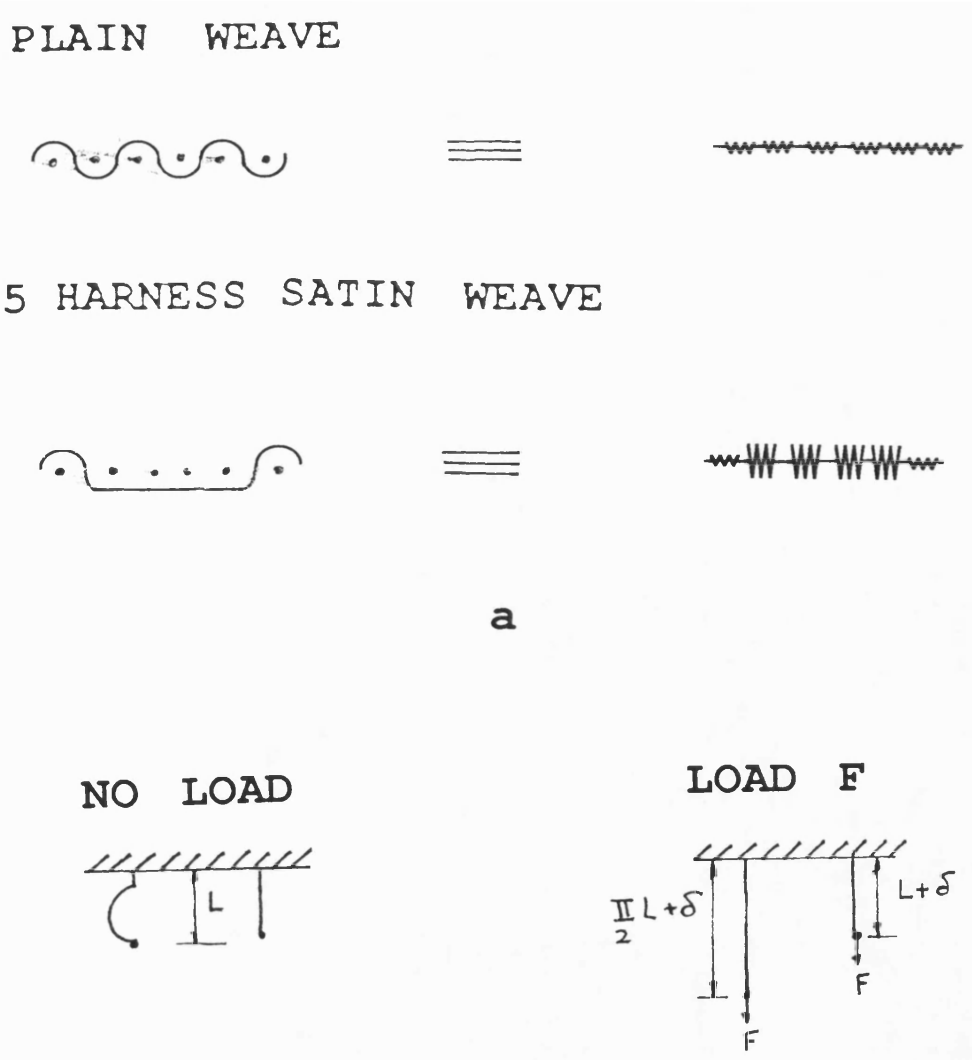

FIG 5.2 EQUIVALENT SPRING SYSTEMS FOR a) WEAVE PATTERNS, b) STRAIGHT AND CURVED FIBRES AND c) COMPOSITES

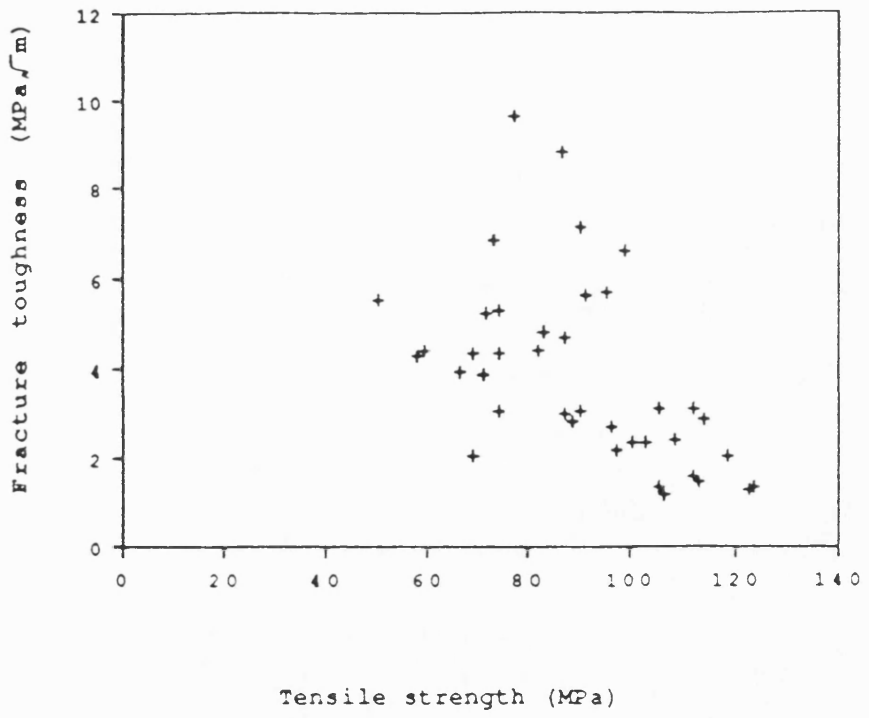

a

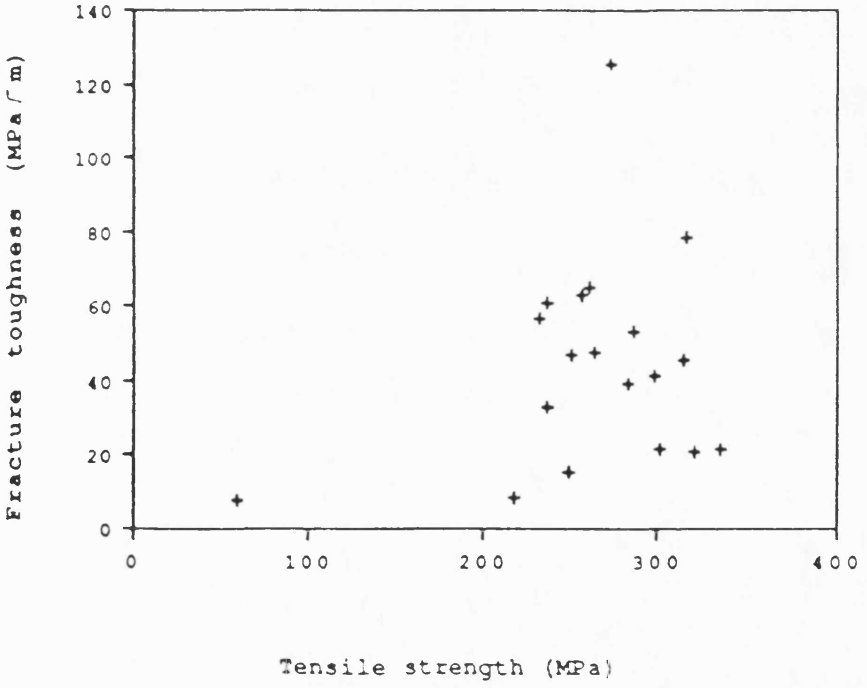

b

FIG 5.3 VARIATIONS OF FRACTURE TOUGHNESS WITH TENSILE STRENGTH FOR a) KKARB AND b) SIGRI